POLITECNICO DI TORINO

Corso di Laurea Magistrale in Ingegneria Civile

Tesi di Laurea Magistrale

Scenario analysis of risk-oriented design for geotechnical structures

Relatori:

Prof. Marco Barla

Dr. Claudia Klotz

Candidato:

Ina Valodzka

Marzo 2018

TABLE OF CONTENTS

ABSTRACT

Geotechnical problems are one of the major contributors to cost and schedule overruns and lack of quality on large civil engineering projects. That is why it is very important to recognize and identify the root causes. A risk management process includes identifying and analyzing risks. Risk identification is the first and perhaps the most important step in the risk management process, as it attempts to identify the source and type of risks. It develops the basis for the next steps: analysis and control of risk management. Correct risk identification ensures risk management effectiveness. The risk identification process would have highlighted risks that may be considered more significant for further analysis. Generally two broad categories, namely, qualitative and quantitative analysis are distinguished in literature on risk assessment. A qualitative analysis allows the key risk factors to be identified. Qualitative risk analysis assesses the impact and likelihood of the identified risks.

This master thesis was carried out in the city of Stuttgart with the guidance of Dr. Claudia Klotz, a professor at the University of Applied Science of Stuttgart and a project engineer at Züblin AG. This work aims to the study of the variety of risks to which various geotechnical structures are amenable, the reasons and the consequences of those risks. Then, the formulation and the quantification of the criterions for the risk evaluation in accordance with euronorms and national standards. Finally, the implementation of those criterions in a case study modelled with the finite element method.

In the first chapter some definitions and common notions of *risk* and *level of risks* are given. Then, the main reasons of failures in constructions are reported with detailed review of failures in geotechnical structures such as shallow and deep foundations, deep

excavations and tunneling. Different causes and factors that may lead catastrophic consequences are described here.

In the second chapter the most significant control parameter are considered for the evaluation of risks during the deep excavation process. Deep excavation implies an excessive soil movements, hence mobilized active earth pressure, and causes excessive settlements of adjacent buildings that, in turn, may lead to the various damages. Qualitative and quantitative criterions of the control parameters are defined concerning geotechnical structures that are supposed to be executed, as well as concerning the stability of the adjacent buildings.

The next chapter represents the summary and more detailed review of the most important characteristics related to the excavation process such as movement and deflection of retaining walls, determined by the excavation-induced unbalanced forces, presence of the piled foundations in the vicinity, behaviour of soil (drained/ undrained) and ground water lowering.

In the chapter four some costitutive models for soils are represented, that are commonly used for analysis of soil behaviour. The choice of a constitutive model depends of many factors but, most of all, it is related to the type of analysis that the users intend to perform, to an expected precision of predictions and to available knowledge of soil. Three constitutive models of soil are explained here that further are implemented in calculations. One is a simple linear-elastic perfectly plastic Mohr-Coulomb model; the other two are advanced nonlinear-elastoplastic models: a Hardening Soil and a Hardening Soil Small Strain models. For these models the significant parameters are considered and a formulation of each model is given.

Chapter five introduces a case study: construction of a multistorey building in the central area of Stuttgart. First, the geology of the interested area is investigated by means of *in situ* tests in order to explore the composition and the sequence of the soil layers and their depths, as well as the level of ground water. Then, samples of every layer are examined in laboratory for the purpose to obtain necessary parameters of soil such as grain size of soil particles, permeability, cohesion, shear strength, compressibility and others. Moreover, calculations of the ground water lowering are represented here. As a basement of the building is supposed to lie beneath the ground water level, the water lowering is required during the excavation process. Further, a numerical modelling of the case study is described with detailed explanation of every

unit used in FEM-model and the sequences of the construction phases are given. The simulation carried out in three models of soil: Mohr- Coulomb, Hardening Soil and Hardening Soil Small Strain models. For the Hardening Soil Small Strain model four more variations are studied: an increase of the soil stiffness of all layers by one quarter in relation to the original value, a decrease of the soil stiffness by one quarter, an increase the stiffness of the retaining wall and a decrease the stiffness of the wall.

In the last chapter a risk analysis is carried out. First, the values of the parameters of the quantitative criterions of risks are introduced (that were previously discussed in chapter two) as for geotechnical structures as well as for the adjacent structure for the presented study case. Then, the obtained results are collected, careful analysed and discussed.

RIASSUNTO

I problemi geotecnici rappresentano uno dei maggiori contributi ai ritardi nei lavori e superamenti dei costi previsti, altre ai peggioramenti nei termini di qualità nei grandi progetti di ingegneria civile.

Ecco perché è molto importante riconoscere e identificare le cause di tali problemi. Un processo di gestione del rischio include l'identificazione e l'analisi dei rischi. L'identificazione del rischio è il primo passo, e forse il più importante, nel processo di gestione del rischio, dato che tenta di identificare la fonte ed il tipo di rischio. L'identificazione dei rischi sviluppa la base per i passi successivi: analisi e controllo della gestione del rischio. La corretta identificazione assicura che la gestione del rischio sia efficace. Il processo di identificazione evidenzia i rischi che possono essere considerati più significativi per ulteriori analisi. Generalmente in letteratura si distinguono due grandi categorie nella valutazione del rischio: analisi qualitativa e analisi quantitativa. Un'analisi qualitativa permette di identificare i principali fattori del rischio. L'analisi quantitativa valuta l'impatto e la probabilità dei rischi identificati.

Questa tesi di laurea propone lo studio della varietà dei rischi ai quali sono suscettibili varie strutture geotecniche, le cause e le conseguenze di tali rischi. Si è inoltre approfondito il tema relativo alla formulazione e dalla quantificazione di alcuni criteri per la valutazione dei rischi secondo gli standard europei e nazionali. Infine, tali criteri sono stati applicati aduncaso di studio modellato tramite il software agli elementi finiti.

Nel primo capitolo vengono fornite alcune definizioni e nozioni comuni di *rischio* e *livello di rischio*. L'istituto di Risk Management non propone una definizione ufficiale

del termine "rischio", sebbene nei suoi documenti vengano usate termini come "possibilità di cattive conseguenze o esposizione a disgrazie". Quindi, hanno principalmente un effetto negativo. [1]

Il livello di rischio è definito come "grandezza di un rischio o combinazione dei rischi, espressa in termini di combinazione di conseguenze e di probabilità". Questa definizione consente la pratica comune di quantificare il rischio come un prodotto di probabilità di verificarsi un evento e le conseguenze di tale evento. [2]

È importante riconoscere che nell'ingegneria geotecnica molte delle fonti di rischio o dei rischi derivano dall'incertezza o errore geotecnico. Questo argomento è stato ampiamente discusso in letteratura. Ad esempio, [3] ha classificato le fonti di incertezza come segue:

(1) variabilità spaziale e temporale intrinseca;

(2) errori di misura (sistematici o casuali);

(3) incertezza del modello;

(4) incertezza del carico;

(5) omissioni.

Poi vengono viste le cause principali del collasso delle costruzioni. Le cause del collasso strutturale possono essere classificate come segue: [5]

- Inadeguato design
- Costruzione difettosa
- Collasso della fondazione
- Carichi straordinari
- Materiali e elementi strutturali non ancora raggiunto la resistenza di progettazione
- Modalità di guasto imprevisto
- Combinazione delle cause

Inadeguato design significa sia errori di calcolo, come guasti e collassi dovuti ai carichi calcolati non precisamente o erratamente che la struttura deve portare dopo essere completata, così come le teorie errate, affidamento sui dati imprecisi, l'ignoranza degli effetti di sollecitazioni ripetute o impulsive (carichi dinamici), scelta errata dei materiali o incomprensione delle loro proprietà. È l'ingegnere chi è responsabile di questi errori creati in ufficio.

I guasti dovuti ad una progettazione errata possono verificarsi in una struttura in qualsiasi momento durante la vita utile prevista della struttura. Ad esempio, i crolli catastrofici dei ponti e delle altre strutture sono dovuti alla mancanza di manutenzione dopo molti anni di prestazioni soddisfacenti. Allo stesso modo, un errore commesso durante la progettazione o la costruzione può essere ignorato fino a quando si verifica un guasto, dopo anni di un adeguato utilizzo della struttura.

In seguito vengono representate le cause dei collassi delle strutture geotecniche tali come fondazioni superficiali e profonde, scavi profondi e gallerie. Nel lavoro presente i scavi profondi e le fondazioni profonde sono di maggior interesse.

Scavo profondo nel terreno ha due effetti principali. Il primo è che la rimozione del peso del terreno scavato provoca una diminuzione delle tensioni verticali nel suolo sotto lo scavo. Il secondo è che la rimozione del terreno nello scavo comporta una perdita di supporto laterale del terreno attorno allo scavo stesso [9]. La deformazione del terreno attorno agli scavi può danneggiare gli edifici, le strade e i servizi pubblici adiacenti. La gravità e l'entità del danno dipendono dall'entità e dalla struttura dei movimenti del terreno intorno allo scavo.

Allo scopo di fornire un supporto laterale al terreno attorno a uno scavo profondo e per limitare i movimenti del terreno circostante, deve essere fornito un sistema di supporto. I sistemi di supporto per lo scavo profondo sono costituiti da due componenti principali: una paratia e un supporto dell paratia stessa.

Le seguenti cause possono portare al fallimento delle strutture di supporto:

- Stima della spinta attiva e passiva
- Stima dell'acqua interstiziale
- Considerazione della pressione dell'acqua artesiana
- Esistenza della forza di filtraggio
- Estrusione/flusso del terreno
- Sollevamento del terreno (heaving)
- Errori nella modellazione numerica geotecnica
- Terremoti o vibrazioni che provocano deformazion/spostamentii laterali
- Costruzione non adeguata

Nel secondo capitolo vengono riportati alcuni nozioni della ricerca qualitativa e quantitativa e presi in considerazione i parametri di controllo più significativi per la

valutazione dei rischi durante il processo di scavo profondo. Scavi profondi implicano un eccessivo movimento del terreno (cioè, appaia una spinta attiva mobilizzata nel terreno), e provocano eccessivi cedimenti degli edifici adiacenti che, a loro volta, possono portare a vari danni. I criteri qualitativi e quantitativi dei parametri di controllo sono definiti per quanto riguarda le strutture geotecniche che devono essere eseguite, nonché per quanto riguarda la stabilità degli edifici adiacenti.

La ricerca qualitativa è generalmente di natura esplorativa e/o investigativa. Essa implica un'interazione continua tra la teoria e l'analisi e le sue conclusioni spesso non sono definitive. Tuttavia, queste scoperte sono preziose per una profonda comprensione di un dato problema e per un ulteriore processo decisionale.

Come suggerisce il nome, la ricerca quantitativa si basa sulla misurazione delle quantità, è di natura statistica e/o empirica. [14] descrive la ricerca quantitativa come "Spiega i fenomeni raccogliendo dati numerici che vengono analizzati usando metodi matematici". L'obiettivo della ricerca quantitativa è sviluppare e impiegare modelli matematici, teorie e/o ipotesi relative ai fenomeni e impiega diverse forme di strumenti statistici ed è di natura.

Quali parametri devono essere controllati per garantire il processo di scavo sicuro e la stabilità delle strutture adiacenti?

Per quanto riguarda le strutture geotecniche, i seguenti parametri dovrebbero essere presi in considerazione:

- spostamento orizzontale della struttura di sostegno, u_x [mm]
- capacità portante del terreno, q [kN/m^2]
- tensioni normali alla base del palo, q_b [kN/m^2]
- tensioni tangenziali lungo fusto del palo, τ_s [kN/m^2]
- compressibilità del terreno, E [kPa]
- geometria della struttura di sostegno, EA [kN], EI [kN m^2]
- fattore di sicurezza, η [-]
- modello di comportamento del terreno

Una deflessione della paratia verso l'interno dovuta al movimento del terreno dovrebbe essere limitata in modo tale da non creare eccessivi cedimenti del terreno superficiale (quindi, cedimenti degli edifici adiacenti) e inoltre, non creare gli effetti del secondo ordine (momento flettente aggiuntivo, ecc.).

Per quanto riguarda la stabilità degli edifici adiacenti, è necessario controllare i seguenti parametri:

- cedimenti, ρ [mm]
- distorsione angolare, β [-]
- larghezza delle crepe visibili negli edifici adiacenti, w [mm]
- sollecitazioni di compressione e di trazione nella struttura adiacente, σ_c, σ_t [kN/m^2]

Un riassunto degli effetti creati dal movimento del terreno indotto dallo scavo profondo è rappresentato nella figura 2.4 del capitolo 2.2. Mentre i criteri qualitativi dei parametri di controllo dello scavo profondo sono riportati nella tabella 2.3 - per le strutture geotecniche e nella tabella 2.4 - per le strutture adiacenti allo scavo; nel frattempo i criteri quantitativi raccolti nella tabella 2.5 - per le strutture geotecniche e nella tabella 2.6 - per le strutture adiacenti.

Il prossimo capitolo rappresenta la sintesi e la revisione più dettagliata delle caratteristiche più importanti relative al processo di scavo come il movimento e la deflessione dei muri di sostegno, determinate dalle forze sbilanciate indotte dallo scavo, la presenza in vicinanza di una fondazione su pali, il comportamento del suolo (drenato/non drenato) e l'abbassamento delle falde acquifere.

Nel capitolo quattro sono rappresentati alcuni modelli costitutivi, comunemente usati per l'analisi del comportamento del suolo. La scelta di un modello costitutivo dipende da molti fattori ma, soprattutto, è legata al tipo dell'analisi che l'utente intende eseguire, alla precisione prevista dalle previsioni e alla conoscenza disponibile del suolo.

Per quanto riguarda il tipo di analisi, i calcoli in ambito geotecnico possono essere divisi in due gruppi (figura 4.1):

- coloro il cui obiettivo è valutare la capacità portante e la pendenza o la stabilità di una paratia sono riferiti all'analisi di stato limite ultimo (SLU), e
- quelli che sono riferiti all'analisi di stato limite di esercizio (SLE), come scavi profondi e gallerie in aree urbane. [26]

In generale, purché sia prevista la valutazione allo SLU della capacità portante o della stabilità del pendio, l'analisi può essere limitata ai modelli basici lineari come il modello alla Mohr-Coulomb. Da l'altra parte, un'analisi precisa della deformazione richiede l'applicazione di modelli costitutivi avanzati che approssimano la relazione sforzo-

deformativa in modo più accurato del semplice modello lineare-elastico, perfettamente plastico. [28]

Qui vengono spiegati tre modelli costitutivi del terreno che vengono ulteriormente implementati nei calcoli. Il primo è un semplice modello lineare-elastico perfettamente plastico alla Mohr-Coulomb; gli altri due sono modelli avanzati non lineari elastoplastici incrudenti: Hardening Soil e Hardening Soil Small Starin.

Modello alla Mohr-Coulomb è un modello ben conosciuto che viene utilizzato come una prima approssimazione del comportamento del terreno. La parte elastica lineare si basa sulla legge di Hooke (elasticità isotropa). La parte perfettamente plastica si basa sul criterio di rottura di Mohr-Coulomb (figura 4.2 e equazione 4.1), formulato in un campo plastico non associato. [27] I concetti del presente modello sono riportate in detaglio in capitolo 4.2. Il modello richiede cinque parametri di input: il modulo di Young E, il coefficiente di Poisson ν, la coesione c', l'angolo d'attrito φ', e l'angolo di dilatanza ψ.

Hardening Soil (HS) è un modello avanzato per la simulazione del comportamento di diversi tipi del terreno, sia per i terreni teneri come per i quelli rigidi. Il modello riproduce realisticamente le deformazioni del terreno, poiché la relazione sforzo-deformazione (σ-ε) è approssimata con una curva non lineare (la funzione iperbolica di Duncan-Chang [29], [28]). In contrasto con un modello elastico perfettamente plastico, la superficie di snervamento di un modello plasticito indurente non è fissata nello spazio principale di sollecitazione, ma può espandersi a causa delle deformazioni plastiche.

Inoltre, poiché la formulazione del modello HS incorpora due meccanismi di indurimento, è adatta a modellare bene sia i terreni granulari sia quelli coesivi sovraconsolidati, come i terreni teneri. [30]

Il modello Hardening Soil (HS-Standard) è stato progettato da [31], [32] allo scopo di riprodurre i fenomeni macroscopici di base esposti dai terreni quali sono:

- densificazione, cioè una riduzione nel volume dei vuoti nel terreno a causa delle deformazioni plastiche;
- rigididezza è dipendente dallo sforzo applicato; vale a dire, che questo fenomeno è comunemente osservato quando i moduli di rigididezza crescono con il crescere delle pressioni di confinamento;

- storia dello stato tensionale, ossia tiene in conto degli effetti di preconsolidamento;
- cedimento plastico del materie, cioè sviluppo delle deformazioni irreversibili con il raggiungimento del criterio di snervamento del materiale;
- dilatanza, deformazioni volumetriche negative dovuti alle tensioni di taglio.

Analogamente al modello di Mohr-Coulomb, gli stati limite di sollecitazione vengono simulati mediante i parametri efficaci di taglio: coesione c', angolo di attrito φ' e l'angolo di dilatanza, ψ. Mentre gli stati precedenti al collasso sono descritti in modo più accurato usando i tre nuovi parametri di input:

- rigiddezza edometrica, E_{oed} (equazione 4.11 e figura 4.5)
- rigidezza triassiale di carico, E_{50} (equazione 4.14 e figura 4.6)
- rigidezza triassiale di scarico, E_{ur}. (equazione 4.15 e figura 4.6)

Dalle formule 4.11, 4.14 e 4.15 è visto che tali rigidezze cambiano in modo non lineare ma iperbolico al crescere dello sforzo applicato. La spiegazione più ampia del modello é presente nel capitolo 4.3.

Una versione estesa del modello HS-Standard, è il modello Hardening Soil Small Strain (HSS Strain model) che è stato formulato da Benz [38] per tener conto della non-linearità del terreno anche alle deformazioni piccole. Il modello, infatti, consente di descrivere un comportamento esteretico del terreno per stati all'interno della superficie di snervamento per mezzo di due parametri aggiuntivi rispetto alla versione originale:

- G_0 è il modulo di rigidezza a taglio iniziale (formula 4.36)
- $\gamma_{0,7}$ è il modulo di deformazione di taglio in corrispondenza della quale il modulo di rigidezza a taglio seccante G si riduce al 70% del modulo iniziale.

Esso inoltre consente di scrivere un andamento variabile con la profondità del modulo di rigidezza a taglio iniziale, attraverso la dipendenza non lineare dallo stato tensionale (vedi figura 4.8).

Il modello Hardening Soil Small Strain è in grado di fare un'approssimazione più accurata e affidabile degli spostamenti che può essere utile per gli applicazioni dinamiche o nella modellazione dei problemi condizionati allo scarico, ad es. per gli scavi con paratie o scavi nelle gallerie. La descrizione del modello più ampia è presentata in capitolo 4.4.

Il quinto capitolo introduce un caso di studio che consiste nella costruzione di un hotel multipiano nella zona centrale di Stoccarda. L'edificio ha una forma triangolare con le

lunghezze laterali di 70,2 m, 47,7 m e 63,3 m. (figura 5.4, allegato A3) e che è costituito dal pianoterra, due livelli sotteranei previsti per il parchieggio e nove piani sovrastanti (figura 5.3, allegato A1-2).

L'edificio si trova all'incrocio di Wolframstrasse e Nordbahnhofstrasse (vedi figura 5.2); al sud confina con un ponte ferroviario, mentre ad ovest del cantiere (Lissabonnerstrasse) si trova un centro commerciale.

Innanzitutto, la geologia dell'area interessata viene investigata mediante tre fori di sondaggio a carotaggio continuo e altri tre fatti con il penetrometro dinamico pesante (DPH). I dati ottenuti sono raccolte nelle tabelle 5.1, 5.2 e 5.8. Questi sondaggi ci permettono di conoscere la sequenza e la composizione degli strati del terreno e le loro profondità, nonché il livello delle falde acquifere.

Poi, i campioni di ogni strato vengono prelevati e esaminati in laboratorio per ottenere i parametri necessari del terreno: granulometria delle particelle del suolo, contenuto d'acqua, permeabilità, resistenza al taglio, compressibilità, coesione e altri (vedi tabelle 5.3-5.6).

Inoltre, vengono rappresentati i calcoli dell'abbassamento della falda acquifera. Poiché il seminterrato dell'edificio è profondo di circa 8 metri, cioè è supposto di giacere al di sotto del livello della falda acquifera (quella è situata circa 3 metri sotto il livello del terreno), è necessario far abbassare il livello della falda durante il processo di scavo (vedi paragrafo 5.3.3).

Inoltre, è stata effettuata modellazione numerica agli elementi finiti del caso di studio, caratterizzando ogni componente strutturale utilizzata e seguendo l'ordine del processo di costruzione.

Nella fase iniziale è ricreata la geologia della area di costruzione, poi viene inserito in modello il ponte ferroviario. Queste due fasi riproducono le condizioni pre-esistenti alla costruzione. Nella seconda fase viene eseguito lo sbancamento per preparare l'area di costruzione e ottenere il "livello zero". Poi vanno realizzate le paratie per assicurare il processo di scavo e la stabilità delle strutture adiacenti: dal lato del ponte e dal lato del centro commerciale vengono costruiti due muri di pali seccanti in profondità di 10,4m e 8,8m rispettivamente, mentre dal terzo lato va eseguita una berlinese di 12m. Dopo di que si parte con la realizzazione dello scavo. Lo scavo va fatto nei seguenti step:

- primo step: uno scavo di 2,5m
- installazione del primo livello di puntoni
- secondo step: abbassamento delle falde acquifere per 1,5m e lo scavo successivo di 2,5m
- installazione del secondo livello di puntoni
- terzo step: abbassamento delle falde acquifere per 2,7m e lo scavo successivo di 2,7m
- installazione del secondo livello di puntoni
- quarto step: abbassamento delle falde acquifere per 1,55m e lo scavo successivo di 1,55m

Dopo aver eseguito lo scavo viene realizzata la fondazione dell'hotel in calcestruzzo armato di spessore 1,2m e, poi, i piani sovrastanti dell'edificio. Dopo la conclusione lo spazio vuoto tra le paratie e le pareti dell'edificio si riempie con il calcestruzzo di classe C20/25.

La simulazione viene eseguita in tre modelli costitutivi del terreno: modello alla Mohr-Coulomb, Hardening Soil e Hardening Soil Small Strain. In più, nel modello Hardening Soil Small Strain vengono modificati i seguenti parametri ognuno alla volta: un aumento della rigidezza del terreno di tutti gli strati di un quarto in relazione al valore originale, una diminuzione della rigidezza del terreno di un quarto, un aumento della rigidezza del muro di sostegno e una diminuzione della rigidezza del muro cambiando la classe del calcestruzzo con cui deve essere realizzato. Nella versione originale si utilizza la classe C20/25, mentre negli altri due si utilizzano C30/37 e C12/16 corrispondente.

Nell'ultimo capitolo viene effettuata un'analisi dei rischi. Innanzitutto, vengono introdotti i valori numerici dei parametri dei criteri quantitativi dei rischi (che sono stati precedentemente discussi nel secondo capitolo) sia per gli elementi strutturali geotecnici come per gli elementi della struttura adiacente.

Nella tabella I sono rappresentati i criteri qualitativi per la stima dei parametri di controllo dei rischi del ponte ferroviario (vedi figure 6.3-6.5).

Tabella I: Criteri quantitativi per la valutazione dei rischi del ponte

Parametero	Livello di rischio basso (LR)	Livello di rischio medio (IR)	Livello di rischio alto (HR)
Spostamento orizzontale, u_x [mm]	$u_x < 9$	$9 \leq u_x \leq 11,7$	$u_x > 11,7$
Spostamento verticale, u_y [mm]	$u_y < 11$	$11 \leq u_y \leq 14,3$	$u_y > 14,3$
Distorsione angolare, β [-]	$\beta < 1/500$	$1/500 \leq \beta \leq 1/300$	$\beta > 1/300$
Sollecitazione di compressione, σ_c [kN/m^2]	$\sigma_c < 50000$	$50000 \leq \sigma_c \leq 65000$	$\sigma_c > 65000$
Sollecitazione di trazione, σ_t [kN/m^2]	$\sigma_t < 4100$	$4100 \leq \sigma_t \leq 5330$	$\sigma_t > 5330$

Nella tabella II sono rappresentati i criteri qualitativi per la stima dei parametri di controllo dei rischi del palo situato più vicino allo scavo (figure 6.6-6.7).

Tabella II: Criteri quantitativi per la valutazione dei rischi del palo

Parametero	Livello di rischio basso (LR)	Livello di rischio medio (IR)	Livello di rischio alto (HR)
Spostamento orizzontale, u_x [mm]	$u_x < 8$	$9 \leq u_x \leq 10,4$	$u_x > 10,4$
Attrito laterale, T_{skin} [kN/m^2]	$T_{skin} < 65$	$65 \leq T_{skin} \leq 84,5$	$T_{skin} > 84,5$

Nella tabella III sono rappresentati i criteri qualitativi per la stima dei parametri di controllo dei rischi nel della paratia (vedi figure 6.8).

Tabella III: Criteri quantitativi per la valutazione dei rischi della paratia

Parametero	Livello di rischio basso (LR)	Livello di rischio medio (IR)	Livello di rischio alto (HR)
Spostamento orizzontale, u_x [mm]	$u_x < 10,4$	$10,4 \leq u_x \leq 13,52$	$u_x > 13,52$

Nella tabella IV sono rappresentati i criteri qualitativi per la stima dei parametri di controllo dei rischi dell'hotel (figura 6.9-6.12).

Tabella IV: Criteri quantitativ per la valutazione dei rischi dell'hotel

.Parametero	Livello di rischio basso (LR)	Livello di rischio medio (IR)	Livello di rischio alto (HR)
Spostamento orizzontale nella sezione 1, u_x [mm]	$u_x < 3$	$3 \leq u_x \leq 3{,}9$	$u_x > 3{,}9$
Spostamento verticale nella sezione 2, u_y [mm]	$u_y < 8{,}5$	$8{,}5 \leq u_y \leq 11{,}05$	$u_y > 11{,}05$
Distorsione angolare, β [-]	$\beta < 1/500$	$1/500 \leq \beta \leq 1/300$	$\beta > 1/300$
Sollecitazione di compressione nella sezione 3, σ_c [kN/m^2]	$\sigma_c < 20000$	$20000 \leq \sigma_c \leq 26000$	$\sigma_c > 26000$
Sollecitazione di trazione nella sezione 3, σ_t [kN/m^2]	$\sigma_t < 2200$	$2200 \leq \sigma_t \leq 2860$	$\sigma_t > 2860$

Nella tabella V sono rappresentati i criteri qualitativi per la stima dei parametri di controllo dei rischi del terreno (figure 6.13).

Tabella V: Criteri quantitativ per la valutazione dei rischi del terreno

Parametero	Livello di rischio basso (LR)	Livello di rischio medio (IR)	Livello di rischio alto (HR)
Capacità portante nei parti laterali, q [kN/m^2]	$q < 138{,}5$	$138{,}5 \leq q \leq 180$	$q > 180$
Capacità portante nella parte centrale, q [kN/m^2]	$q < 184{,}6$	$184{,}6 \leq q \leq 240$	$q > 240$

Dopo l'analisi numerica i risultati ottenuti vengono raccolti, analizzati con attenzione e discussi.

Riassunto dei risultati ottenuti

1) Spostamenti orizzontali, u_x, cedimenti, u_y e distorsione angolare, β cambiano con il modello del terreno (Mohr-Coulomb, Hardening Soil o Hardening Soil Small Strain) e con la rigidezza del terreno ($E_{50}^{ref}, E_{oed}^{ref}, E_{ur}^{ref}$).
2) Tensioni di compressione, σ_c e di trazione, σ_t e capacità portante del terreno, q sono meno influenzati dal modello o dalla rigidezza del terreno.
3) La rigidezza delle paratie (C20/25-originale, C30/37, C12/16) influenza meno i parametri studiati nel presente caso di studio.

4) L'incremento della rigidezza del terreno del il 25% mostra i valori considerevolmente minori: sono più piccoli le deformazioni e la distorsione rispetto alla rigidezza originale.
5) La riduzione della rigidezza del terreno del il 25% mostra i valori considerevolmente maggiori: le deformazione e la distorsione sono più grandi rispetto al caso con la rigidezza originale.
6) I modelli Hardening Soil and Hardening Soil Small Strain mostrano i risultati pressoché identici.
7) Il modello alla Mohr-Coulomb fornisce i risultati notevolmente più elevati rispetto ai modelli Hardening Soil e Harderning Soil Small Strain per gli spostamenti: gli spostamenti e i valori di distorsione angolare sono maggiori fino all'80%, mentre per le tensioni fino al quarantacinque percento.

Conclusioni

In questa tesi sono stati proposti e descritti alcuni scenari di rischio per le fondazioni profonde e scavi. L'impatto qualitativo e quantitativo degli scenari di rischio è stato mostrato nel caso di studio. I criteri di rischio raccomandati in questo lavoro si basano su incertezze qualitative e quantitative dei metodi di progettazione e seguono i parametri che li controllano. Questi parametri (comportamento e rigidezza del terreno, proprietà dei materiali della struttura, deformazione della struttura, ecc.) hanno un'influenza importante sul design di progetto. L'applicazione di questi risultati nella progettazione richiede ulteriori ricerche nel contesto delle diverse progettazioni geotecniche.

Per ottenere una determinazione e valutazione degli scenari di rischio più efficace, è necessario seguire il seguente ordine:

- Descrizione del processo reale del problema geotecnico.
- Analisi qualitativa del rischio mediante l'identificazione di: rischi, scenari e conseguenze.
- Valutazione e conseguenze del rischio di quantificazione.
- Accettazione dei rischi o misure di attenuazione.

Il compito principale degli ingegneri geotecnici è quello di ridurre questi rischi con l'aiuto dei nuovi metodi di progettazione e costruzione.

CHAPTER 1
STATE OF THE ART

1.1 Introduction: What is Risk?

The international literature on risk analysis, assessment and management contains a range of definitions of risk and associated terms. [1]

The Institute of Risk Management have no official definition of "risk", although in its documents phrases such as "chance of bad consequences, or exposure to mischance" are used. Thus, they have mostly negative effect. More recently a neutral view of risk have been taken, and define risk as "an uncertain event or set of circumstances which, should it occur, will have an effect on achievement of objectives". The nature of the effect is undefined, so implicitly this could include both negative and positive effects. [1]

In the safety field, it is generally recognized that consequences are only negative and therefore the management of safety risk is focused on prevention and mitigation of harm.

The level of risk is defined as the "magnitude of a risk or combination of risks, expressed in terms of the combination of consequences and their likelihood". This definition allows for the common practice of quantifying risk as the product of the likelihood of the occurrence of an event and the consequences of that event. [2]

Uncertainty and error in geotechnics

It is important to recognize that in geotechnical engineering many of the risk sources or hazards arise from geotechnical uncertainty or error. This topic has been discussed widely in the literature. For example, [3] *classified the sources of uncertainty* as:

(1) inherent spatial and temporal variability;

(2) measurement errors (systematic or random);

(3) model uncertainty;

(4) load uncertainty;

(5) omissions.

[4] has described *these sources of uncertainty as being aleatory or epistemic*. Aleatory uncertainty is the *irreducible randomness or variability associated with phenomena that are naturally variable in time or space*, even when the system is well known. For example, the discontinuous geometries and the mechanical and hydraulic properties of soil masses provide good examples of this natural variability. Epistemic uncertainty, on the other hand, arises from *limitations in our fundamental knowledge or understanding of some aspects of a problem*. This is sometimes termed conceptual uncertainty and may be reflected in the use of inappropriate models in analyses, for example. [4]

1.2 Failures in construction

All structures are designed to support certain loads without deforming excessively. *Live loads* are the weights of people and objects, the weight of rain and snow and the pressure of wind. A *dead load* is the weight of the structure itself.

Due to these loads or/and another factors structures could be subjected to catastrophic collapses. The causes of structural collapse can be classified as following: [5]

- Inadequate Design
- Faulty Construction
- Foundation Failure
- Extraordinary Loads
- Materials and assemblies not yet at design strength
- Unexpected Failure Modes
- Combination of Causes

Inadequate design means as errors of computation, as failures due to inaccurate or erroneous calculated loads that the structure will carry after to be completed, as well as erroneous theories, reliance on inaccurate data, ignorance of the effects of repeated or

impulsive stresses (dynamic loads), and improper choice of materials or misunderstanding of their properties. The engineer is responsible for these failures, which are created at the drawing board.

Failures due to bad design may occur at any time during the expected useful life of a structure. For example, catastrophic collapses of bridges and other structures have due to lack of maintenance after many years of satisfactory performance. Similarly, an error made during design or construction may go undiscovered until failure occurs, years after satisfactory occupancy of the facility.

Faulty construction has been the most important cause of structural failure. A structure is extremely vulnerable to failure while it is under construction. The construction process can be named "the first test of the adequacy of design", but also the construction process itself provides several opportunities for failure. This may include the use of salty sand to make concrete, bad welds, and many other practices well known to the construction worker. The engineer is also at fault here, if inspection has not been run properly.

Even an excellently designed and constructed structure will not stand on *not appropriate foundation*. Although the structure will carry its loads, the earth beneath it may not. The displacements due to bad foundations may alter the stress distribution significantly. One of the famous example of bad foundations is the tower of Pisa, but there are many others.

Extraordinary loads are often natural, such as repeated heavy snowfalls, or the shaking of an earthquake, or the winds of a hurricane. Structures that are intended to stand for some years should be able to meet these challenges. A flexible structure may avoid destruction in an earthquake, while a solid masonry building would be destroyed. Earthquakes may also cause foundation problems when moist filled land liquefies.

One more extraordinary load that may occur is wind. Wind is called the motion of the air in the atmosphere that flowing from high to low pressure zone. Dominant direction of this motion is horizontal, therefore the intensive air streams are considered as an excessive horizontal load that can cause the instability of structures, especially such as high rise buildings and bridges.

Another common cause of structural failure during construction is the presence of materials and structural assemblies that are working at less than anticipated *design strength*. For certain types of construction, especially cast-in-place reinforced concrete, this may be the principal source of construction failure.

Unexpected failure modes are the most complex of the reasons for collapse. Any new type of structure is subjected to unexpected failure, until its properties are well understood. For example, times ago the suspension bridges seemed to be a good answer to bridging large gaps. Everything was expected to be supported by a strong cable in tension, a reliable and understood member. However, sad experience showed that in several cases a bridge deck was capable of galloping and twisting without restraint from the supporting cables. One of the example of that is the Ellet's bridge at Wheeling, USA collapsed from this cause in the 1840's. [5]

1.3 Shallow foundations

Foundations have the function of spreading the load from the upper structure to the soil ground. Inadequate foundation design, excessive loads or soft soil may cause the ground fails in shear or/and induce excessive settlements in the ground that, in terms, cause distortion and structural failure or architectural damage.

A shallow foundation is a type of foundation which transfers building loads to the earth very near the surface.

Eurocode 7 defines following most common limit states for spread foundations (schematically represented in fig. 1.1):

- loss of overall stability
- bearing capacity failure
- failure by sliding
- combined failure in the ground and in the structure
- structural failure due to foundation movement
- excessive settlements
- excessive heave due to swelling, frost and other causes
- unacceptable vibrations. [7]

The most pronounced failure modes are considered bearing capacity failure and excessive settlements.

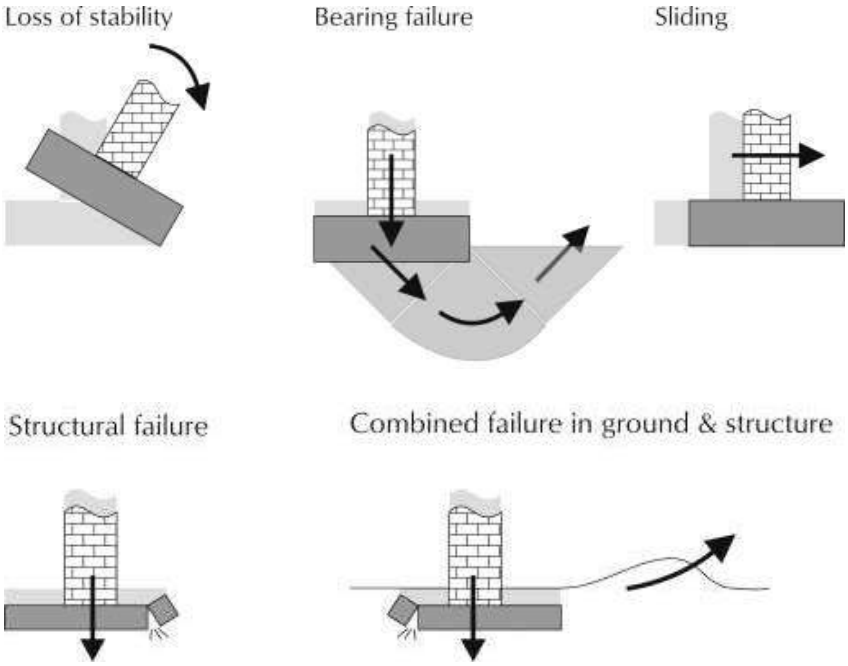

Figure 1.1: Failure modes in shallow foundations

1.4 Deep foundations

A deep foundation (called also pile foundation) is a type of foundation where the embedment is larger than its maximum plane dimension. Deep foundation is designed to be supported on deeper geologic materials because the soil or rock near the ground surface is not competent enough to take the design loads or result less economical. By involving deeper geologic materials, a deep foundation occupies a relatively smaller area of the ground surface and take lager loads than shallow foundation.

Laterally loaded piles

Structures founded on piles are often *subjected to lateral loads and moments in addition to vertical loads*. Lateral loads may come from wind, traffic, seismic events, waves, docking ships, and earth pressures. Moments may come from the eccentricity of the vertical force, fixity of the super structure to the piles, and the location of the lateral forces on the pile.

The *mechanism of failure depends on the width ratio (length to diameter), soil type, and the fixity of the pile head*.

Further the fundamental mechanisms that may cause yielding/failure of the pile are described. [8]

Shear failure

Shear failure of pile may occur due to lateral loads such as inertia or kinematic loads or a combination of the above. Figure 1.2b shows this mechanism of pile failure due to inertia load. This is particularly damaging to hollow, circular, concrete piles (non-ductile) with low shear capacity.

Bending failure

Bending failure of piles may occur due to the lateral loads either due to inertia or due to kinematic loads or a combination of the two. This would depend on the type of earthquake motion, the time of onset of liquefaction and regaining of strength of the soil after liquefaction. Bending in the pile due to lateral spreading of ground is often regarded as the root cause of many bridge failures. Figure 1.2c explains the hypothesis of this failure mechanism.

Buckling instability

Buckling failure (fig. 1.2d) may occur due to the effect of axial load acting on the pile and loss of the surrounding confining pressure offered by the soil owing to liquefaction. Lateral loading due to slope movement, inertia or out-of-line straightness in the pile will increase lateral deflections, which in turn can increase the chances of instability failure even at lower axial loads. This may cause plastic hinges in the piles leading towards collapse of the structure.

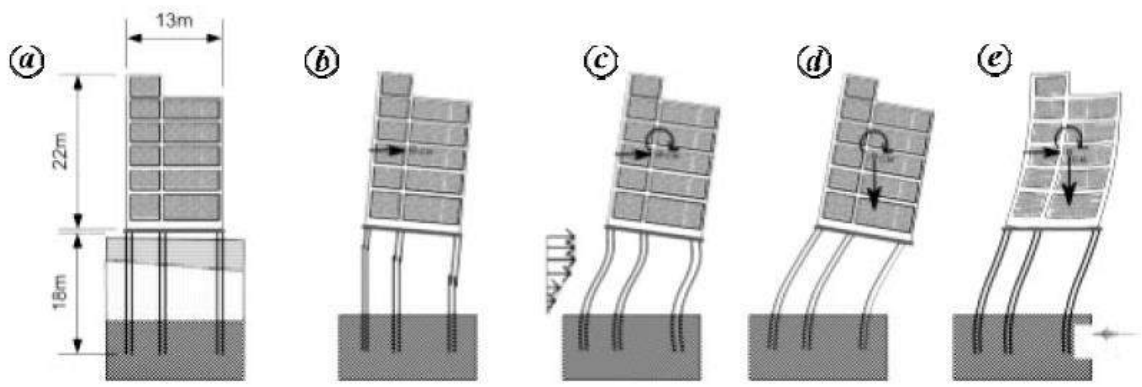

Figure 1.2: Different failure mechanisms: a) building with pile foundations; b) shear failure mechanism; c) bending failure mechanism; d) buckling mechanism; e) dynamic amplification mechanism.

Dynamic failure

All the above failures can occur due to static loads. During the earthquake, the dynamic soil–pile interaction becomes much complicated and has significant effect on the pile response. The dynamic properties of soil and pile and their interaction properties change during the earthquake. This change can lead to amplification of structural response and eventually to the failure of the structure (fig. 1.2e). [8]

The following diagram show the summary of causes of deep foundation failures (fig. 1.3).

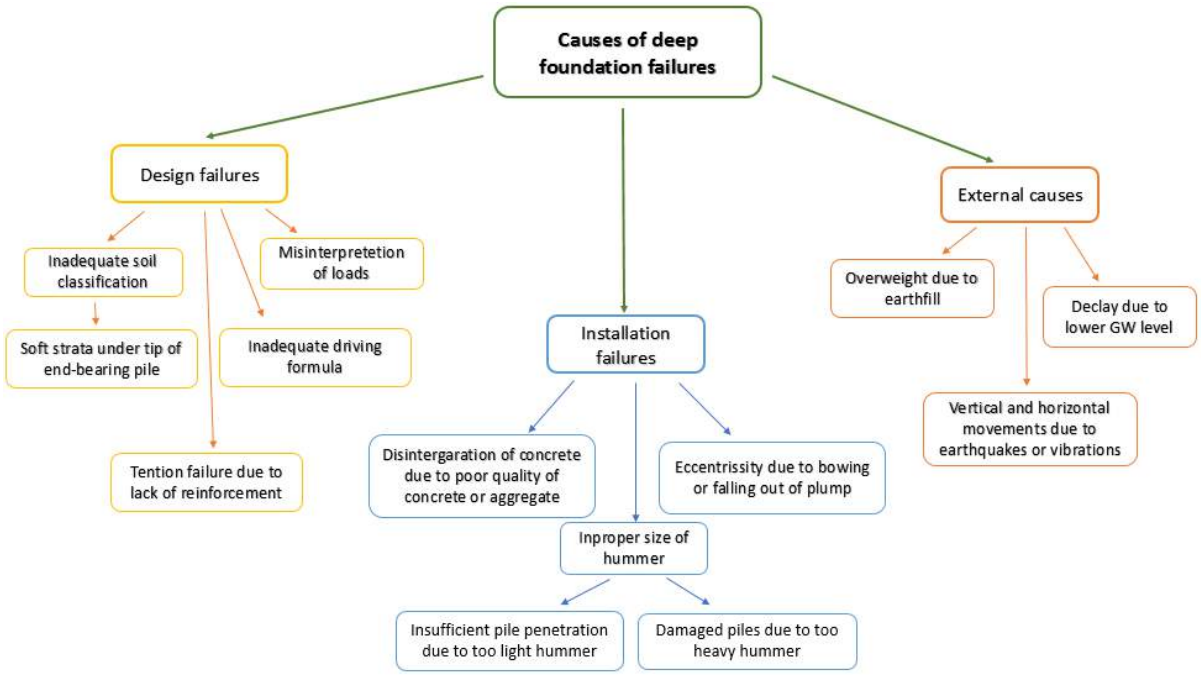

Figure 1.3: Causes of deep foundation failures

1.5 Deep excavations

Excavation is an important segment of foundation engineering. For example, in the construction of the foundations or basements of high buildings, underground oil tanks, subways or mass rapid transit systems, etc.

The excavation of soil from a deep excavation has two main effects. The first is that the removal of the weight of the excavated soil results in decrease in the vertical stress in the soil beneath the excavation. The second is that the removal of the soil in the excavation results in a loss of lateral support for the soil around the excavation [9]. Ground deformation around excavations can damage adjacent buildings, streets and utilities. The

severity and extent of damage depends on the magnitude and pattern of ground movements around the excavation.

For the purpose to provide lateral support for the soil around an excavation and to limit movement of the surrounding soil a deep excavation support system is provided. Support systems for deep excavation consist of two main components: retaining wall and the support provided for the retaining wall. The principle types of wall are diaphragm (structural slurry), sheet pile, soldier piles and lagging, tangent piles, contiguous piles, and deep soil mixed walls. The principal types of supports are struts (braces), rakers and tieback anchors. [10]

The following causes may lead to failure of support structures:

- Estimation of active and passive earth pressure
- Estimation of water pressure
- Consideration of artesian water pressure
- Existence of seepage force
- Squeezing / soil flow
- Heaving
- Errors in geotechnical numerical modelling
- Earthquakes or vibrations that cause lateral displacement/ deformation
- Inadequate construction

Determination an active and passive earth pressure for cohesive soil

Active and passive earth pressure values play eminent role in design of retaining structures. In the calculation of the lateral earth pressures acting on a retaining wall system, the engineers generally use the following formula formulated by Rankine:

$$e_a = K_a \cdot \sigma'_v - 2c'\sqrt{K_a} \quad (1.1)$$

$$e_p = K_p \cdot \sigma'_v + 2c'\sqrt{K_p} \quad (1.2)$$

where: e_a - active earth pressure, [kN/m^2]

e_p - passive earth pressure, [kN/m^2]

K_a - coefficient of active earth pressure, [-]

K_p - coefficient of passive earth pressure, [-]

σ_v' - effective vertical pressure, [kN/m^2]

c' - cohesion intercept in Mohr-Coulomb failure criterion, [kN/m^2]

Seepage Force

It is very important to prevent the ground water to flow out from the slope of the open cut excavations or through the walls of the retaining wall system.

The mode of the seepage depends on whether water can pass through the retaining wall or not.

For an excavation with impervious retaining walls, e.g. diaphragm walls or secants piles, where *the toe of the walls is located in a permeable soil layer*, then the walls will not act as a water cut-off system. This means, water can seep from outside the walls into the excavation area through the permeable soil layer below the walls' toe as shown in figure 1.4.

This ground water seepage creates seepage force which *increases the effective overburden pressure in the active side of the walls, and on the other hand, reduces the effective stress in the passive side of the walls*. This means the seepage force increases the lateral pressure to the walls and decreases the passive pressure. A large *seepage force may significantly reduce the effective overburden pressure and subsequently will induce piping and boiling*.

If the *retaining wall is embedded into an impermeable layer* (fig. 1.5), there will be unbalance water pressure within the active and passive sides. When the base of an excavation is impermeable, say by jet grouting a layer at the base of the excavation, *the base of the excavation is then subjected to an uplifting force* (fig. 1.6). Therefore, to withstand this uplifting force, the thickness of the base has to be calculated. *Ignorance in calculating this uplifting force can cause failure*.

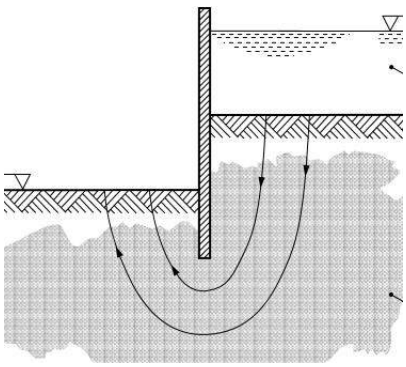

Figure 1.4: Groundwater seepage through impervious wall

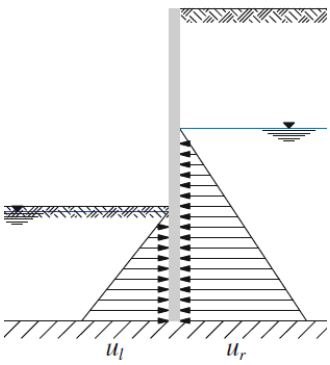

Figure 1.5: Unbalance water pressure

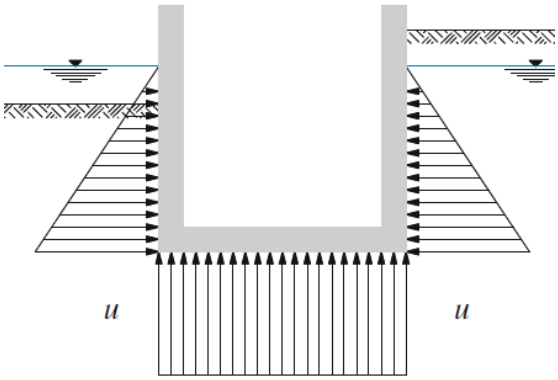

Figure 1.6: Impermeable layer at base

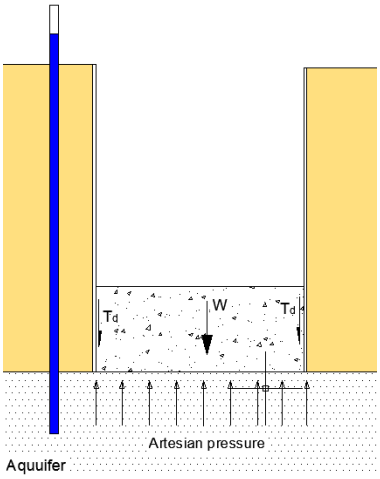

Figure 1.7: Artesian water pressure

Artesian Water Pressure

The existence of artesian water pressure can greatly affect the stability of an excavation. The weight of the soil from the excavation level to the top of the aquifer layer and the friction of the soil-wall system should be able to withstand the artesian pressure (fig. 1.7); otherwise the base of the excavation shall fail. This type of failure is known as *bursting or boiling*. Undetected artesian water pressure beneath an excavation may lead to unsafe excavation.

Squeezing / Soil Flow

When soldier piles system is used as retaining structures for soft soils, soil squeezing or soil flow through the gaps within the soldier piles may take place (fig. 1.8).This phenomenon may affect *the stability of the structures/facilities adjacent to the excavation area*. Therefore, it should be noted that *the gaps within the soldier piles must be close enough to ensure the formation of arching* (arching effect) where the soft soils could not penetrate or squeeze out of the gaps.

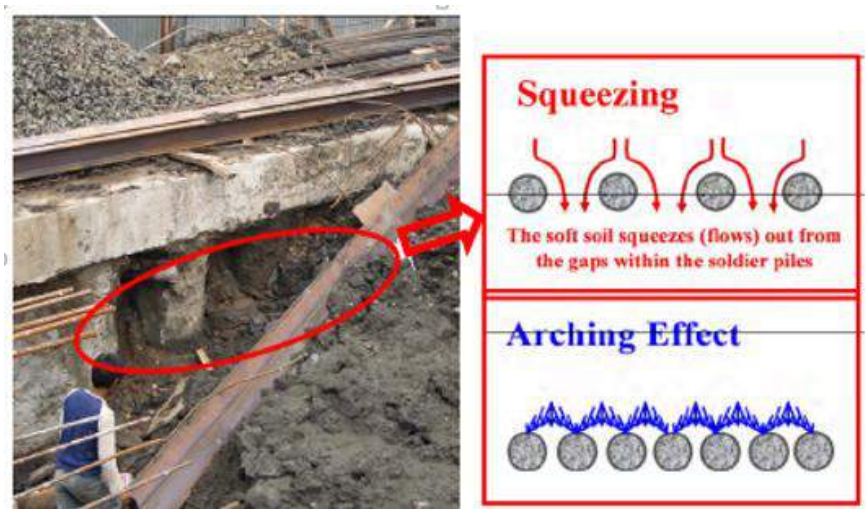

Figure 1.8: Squeezing or flow of soft soil through the gaps within soldier piles [10]

Heaving

For braced excavation system, it is quite common that the heaving mode of failure should be taken into account. This mode of failure can take place due to the weight of the soil columns, of 0.7 excavation width, at the sides of the excavation pushing inward from the bottom of the excavated area. If the bearing capacity of the soil beneath the excavation area is unable to withstand the soil column weight, then heaving failure can take place (fig. 1.9).

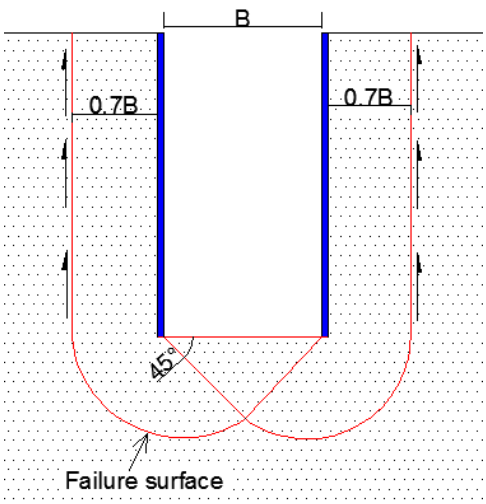

Figure1.9: Heaving mode of failure

Geotechnical Design Errors

There are many soil models available for geotechnical analysis, e.g.: Mohr-Coulomb Model, Soft Soil Model, Hardening Soil Model, etc. Choosing not appropriate soil model may lead to wrong estimation on the performance of the geotechnical structure.

1.6 Tunneling

Tunneling is world-wide environmentally preferable means used to provide infrastructure such as transportation and utilities to densely populated urban areas. [11]

There are two major risk scenarios in urban tunneling as shown in figure 1.10, i.e. *collapse up to the ground surface* and *damage due to ground settlements*. Both of these scenarios are referred to a *ground movement*. [12]

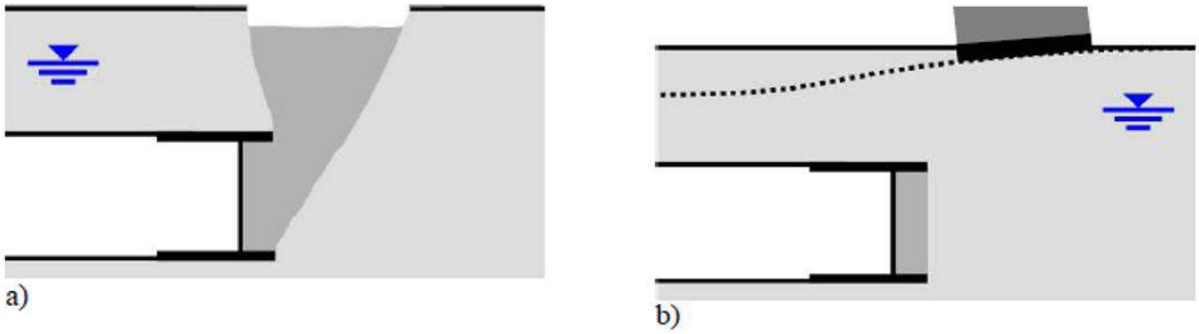

Figure 1.10: Major risk scenarios in urban tunneling: a) Collapse up to the ground surface b) Damage due to ground settlements

The relationship between surface settlements and tunnel depth is neither simple nor linear. In reality, ground movements depend on a number of factors including:

- geological, hydro-geological and geotechnical conditions;
- tunnel geometry and depth;
- excavation methods;
- quality y of workmanship and management.

It is however clear that a shallow tunnel will tend to have a greater effect on surface structures

Face stability

During tunnel construction, soil is removed from the tunnel face. The soil layer in front and above the tunnel face exerts active earth pressure. The presence of infrastructures or surcharge also contributes as additional earth pressure. For the tunnel alignment below the groundwater table, water pressure is an another significant component of pressure acting at the tunnel face. The face may not be strong enough to bear such pressures or may be unstable. Therefore, the soil mass in front of the cutterhead can collapse which would then result in excessive settlement at the surface (fig. 1.11).

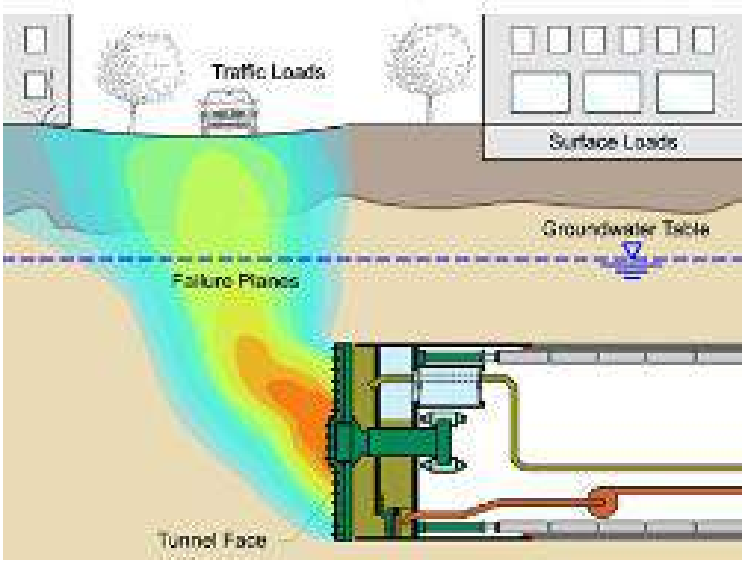

Figure 1.11: Failure mechanism at tunnel face

Based on the nature of the grounds encountered, two types of failure mechanisms may be observed.

- In the *case of cohesive soils* (fig. 1.12a) face failure involves a large volume of ground ahead of the working front. This mechanism leads to the formation of a sinkhole at the ground surface with a width larger than one tunnel diameter.
- In the case of *cohesionless soils*, failure tends to propagate along a chimney like mechanism above the tunnel face (fig. 1.12b).

Both based on the consideration of idealized conditions and should, of course, be adjusted to account for the actual conditions found on each individual worksite: non-homogeneous grounds and water inflows. In particular, in water-bearing sands, ground stability will be considerably influenced by hydraulic gradients induced by seepage towards the face.

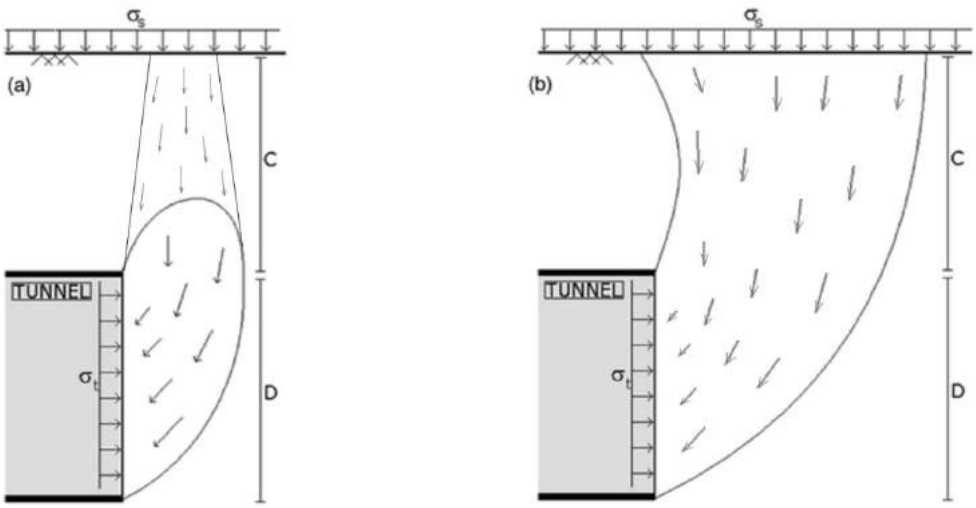

Figure 1.12: Face collapse: a) basic diagram in cohesive soils; b) basic diagram in granular soils

Causes for construction induced settlements

Generally speaking, movements along the tunnel center-line are initiated at some distance ahead of the face and keep increasing until a complete support system is in place. Therefore one must differentiate between the settlements associated with the methods of excavation used at the face, and the settlements that occur behind the face.

Case of the conventional method

For works of this type, four major settlement sources can be identified:

- settlements associated with the stability at the face;
- settlements associated with the characteristics and conditions of installation of a temporary support system;
- settlements associated with the cross-sectional staging (sequencing) of the excavation works;
- settlements associated with the final lining installation and response.

Case of shield-driven tunnels

Settlements induced by shield tunneling can be broken down into four contributions (fig. 1.13):

- settlements ahead and above the face;
- settlements along the shield;
- settlements at the shield tail skin;
- settlements due to liner deformations.

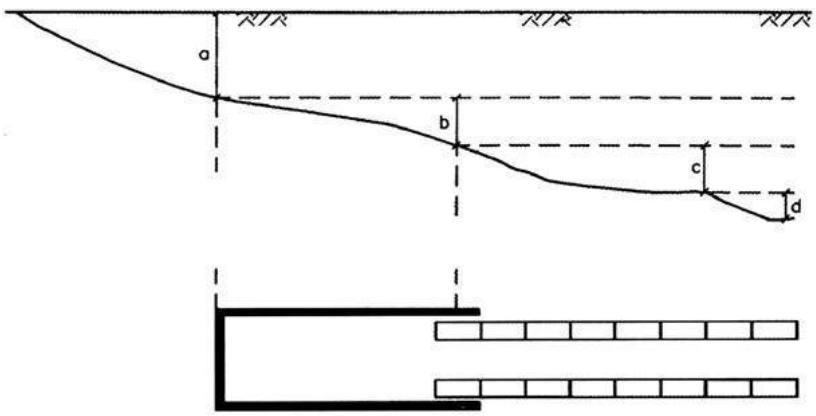

Figure1.13: Evolution of settlements along a shield

Effect of groundwater

Settlements induced by groundwater typically fall under two categories.

The first category refers to the occurrence of settlements almost concurrently with construction. Lowering of the groundwater table, prior to excavation(through drainage) or as a consequence of tunneling, may cause immediate settlements to occur in layers or lenses of compressible soils, as well as in weathered rocky materials. The impact of such lowering of the groundwater table varies in proportion to its magnitude and radius of influence:

- when localized, induced deformations are often prone to generate large differential settlements that can be damaging to the surrounding buildings;
- when widely spread, their consequences are generally less severe

The occurrence of groundwater at the tunnel face may induce settlements as a result of:

- the hydraulic gradient weakening the mechanical conditions at the face and on the tunnel walls thereby increasing ground deformations;
- worsening effects on preexisting mechanical instabilities (washed out karsts, etc.);
- worsening of the mechanical properties of the ground in the invert, particularly when the sequential method is used, with the risk for punching of the foundation ground by the temporary support due to loss of confinement.

The second category refers to delayed settlements that are typically observed in soft compressible grounds. As a result of the tunneling works, the ground can be locally subjected to stress increase and subsequently excess pore pressures. Similar mechanisms can develop at a larger scale with fully pressurized shield tunneling. Moreover, as a result of seepage towards the tunnel walls that inevitably occurs during and/or after construction, either along the more pervious materials present around the opening or through the tunnel liner, consolidation will take place within the entire ground mass. The magnitude of consolidation settlements will be larger in areas experience in higher reductions in pore pressures.

Effect of worksite conditions

This includes the settlements induced by the general worksite conditions, especially *vibrations* induced by boring whether with the sequential or shielded method and muck removal operations. Settlements of this type have been observed in soft ground conditions, or in good ground with poor surface backfill material. [12]

CHAPTER 2
RISK EVALUATION

2.1 Risk evaluation: qualitative research vs quantitative research

Qualitative research

Qualitative research has to do with qualifying or expressing the characteristics of a phenomenon. Instead of testing, measuring, and experimenting, qualitative research aims at understanding the subject of study. [13]

In the field of civil and environmental engineering, qualitative research approach method is being used in studying and investigating reasons, relationships and phenomena.

Quantitative research

As the name implies, quantitative research is based on the measurement of quantities, i.e. quantity or amount. [14] describes quantitative research as "Explaining phenomena by collecting numerical data that are analyzed using mathematically based methods". The objective of quantitative research is to develop and employ mathematical models, theories and/or hypotheses pertaining to phenomena.

Relationship between theory and data

In qualitative researches, the techniques are often unstructured or semi-structured unlike in quantitative research they are usually highly structured. While quantitative research relies on responses to pre-formulated questions, qualitative research allows unlimited expression from respondents. [15]

Qualitative research is typically exploratory and/or investigative in nature. It involves a continual interplay between theory and analysis and its findings are often not conclusive. However, these findings are valuable for a deep understanding of a given problem and for further decision making. On the other hand, quantitative research is statistical in nature. It employs different forms of statistical tools and it is empirical in nature.

In qualitative research, data largely comprises of texts and pictures while in quantitative research, the data are in numbers and empirical in nature.

Qualitative research usually adopts an inductive approach to its reasoning: observations are made, data are collected and then the work proceeds towards a theoretical integration of what it has found. So, *it moves from the data to a theory*. The focus is on individuality and uniqueness. Hence, the data collected in qualitative research tends to be *oriented toward individuals and case studies*. In the case of quantitative research (adopts a deductive approach), its focus is on generalization and working towards the development of universal statements or laws. Hence, the data collected tend to be *aggregated across individuals*. In short, *qualitative approach explores causality* while *quantitative approach suggests causality*. [15]

2.2 Control parameters to evaluate risks in deep excavations

2.2.1 Introduction

Engineers are required to design structures which are safe, serviceable and economical. That means they must do not fall, not move too much and they should not be very expensive. Different analyses are needed to meet these criteria.

Figure 2.1 shows the relationship between loading and movement of a structure. [24]

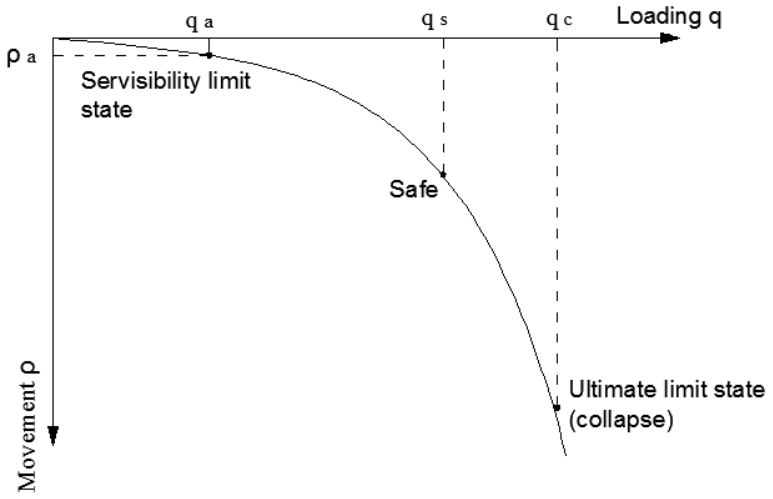

Figure 2.1: Loading and movement of structures after [24]

q_c is a load in ultimate limit state when the movement are very large and the structure is collapsing. There a safe state where the load is q_s, the movements are relatively large but the structure is not collapsing. There is a serviceability limit state where the allowable movements ρ_a are very small. There is a load factor, L_f given by

$$q_a = L_f \cdot q_c$$

such that the allowable bearing pressure, q_a causes movements that are acceptably small. [24]

Values for factors of safety and for load factors should be chosen by the designer. Typical values can be taken from eurocodes or national standards, as well as from the experience.

2.2.2 Control parameters of risks in deep excavation

Soil movement occurring during deep excavation process is considered of a great importance. Excessive soil movement (hence, mobilized active earth pressure) causes excessive settlements of adjacent buildings and may cause various damages.

What parameters have to be controlled to ensure the deep excavation process and the stability of adjacent structures?

Concerning geotechnical structures, the following parameters should be taken into account:

- horizontal displacement of the retaining structure, u_x [mm]
- bearing capacity of the soil, q [kN/m^2]
- normal stresses at base of piles, q_b [kN/m^2]
- shear stresses along the shaft of piles, τ_s [kN/m^2]

- compressibility of soil, E [kPa]
- retaining structure geometry, EA [kN], EI [kN·m^2]
- factor of safety, η [-]
- model of soil behavior

A wall deflection due to inward movement of the ground should be limited such that not create excessive surface ground settlements (hence, the settlements of adjacent buildings), moreover, not create the second order effects (additional bending moment, etc.).

Concerning to stability of adjacent buildings the following parameters should be controlled:

- settlements, ρ [mm]
- angular distortion, β [-]
- width of visible cracks in the buildings, w [mm]
- compressive and tensile stresses in the adjacent structure, σ_c, σ_t [kN/m^2]

Surface ground movement generated during excavation may cause various effects on the nearby standing buildings, the main of which are: total and differential settlements. The effect of differential settlements can be split in two components: angular distortion and horizontal displacement (fig. 2.2) that cause additional stresses in buildings' basement and walls. Thus, the total stresses can arise considerably. When the resulting total stresses high enough the process of cracking starts to occur.

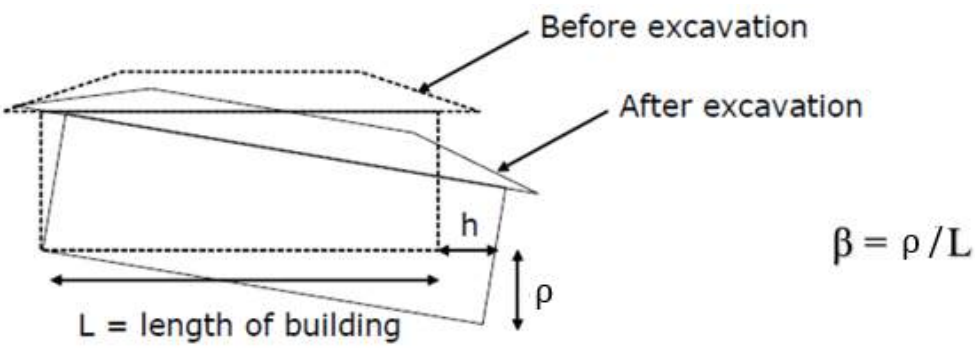

Figure 2.2: Example of angular distortion, settlements and horizontal displacement

Some significant values for angular distortion are shown in figure 2.3.

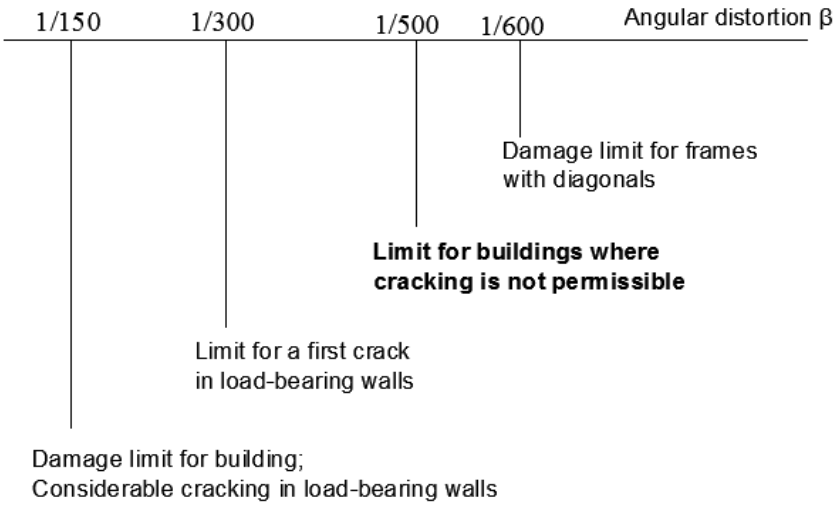

Figure 2.3: Limits for angular distortion after [18]

A summary of the effects created by ground movement induced by deep excavation is represented in figure 2.4.

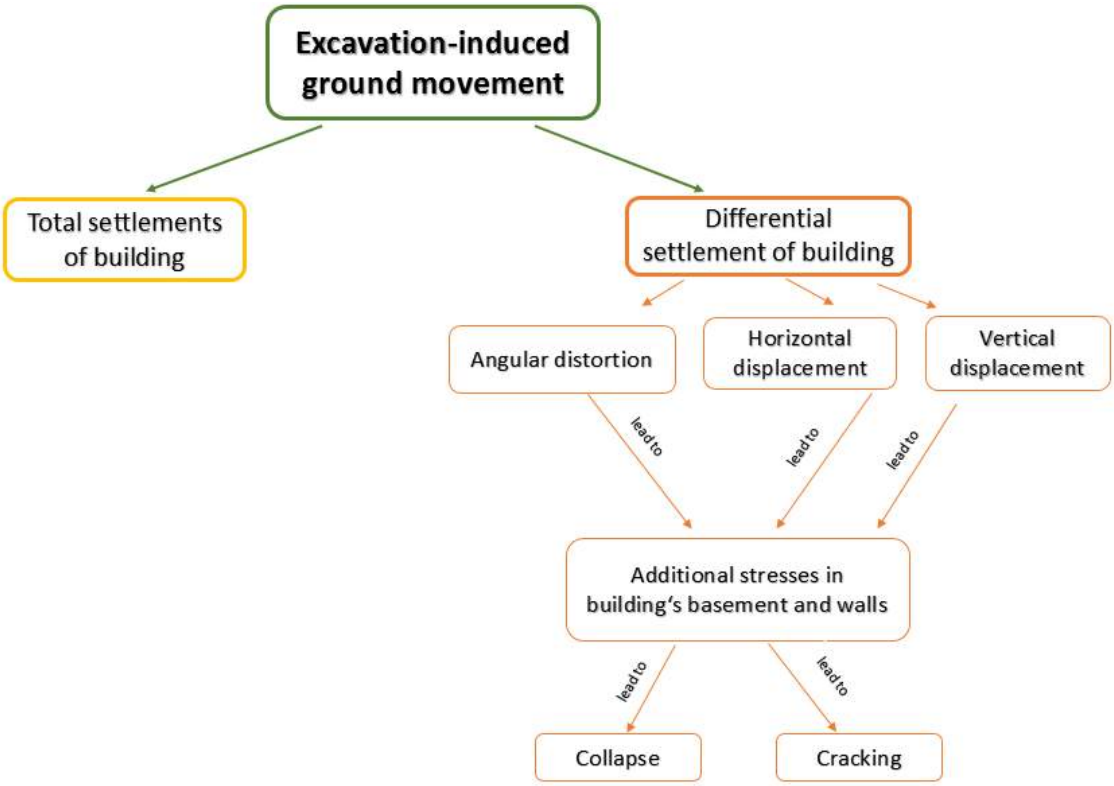

Figure 2.4: Main effects created by excavation-induced ground movement

Compression and tensile stresses generated in structures may exceed the material resistance that leads to cracking and, in worst case, to considerable damages in the structures. Therefore, the resulting stresses should not exceed the admissible stresses. Tables 2.1 and 2.2 represents admissible compressive and tensile stresses in concrete for different strength classes according to Eurocode 2.

Table 2.1: Mean compressive cylinder and cube strength for different strength classes of concrete (EC 2).

Mix designation	C12/16	C16/20	C20/25	C25/30	C30/37	C35/45	C40/50	C45/55	C50/60	C55/67
Characteristic cylinder strength f_{ck}	12	16	20	25	30	35	40	45	50	55
Target mean cylinder strength f_{cm}	20	24	28	33	38	43	48	53	58	63
Characteristic cube strength $f_{ck,cube}$	16	20	25	30	37	45	50	55	60	67
Target mean cube strength $f_{cm,cube}$	26	30	35	40	47	55	60	65	70	77

Table 2.2: Values of tensile strength in relation to strength class of concrete (EC 2).

Mix designation	C12/16	C16/20	C20/25	C25/30	C30/37	C35/45	C40/50	C45/55	C50/60	C55/67
Mean axial tensile strength f_{ctm}	1.6	1.9	2.2	2.6	2.9	3.2	3.5	3.8	4.1	4.2
Mean splitting tensile strength $f_{ctm,sp}$	1.7	2.1	2.5	2.8	3.2	3.6	3.9	4.2	4.5	4.7
Mean flexural tensile strength $f_{ctm,fl}$	2.4	2.9	3.3	3.8	4.3	4.8	5.3	5.7	6.1	6.3

The qualitative criterions of the control parameters of deep excavation are summarized in tables 2.3 – for geotechnical structures and in table 2.4 - for adjacent to deep excavation structures; meanwhile the quantitative criterions gathered in table 2.5 - for geotechnical structures and in table 2.6 - for adjacent structures.

Table 2.3: Qualitative criterions for risk evaluation of deep excavation for geotechnical structures.

GEOTECHNICAL STRUCTURES				
Control parameter	Low Level of Risk	Intermediate Level of Risk	High Level of Risk	Note
Wall deflection, u_x [mm]	$u_x < u_{x,adm}$	$u_{x,adm} \leq u_x \leq 1{,}3 \cdot u_{x,adm}$	$u_x > 1{,}3 \cdot u_{x,adm}$	$u_{x,adm}$ is an admissible value of wall deflection.
Bearing capacity of soil, q [kN/m^2]	$q < q_{adm}$	$q_{adm} \leq q \leq 1{,}3 \cdot q_{adm}$	$q > 1{,}3 \cdot q_{adm}$	q_{adm} is an admissible value of load on the soil.
Shear stresses along the shaft of the pile, τ_s [kN/m^2]	$\tau_s < \tau_{s,adm}$	$\tau_{s,adm} \leq \tau_s \leq 1{,}3 \cdot \tau_{s,adm}$	$\tau_s > 1{,}3 \cdot \tau_{s,adm}$	$\tau_{s,adm}$ is an admissible value of shear stresses along the shaft of the pile.
Compressibility of soil, E [kPa]	$E > E_{max}$	$E_{max} \geq E \geq E_{min}$	$E < E_{min}$	E_{min} is a minimal value of the soil compressibility. E_{max} is a maximal value of the soil compressibility.
Geometry EA, EI	$EA > 1{,}3 \cdot (EA)_{adm}$	$1{,}3 \cdot (EA)_{adm} \geq EA \geq (EA)_{adm}$	$EA < (EA)_{adm}$	E is a Young's modulus A is an area I is an inertia moment
Factor of safety, η [-]	$\eta > 1{,}3 \cdot \eta_{adm}$	$1{,}3 \cdot \eta_{adm} \geq \eta \geq \eta_{adm.}$	. $\eta < \eta_{adm}$	η_{adm} is an admissible value of the factor of safety.
Modelling of soil behavior	non-linear elastic	elasto-plastic	linear -elastic	

Table 2.4: Qualitative criterions for risk evaluation of deep excavation for adjacent buildings.

ADJUCENT STRUCTURES				
Control parameter	Low Level of Risk	Intermediate Level of Risk	High Level of Risk	Note
Angular distortion, β [-]	$\beta < \beta_{adm}$	$\beta_{adm} \leq \beta \leq 1{,}3 \cdot \beta_{adm}$	$\beta > 1{,}3 \cdot \beta_{adm}$	β_{adm} is an admissible value of angular distortion
Compressive stresses, σ_c [kN/m^2]	$\sigma_c < \sigma_{c,adm}$	$\sigma_{c,adm} \leq \sigma_c \leq 1{,}3 \cdot \sigma_{c,adm}$	$\sigma > 1{,}3 \cdot \sigma_{adm}$	σ_{adm} is admissible compressive stresses
Tensile stresses, σ_t [kN/m^2]	$\sigma_t < \sigma_{t,adm}$	$\sigma_{t,adm} \leq \sigma_t \leq 1{,}3 \cdot \sigma_{t,adm}$	$\sigma_t > 1{,}3 \cdot \sigma_{t,adm}$	$\sigma_{t,adm}$ is admissible tensile stresses.
Width of visible cracks, w [mm]	$w < w_{adm}$	$w_{adm} \leq w \leq 1{,}3 \cdot w_{adm}$	$w > 1{,}3 \cdot w_{adm}$	w_{adm} is an admissible value of crack width
Total settlements, ρ [mm]	$\rho < \rho_{adm}$	$\rho_{adm} \leq \rho \leq 1{,}3 \cdot \rho_{adm}$	$\rho > 1{,}3 \cdot \rho_{adm}$	ρ_{adm} is an admissible value of total settlement

Table 2.5: Quantitative criterions for risk evaluation of deep excavations for geotechnical structures.

GEOTECHNICAL STRUCTURE				
Control parameter	Low Level of Risk	Intermediate Level of Risk	High Level of Risk	Source
Wall deflection, u_x [mm]	$u_x < 0{,}001H$	$0{,}001H \leq u_x \leq 1{,}3 \cdot (0{,}001H)$	$u_x > 1{,}3 \cdot 0{,}001H$	[18] H is a wall height
Bearing capacity of soil, q [kN/m^2]	$q > q_{lim}/1{,}3$	$q_{lim}/1{,}3 \geq q \geq q_{lim}$	$q < q_{lim}$	
Shear stresses along the shaft of the pile, τ_s[kN/m^2]	$\tau_s < \tau_{s,adm}$	$\tau_{s,adm} \leq \tau_s \leq 1{,}3 \cdot \tau_{s,adm}$	$\tau_s > 1{,}3 \cdot \tau_{s,adm}$	
Compressibility of soil, E [kPa]	$E > 1{,}3 \cdot E_{min}$	$1{,}3 \cdot E_{min} \geq E \geq E_{min}$	$E < E_{min}$	
Geometry EA, EI	$EA > 1{,}3 \cdot (EA)_{adm}$	$1{,}3 \cdot (EA)_{adm} \geq EA \geq (EA)_{adm}$	$EA < (EA)_{adm}$	
Factor of safety, η [-]	$\eta > 1{,}5$	$1{,}5 \geq \eta \geq 1{,}3$	$\eta < 1{,}3$	
Modelling of soil behavior	Hardening Soil, Hardening Soil-Small, (Modified) Cam Clay	Von Mises, Mohr-Coulomb, Drucker-Prager	Hoock´s low	

Table 2.6: Quantitative criterions for risk evaluation of deep excavation for adjacent buildings

ADJUCENT STRUCTURES				
Control parameter	Low Level of Risk	Intermediate Level of Risk	High Level of Risk	Source
Angular distortion, β [-]	$\beta < 1/500$	$1/500 \leq \beta \leq 1/300$	$\beta > 1/300$	[18]
Compressive stresses, σ_c [kN/m^2]	$\sigma_c < \sigma_{ck}$	$\sigma_{ck} \leq \sigma \leq 1{,}3 \cdot \sigma_{ck}$	$\sigma > 1{,}3 \cdot \sigma_{ck}$	[37]
Tensile stresses, σ_t [kN/m^2]	$\sigma_t < \sigma_{ctm}$	$\sigma_{ctm} < \sigma_t < 1{,}3 \cdot \sigma_{ctm}$	$\sigma_t > 1{,}3 \cdot \sigma_{ctm}$	[37]
Width of visible cracks, w [mm]	$w < w_{max}$	$w_{max} \leq w \leq 1{,}3 \cdot w_{max}$	$w > 1{,}3 \cdot w_{max}$	[37]
Total settlements, ρ [mm]	$\rho < \rho_{adm}$	$\rho_{adm} < \rho < 1{,}3 \cdot \rho_{adm}$	$\rho > 1{,}3 \cdot \rho_{adm}$	

CHAPTER 3
IMPORTANT FEATURES FOR RISK EVALUATION IN EXCAVATIONS

3.1 Introduction

In this chapter are summarized the most important characteristics related to a deep excavation process such as: wall deflection, ground movement, allowable settlements, groundwater lowering and soil behavior. Moreover, pile response to deep excavation is considered.

The stress and deformation induced by excavation from either unbalanced forces or construction defects. The larger the unbalanced forces, the larger the movements of soils within the influence range of excavation. Construction defects can cause, in less serious situations, extra wall deflection, greater ground settlements and excavation bottom movements or, in serious conditions, collapses of excavation and damage to adjacent buildings and public facilities. The magnitude of stress and deformation due to construction defects cannot be predicted through theoretical simulation or empirical formulas. Such conditions can only be prevented by the improvement of construction quality. [16]

3.2 Characteristics of wall movement induced by excavations

The magnitude of wall movement is determined by the excavation-induced unbalanced forces, the stiffness of the retaining-strutting system, the excavation width, the excavation depth, the preload, etc. The relations of these factors with the deformation of a retaining wall can be inferred theoretically. For example, the thicker the retaining wall, the narrower and the shallower the excavation, the stronger the strut stiffness, the larger the preload; and the greater the safety factor of stability, the smaller the wall deformation.

Excavation width

[17] found that the wider the excavation, the lager the deformation of retaining wall. As a matter of fact, for a typical excavation the wider excavation, the lager the unbalanced forces; the lager the unbalanced forces, the greater is the wall deformation.

Excavation depth

Deformation of retaining walls deteriorates with the increase of excavation depth. According to a German standard DIN 4085 a wall deflection depends on the type of the ground and on the type of retaining structure and can be estimated with the following equations [18]:

$u_x = (0,1\text{-}0,2\%) \cdot H$. for soft soils and

$u_x = (0,1\text{-}0,2\%) \cdot H$ for stiff soils,

where H is excavation depth and u_x is a maximal horizontal displacement of the wall.

Wall stiffness

Theoretically, the deformation of a retaining wall will decrease with the increase of the stiffness of the retaining wall. However, the amount of decrease does not have a linear relationship with the increment of stiffness.

The increase of wall thickness or wall stiffness to reduce wall deformation is certainly effective, but only to a certain extent. [19]

Strut stiffness

Strut can be of high or low stiffness. With the start of the first stage of excavation, wall movement will be produced and form a cantilever shape (fig. 3.1a). The second stage of excavation starts after the installation of the first level of struts. If the stiffness of the struts is high enough, the compression of the struts will be rather small, so that the retaining wall

will rotate about the contact point between the struts and the wall, and the wall deformation is thus generated. The maximum wall deformation will occur near the excavation surface (fig. 3.1b). After the second level of the struts the third level of excavation starts. The retaining wall will continue rotating about the contact point with the second level of the struts, ant wall deformation is produced again. The location of the maximum deformation for soft soils will be mostly below the excavation surface (fig. 3.1c), for the stiff soils (such as sand) will be mostly below the excavation surface.

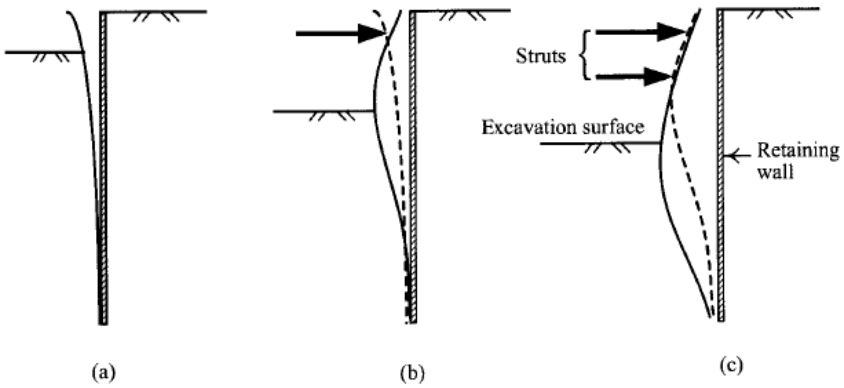

Figure 3.1: Relationship between the shape of wall deformation and high struts stiffness: (a) first stage of excavation, (b) second stage of excavation, (c) third stage of excavation

If the stiffness of struts not high, the compression of the struts should be quite large. There will be lager wall displacement around the contact points during the second and the third stages of excavation. The final pattern of the retaining wall will be close to that of the cantilever type and the maximum deformation will be produced at the top of the retaining wall (fig. 3.2 b, c).

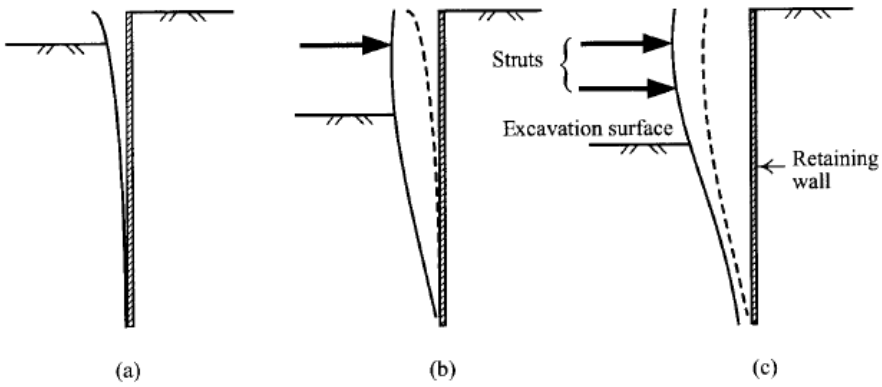

Figure 3.2: Relationship between the shape of wall deformation and low struts stiffness: (a) first stage of excavation, (b) second stage of excavation, (c) third stage of excavation

Strut spacing

The problem of struts spacing can be distinguished into horizontal spacing and vertical spacing. Narrowing the horizontal spacing can increase the stiffness of the struts per unit width. Shortening the vertical spacing of struts can effectively decrease the deformation of a retaining wall because the stiffness of the strut system is raised.

Strut preload

When applying the braced (or anchored) excavation method, preload is often exerted onto struts. When the preloaded struts are placed at shallower levels, the preload will be cable of pushing the retaining wall out. If the struts are placed at deeper levels, with the earth pressure growing with the depth, the preload of struts will not be able to push the wall outward easily [19]. In any case, preload is always helpful to reduce the displacement of a retaining wall or the ground settlement.

3.3 Response of piled foundation situated in the vicinity of deep excavation

The behavior and capacity of piles under loading is governed by complex mechanisms such as:

- Installation effects which cause very high strain levels and plasticity
- Skin friction, which can be both negative and positive and changing under external loading
- Bearing capacity and stress distribution around the pile tip.

These effects lead to changes in stresses in the ground behind the deep excavation if pile foundation appear into the active zone (fig. 3.3).

The excavation process, in turn, also induces some changes on pile behavior. That is why it is important to understand the stress changes in pile foundations that situated behind the excavation pit.

Soil around the piles is subjected to vertical settlements and horizontal displacements, similar to the ground surface. In stress terms the vertical and horizontal stresses around the pile decrease. Outside the active zone (fig.3.3), the stresses are assumed to remain constant. For end bearing piles which settle less than the surrounding soil, negative skin friction may develop.

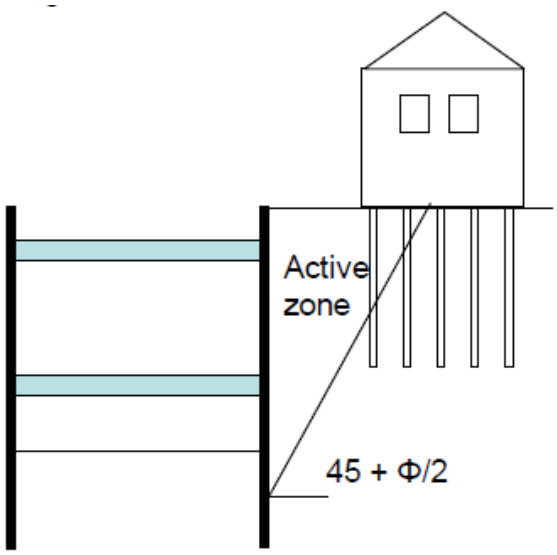

Figure 3.3: Active zone behind the wall

[20] conducted a research using the finite element analysis to study the effects of excavation depth, distance of pile from side supported excavation, pile stiffness and wall stiffness. Results indicate that the distance of pile from excavation and the excavation depth have a significant effect on the lateral deformation and bending moment on pile. The induced maximum bending moment and deflection on the pile decrease as the distance between the pile and the excavation increases. In multilayer soil deflection of pile depends on the properties of each soil layer. [21]

3.4 Drained and undrained soil behavior

The concepts of drained and undrained conditions are of fundamental importance in the mechanical behavior of soils. The definitions *of drained and undrained (drained = dry or emptied, undrained = not dry or not emptied)* used in soil mechanics are related to the ease and speed with water moves in or out of soil in comparison with the length of time that the soil is subjected to some change in load. The cause of the issue is whether or not changes in load cause changes in pore pressure. [22]

Drained is the condition under which water is able to flow into or out of a mass of soil in the length of time that the soil is subjected to some change in load. Under drained conditions, changes in the loads on the soil do not cause changes in the water pressure in the voids in the soil, because the water can move in or out of the soil freely when the volume of voids increase or decreases in response to the changing loads. [23]

Drained analysis assumes that in analysis the excess pore water pressure has been all dissipated (i.e. $u_e = 0$) and the volume of soils thereby changes. Drained analysis is mainly

applied to the analysis of long-term behavior of clayey soils. That is to say, the analysis has to adopt the effective stress analysis and the required parameters in the analysis are effective parameters, that is *c'* and *φ'*. [16]

Undrained is the condition under which there is no flow of water into or out of a mass of soil in the length of time that the soil is subjected to some change in load. Changes in the loads on the soil cause changes in the water pressure in the voids, because the water cannot move in or out in response to the tendency for the volume of voids to change. [23]

The undrained analysis, instead, except that the excess pore water is not dissipated ($u_e \neq 0$) and the total stress analysis is adopted accordingly. Suppose the soil is in the saturated state, no volume change can be observed under the undrained conditions. The parameter to be used in analysis would be s_u and $\varphi = 0$. [23]

Now let us have a look onto σ-τ diagram (fig. 3.4a) for a wall retaining excavation in soft soil (undrained behavior).The effective stress path A′→ B′ corresponds to undrained loading and B′→ C′ corresponds to swelling and reduction in the mean normal effective stress. The pore pressure immediately after construction u_i is less than the final steady state pore pressure, u_c and so there is an initial excess pore pressure which is negative. As time passes the total stresses remains approximately unchanged at B but the pore pressure rises. The wall will fail in some way if the states of all elements along the slip surfaces reach the failure line; if B′ reaches the failure line the wall fails during the undrained excavation and if C′ reaches the line the wall fails some times after construction. The figure demonstrate that unlike footing foundations or embankment foundations or retaining walls loaded by fill, where the foundation becomes stronger with drainage, the factor of safety of a retaining walls supporting an excavation will decrease with time. [24]

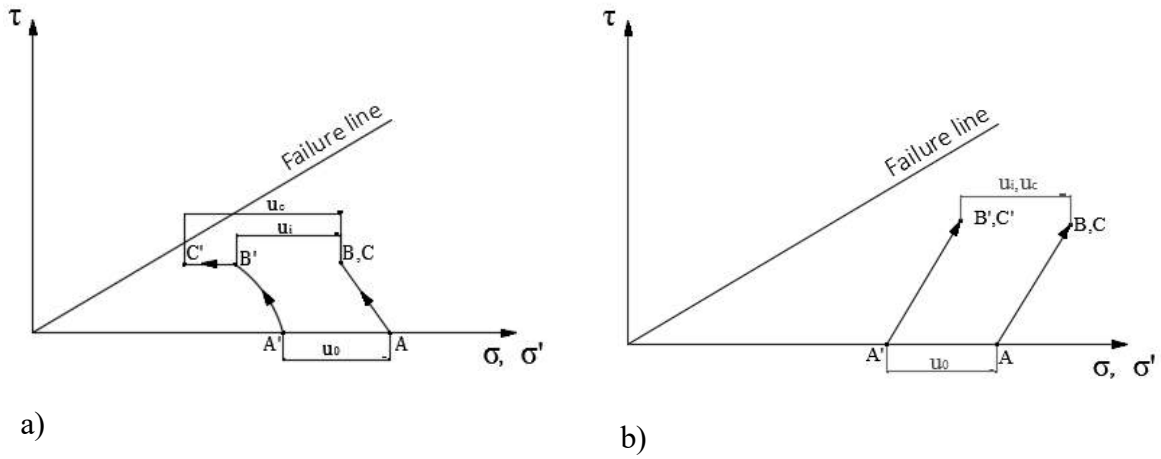

Figure 3.4: Change of stress and pore pressure for a wall retaining excavation (after [29]): a) undrained behavior; b) drained behavior

Since the un/reloading modulus of elasticity for soft soils is 5 to 7 times higher than the modulus of elasticity in primary loading (for sand 2 to 3 times), the time required to reach an approximate steady condition after excavation is usually measured in weeks or months ,i.e. during the normal construction periods [22]. [25] reviewed several cases of excavation in clayey soils and concluded that the stability is best expressed in terms of effective stress analysis. He reasoned that the readjustment of stresses and pore water pressures to correspond with a state of steady seepage may often take place in the course of few days or few weeks or at most some months. He further commented that the simple total stress analysis for excavations in clay will frequently lead to overestimation of the results both for safety factor and shear surface location. [22], [39]

From the above discussions it is clear that there is a possibility of undrained failure in excavation, although the drained (steady state) condition is most critical. [22]

3.5 Groundwater lowering

According to investigations, most problems encountered in deep excavation have direct or indirect relations with groundwater.

The permeability of clay is lower than 10^{-7} m/s, from which it follows that the velocity of groundwater in clay is rather slow. That means that the possibility of groundwater leaking into the excavation zone, which will cause much inconvenience during the construction, need not be considered. There is no occurrence boiling in clay either. Therefore, when clays is encountered in an excavation, the groundwater level can be ignored in practical engineering applications. When the groundwater level is lowered or the water content is decreased, the properties of clay will change significantly. The shear strength will increase and the compressibility will decline. [16]

The permeability of sand or gravel is usually greater than 10^{-4}m/s, which follows that the flow velocity of groundwater in sand or gravel is rather high and groundwater probably will leak into the excavation zone, which will cause much trouble. In worst, it may bring to the leakage of groundwater or soil, sand liquefaction, upheaval failure or floating of the basement.

Dewatering will decrease the pore water pressure and increase accordingly the effective stress of soils. In sandy or gravelly soils, the increase of the effective stress will produce elastic settlement. In clayey soils, not only elastic settlements but consolidation settlement

will be induced. The elastic settlements in this case is far less than that of consolidation settlements. [16]

CHAPTER 4
MATERIAL MODELS FOR SOILS

4.1 Introduction

There is a variety of soil models at the present: from simple linear elastic perfectly plastic (e.g. Mohr Coulomb), elastoplastic cap models (e.g. Cap, Modified Cam Clay) to advanced nonlinear-elastoplastic Hardening Soil Model and HS-Small Strain Model. The choice of a constitutive model depends on many factors but, in general, it is related to the type of analysis that the user intends to perform, expected precision of predictions and available knowledge of soil.

As regards the type of analysis, geoengineering computings can be divided into two groups (fig.4.1):

- those whose goal is to assess bearing capacity and slope or wall stability which are related to the ultimate limit state analysis (ULS), and
- those whose are related to the serviceability limit state analysis (SLS), such as deep excavations or tunnel excavations in urban areas. [26]

In general, as long as assessment of ULS for bearing capacity or slope stability is foreseen, the analysis may be limited to basic linear models such as the Mohr-Coulomb model. On the other hand, a precise deformation analysis requires the application of advanced constitutive models which approximate the stress-strain relation more accurately than simple linear-elastic, perfectly plastic model, and in effect, the form of displacement fields can be modeled more realistically. [28]

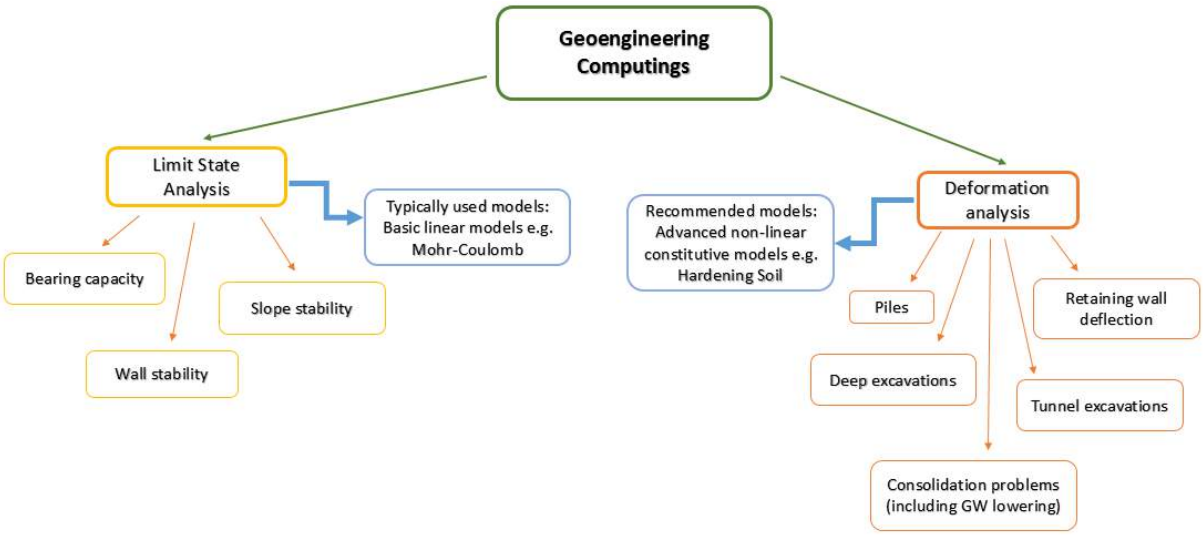

Figure 4.1: General types of geoengineering computing

4.2 Mohr-Coulomb Model

The Mohr-Coulomb Model is a simple and well-known linear elastic and perfectly plastic model, which can be used as a first approximation of soil behavior. The linear elastic part is based on Hooke's law of isotropic elasticity. The perfectly plastic part is based on the Mohr-Coulomb failure criterion, formulated in a non-associated plasticity framework. [27]

MC Model involves five input parameters: Young´s modulus E and Poisson´s ratio ν for soil elasticity, affective shear parameters cohesion c' and angle of friction φ' for soil plasticity and ψ as an angle of friction.

Coulomb failure criterion

If the results of laboratory tests are plotted in terms of effective stresses, the Mohr´s circles of stress at failure are often idealized as shown in figure 4.2. It is usual to assume that the tangent to the failure circles from several tests, performed with different initial effective stresses, is straight. This line is called the Coulomb failure criterion and can be expressed as:

$$\tau = c' + \sigma_f' \cdot tan\varphi', \qquad (4.1)$$

where τ and σ_f' are the shear and normal effective stresses on the failure plane and the cohesion, c', and angle of shearing resistance, φ', are material parameters [34].

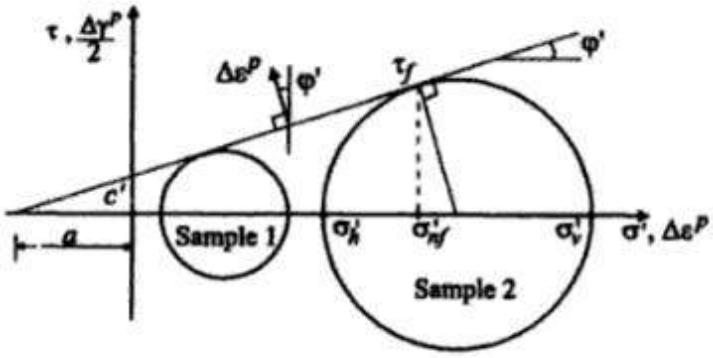

Figure 4.2: Mohr´s circles of effective stress

Formulation of the Mohr-Coulomb model

As shown in figure 4.3a for primary loading the stress-strain behavior is modelled elastic with a constant stiffness up to a certain failure stress σ_f. Similarly unloading-reloading is modelled, adopting the same material response and stiffness as a primary loading. When the failure stress is reached, perfectly plastic deformation takes place, involving the development of reversible strains. In order to evaluate whether or not plasticity takes place, yield function are introduced. As shown in figure 4.3b, for general states of stress soil failure can be represented as a fixed hexagonal yield surface in principal stress space. By extending Coulomb´s friction law to general states of stress the equations of the hexagonal yield surface are obtained as:

$$f_1 = 0 \text{ with } \quad f_1 = \frac{1}{2} \cdot |\sigma_2' - \sigma_3'| - \frac{1}{2} \cdot (\sigma_2' + \sigma_3') \cdot sin\varphi' - c' \cdot cos\varphi' \leq 0$$

$$f_2 = 0 \text{ with } \quad f_2 = \frac{1}{2} \cdot |\sigma_3' - \sigma_1'| - \frac{1}{2} \cdot (\sigma_3' + \sigma_1') \cdot sin\varphi' - c' \cdot cos\varphi' \leq 0 \qquad (4.2)$$

$$f_3 = 0 \text{ with } \quad f_3 = \frac{1}{2} \cdot |\sigma_1' - \sigma_2'| - \frac{1}{2} \cdot (\sigma_1' + \sigma_2') \cdot sin\varphi' - c' \cdot cos\varphi' \leq 0$$

For stress states that are within this yield surface the MC Model responds linear elastic and all strains are reversible.

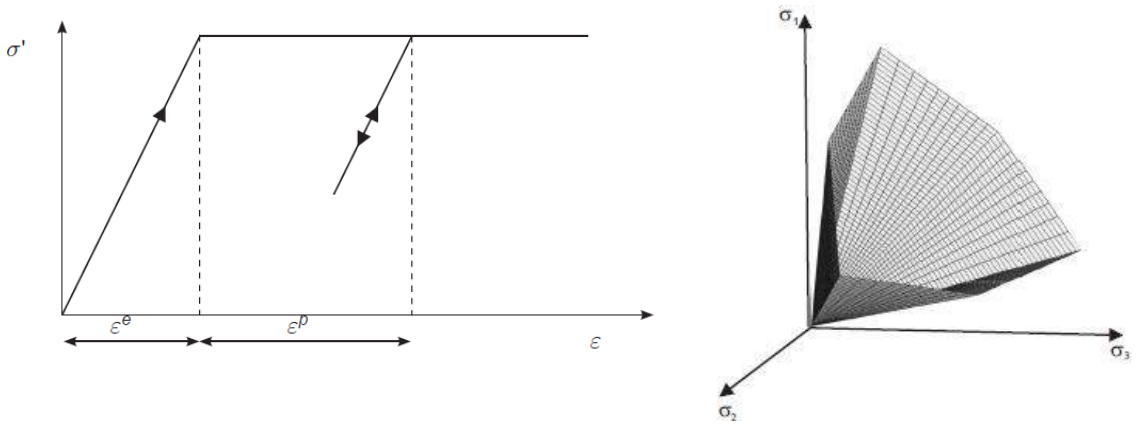

a) b)

Figure 4.3: Basic idea of an elastic perfectly plastic model: a) linear elastic perfectly plastic material behavior, b) yield surface in principal stress space with c'= 0

According to Hook´s low of isotropic elasticity the elastic stress-strain relationship is written as:

$$\dot{\sigma}' = D^e \dot{\varepsilon}^e \tag{4.3}$$

where $\dot{\sigma}'$ is the tress rate, $\dot{\varepsilon}^e$ the corresponding elastic strain rate and D^e is the elastic material stiffness matrix.

For elastoplastic model strain can be decomposed into elastic and plastic components:

$$\dot{\varepsilon} = \dot{\varepsilon}^e + \dot{\varepsilon}^p, \tag{4.4}$$

where e is used to denote elastic strains and p denotes plastic strains.

Combining eqs.4.3 and 4.4:

$$\dot{\sigma}' = D^e(\dot{\varepsilon} - \dot{\varepsilon}^e) \tag{4.5}$$

If associated plasticity is assumed, the plastic strain rate can then be formulated using the yield function introduced in eqs. 4.2. Doing so, the plastic strain rates become vectors perpendicular to the surface of the yield function. However, the use of MC type of plastic potential functions would lead to a considerable overprediction of the angle of dilatancy. Therefore, in addition to yield functions, different plastic potential function g are employed. Using the plastic potential functions, non-associated plasticity is adopted and the plastic strain rates are formulated as [35]:

$$\dot{\varepsilon}^p = \lambda_1 \frac{\partial g_1}{\partial \sigma'} + \lambda_2 \frac{\partial g_2}{\partial \sigma'} + \lambda_3 \frac{\partial g_3}{\partial \sigma'}, \tag{4.6}$$

where $\dot{\varepsilon}^p$ is the plastic strain rate and λ_1, $\lambda 2$ and λ_3 are plastic multipliers. The plastic potential functions are:

$$g_1 = \frac{1}{2} \cdot |\sigma_2' - \sigma_3'| - \frac{1}{2} \cdot (\sigma_2' + \sigma_3') \cdot sin\psi$$

$$g_2 = \frac{1}{2} \cdot |\sigma_3' - \sigma_1'| - \frac{1}{2} \cdot (\sigma_3' + \sigma_1') \cdot sin\psi \qquad (4.7)$$

$$g_3 = \frac{1}{2} \cdot |\sigma_1' - \sigma_2'| - \frac{1}{2} \cdot (\sigma_1' + \sigma_2') \cdot sin\psi$$

The plastic potential function contain a third plasticity parameter, the dilatancy angel ψ. This parameter is required to model positive plastic volumetric strain increments (dilatancy) as actually observed for dense soils.

Using the consistency condition:

$$\dot{f} = \frac{\partial f}{\partial \sigma'} \dot{\sigma}' = 0 \qquad (4.8)$$

And employing eqs. 3.12, 3.13 and 3.14, the plastic multipliers λ_1, λ_2 and λ_3 are solved from the equation:

$$\dot{f}_i = \frac{\partial f_i}{\partial \sigma'} \left(\dot{\varepsilon} - \lambda_1 \frac{\partial g_1}{\partial \sigma'} + \lambda_2 \frac{\partial g_2}{\partial \sigma'} + \lambda_3 \frac{\partial g_3}{\partial \sigma'} \right) = 0 \qquad (4.9)$$

where *i* runs from 1 to 3.

When implementing the Mohr-Coulomb model for general stress states, special treatment is required for the intersection of two yield surfaces. In Plaxis the exact form of the full Mohr-Coulomb model is implemented using a sharp transition from one yield function to another. For $c > 0$, the standard Mohr-Coulomb criterion allows for tension. In fact, allowable tensile stresses increase with cohesion. In reality, soils can sustain none or very small tensile stresses. This behavior can be included by specifying a tension cut-off. In this case, Mohr circles with positive principal stress are not allowed. The tension cut-off introduces three additional yield functions, defined as:

$$f_4 = \sigma_1' - \sigma_t \leq 0$$

$$f_5 = \sigma_2' - \sigma_t \leq 0 \qquad (4.10)$$

$$f_6 = \sigma_3' - \sigma_t \leq 0$$

where σ_t' is a tensile stress. [27]

The Mohr-Coulomb Model requires a total of five parameters which can be obtained from basic tests on soil samples:

E – Young modulus

v – Poisson's ratio

φ' – angle of friction

c' – cohesion

ψ – angle of dilatancy.

4.3 Hardening Soil Model

When soils subjected to changes of stress or stain their behavior is non-linear. In reality, the stiffness of soils depends at least on the stress level, the stress path and the strain level.

The Hardening Soil model is an advanced model for simulating the behavior of different types of soils, both soft soils and stiff soils (fig. 4.5). The Hardening-Soil model realistically reproduces soil deformations, as the σ-ε relation is approximated with a non-linear curve (the hyperbolic function by Duncan-Chang [29], [28]).In contrast to an elastic perfectly plastic model, the yield surface of a hardening plasticity model is nor fixed in principal stress space, but it can expand due to plastic straining. Moreover, as the formulation of the HS model incorporates two hardening mechanisms, it is suitable for modelling both domination of shear plastic strains which can be observed in granular soils and in overconsolidated cohesive soils, as well as domination of compressive plastic strains which is typical for soft soils, see figure 4.4. [30]

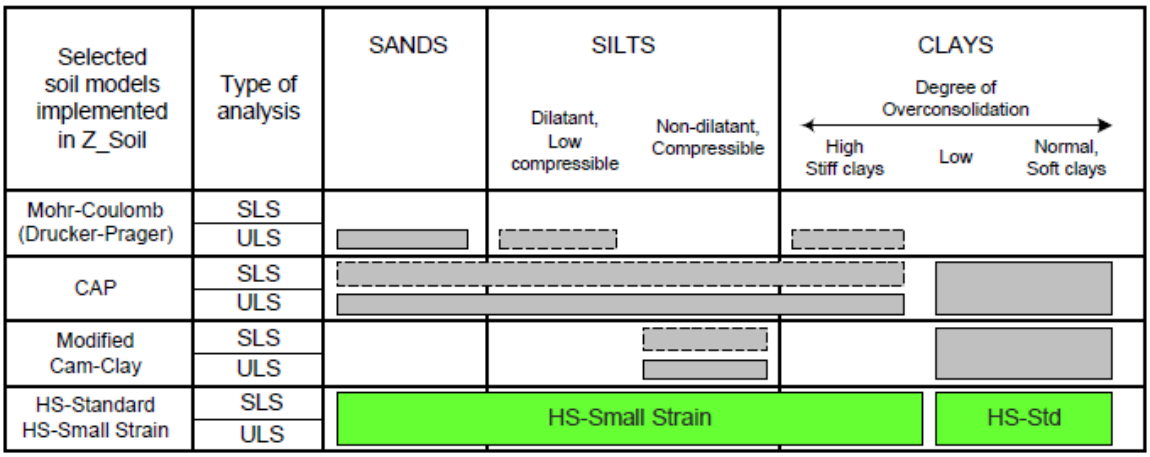

Figure 4.4: Recommendations for the model choice for soil type and types of analysis. Dashed line: may be used but not recommended in terms of quality of results; Solid line: can be applied; Green fill: recommended

The Hardening Soil model (HS-Standard) was designed by [31], [32] in order to reproduce basic macroscopic phenomena exhibited by soils such as:

- densification, i.e. a decrease of voids volume in soil due to plastic deformations,
- stress dependent stiffness, i.e. commonly observed phenomena of increasing stiffness modules with increasing confining stress (also related to increasing depth);
- soil stress history, i.e. accounting for preconsolidation effects;
- plastic yielding, i.e. development of irreversible strains with reaching a yield criterion;
- dilatancy, i.e. an occurrence of negative volumetric strains during shearing.

Similarly to the MC Model limiting states of stress are simulated by means of the effective shear parameters: cohesion c', friction angle φ' and the angle of dilatancy, ψ. But the pre-failure states of soil behavior are more accurately described by using three input stiffnesses:

- oedometer loading stiffness, E_{oed}
- triaxial loading stiffness, E_{50}
- triaxial unloading stiffness, E_{ur}.

In the following basic features of the HS Model will be explained, adopting a standard drained triaxial test. Compression is considered positive.

A basic feature of the present Hardening Soil model is the stress dependency of soil stiffness. For oedometer conditions of stress and strain, the model implies the relationship:

$$E_{oed} = E_{oed}^{ref} \cdot \left(\frac{c' \cdot cot\varphi' + \sigma'_1}{c' \cdot cot\varphi' + p^{ref}}\right)^m, \tag{4.11}$$

m is the exponent of the power low (the stress dependent stiffness parameter), σ_1 is the vertical stress and E_{oed}^{ref} is an oedometer reference stiffness modulus corresponding to the reference confining pressure p^{ref} (see fig. 4.5).

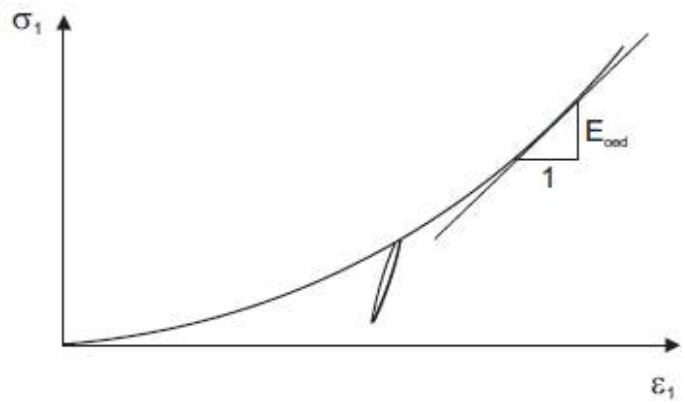

Figure 4.5: Characteristic curve of an oedometer test

Hyperbolic stress-strain relationship

When soil is subjected to primary deviatoric loading a decrease in stiffness is observed and irreversible plastic strains develop. In 1963 Kondner [40] formulated for a special case of a drained triaxial test a hyperbolic relationship between the deviatoric stress $q = \sigma_1 - \sigma_3$ and the axial strain ε_1 and later a hyperbolic model was presented by Duncan and Chang [33]:

$$\varepsilon_1 = \frac{q_a}{2 \cdot E_{50}} \cdot \frac{q}{q_a - q}, \tag{4.12}$$

where q_a is the asymptotic failure stress as shown in figure 4.6.

This figure also shows the typical curve of a drained triaxial test with constant lateral pressure σ_3, assuming that under primary loading the behavior is distinctly nonlinear and hyperbolic up to a Mohr-Coulomb failure stress q_f. The asymptotic failure stress has a relation:

$$q_a = \frac{q_a}{R_f} = (c \cdot cot\varphi' + \sigma'_3) \cdot \frac{2 \cdot sin\varphi'}{R_f \cdot (1 - sin\varphi')} \tag{4.13}$$

where R = 0.9 for many soils. While the maximum stress is determined by the Mohr-Coulomb failure criterion, the hyperbolic part of the curve can be defined using a single secant modulus as additional input parameter. In the HS Model this is the stress dependent modulus E_{50}, as used in eq. 4.11, which defined as:

$$E_{50} = E_{50}^{ref} \cdot \left(\frac{c' \cdot cot\varphi' + \sigma'_3}{c' \cdot cot\varphi' + p^{ref}}\right)^m, \tag{4.14}$$

where E_{50}^{ref} is a triaxial reference stiffness modulus corresponding to the reference confining pressure p^{ref}.

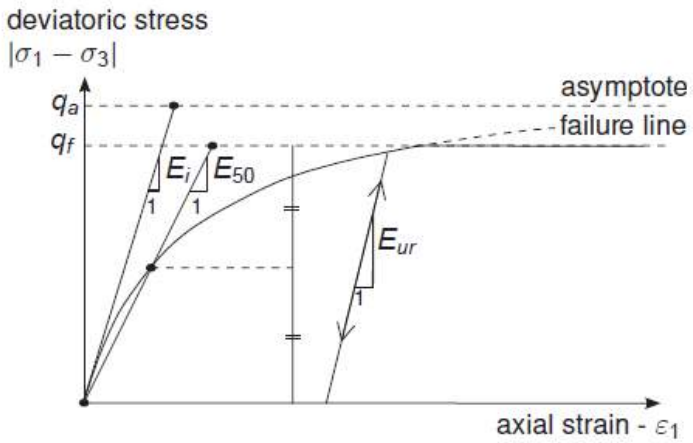

Figure 4.6: Hyperbolic stress-strain relation in primary loading for a standard drained triaxial test

The amount of stress dependency is governed by the exponent *m*, which can be measured both in oedometer tests and triaxial tests [34]. A value of 0.5 is typical for sands and clays tend to have *m* = 1.

In contrast to E_{50}, which determines the magnitude of both the elastic and the plastic strains, E_{ur} is a true elasticity modulus. In conjunction with a Poisson´s ratio ν_{ur} it determines the ground behavior under unloading and reloading; the indices *ur* stand for *unloading/reloading*. As the average primary loading modulus E_{50} the unloading and reloading E_{ur} is stress-level dependent:

$$E_{ur} = E_{ur}^{ref} \cdot \left(\frac{c' \cdot cot\varphi' + \sigma'_3}{c' \cdot cot\varphi' + p^{ref}}\right)^m \tag{4.15}$$

where E_{ur}^{ref} is a reference stiffness modulus corresponding to the reference confining pressure p^{ref}.

When comparing the hardening model to the previous elastic perfectly-plastic MC Model another significant difference is that plastic strains may already occur before the limit

MC-failure stress is reached. This implies that the HS Model incorporates another yield surface, which is not fixed in principal stress space, but it may expand and soil hardening is simulated due to plastic straining. As shown in figure 4.7a, as a distinction is made between two types of hardening, namely shear hardening and compression hardening. For the shear hardening law a yield function f^s is introduced, which is function of the triaxial loading stiffness E_{50} and for the compression hardening a yield function f^c is formulated, being governed by the oedometer loading stiffness E_{oed}. As also indicated in figure 4.7a for unloading-reloading elastic soil behavior is assumed, adopting Hook´s law with Young´s modulus E_{ur}. Figure 4.7b shows the total contour of the HS yield surface in principal stress space.

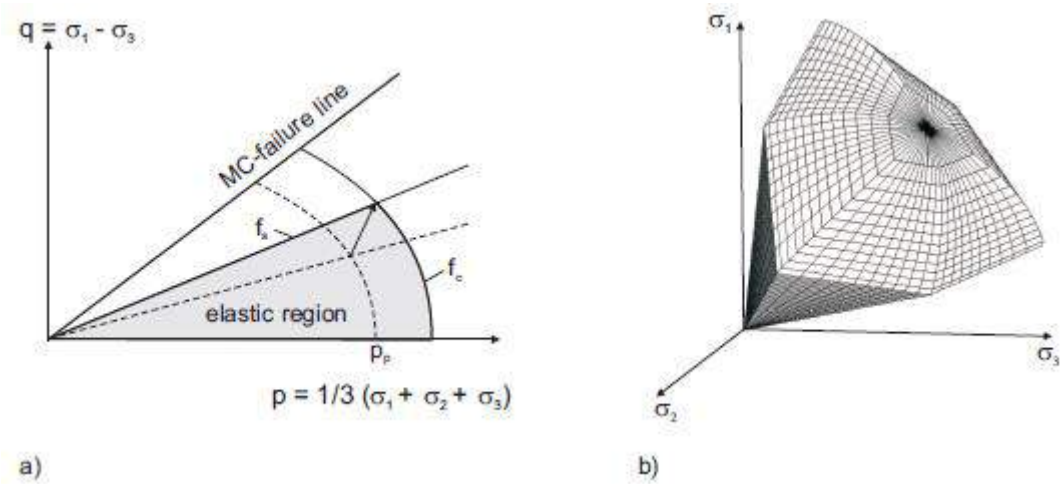

Figure 4.7: Yield surface of the HS Model for c = 0: a) successive yield loci for shear hardening and compression hardening in p-q-space; b) total yield contour in principal stress space.

Yield function f^s

The yield function f^s adopted in the HS Model has the formulation:

$$f^s = \bar{f} - \gamma^p, \tag{4.16}$$

where $\bar{f}$ is a function of stress and the hardening parameter and is formulated:

$$\bar{f} = \frac{q_a}{E_{50}} \cdot \frac{q}{q_a - q} - \frac{2q}{E_{ur}}, \tag{4.17}$$

and γ^p is a function of plastic strains:

$$\gamma^p = \varepsilon_1^p - \varepsilon_2^p - \varepsilon_3^p = 2 \cdot \varepsilon_1^p - \varepsilon_v^p \approx 2 \cdot \varepsilon_1^p, \tag{4.18}$$

Similar to the MC Model the HS Model adopts non-associated plasticity to determine the rates of plastic strain with the plastic potential function:

$$g^s = (3 - sin\psi_m) \cdot q - 6 \cdot sin\psi_m \cdot p \tag{4.19}$$

with $p = 1/3\ (\sigma_1 + \sigma_2 + \sigma_3)$. The mobilized angle of dilatancy ψ_m is calculated according to the so-called stress-dilatancy equation of Rowe. [35]

$$sin\psi_m = \frac{sin\varphi_m - sin\varphi_{cv}}{1 - sin\varphi_m \cdot sin\varphi_{cv}} \tag{4.20}$$

where φ_m is a mobilized friction angle, governed by the equation:

$$sin\varphi_m = \frac{\sigma_1' - \sigma_3'}{\sigma_1' + \sigma_3' - 2c \cdot cot\varphi}, \tag{4.21}$$

and φ_{cv} is a constant-volume angle (also called critical state friction angle), governed by the equation:

$$sin\varphi_{cv} = \frac{sin\varphi - sin\psi}{1 - sin\varphi \cdot sin\psi} \tag{4.22}$$

Yield function f^c

A compression hardening low is formulated by means of cap-type yield surfaces, which makes the model both suitable for hard soils as well as very soft clays. The cap-type yield function has the formulation:

$$f^s = \frac{q^2}{M^2} + (p + c \cdot cot\varphi)^2 - (p_p + c \cdot cot\varphi)^2, \tag{4.23}$$

with $M = \frac{6 \cdot sin\varphi}{3 - sin\varphi}$ (4.24)

The position and shape of the cap in stress space is governed by the isotropic preconsolidation pressure p_p as indicated in fig. 3.14a. The hardening law formulates the relationship between the plastic volumetric cap-strain ε_v^{pc} and the preconsolidation stress p_p:

$$\varepsilon_v^{pc} = \frac{E_{oed}}{1-m} \left(\frac{p_p}{p^{ref}}\right)^{1-m} \tag{4.25}$$

p^{ref} is an isotropic reference pressure. E_{oed} is the oedometer stiffness (fig. 4.6), which obeys a stress dependency according to the formula 4.11.

In addition to the moduli E_{50} and E_{ur}, the oedometer modulus E_{oed} is also an input modulus for the HS Model. Together with the parameters m, υ_{ur}, c', φ' and the dilatancy angle ψ, there are a total of eight input parameters.

To determine the rates of plastic volumetric strains associated plasticity, i.e. $g^c = f^c$ is adopted.

Strain and plastic multipliers

The strain rates are decomposed into an elastic part $\dot{\varepsilon}^e$ and into a plastic shear hardening part $\dot{\varepsilon}^{ps}$ and/or compression hardening part $\dot{\varepsilon}^{pc}$:

$$\dot{\varepsilon} = \dot{\varepsilon}^e + \dot{\varepsilon}^{ps} + \dot{\varepsilon}^{pc} \tag{4.26}$$

$$\dot{\varepsilon} = D^{-1}\dot{\sigma} + \lambda^s \frac{\partial g^s}{\partial \sigma} + \lambda^c \frac{\partial g^c}{\partial \sigma} \tag{4.27}$$

The plastic multipliers λ^s and λ^c are then solved from the consistency conditions $\dot{f}^s = 0$ and $\dot{f}^c = 0$ and result:

$$\lambda^s = \frac{1}{H^s - d^s} \frac{\partial f^s}{\partial \sigma} D^e \dot{\varepsilon} \quad (4.28) \qquad \text{and} \qquad \lambda^c = \frac{1}{H^c - d^c} \frac{\partial f^c}{\partial \sigma} D^e \dot{\varepsilon}, \quad (4.29)$$

where H^s is a shear hardening modulus:

$$H^s = \frac{\partial f^s}{\partial \gamma^p} \frac{\partial \gamma^p}{\partial \varepsilon^{ps}} \frac{\partial g^s}{\partial \sigma} \quad (4.30) \qquad \text{and} \qquad d^s = \frac{\partial f^s}{\partial \sigma} D^e \frac{\partial g^s}{\partial \sigma}. \quad (4.31)$$

H^c is a compression hardening modulus:

$$H^c = \frac{\partial f^c}{\partial \varepsilon_v^{pc}} \frac{\partial \gamma^p}{\partial \varepsilon^{pc}} \frac{\partial g^c}{\partial \sigma} \quad (4.32) \qquad \text{and} \qquad d^c = \frac{\partial f^c}{\partial \sigma} D^e \frac{\partial g^c}{\partial \sigma}. \quad (4.33)$$

Limitations of HS Model

Although the HS Model can be considered an advanced soil model which is able to faithfully approximate complex soil behavior, it includes some limitations related to specific behavior observed for certain soils. The models are not able to reproduce softening effects associated with soil dilatancy and soil restructuration (debonding of cemented particles) which can be observed, for instance, in sensitive soils.

The HS Model does not account for large amplitudes of soil stiffness related to transition from very small strain to engineering strain levels ($\varepsilon \approx 10^{-3}$–$10^{-2}$). Therefore, the user should adapt the stiffness characteristics to the strain levels, which are expected to take place in conditions of the analyzed problem.

4.4 Hardening Soil Small Strain Model

The original Hardening Soil Model assumes elastic material behavior during unloading and reloading. However, the strain range in which soils can be considered truly elastic, is very small. With increasing strain amplitude, soil stiffness decays nonlinearly (fig. 4.8).

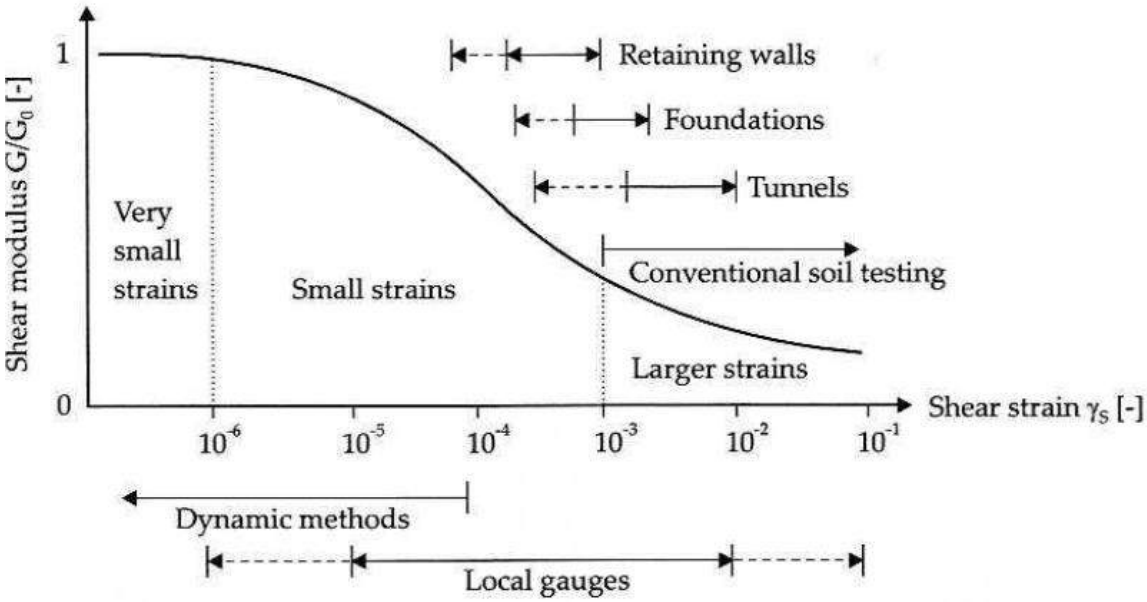

Figure 4.8: Characteristic stiffness-strain behavior of soil with typical strain ranges for laboratory tests after [26]

An extended version of the HS-Standard, the Hardening Soil Small Model (HS Small-Strain) was formulated by Benz [38] in order to handle the commonly observed phenomena: of a strong stiffness variation with increasing shear strain amplitudes in the domain of small strains (S-shape curve presented in figure 4.9); and of a nonlinear elastic stress-strain relationship which is applicable in the range of small strains.

As seen in figure 4.9, small unloading-reloading stress-strain paths result in a considerably higher elasticity modulus E_0. In fact, maximum soil stiffness is observed at very low strain levels, e.g. strains smaller than 10^{-5} [31]. The strain levels obtained here, are far below conventional laboratory testing, requiring special measuring devices such as dynamic methods or local strain gauges.

The formulation of small strain stiffness in the HS-Small Model assumes that the decay of small strain stiffness is primary related to either break up of bonding forces between soil particles or frictional particle forces exceeding their elastic limit. Thus, a drop of stiffness can be observed whenever inter-particle forces are reorganized and concentrated.

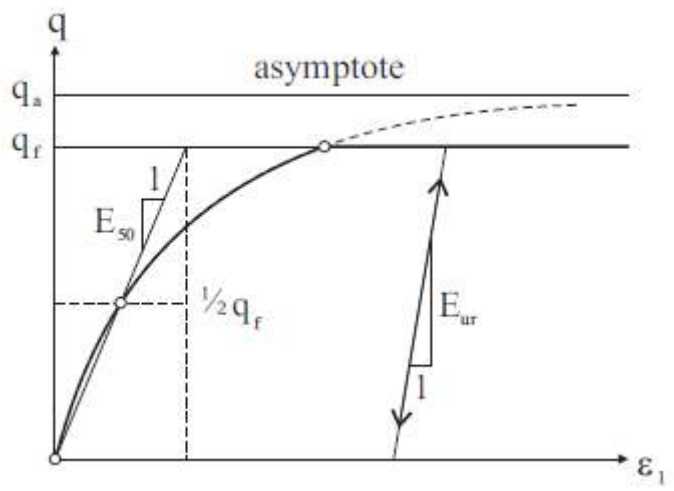

Figure 4.9: HS-Small Model: extension of the HS Model incorporating small strain stiffness.

These very small-strain stiffness and its non-linear dependency on strain amplitude should be properly taken into account. The Hardening Soil Small-Strain model offers the possibility do so. The Hardening Soil Small-Strain Model is able to produce more accurate and reliable approximation of displacements which can be useful for dynamic applications or in modeling unloading-conditioned problems, e.g. excavations with retaining walls or tunnel excavations.

The HS Small-Strain model is based on the Hardening Soil Model and uses almost entirely the same parameters. Only two additional parameters are needed to describe the variation of stiffness with strain:

- G_0 is an initial shear modulus
- $\gamma_{0,7}$ is a shear strain level at which the initial shear modulus G_0 has reduced to 70% of G_0

To incorporate small strain stiffness effects into HS Model a relatively simple expression for the small strain stiffness decay of the shear modulus is adopted:

$$G = \frac{G_0}{1+0{,}43\cdot\frac{\gamma}{\gamma_{0,7}}} \tag{4.34}$$

where G is the actual shear modulus at shear strain γ, G_0 is the initial shear modulus and $\gamma_{0,7}$is the shear strain at which the initial shear modulus has reduced to $0{,}7G_0$, as shown in figure 4.9. For general states of stress the shear strain is expressed using the strain invariant:

$$\gamma = \frac{1}{\sqrt{2}}\cdot\sqrt{(\varepsilon_1-\varepsilon_2)^2+(\varepsilon_2-\varepsilon_3)^2+(\varepsilon_3-\varepsilon_1)^2}, \tag{4.35}$$

which in case of triaxial loading reduces to $\gamma = |\varepsilon_1 - \varepsilon_2|$. While reducing the shear modulus with increasing shear strain, the Poisson´s ratio ν_{ur} is kept constant, such that the resulting bulk modulus is reducing as a function of shear strain.

A number of factors influence the small-strain parameters G_0 and $\gamma_{0,7}$. Most importantly they are influenced by the material's actual state of stress and void ratio e. The stress dependency of the shear modulus G_0 is taken into account with the power law:

$$G_0 = G_0^{ref} \cdot \left(\frac{c' \cdot cot\varphi' + \sigma'_3}{c' \cdot cot\varphi' + p_{ref}}\right)^m, \tag{4.36}$$

Figure 4.8 shows the stiffness degradation curve, reaching far into the plastic material behavior at lager strains. According to the formulation of the HS Model, stiffness degradation due to plastic straining is modelled by involving material hardening. Therefore, before reaching plastic material behavior, the formulation of the small strain stiffness curve is cut off at the unloading-reloading shear modulus G_{ur}, defined as:

$$G_{ur} = \frac{E_{ur}}{2 \cdot (1 + \nu_{ur})} \tag{4.37}$$

The elastic constant E_{ur} and ν_{ur} have already been introduced in the HS Model.

Equation 4.37 indicates that G_{ur} is the shear modulus in complete deviatoric unloading as illustrated in fig. 4.9.

CHAPTER 5:
CASE STAUDY FOR THE EVALUATION OF RISK

5.1 Project description

Stuttgart is the capital of Baden-Württemberg region, situated on the south-west of Germany (fig. 5.1). With about 600.000 inhabitants Stuttgart is the sixth largest city in Germany.

Figure 5.1: Location of Stuttgart

The case study is a multistorey building that will be constructed in the central area of the city, in Wolframstrasse on the North of Stuttgart Central Station. The exact location is

situated on the cross-road of the Wolframstrasse and Nordbahnhofstrasse, and is also bordered by a railway bridge on the South. On the West of the construction site (Lissabonnerstrasse) a shopping centre “Milaneo” is situated (fig. 5.2).

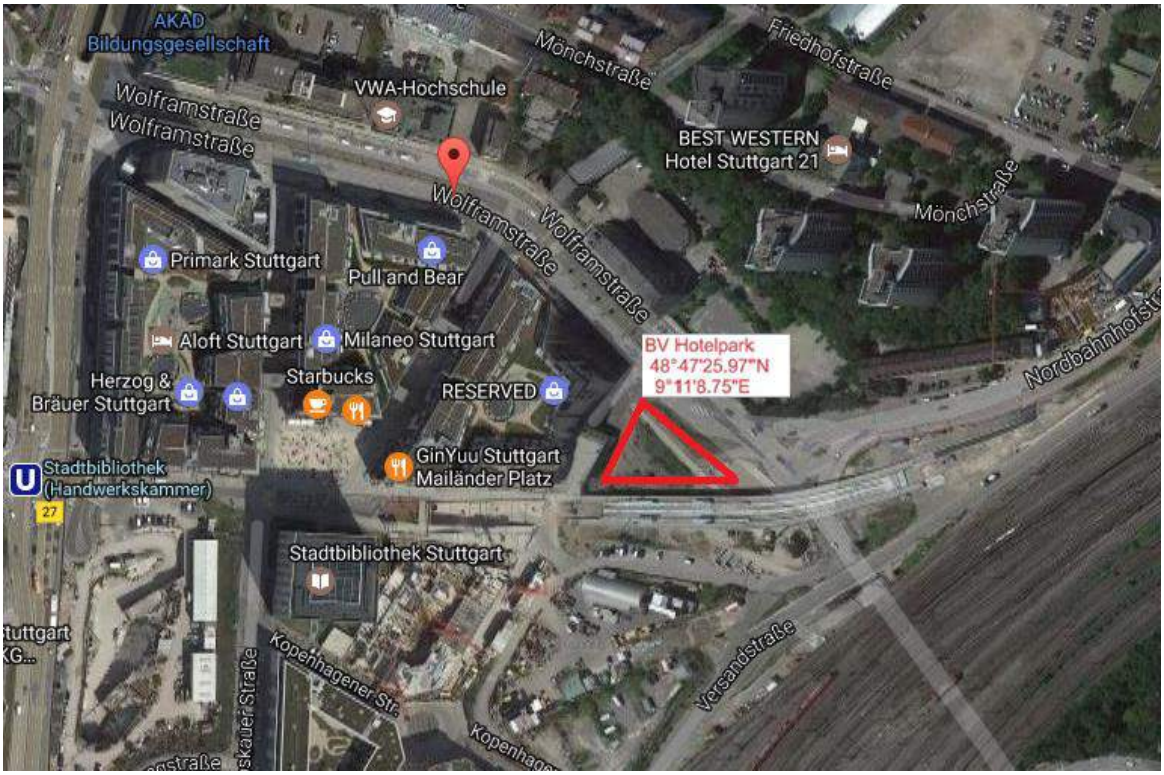

Figure 5.2: Location of the case study.

The multistorey building is a 10-storay hotel “Parkhotel” that accounts 2 underground levels, a ground floor and 9 upper-floors (fig. 5.3, Annex A1-2). The building has a triangular shape with side lengths of 70,2 m, 47,7 m and 63,3 m. (fig. 5.4, Annex A3).

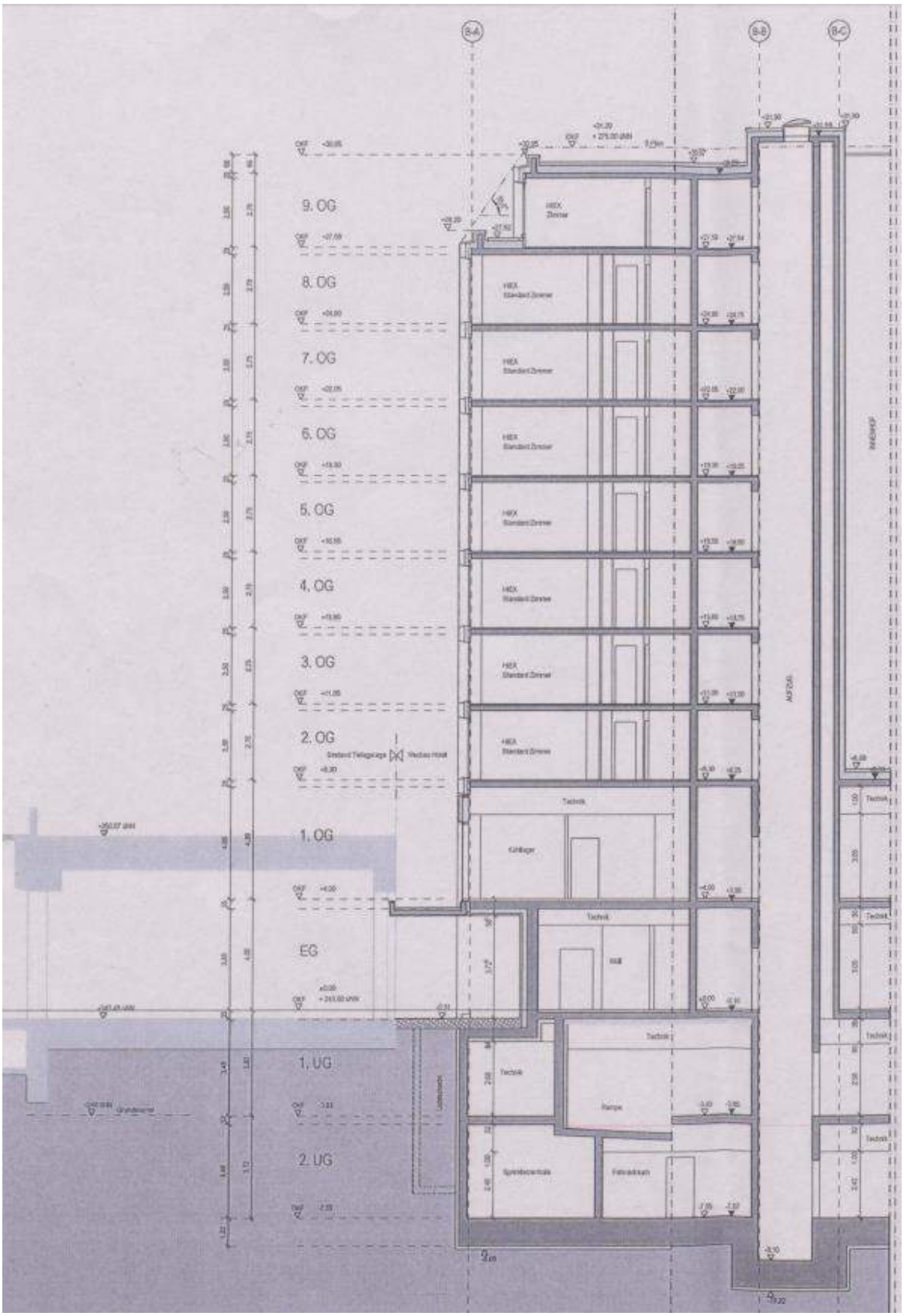

Figure 5.3: Parkhotel – cross-section.

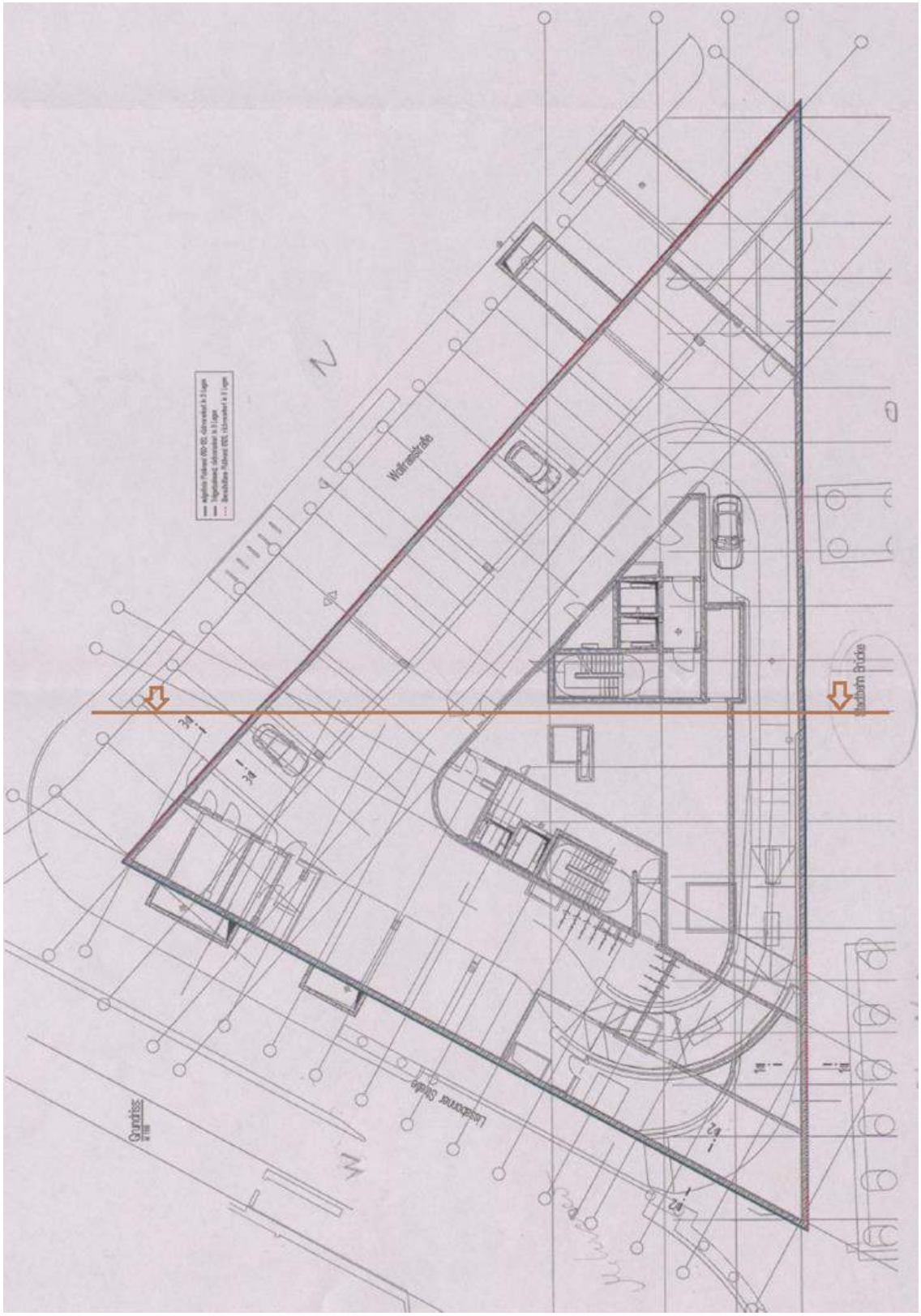

Figure 5.4: Parkhotel – plan view.

5.2 Geology and soil properties

5.2.1 Geomorphology of the research area

From the morphological point of view, the investigated area is located in the valley of Nesenbach and contains the sequence of so-called grave-formations that are the lithostratigrafic formation of Mittelere Keuper (or Gipskeuper) - fine-sediment deposits of various colours.

The lower edge of the excavated area is a Grenzdolomit formation that is a geological formation typical for Germany dated back to the Triassic period. Grenzdolomit formation contains two types of soil: Bochinger Horizont and Dunkelrote Mergel (Dark Red Marl) that, due to chemical and physical weathering processes, are presented in unstable weathered state.

Grenzdolomit underlays Grundgipsschichten that is characterized as a stable unweathered rock.

Above the Grenzdolomit lays a Fließerde (or Quartäre Fließerde) that can be characterized as a plastic clay.

In general, the sequence of layers of the investigated area is following:

Auffüllung (Fill) – recent, man-made

Quartäre Fließerde – Pleistocene

Dunkelrote Mergel – Mittelerer Keuper

Bochinger Horizont – Mittelerer Keuper

Grenzdolomit – Triassic

A field investigation was carried out from 02.02.2015 to 04.02.2015 and constitutes of three boreholes: BK 1-3/15 of maximum 16 m depth and three DPH 1-3/15 (Dynamic Probing Heavy) (in accordance with DIN EN ISO 22476-2), see Annex B1, B2-1.

The layers were studied in details through boring logs of BK 1-3/15 and during DHP 1-3/15 (see Annex B2-2). The layer sequence and their depths are summarized in table 5.1 and 5.2, and represented in figure 5.5 and in Annex B2-2, B3.

Table 5.1: Layers sequence and its depth detected in boring logs.

Outcrop	Auffüllung (Fill)	Fließerde	Dunkelrote Mergel	Bochinger Horizont
BK 1/15	0,00 – 4,00	4,00 – 6,30	6,30 – 15,00	15,00 – 16,00
BK 2/15	0,00 – 4,80	4,80 – 7,50	7,50 – 13,60	13,60 – 16,00
BK 3/15	0,00 – 4,10	4,10 – 4,50	4,50 – 11,70	11,70 – 16,00

Table 5.2: Layers sequence and its depth detected during DHP.

Outcrop	Auffüllung (Fill)	Fließerde	Dunkelrote Mergel	Bochinger Horizont
BK 1/15	0,00 – 3,90	3,90 – 6,10	6,10 – 14,80	14,80 – 16,00
BK 2/15	0,00 – 5,00	5,00 – 7,00	7,00 – 13,90	13,90 – 16,00
BK 3/15	0,00 – 3,90	3,90 – 4,40	4,40 – 12,10	12,10 – 16,00

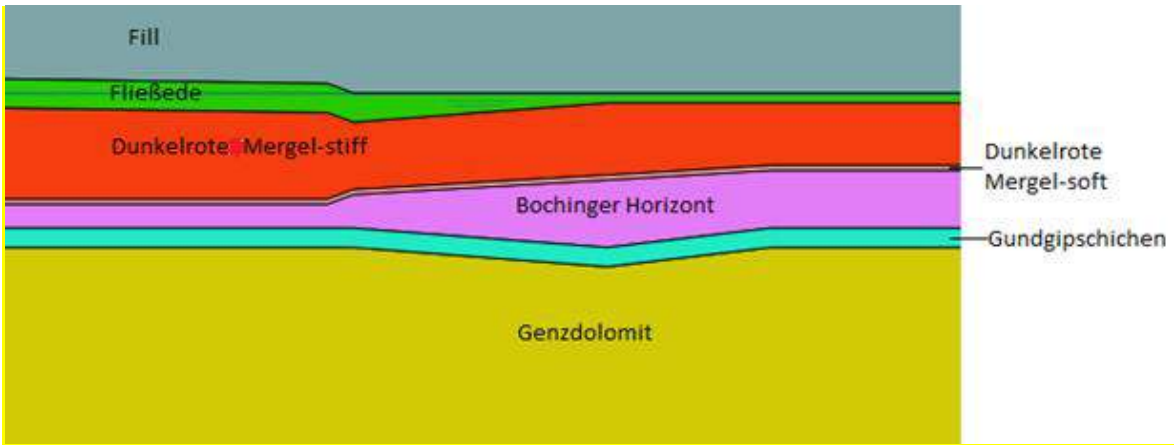

Figure 5.5: Geology of the investigated area in Plaxis.

5.2. Water content

The water content of all soil layers was determined in laboratory. Samples were taken from the borehole BK-2/15 at depth between 2 and 14 meters. Results are represented in table 5.3:

Table 5.3: Water content results.

Outcrop	Depth [m]	Water content [%]	Stratigraphic layer
BK 2/15	2,0	23,81	Fill
	4,0	27,14	
	6,0	18,92	Fließerde
	8,0	20,41	Dunkelrote Mergel
	10,0	21,08	
	12,0	18,47	
	14,0	14,79	Bochinger Horizont

5.2.3 Soil particle sizes

Grain size is an important aspect of soil mechanics and geotechnical engineering because it is an indicator of other engineering properties. Grain size distribution curves provides approximate assessment of soil with regard to its permeability (hydraulic conductivity), sensibility to frost, compressibility, shear strength and its suitability as a filter material.

In order to determine the grain size distribution of the Dunkelrote Mergel, three samples at the depth of 6-8 m were tested. For grains with diameter more than 0,063 mm a sieve analysis was carried out, meanwhile, for grain size with diameter less than 0,063mm a sedimentation analysis was executed. Results are represented in table 5.4 and Annex C.

In accordance with DIN 18122, in saturated conditions the Dunkelrote Mergel has the consistency index I_c = 0,55 and can be rated to the soil group TL/ TM (slightly to middle plastic clay).

Table 5.4: Grain size analysis results.

Outcrop	Depth [m]	Gravel content [%]	Sand content [%]	Silt/Clay content [%]	Soil type	Stratigraphical belonging	Permeability coefficient k_f [m/s]
BK 1/15	6,0 – 7,0	25,9	34,0	28,3/11,5	Silty sand with gravel, slightly clayey	Dunkelrote Mergel	$6,9 \cdot 10^{-8}$
BK 2/15	7,5 – 7,8	21,5	40,9	24,9/12,6	Sand, highly silty, slightly clayey	Dunkelrote Mergel	$3,3 \cdot 10^{-8}$
BK 3/15	6,0 – 7,0	6,4	52,1	32,5/9,0	Silty sand, slightly clayey	Dunkelrote Mergel	$4,7 \cdot 10^{-8}$

From the grain distribution curves the soil permeability coefficient, k_f, according to Malet, is obtained. It varies from $3,3 \cdot 10^{-8}$ m/s to $6,9 \cdot 10^{-8}$ m/s that, according to DIN 18130, is classified as a low permeable soil.

5.2.4 Soil parameters

One of the most important parameters of soils is a compressibility modulus, E_s that describes deformation behaviour of soil under the vertical load and can be determined by means of Oedometer test.

One-dimentional oedometer test is one of the simplest soil tests that may be used to investigate compression and swelling of soil (i.e. the relationship between effective stress and volumetric strain) or consolidation (i.e. the relationship between compression and seepage). The soil sample is a disc contained in a stiff metal cylinder (hence, the radial strains are zero). Porous disc at the bottom and the top act as drains and so seepage of pore water is vertical and one-dimensional.

The axial stress σ_v is applied by adding or removing weight. The axial strain ε_a is measured using a displacement transducer or a dial gauge. Implementing ε_a in a Hoock's low, the compressibility modulus E_s can be calculated. For Dunkelrote Mergel the results of the oedometer test is represented in table 5.5.

Table 5.5: Oedometer test results.

Sample 1	Loading	Vertical stresses, σ_v [kN/m^2]	Compressibility modulus, E_s [MN/m^2]
BK 1/14 Depth: 7,75-8,00 m	First loading	20 – 50	3,8
		50 – 150	7,3
		150 – 250	12,8
	Secondary loading	50 – 150	27,5
		150 – 250	35,9
		250 – 350	22,2
		350 – 550	23,0
Sample 2	Loading	Vertical stresses, σ_v [kN/m^2]	Compressibility modulus, E_s MN/m^2]
BK 1/14 Depth: 12,00-12,75 m	First loading	20 – 50	2,4
		50 – 150	5,0
		150 – 250	8,7
	Secondary loading	50 – 150	19,7
		150 – 250	23,0
		250 – 350	13,9
		350 – 550	13,8

Another parameters, that are necessary for engineering purposes to design the soil behaviour, are indicated in table 5.6.

Table 5.6: Characteristic soil parameters.

Layer	Soil unit weight (moist), γ_k [kN/m^3]	Soil submerged unit weight, γ'_k [kN/m^3]	Drained angle of friction, φ'_k [°]	Drained cohesion, c'_k [kN/m^2]	Compressibility modulus, E_s [kN/m^2]
Fill	18 – 20	8 – 10	25, 0 – 27, 5	3 – 5	2 – 8
Fließerde	19 – 21	9 – 11	22,5 – 30,0	5 – 10	5 – 10
Dunkelrote Mergel (soft to stiff)	18 – 20	10 – 12	22,5 – 27,5	4 – 8	10 – 20
Dunkelrote Mergel (stiff to firm)	19 – 21	11 – 12	25, 0 – 27,5	10 – 20	25 – 45
Bochinger Horizont	21 – 22	14 – 16	25, 0 – 27,5	30 – 50	40 – 60

E_s modulus can be used directly only in Mohr-Coulomb Model, meanwhile for HS Model such parameters as: E_{oed}^{ref}, E_{50}^{ref}, E_{ur}^{ref}, m are required. For HS-Small Model, in addition, G_0^{ref} and $\gamma_{0,7}$ are required.

1) m is the exponent of the power low (the stress dependent stiffness parameter). m varies from 0,5 for sands to 1 for soft soils.

2) E_{oed}^{ref} is the reference oedometer stiffness modulus at reference pressure p^{ref}.

It is assumed: $E_s \cong E_{oed} \cong E_{oed}^{50}$

3) E_{50}^{ref} is the reference triaxial stiffness modulus at reference pressure p^{ref}.

$E_{50}^{ref} = E_{oed}^{ref}$ is assumed.

4) E_{ur}^{ref} is reference triaxial stiffness modulus due to unloading/ reloading at reference pressure p^{ref}.

It is assumed that $E_{ur}^{ref} = 3 \cdot E_{50}^{ref}$.

5) G_0^{ref} is initial shear modulus at reference pressure p^{ref}.

Assuming that $\frac{E_0}{E_{ur}} \cong \frac{G_0}{G_{ur}}$,

where E_0 is an initial stiffness modulus (at very small strains) and G_{ur} is shear modulus of unloading/ reloading, the ratio $\frac{G_0}{G_{ur}}$ can be found from the chart proposed by Alpan [41] shown in figure 5.6.

It is known that $G_{ur} = \frac{E_{ur}}{2\cdot(1+\nu_{ur})}$

Then, multiplying G_{ur} per number obtained from the chart, the initial shear modulus, G_0 can be calculated.

Finally, the initial shear modulus at reference pressure, G_0^{ref} can be obtained from the following equation:

$$G_0 = G_0^{ref} \cdot \left(\frac{c'\cdot cot\varphi' + \sigma'_3}{c'\cdot cot\varphi' + p_{ref}}\right)^m \rightarrow \qquad G_0^{ref} = G_0 \cdot \left(\frac{c'\cdot cot\varphi' + \sigma'_3}{c'\cdot cot\varphi' + p_{ref}}\right)^{-m}$$

where σ'_3 is effective horizontal earth pressure.

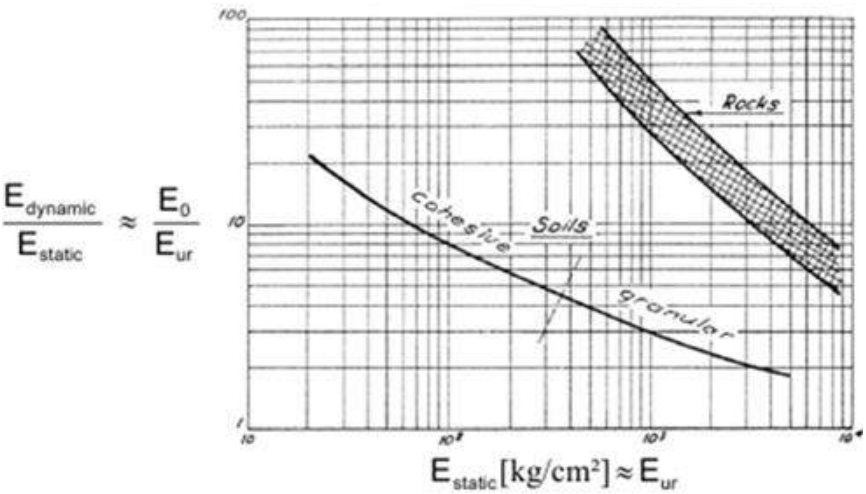

Figure 5.6: Correlation between very small-strain stiffness at larger strain from conventional laboratory tests after Alpan.

6) $\gamma_{0,7}$ is shear strain at 70% of G_0. Values of $\gamma_{0,7}$ are usually known from the experience.

$\gamma_{0,7} = 1\cdot10^{-4}$ is assumed for Fill

$\gamma_{0,7} = 1\cdot10^{-5}$ is assumed for Fließerde, Dunkelrote Mergel-soft and Grundgipschihten

$\gamma_{0,7} = 1\cdot10^{-6}$ is assumed for Dunkelrote Mergel-stiff, Grenzdolomit and Bochinger Horizont.

The complete list of soil parameters is represented in Annex D – Material report from Plaxis.

5.2.5 Georisk: seismic activity

In accordance with DIN EN 1998-1/NA:2011-01 the examined area is situated in seismic zone 1: maximal intensity expected reaches magnitudes 6,5 – 7,0. Subsoil belongs to class R: areas with missing or only low degree of covering with loose rock over solid rock.

Ground type B: deposits of very dense sand, gravel, or very stiff clay, at least several tens of meters in thickness, characterised by a gradual increase of mechanical properties with depth.

5.3 Hydrology

5.3.1 Ground water level

In order to study a ground water flow, as well as a ground water level, the necessary measurements in boreholes were made. Boreholes BK 1-3/15 were observed while drilling and immediately after completion for the presence and level measurement of ground water. The water levels observed are noted on the attached boring logs in Annex B4 and are summarized in tables 5.7 – 5.8.

Table 5.7: Ground water measurements on 02-03.02.2015.

Borehole	GW while drilling		GW	
	Depth in borehole, [m]	[m a.s.l.]*	Depth in borehole, [m]	[m a.s.l.]
BK 1/15	14,30	229,14	5,40	238,04
BK 2/15	11,70	231,91	5,60	238,01
BK 3/15	10,50	233,64	6,20	237,94

* m a.s.l. means meters above see level

Table 5.8: Ground water measurements on 17.02.2015.

Borehole	GW at 17.02.2015	
	Depth in borehole, [m]	[m a.s.l.]
BK 1/15	5,62	237,82
BK 2/15	5,80	237,81
BK 3/15	6,42	237,72

While drilling the ground water was detected at depth 10,5 – 14,3 m. After completion of the boreholes the GW level rose till 5,40 – 6,20 m (238,00 m a.s.l. – meters above see level) due to the presence of the confined aquifer.

On the 17.02.2015 subsequent measurements were carried out and the GW level was detected at 237,80 m a.s.l.

Longer monitoring during a year with piezometers shows the long-term GW conditions. During some periods of year, the water level varies. The maximum highest level detected is 240,00 m a.s.l. This value will be used for further calculations.

5.3.2 Aggressivity to concrete

From borehole BK-2/15 a sample for the analysis of the aggressivity to concrete were taken and carried out according to DIN 4030-1. Results show that the ground water is not aggressive to concrete.

5.3.3 Ground water lowering

As a null level the ground floor level, that equal to 243,49 m a.s.l., was fixed. First and second underground levels have 3,1 m height and lay on 240,49 m and 237,29 m a.s.l. accordingly. The foundation level is situated 1,20 m below the second underground floor (fig.5.7).

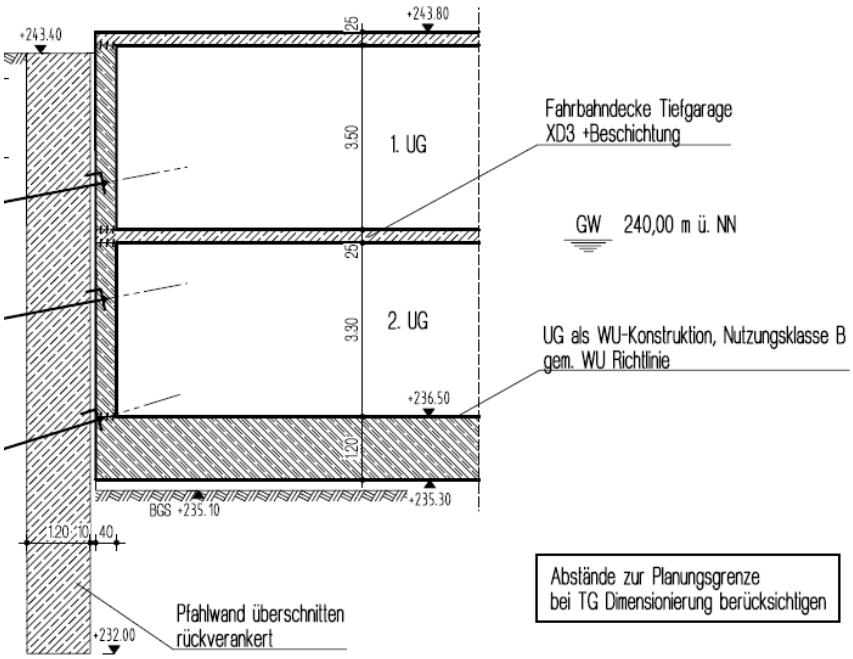

Figure 5.7: Frontal cross-section of the underground part of the Parkhotel.

According to the hydrological situation, described above, a watertight covering of the underground floors is required, as well as the lowering of ground water during basement construction.

According to phase constructions, ground water lowering will be made in three steps:

1) First lowering from 240,00 to 238,50 m a.s.l., soil – Flißerde with permeability coefficient $k_f = 1{,}5 \cdot 10^{-7}$ [m/s] (fig. 5.8)

Excavation at phase 5 should be carried out till the 239,00 m a.s.l. Ground water level must be at least 0,5 m lower; hence, the first ground water lowering, s_1 [m] amounts:

s_1 = 240,00 - (239,00 - 0,50) = 1,5 m

In absence of pumping test data, the distance of influence, L_1 [m] can be estimated from the equation:

$L = 1750 \cdot s \cdot \sqrt{k_f}$, where k_f [m/s] is the permeability coefficient of soil, s [m] is the depth of the water lowering.

$$L_1 = 1750 \cdot s_1 \cdot \sqrt{k_f} = 1750 \cdot 1{,}5 \cdot \sqrt{1{,}5 \cdot 10^{-5}} = 1{,}0\ m$$

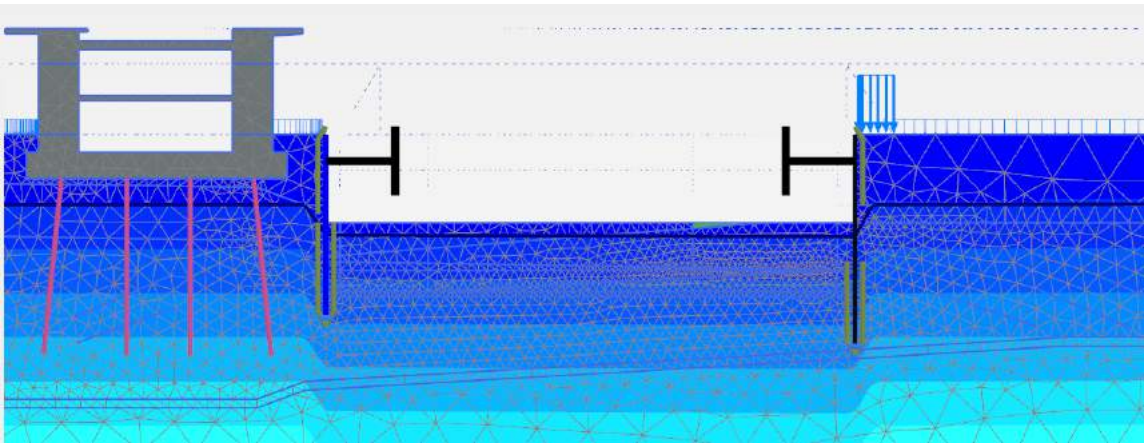

Figure 5.8: Ground water lowering 1.

2) Excavation at phase 8 should be carried out till the 236,30 m a.s.l., means that the second lowering drawdowns till 235,80 m a.s.l. – in Dunkelrote Mergel with $k_f = 1{,}0 \cdot 10^{-7}$ m/s. (fig.5.9)

Second GW lowering, s_2:

s_2 = 240,0 - (236,30 - 0,50) = 4,2 m

L_2 distance of influence:

$$L_2 = 1750 \cdot s_2 \cdot \sqrt{k_f} = 1750 \cdot 4{,}2 \cdot \sqrt{1{,}0 \cdot 10^{-5}} = 2{,}3\ m$$

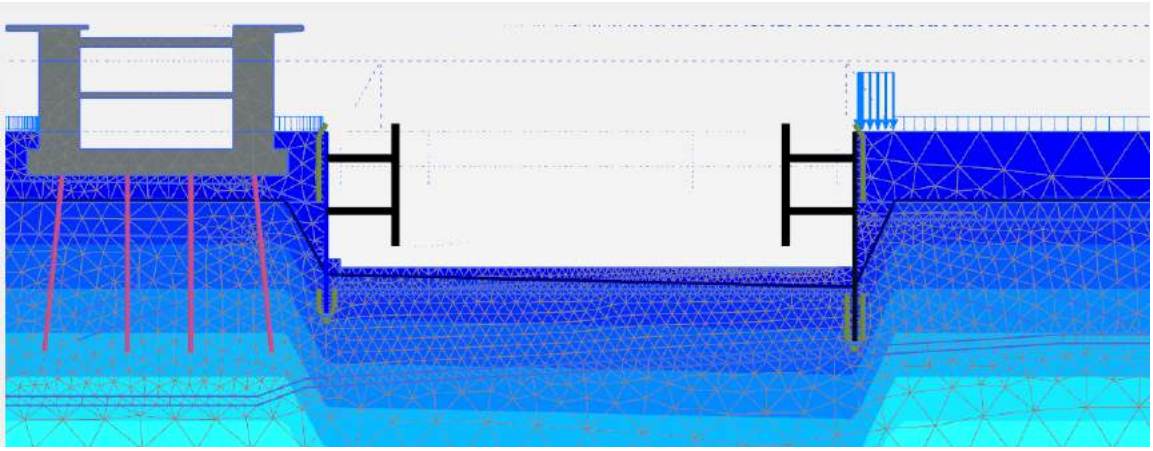

Figure 5.9: Ground water lowering 2 in.

Next excavation at phase10 should be carried out till the 234,75 m a.s.l., means that the third lowering drawdowns till 235,80 m a.s.l. – in Dunkelrote Mergel with k_f = 1,0·10^{-7} m/s.

Third GW lowering, s_3:

s_3 = 240,00 - (234,75- 0,50) = 5,75 m

L_3 distance of influence:

$$L_3 = 1750 \cdot s_3 \cdot \sqrt{k_f} = 1750 \cdot 5{,}75 \cdot \sqrt{1{,}0 \cdot 10^{-5}} = 3{,}2\ m$$

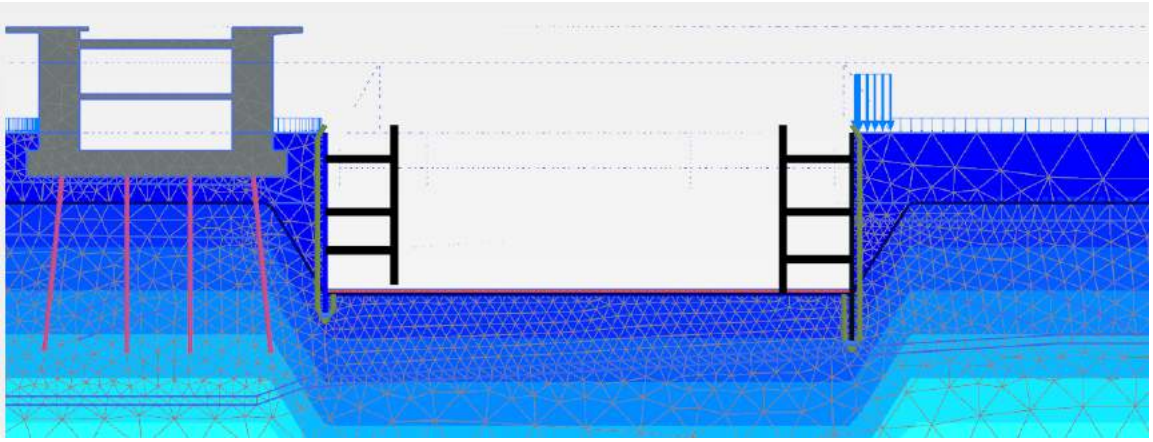

Figure 5.10: Ground water lowering 3 in.

Calculations are represented also schematically in figure 5.11.

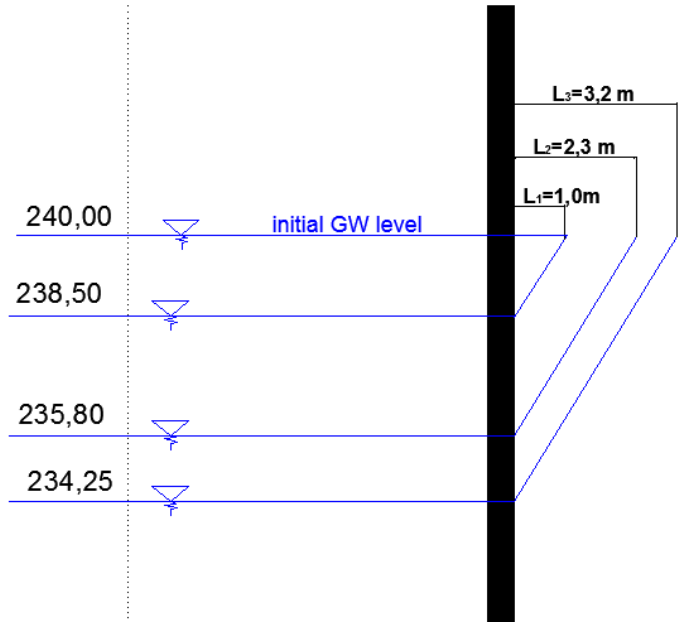

Figure 5.11: Ground water lowering and distance of influence.

5.4 Numerical modelling

5.4.1 Introduction

This thesis aims for the evaluation of the numerical solution performance of the case study, i.e. the realization of the multistorey building in the center of Stuttgart. The numerical modelling of the problem is performed using the FEM software PLAXIS 2D. This software is well-known to geotechnical engineers, and its application to problems of this sort is therefore of great interest. The challenge of the present case study is that the construction site is situated in the dense constructed area, where there is the railway bridge in the very vicinity from the construction site. Therefore, the allowable settlements and deformations of the bridge are high restricted.

The performance of a FEM-software is highly dependent on the material model and its applicability to the problem. So, three different soil models are used: Mohr- Coulomb, Hardening Soil and Hardening Soil Small. Then, the most appropriate model is chosen and more parameters are varied such as:

- increase in stiffness of all soil layers
- decrease in stiffness of all soil layers
- increase in stiffness of the excavation retaining structure
- decrease in stiffness of the excavation retaining structure

The numerical model (fig. 5.12) is based on the cross-section indicated in figure 5.4. In Annex D the material report from Plaxis is placed, where represented the soil parameters and the material parameters of the modelled structures.

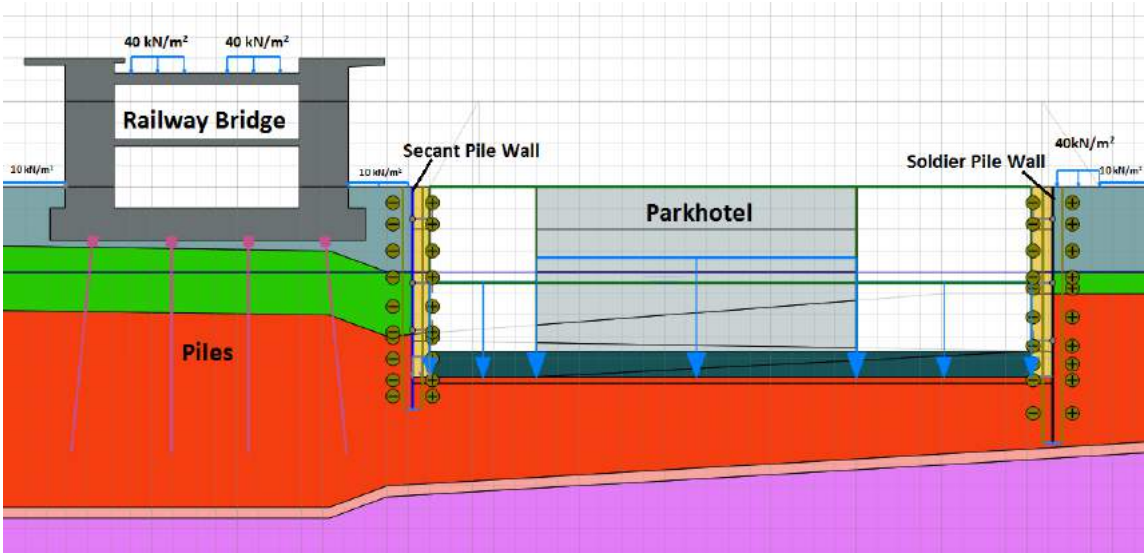

Figure 5.12: Numerical model of the case study in FEM.

5.4.2 Modelling of piles

Foundation of the bridge carries and transmits loads from the bridge to the ground and consists of 4 piles per every 3,1 m for the bridge length (fig. 5.13). Two inner piles are installed perpendicular to the bridge, while another two have an inclination about 5,7°. The piles have the following geometry properties:

- length: 10 m
- diameter: 1,2 m
- material: concrete C 20/25

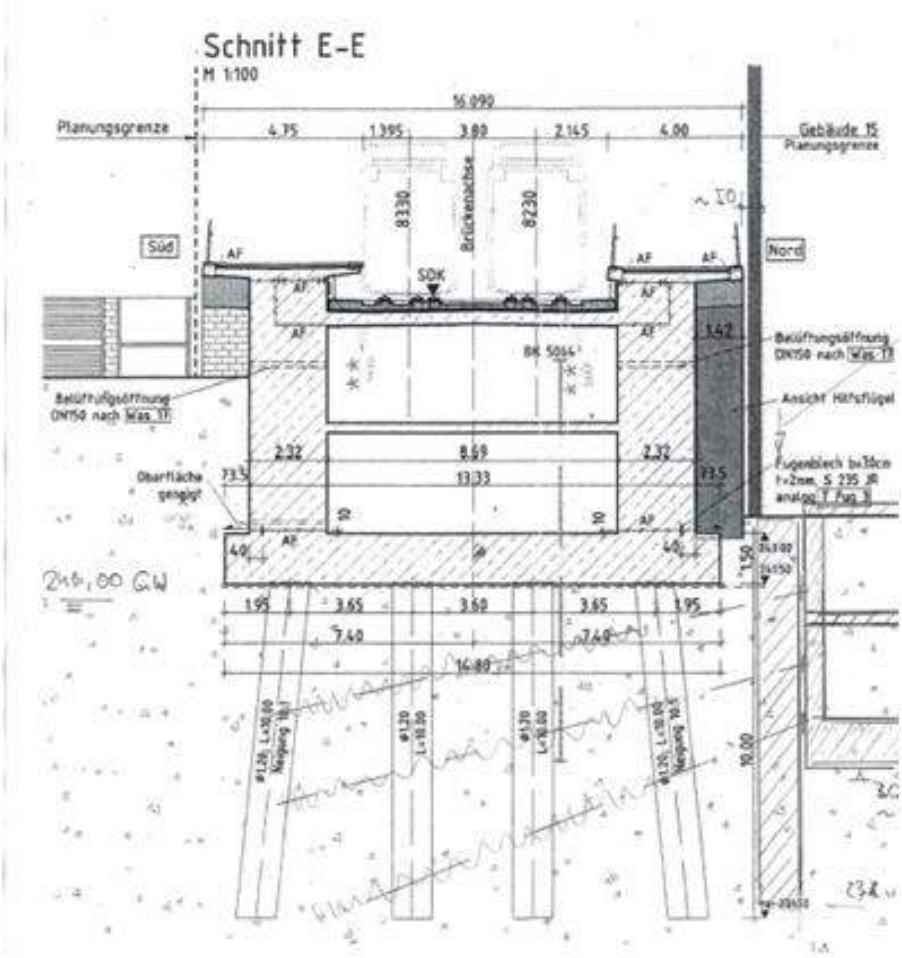

Figure 5.13: Cross-section of the railway bridge.

In order to design correctly the piles, a load test on a single bored pile of 1,2 m in diameter was carried out. This test shows the relationship between the applied loads and the associated settlements of the pile top, as well as the values of pile resistance. The calculation combination is BS-P (persistent situations) and the stratigraphic profile is the same as in the borehole BK-1/15. Load variation makes up 50% of the total load.

As can be seen from the Pile Resistance-Settlements diagram of the observed bored pile, the resistance, R_d depends on the length of the pile (table 5.9, Annex F).

Table 5.9: Pile resistance and pile head settlements with the pile length of 1,2 m in diameter.

Pile length, L [m]	Pile resistance, R_d [kN]	Pile head settlements, s [m]
10,80	2602	1,07
11,80	2723	1,10
12,80	2845	1,14
13,80	2996	1,17

Represented values can be used for the preliminary design of bored piles, although the behaviour of group of piles (interaction between piles) is not taken into consideration.

In Plaxis the piles are designed as "embedded beam row" (fig. 5.14) with parameters represented in table 5.10.

Table 5.10: Design parameters for embedded beam row in Plaxis.

Identification		**Piles-Bridge**
Identification number		1
Comments		
Colour		
E	kN/m²	30,00E6
γ	kN/m³	25,00
Pile type		Predefined
Predefined pile type		Massive circular pile
Diameter	m	1,200
A	m²	1,131
I_3	m⁴	0,1018
I_2	m⁴	0,1018
Rayleigh α		0,000
Rayleigh β		0,000
Axial skin resistance		Linear
$T_{skin, start, max}$	kN/m	65,00
$T_{skin, end, max}$	kN/m	65,00
F_{max}	kN	1500

The modelling of piles in a 2D finite element model brings limitations because the pile-soil interaction is a strongly 3D phenomenon. Pile-soil interaction is difficult to model and traditional methods in which pile rows are modelled either as plates or as node-to-node anchors have clear limitations. The embedded pile row combines the advantages of the plate and node-to-node anchor. It has pile properties similar to the plate element and a continuous mesh similar to the node-to-node anchor. The embedded pile row has been developed to model a row of piles in the out-of-plane direction, which is available in PLAXIS 2D. It is supposed to result in a more realistic pile-soil interaction behaviour compared to other methods. The "embedded pile row" element can be used to simulate a

row of piles with a certain spacing perpendicular to the model area. The stiffness properties are entered per pile, the program calculates the smeared properties per meter width. [44]

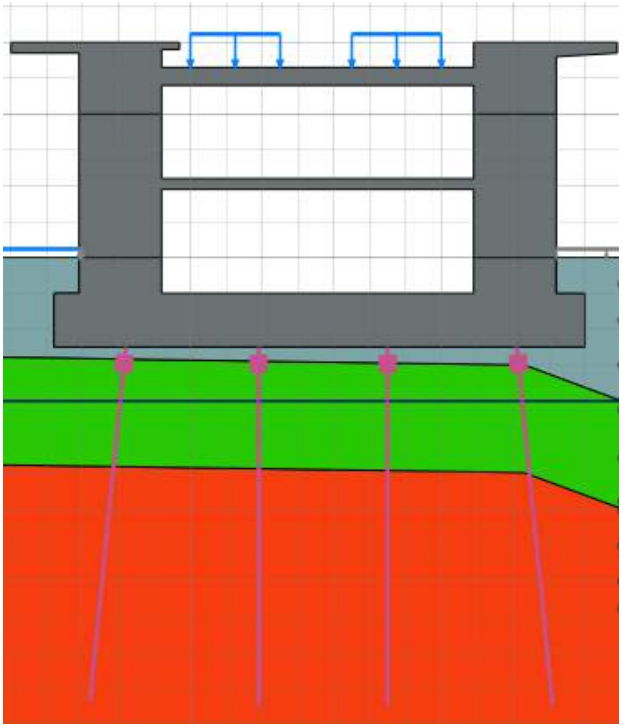

Figure 5.14: Railway bridge represented in FEM.

5.4.3 Modelling of bridge

Railway bridge was executed before the construction of the Parkhotel. It is situated in the very proximity to the construction site (fig. 5.12). The bridge has following geometry properties:

- height: 8,5 m
- width: 13,3 m
- material: concrete C 50/60
- foundation: 4 embedded piles with longitudinal spacing of 3,1 m.

In Plaxis the bridge is designed as a volume element (fig. 5.14) with parameters represented in table 5.11.

As the bridge is an operational structure- a two rails traffic is presented. That means, the additional loads should be applied - one train can be considered as the load of 40 kN/m (fig.5.14).

Table 5.11: Design parameters for the elements with the linear elastic behaviour.

Identification		**Railway Bridge**	**Building Stiffness**	**Backfill Material**	**Basement Hotel**
Identification number		8	9	12	13
Drainage type		Non-porous	Non-porous	Drained	Non-porous
Colour					
Comments					
γ_{unsat}	kN/m³	25,00	0,000	24,00	0,000
γ_{sat}	kN/m³	25,00	0,000	24,00	0,000
Dilatancy cut-off		No	No	No	No
e_{init}		0,5000	0,5000	0,5000	0,5000
e_{min}		0,000	0,000	0,000	0,000
e_{max}		999,0	999,0	999,0	999,0
Rayleigh α		0,000	0,000	0,000	0,000
Rayleigh β		0,000	0,000	0,000	0,000
E	kN/m²	37,00E6	150,0E3	29,96E6	30,00E6
v (nu)		0,2000	0,2000	0,2000	0,2000
G	kN/m²	15,42E6	62,50E3	12,48E6	12,50E6
E_{oed}	kN/m²	41,11E6	166,7E3	33,29E6	33,33E6

5.4.3 Modelling of hotel

For the simplicity of the FE calculation it is convenient to substitute the upper floors of the hotel with the correspondent linear loads that include the building self-weight, including the basement, and other additional loads according to design values (fig. 5.15).

The basement of the “Parkhotel” is a 1,2 m of thickness made of concrete C 20/25. The basement is modelled in Plaxis as a volume element that is not provided by the self-weight (it is included in the applied loads), but only by the stiffness (table 5.11).

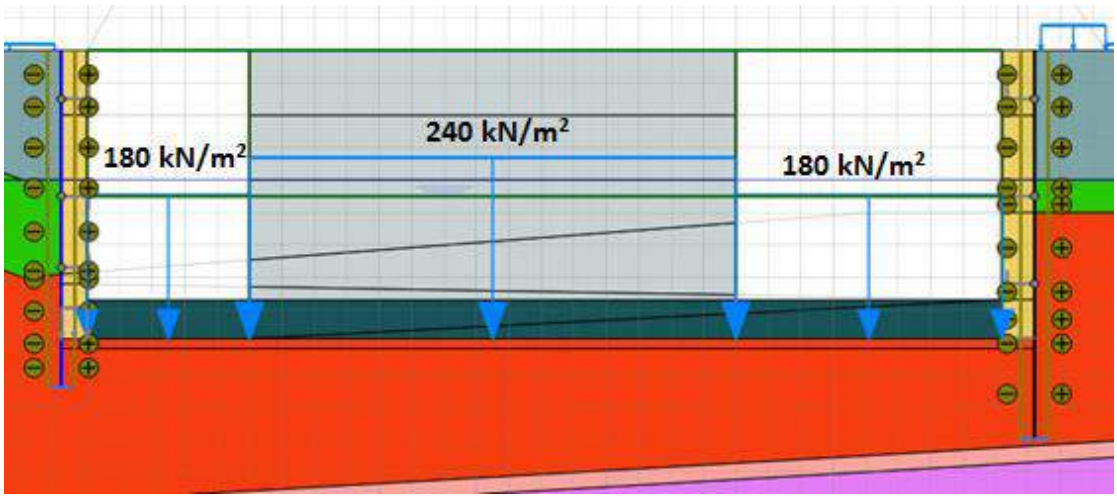

Figure 5.15: Building of the hotel represented in FEM.

In order to obtain realistic behaviour of the interaction soil-structure, it is necessary to model a rigid core of the building. The rigid core is also modelled as a volume element provided by the correspondent stiffness but not by the self-weight (column Building Stiffness in the table 5.11).

Design loads to be applied to the hotel are based on the bearing capacity of soil under the hotel basement (see Annex E) In order to simplify the model they can be divided as following (fig.5.15):

- central part (rigid core): 240 kN/m^2
- lateral parts: 180 kN/m^2

5.4.4 Modelling of retaining walls

Choose of the retaining structures for the excavation site.

The hotel basement is situated at the depth of 8 m under the ground level. Considering the inner city location and restricted space conditions, excavation process should be secured with a shoring system. With regards to adjacent structures (railway bridge, shopping centre) it is recommended to use a low-deformation shoring system to prevent excessive displacements and to resist against the active earth pressure.

As the sheet piling, as well as the soldier pile wall, do not pertains to low-deformation trench piling systems, execution of a bored pile wall is required, which should be reinforced with three-level of grouted anchors or supported with struts.

Between the construction site and the railway bridge a secant pile wall (fig. 5.16), as a shoring system, is chosen, as well as at the side of Lissabonnerstraße, where the shopping

centre is situated. At the side of Wolframstraße there are no structures in vicinity - a soldier pile wall (fig. 5.19), as the shoring system, is chosen.

As a retaining system the three level of struts are used.

Secant pile wall

Secant pile wall will be executed between the bridge and the constructon site, as well as between the shopping centre (Lissabonnerstraße) and the construction site. It is formed by interlocking bored piles (fig. 5.17). Primary piles and secondary piles are executed using the concrete C 20/25.

Wall geometry:

- depth: 10,4 m – bridge side: 8,8 m – shopping centre side
- material of piles: C 20/25

Figure 5.16: Example of a secant pile wall.

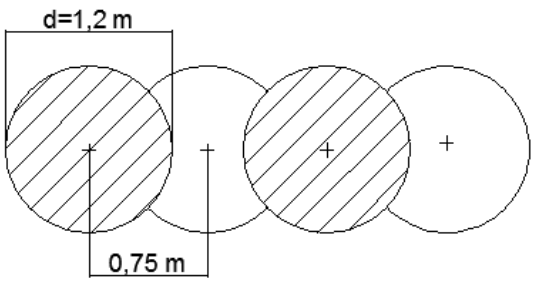

Figure 5.17:Cross-section of the secant pile wall.

In Plaxis the secant pile wall will be design as a plate element (fig. 5.18) with parameters indicated in table 5.12.

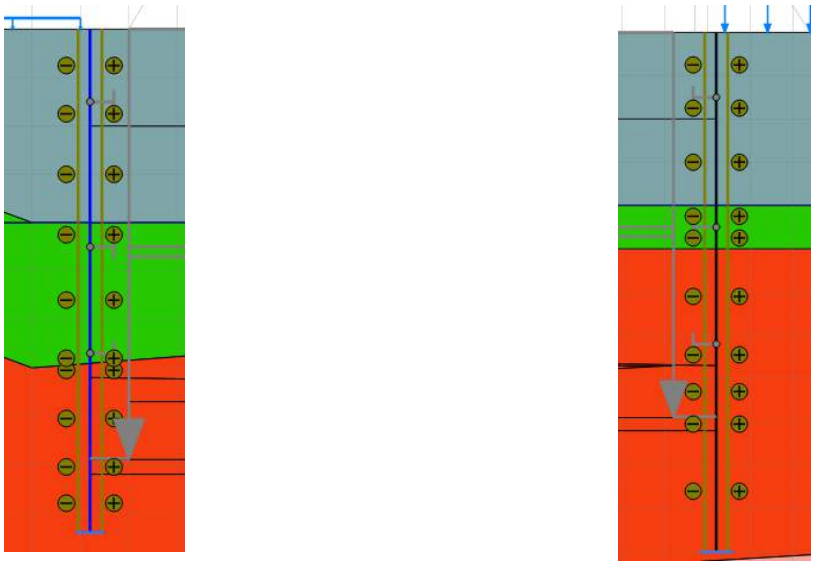

a) b)

Figure 5.18: a) Secant pile wall and b) Soldier pile wall represented in FEMs.

Table 5.12: Design parameters of the plate elements in Plaxis.

Identification		**Secant Pile Wall**	**Soldier Pile Wall**
Identification number		1	2
Comments			
Colour		■	■
Material type		Elastic	Elastic
Isotropic		Yes	Yes
End bearing		No	No
EA_1	kN/m	33,00E6	1,443E6
EA_2	kN/m	33,00E6	1,443E6
EI	kN m²/m	3,320E6	23,97E3
d	m	1,099	0,4465
w	kN/m/m	10,00	0,6000
v (nu)		0,2000	0,1500
Rayleigh α		0,000	0,000
Rayleigh β		0,000	0,000
Identification number		1	2
c	kJ/t/K	0,000	0,000
λ	kW/m/K	0,000	0,000

Soldier pile wall

Soldier pile wall will be executed between the Wolframstraße and the construction site. It is a retaining wall where steel columns and timber lagging are used (fig. 5.19). As a steel column two profiles of U 350 are used (fig. 5.20).

Wall geometry:

- depth: 12 m
- material: columns - 2 U 350/ 2,25 m; timber lagging

In Plaxis the soldier pile wall will be design as a plate element (fig. 5.18) with parameters indicated in table 5.12.

Figure 5.19: Example of a soldier pile wall.

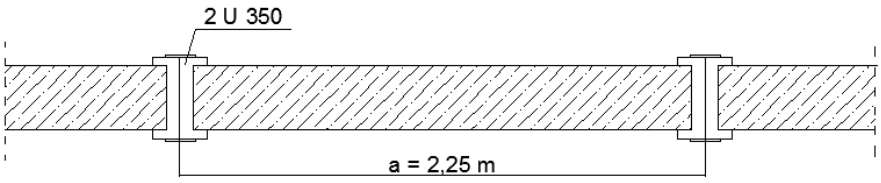

Figure 5.20: Cross-section of the soldier pile wall.

Interface elements

The finite element method is based on continuum mechanics and is incapable to evaluate effectively the loading and displacement conditions induced by relative displacement between materials. Retaining wall used in excavation is stiff, while the adjacent material, soil, is relatively soft. When the retaining wall deforms, relative displacement may be generated between the soil and the wall. To simulate the relative displacement between soil and structure during the excavation, interface elements are used.

As shown in figure 5.21, an interface element is an element that connects structure and soil, with or without thickness, which has a quite large normal stiffness but relatively small shear stiffness; so it can simulate the relative displacement between soil and structures.

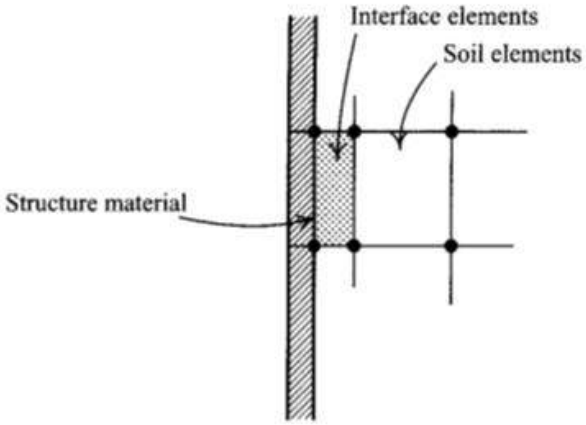

Figure 5.21: Example of an interface element.

The interface element is used to reduce the friction between the structural element and the soil. Introducing interface value, termed as R_{inter}, which has value between 0.01 and 1.0, does this. The lower bound value of 0.01 means there is practically no friction between the structural element and the soil. The upper bound value of 1.0 means the structural element and the soil is completely in contact, it means the soil and the structural component cannot slip one another. In this case, the contact is termed as rigid. Values in between mean the friction is reduced by the given number of R_{inter}, and the structural element and the soil mass can slip between one another. [42]

Numerical exercises show that the lower the interface value, R_{inter}, the larger the soil-structure relative displacements and the bending moment. Therefore, it is important to estimate a reasonably "right" value for this interface or friction reduction factors, R_{inter}.

R_{inter} can be calculated with the following equation:

$$R_{inter} = \frac{tg\delta}{tg\varphi'},$$

where δ is angle of friction between the structure and the soil that depends on the texture of the wall: rough or smooth; and on the type of sliding surface: plane or curved.

In the present case study the secant pile wall is used that, can be considered as a rough wall with the plane sliding surface, therefore $\delta = \frac{2}{3}\varphi'$ [45].

Struts

Horizontal struts, installed in front of the retaining wall, resist the earth pressure on the backs of the wall and pertain to so-called braced excavation methods. [16]

The struts are simulated by Plaxis as "fixed-end anchor" elements (fig. 5.22). That means elastic springs of a given axial stiffness with one fixed (no displacement) end other movable end connected to the pile wall by a given longitudinal distance from the wall.

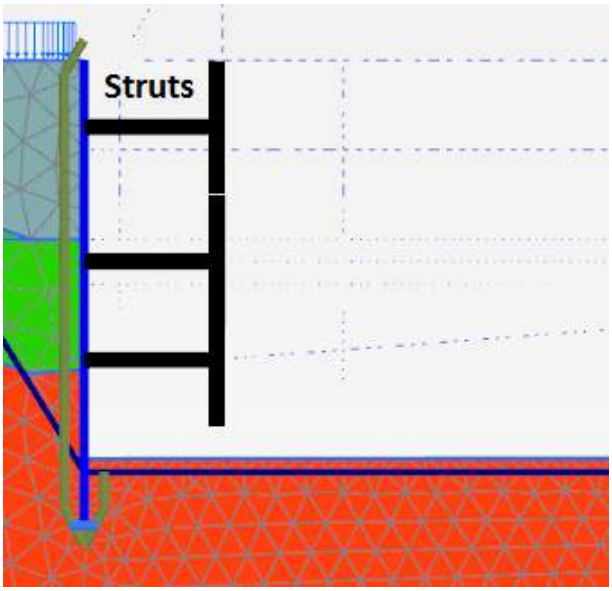

Figure 5.22: Strut element in FEM

The main design parameters of the fixed-end anchor are given in table 5.13 and in Annex D.

Table 5.13: Design parameters of the fixed-end anchor in Plaxis.

Identification		**Strut**
Identification number		3
Comments		
Colour		■
Material type		Elastic
EA	kN	10,00E6
$L_{spacing}$	m	1,000
Identification number		3
c	kJ/t/K	0,000
λ	kW/m/K	0,000
ρ	t/m³	0,000

5.5 Phase construction

In this sub-chapter will be described the construction process of the "Parkhotel". The sequence of construction phases modelled in FEM and their description are placed in the table 5.14 and shown in figures 5.23 – 5.36.

Table 5.14: Sequence of the construction phases in FEM.

Phase	Name of phase	Figure	Description
Initial phase	Geology of the site	Figure 5.24	The geology of the construction site is recreated without any existing structures.
Phase 1	Whish in place bridge	Figure 5.25	The placement of the "wish in place" bridge.
Phase 2	Preliminary excavation	Figure 5.26	The preparation of the construction site for the main works – excavation till the level of 243,40 m a.s.l.
Phase 3	Shoring: installation of the retaining wall	Figure 5.27	Execution of the secant pile wall and the soldier pile wall.
Phase 4	Excavation 1	Figure 5.28	First phase of excavation of 2,5 m (from 244,00 m a.s.l to 241,50 m a.s.l.) is carried out.
Phase 5	Installation of the strut 1[1]	Figure 5.29	After conclusion of the excavation phase the installation of the first level of struts is required.
Phase 6	Excavation 2 with water lowering 1	Figure 5.30	Second phase of excavation of 2,5 m (from 241,50 m a.s.l to 239,00 m a.s.l.) is carried out. Preliminary the first ground water lowering of 1,5 m (from 240,00 m a.s.l to 238,50 m a.s.l.) is achieved.
Phase 7	Installation of the strut 2	Figure 5.31	The installation of the second level of struts is carried out.
Phase 8	Excavation 3 with water lowering 2	Figure 5.32	Third phase of excavation of 2,7 m (from 239,00 m a.s.l to 236,30 m a.s.l.) is carried out. Preliminary the second ground water lowering till 235,80 m a.s.l. is achieved.
Phase 9	Installation of the strut 3	Figure 5.33	The installation of the third level of struts is carried out.
Phase 10	Last excavation with water lowering 3	Figure 5.34	Last phase of excavation of 1,55 m (from 236,30 m a.s.l to 234,75 m a.s.l.) is carried out. Preliminary the third ground water lowering till 234,25 m a.s.l. is achieved.
Phase 11	Construction of the hotel	Figure 5.35	Construction of the hotel.
Phase 12	Backfilling[2]	Figure 5.36	Filling the gap between the hotel walls and the retaining wall with the fill material.

[1] in Plaxis "Strut" names as Fixed-End Anchor.

[2] Backfilling consists of the filling gaps with row concrete C20/25 between the supported wall and the Parkhotel.

Figure 5.23: Sequence of the construction phases in Plaxis.

In the following figures are shown the construction process of the case study.

Figure 5.24 represents the initial phase, where the geology of the constructed area is recreated in Plaxis. In figure 5.25 the "wish in place" bridge is modelled (phase 1). These two phases are preliminary – they recreate conditions that existed before the project starts.

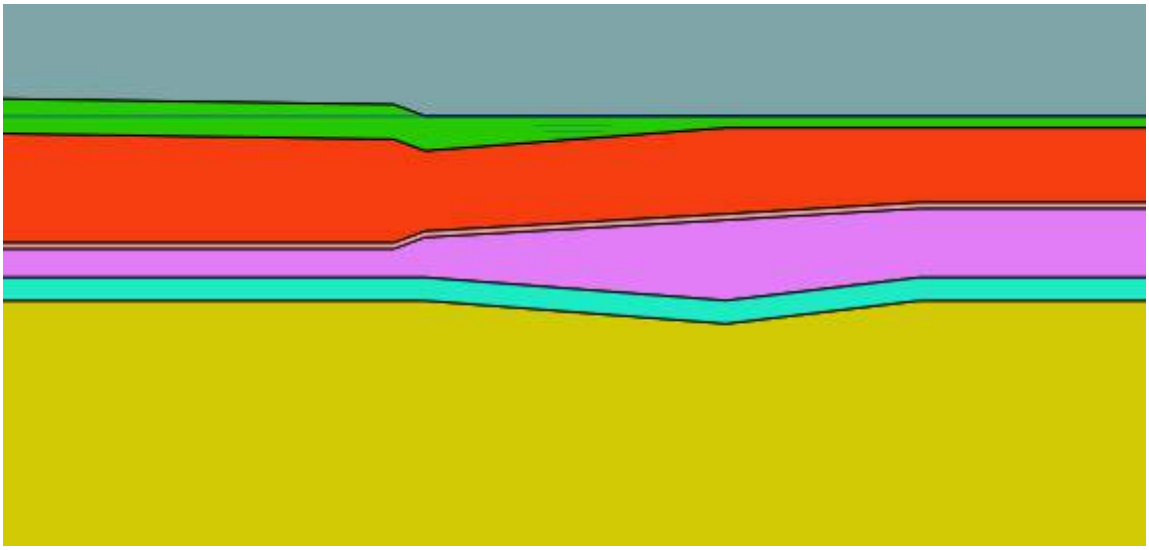

Figure 5.24: Initial phase - Geology of the site.

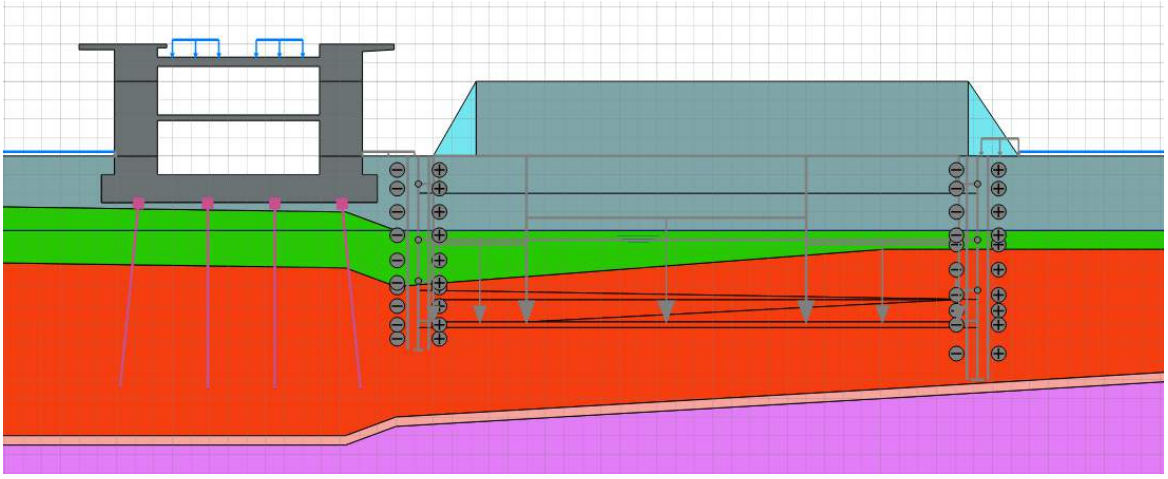

Figure 5.25: Phase 1- Bridge construction.

In phase 2 the preparation of the constructing area starts: the preliminary excavation till the 244 m a.s.l. – so-called "zero level " (the ground floor level of the hotel). According to the project the underground part has about 8 m of depth. In order assure the excavation process and to protect the nearby structures, the shoring system is needed. In figure 5.26 the installation of the retaining walls is shown (phase 3): from the bridge side the secant pile wall is executed, from the other side the soldier pile wall is made. After completion of the shoring system the excavation process stars.

Figure 5.26: Phase 2 – Preliminary excavation.

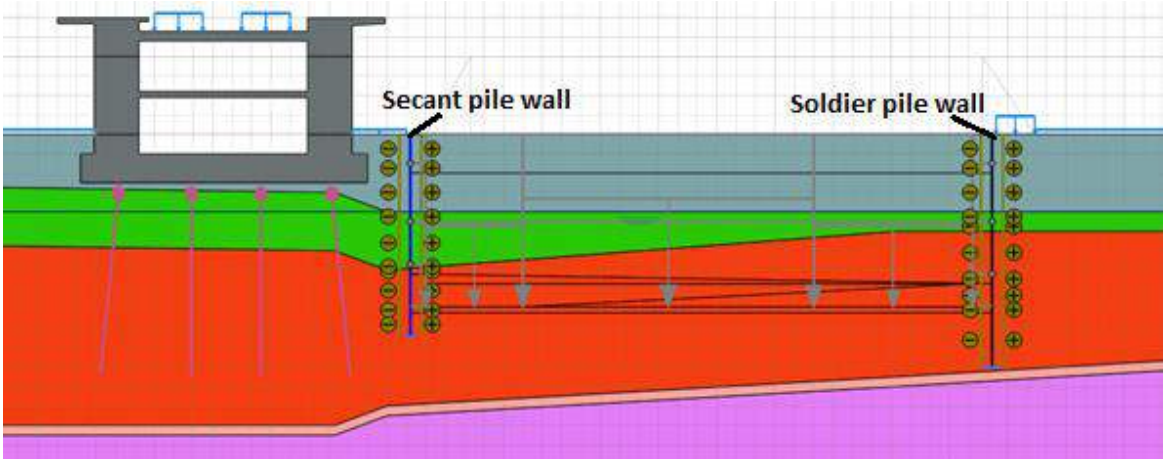

Figure 5.27: Phase 3 – Shoring (execution of the secant pile wall and the soldier pile wall).

The excavation process is conducted in the following steps:

- First, "excavation 1" of 2,5 m is made (phase 4, fig. 5.27).
- Then, the first level of struts is installed (phase 5, fig. 5.28)
- Before the second phase of excavation the ground water lowering of 1,5 m is needed. "Excavation 2" has the 2,5 m of depth (phase 6, fig. 2.29).
- Then, the second level of struts is installed (phase 7, fig. 2.30).
- Third phase of "excavation 3" of 2,7 m is made with preliminary ground water lowering (phase 8, fig. 2.31)
- Third level of struts is installed (phase 9, fig. 2.32).
- Finally, the last ground water lowering and the excavation phase of 1,55 m is made (phase 10, fig. 2.33).

Figure 5.28: Phase 4 - Excavation 1.

Figure 5.29: Phase 5 - Installation of the strut 1.

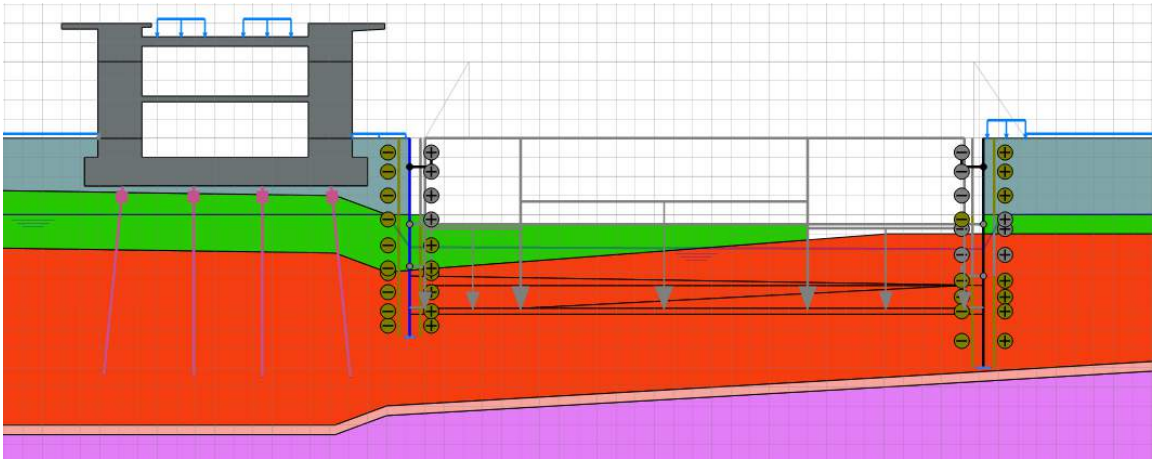

Figure 5.30: Phase 6 - Excavation 2 with water lowering 1.

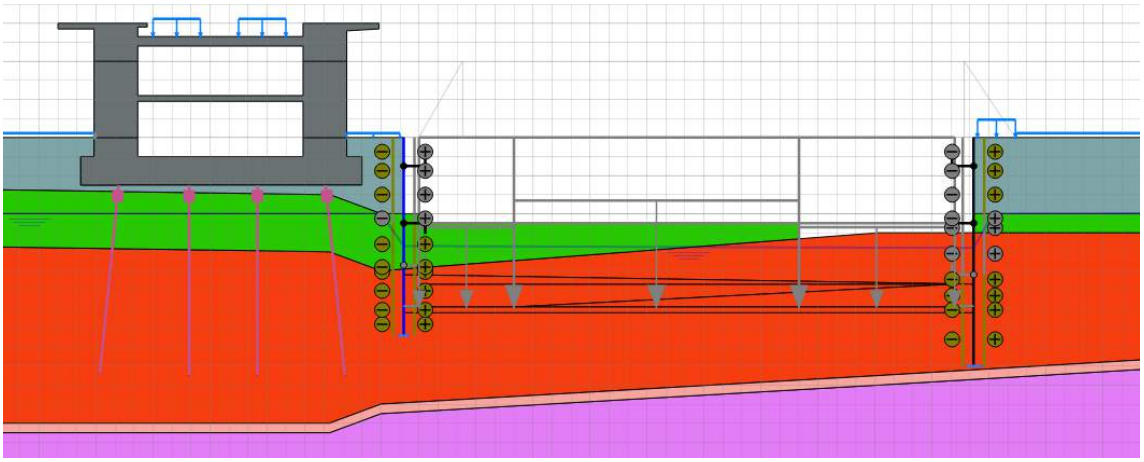

Figure 5.31: Phase 7 - Installation of the strut 2.

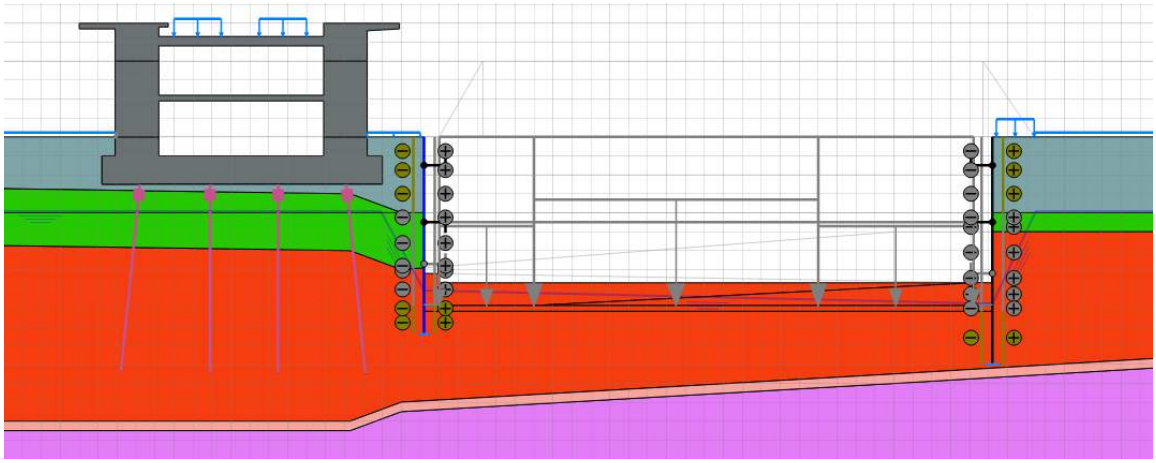

Figure 5.32: Phase 8 - Excavation 3with water lowering 2.

Figure 5.33: Phase 9 - Installation of the strut 3.

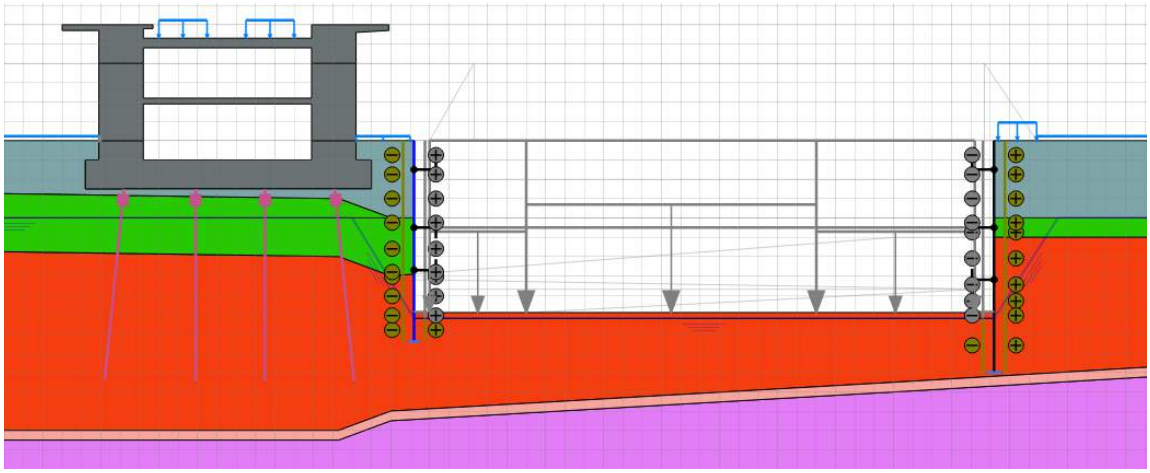

Figure 5.34: Phase 10 - Last excavation with water lowering 3.

Once the excavation pit has the necessary geometry, the construction of the hotel starts (fig. 5.35).

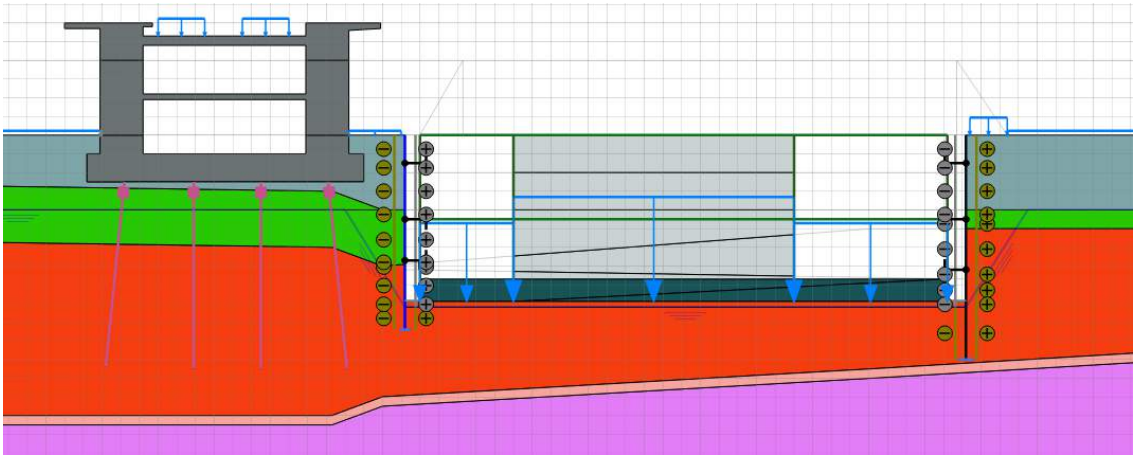

Figure 5.35: Phase 11 - Construction of the Parkhotel.

After termination of the building construction, the space between the buildings walls and the retaining walls is filled with the concrete C20/25 (phase 12, fig. 5.36).

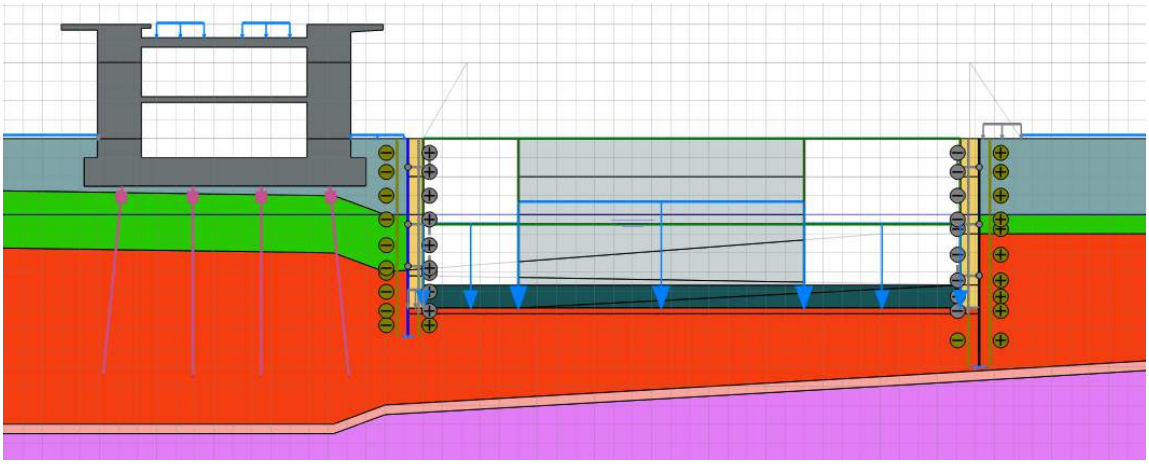

Figure 5.36: Phase 12 – Backfilling.

CHAPTER 6
RISK ANALYSIS

6.1 Investigated parameters for the risk analysis

6.1.1 Introduction

Risk analysis constitutes of the observation of the present case study modelled in FEM Plaxis 2D in three different models of soil: Mohr- Coulomb, Hardening Soil and Hardening Soil Small. For the Hardening Soil Small Model there were four more options studied:

- soil stiffness (E_{50}^{ref}, E_{oed}^{ref}, E_{ur}^{ref}) is increased for 25%,
- soil stiffness is reduced for 25%,
- stiffness of the retaining wall is increased by mince of upgrading the class of concrete to C30/37
- stiffness of the retaining wall is reduced by means of downgrading the class of concrete to C12/16

6.1.2 Bridge

In the railway bridge the following parameters need to be estimated with the quantitative criterions of risk discussed in 2.2:

- Horizontal displacements in section 1, u_x [mm] (fig. 6.1)
  - $u_x < 9$ mm – low level of risk (LR)
  - 9 mm $\leq u_x \leq$ 11,7 mm – intermediate level of risk (IR)
  - $u_x > 11{,}7$ mm – high level of risk (HR)
- Vertical displacements (settlements) in section 2, u_y [mm]

- $u_y < 11$ mm – low level of risk (LR)
- 11 mm $\leq u_y \leq$ 14,3 mm – intermediate level of risk (IR)
- $u_y > 14{,}3$ mm – high level of risk (HR)

- Angular distortion, β [-]
  - $\beta > 1/500$ – low level of risk (LR)
  - $1/500 \leq \beta \leq 1/300$ – intermediate level of risk (IR)
  - $\beta < 1/300$ – high level of risk (HR)
- Compressive stress in section 3, σ_c [kN/m^2]
  - $\sigma_c < 50000$ kN/m^2 – low level of risk (LR)
  - 50000 kN/m^2 $\leq \sigma_c \leq$ 65000 kN/m^2 – intermediate level of risk (IR)
  - $\sigma_c > 65000$ kN/m^2 – high level of risk (HR)
- Tensile stress in section 3, σ_t [kN/m^2]
  - $\sigma_t < 4100$ kN/m^2 – low level of risk (LR)
  - 4100 kN/m^2 $\leq \sigma_t \leq$ 5330 kN/m^2 – intermediate level of risk (IR)
  - $\sigma_t > 5330$ kN/m^2 – high level of risk (HR)

In table 6.1 the summary of the quantitative criterions of risk for the interested parameters is represented.

Table 6.1: Quantitative criterions for risk evaluation for the bridge.

Parameter	Low Level of Risk (LR)	Intermediate Level of Risk (IR)	High Level of Risk (HR)
Horizontal displacements, u_x [mm]	$u_x < 9$	$9 \leq u_x \leq 11{,}7$	$u_x > 11{,}7$
Vertical displacements, u_y [mm]	$u_y < 11$	$11 \leq u_y \leq 14{,}3$	$u_y > 14{,}3$
Angular distortion, β [-]	$\beta < 1/500$	$1/500 \leq \beta \leq 1/300$	$\beta > 1/300$
Compressive stress, σ_c [kN/m^2]	$\sigma_c < 50000$	$50000 \leq \sigma_c \leq 65000$	$\sigma_c > 65000$
Tensile stress, σ_t [kN/m^2]	$\sigma_t < 4100$	$4100 \leq \sigma_t \leq 5330$	$\sigma_t > 5330$

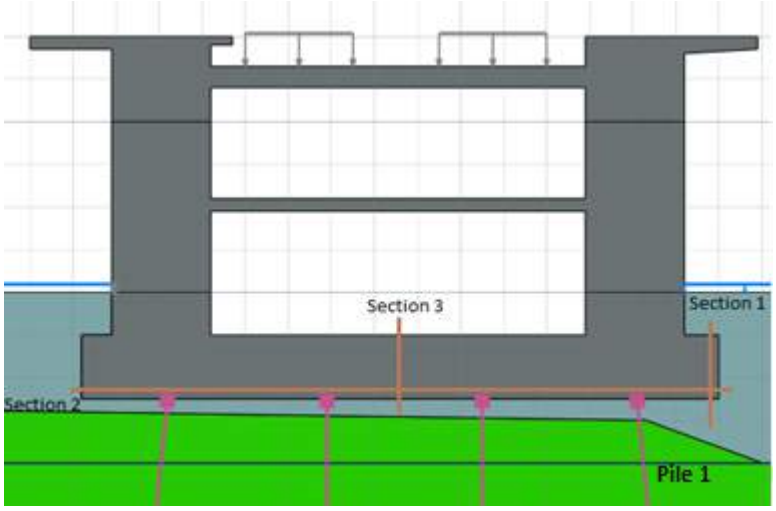

Figure 6.1: Section of interest in the bridge.

6.1.3 Piles

Pile 1 (fig. 6.1) is the most affected by the excavation process because it is the closest pile to the excavation pit. In the pile 1 the following parameters need to be estimated:

- Horizontal displacement, u_x [mm]
- $u_x < 8$ mm – low level of risk (LR)
- 8 mm $\leq u_x \leq$ 10,4 mm – intermediate level of risk (IR)
- $u_x >$ 10,4 mm – high level of risk (HR)
- Lateral skin friction, T_{skin} [kN/m^2]
- $T_{skin} <$ 65 kN/m^2 – low level of risk (LR)
- 65 kN/m^2 $\leq T_{skin} \leq$ 84,5 kN/m^2 – intermediate level of risk (IR)
- $T_{skin} >$ 84,5 kN/m^2 – high level of risk (HR)

In table 6.2 the summary of the quantitative criterions of risk for the interested parameters is represented.

Table 6.2: Quantitative criterions for risk evaluation for piles.

Parameter	Low Level of Risk (LR)	Intermediate Level of Risk (IR)	High Level of Risk (HR)
Horizontal displacements, u_x [mm]	$u_x < 8$	$9 \leq u_x \leq 10,4$	$u_x > 10,4$
Lateral skin friction, T_{skin} [kN/m^2]	$T_{skin} < 65$	$65 \leq T_{skin} \leq 84,5$	$T_{skin} > 84,5$

6.1.4 Secant pile wall

In the secant pile wall only the horizontal displacement, u_x [mm] needs to be controlled:

- $u_x <$ 10,4 mm – low level of risk (LR)

- 10,4 mm ≤ u_x ≤ 13,52 mm – intermediate level of risk (IR)
- u_x > 13,52 mm – high level of risk (HR)

Table 6.3: Quantitative criterions for risk evaluation for secant pile wall.

Parameter	Low Level of Risk (LR)	Intermediate Level of Risk (IR)	High Level of Risk (HR)
Horizontal displacements, u_x [mm]	u_x< 10,4	10,4 ≤ u_x ≤ 13,52	u_x > 13,52

6.1.5 Hotel

In the hotel the following parameters need to be estimated with the quantitative criterions of risk discussed in 2.2:

- Horizontal displacements in section 1 and 2, u_x [mm] (fig.6.2)
  - u_x < 3 mm – low level of risk (LR)
  - 3 mm ≤ u_x ≤ 3,9 mm – intermediate level of risk (IR)
  - u_x > 3,9 mm – high level of risk (HR)
- Vertical displacements (settlements) in section 2, u_y [mm]
  - u_y < 8,5 mm – low level of risk (LR)
  - 8,5 mm ≤ u_y ≤ 11,05 mm – intermediate level of risk (IR)
  - u_y > 11,05 mm – high level of risk (HR)
- Angular distortion, β [-]
  - β > 1/500 – low level of risk (LR)
  - 1/500 ≤ β ≤ 1/300 – intermediate level of risk (IR)
  - β > 1/300 – high level of risk (HR)
- Compressive stress in section 3, σ_c [kN/m^2]
  - σ_c < 20000 kN/m^2 – low level of risk (LR)
  - 20000 kN/m^2 ≤ σ_c ≤ 26000 kN/m^2 – intermediate level of risk (IR)
  - σ_c > 26000 kN/m^2 – high level of risk (HR)
- Tensile stress in section 3, σ_t [kN/m^2]
  - σ_t < 2200 kN/m^2 – low level of risk (LR)
  - 2200 kN/m^2 ≤ σ_t ≤ 2860 kN/m^2 – intermediate level of risk (IR)
  - σ_t > 2860 kN/m^2 – high level of risk (HR)

In table 6.4 the summary of the quantitative criterions of risk for the interested parameters are represented.

Table 6.4: Quantitative criterions for risk evaluation for the hotel.

Parameter	Low Level of Risk (LR)	Intermediate Level of Risk (IR)	High Level of Risk (HR)
Horizontal displacements, u_x [mm]	$u_x < 3$	$3 \leq u_x \leq 3{,}9$	$u_x > 3{,}9$
Vertical displacements, u_y [mm]	$u_y < 8{,}5$	$8{,}5 \leq u_y \leq 11{,}05$	$u_y > 11{,}05$
Angular distortion, β [-]	$\beta < 1/500$	$1/500 \leq \beta \leq 1/300$	$\beta > 1/300$
Compressive stress, σ_c [kN/m^2]	$\sigma_c < 20000$	$20000 \leq \sigma_c \leq 26000$	$\sigma_c > 26000$
Tensile stress, σ_t [kN/m^2]	$\sigma_t < 2200$	$2200 \leq \sigma_t \leq 2860$	$\sigma_t > 2860$

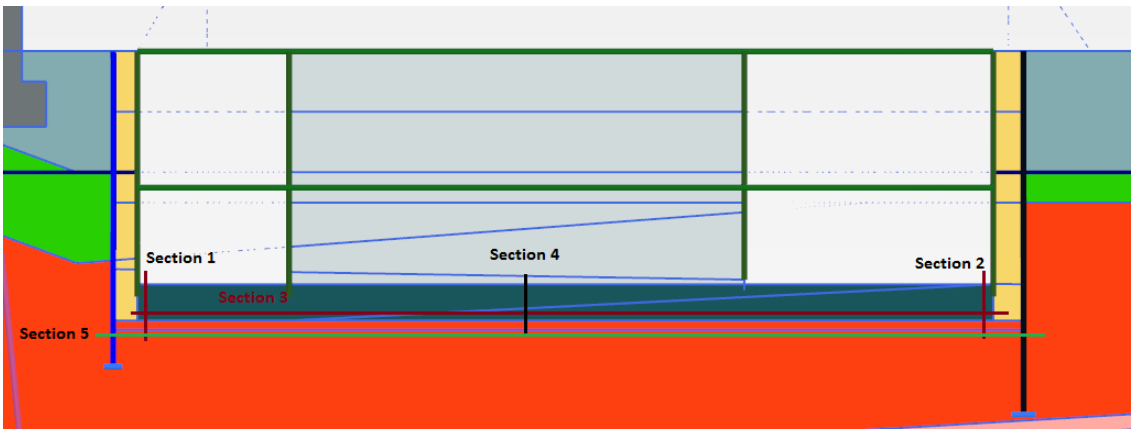

Figure 6.2: Sections of interest in the hotel.

6.1.6 Soil capacity

The bearing capacity of soil in section 5 - under the hotel basement (fig. 6.2) is taken under the study. The limit values for the bearing capacity of soil under the hotel basement is represented in Annex E.

- Bearing capacity of soil in the lateral parts of section 5 (see fig.6.2), q [kN/m^2]
  - $q < 138{,}5$ kN/m^2 – low level of risk (LR)
  - $138{,}5$ kN/m^2 $\leq q \leq 180$ kN/m^2 – intermediate level of risk (IR)
  - $q > 180$ kN/m^2 – high level of risk (HR)
- Bearing capacity of soil in the intermediate part of section 5, q [kN/m^2]
  - $q < 184{,}6$ kN/m^2 – low level of risk (LR)
  - $184{,}6$ kN/m^2 $\leq q \leq 240$ kN/m^2 – intermediate level of risk (IR)
  - $q > 240$ kN/m^2 – high level of risk (HR)

The summary of the quantitative criterions of risk is represented in table 6.5.

Table 6.5: Quantitative criterions for risk evaluation for soil.

Parameter	Low Level of Risk (LR)	Intermediate Level of Risk (IR)	High Level of Risk (HR)
Bearing capacity in the soil of lateral parts, q [kN/m^2]	$q < 138,5$	$138,5 \leq q \leq 180$	$q > 180$
Bearing capacity in the soil of the intermediate part, q [kN/m^2]	$q < 184,6$	$184,6 \leq q \leq 240$	$q > 240$

6.2 Results

6.2.1 Bridge

In figures below are represented results for the bridge, where the soil was modelled with Hardening Soil Small Model for the last construction phase (fig. 6.3 – 6.5).

The entire calculation results are in Annex G1.

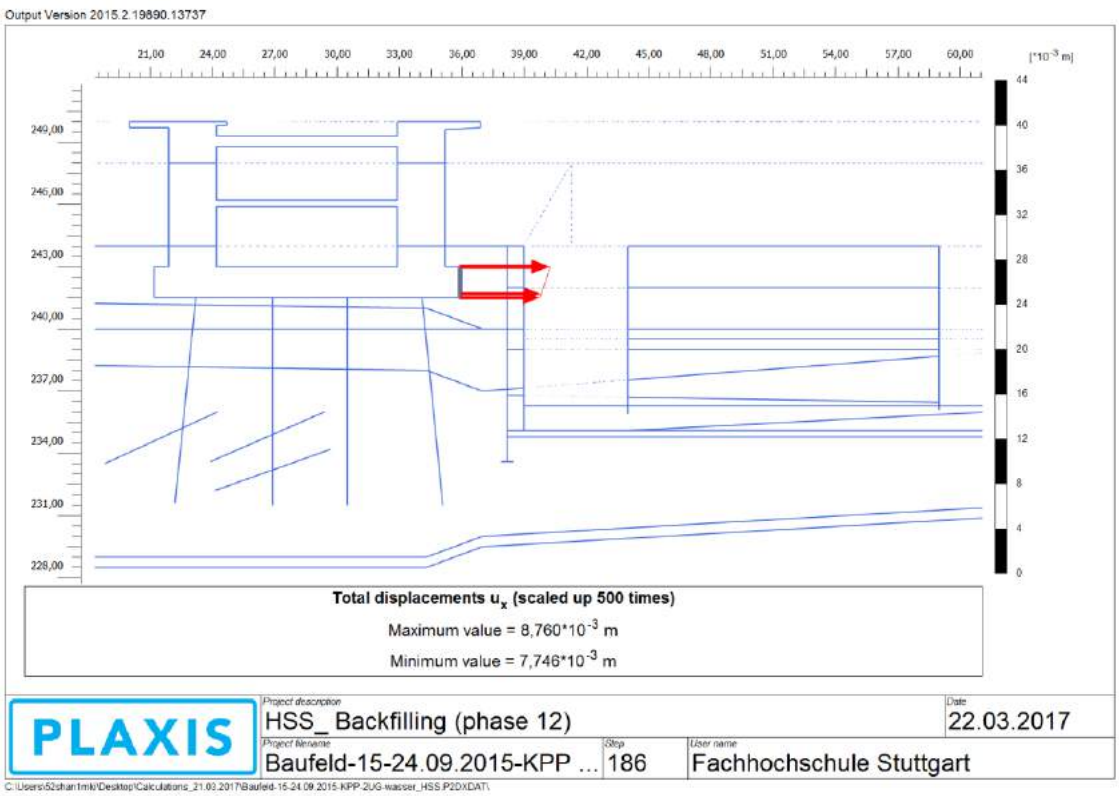

Figure 6.3: Horizontal displacement of the bridge in phase 12.

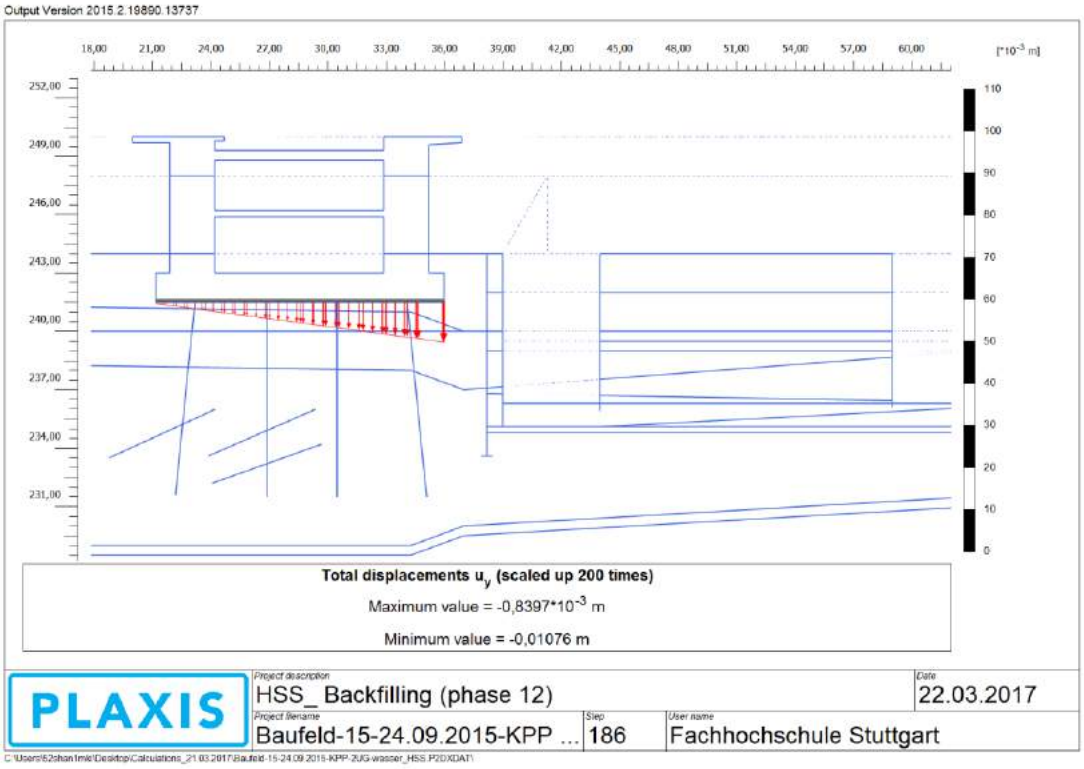

Figure 6.4: Vertical displacement of the bridge in phase 12.

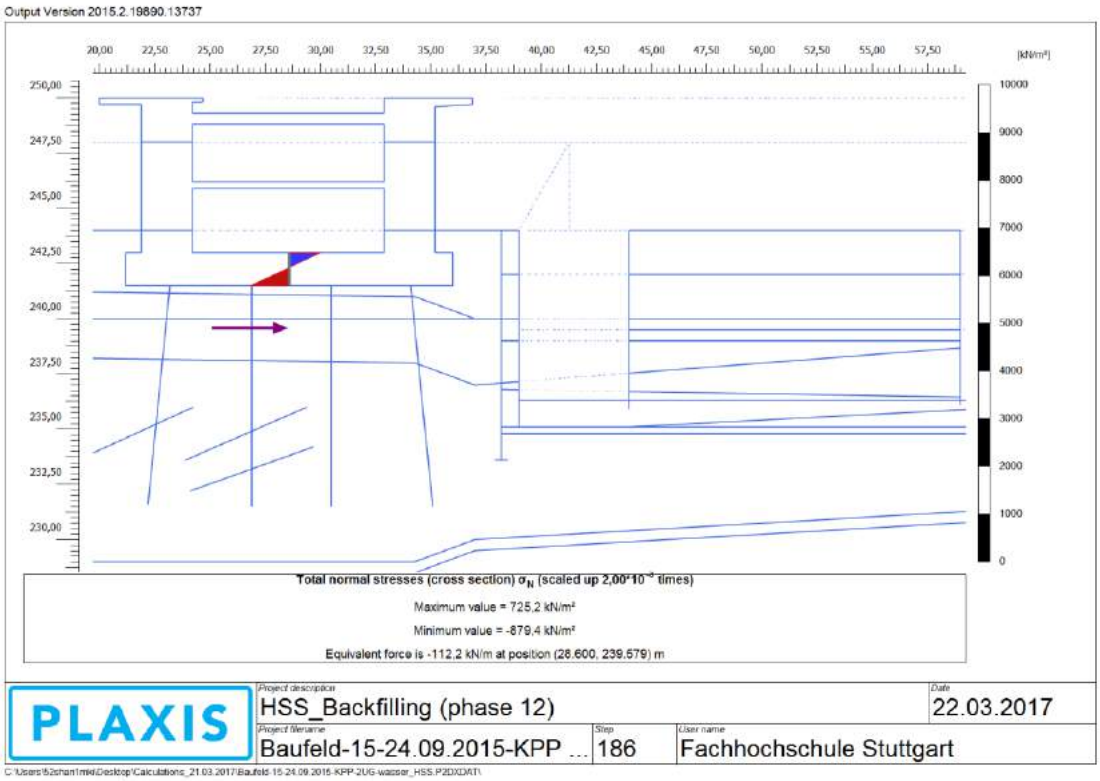

Figure 6.5: Stresses in the bridge in phase 12.

The entire results for all models are summarized in tables below (tables 6.6 – 6.19).

Table 6.6: Horizontal and vertical displacements and angular distortion of the bridge for Mohr-Coulomb Model

MOHR-COULOMB MODEL_BRIDGE						
Stage	Horizontal displacement in section 1, u_x [mm]		Vertical displacement in section 2, u_y [mm]		Angular distortion, β [-]	
	$u_{x,max}$	Risk Level	$u_{y,max}$	Risk Level	β	Risk Level
Phase 1	-0,93	LR	6,60	LR	1/2079	LR
Phase 2	2,10	LR	15,20	IR	1/1618	LR
Phase 3	2,66	LR	11,93	IR	1/2519	LR
Phase 4	3,86	LR	17,80	HR	1/1353	LR
Phase 5	3,61	LR	17,95	HR	1/1335	LR
Phase 6	4,89	LR	20,44	HR	1/1125	LR
Phase 7	4,91	LR	20,28	HR	1/1127	LR
Phase 8	5,94	LR	20,42	HR	1/1152	LR
Phase 9	5,98	LR	20,26	HR	1/1168	LR
Phase 10	6,67	LR	18,20	HR	1/1337	LR
Phase 11	14,80	HR	-13,02	IR	1/903	LR
Phase 12	16,60	HR	-12,14	IR	1/839	LR

Table 6.7: Compressive and tensile stresses of the bridge for Mohr-Coulomb Model

MOHR-COULOMB MODEL_BRIDGE				
Stage	Compressive stresses in section 3, σ_c [kN/m^2]		Tensile stresses in section 3, σ_t [kN/m^2]	
	$\sigma_{c,\ max}$	Risk Level	$\sigma_{c,\ max}$	Risk Level
Phase 1	912,20	LR	726,00	LR
Phase 2	695,60	LR	552,60	LR
Phase 3	739,00	LR	583,5	LR
Phase 4	691,40	LR	560,90	LR
Phase 5	691,60	LR	561,00	LR
Phase 6	687,00	LR	560,50	LR
Phase 7	689,00	LR	562,60	LR
Phase 8	694,00	LR	564,40	LR
Phase 9	696,80	LR	566,30	LR
Phase 10	723,00	LR	589,20	LR
Phase 11	929,60	LR	749,70	LR
Phase 12	926,60	LR	788,50	LR

Table 6.8: Horizontal and vertical displacements and angular distortion of the bridge for Hardening Soil Model.

HARDENING SOIL MODEL_BRIDGE						
Stage	Horizontal displacement in section 1, u_x [mm]		Vertical displacement in section 2, u_y [mm]		Angular distortion, β [-]	
	$u_{x,max}$	Risk Level	$u_{y,max}$	Risk Level	β	Risk Level
Phase 1	1,16	LR	2,46	LR	1/4785	LR
Phase 2	-1,17	LR	6,14	LR	1/4016	LR
Phase 3	-0,67	LR	4,73	LR	1/6369	LR
Phase 4	-0,36	LR	6,90	LR	1/3759	LR
Phase 5	-0,33	LR	6,88	LR	1/3781	LR
Phase 6	0,73	LR	7,11	LR	1/3521	LR
Phase 7	0,76	LR	7,00	LR	1/3610	LR
Phase 8	1,57	LR	5,90	LR	1/3861	LR
Phase 9	1,60	LR	5,80	LR	1/3953	LR
Phase 10	2,00	LR	4,50	LR	1/4926	LR
Phase 11	6,90	LR	-10,50	LR	1/1629	LR
Phase 12	9,10	IR	-10,61	LR	1/1471	LR

Table 6.9: Compressive and tensile stresses of the bridge for Hardening Soil Model.

HARDENING SOIL MODEL_BRIDGE				
Stage	Compressive stresses in section 3, σ_c [kN/m^2]		Tensile stresses in section 3, σ_t [kN/m^2]	
	$\sigma_{c,\ max}$	Risk Level	$\sigma_{c,\ max}$	Risk Level
Phase 1	930,90	LR	682,90	LR
Phase 2	739,70	LR	506,80	LR
Phase 3	781,70	LR	538,20	LR
Phase 4	741,90	LR	535,70	LR
Phase 5	742,10	LR	536,00	LR
Phase 6	716,90	LR	522,80	LR
Phase 7	719,80	LR	525,60	LR
Phase 8	700,10	LR	502,40	LR
Phase 9	703,30	LR	505,50	LR
Phase 10	722,90	LR	523,80	LR
Phase 11	915,50	LR	668,20	LR
Phase 12	899,10	LR	732,90	LR

Table 6.10: Horizontal and vertical displacements and angular distortion of the bridge for Hardening Soil Small Model.

HARDENING SOIL SMALL MODEL_BRIDGE						
Stage	Horizontal displacement in section 1, u_x [mm]		Vertical displacement in section 2, u_y [mm]		Angular distortion, β [-]	
	$u_{x,max}$	Risk Level	$u_{y,max}$	Risk Level	β	Risk Level
Phase 1	1,25	LR	2,60	LR	1/4902	LR
Phase 2	-1,21	LR	5,90	LR	1/4049	LR
Phase 3	-0,74	LR	4,69	LR	1/5882	LR
Phase 4	-0,64	LR	6,80	LR	1/3610	LR
Phase 5	-0,64	LR	6,80	LR	1/3610	LR
Phase 6	0,43	LR	6,89	LR	1/3497	LR
Phase 7	0,43	LR	6,90	LR	1/3484	LR
Phase 8	1,18	LR	5,70	LR	1/2788	LR
Phase 9	1,20	LR	5,60	LR	1/3891	LR
Phase 10	1,61	LR	4,26	LR	1/4854	LR
Phase 11	6,40	LR	-10,56	LR	1/1675	LR
Phase 12	8,80	LR	-10,76	LR	1/1493	LR

HARDENING SOIL SMALL MODEL_BRIDGE

Table 6.11: Compressive and tensile stresses of the bridge for Hardening Soil Small Model. ```

HARDENING SOIL SMALL MODEL_BRIDGE				
Stage	Compressive stresses in section 3, σ_c [kN/m^2]		Tensile stresses in section 3, σ_t [kN/m^2]	
	$\sigma_{c,\ max}$	Risk Level	$\sigma_{c,\ max}$	Risk Level
Phase 1	864,8	LR	621,70	LR
Phase 2	654,1	LR	433,70	LR
Phase 3	703,00	LR	473,20	LR
Phase 4	647,20	LR	458,30	LR
Phase 5	647,60	LR	458,70	LR
Phase 6	631,00	LR	456,50	LR
Phase 7	631,80	LR	457,20	LR
Phase 8	609,10	LR	429,10	LR
Phase 9	612,10	LR	431,90	LR
Phase 10	643,50	LR	461,20	LR
Phase 11	802,20	LR	654,30	LR
Phase 12	879,40	LR	725,20	LR

Table 6.12: Horizontal and vertical displacements and angular distortion of the bridge for Hardening Soil Small Model with increased soil stiffness.

HARDENING SOIL SMALL MODEL +25% Esoil_BRIDGE						
Stage	Horizontal displacement in section 1, u_x [mm]		Vertical displacement in section 2, u_y [mm]		Angular distortion, β [-]	
	$u_{x,max}$	Risk Level	$u_{y,max}$	Risk Level	β	Risk Level
Phase 1	1,00	LR	2,04	LR	1/6098	LR
Phase 2	-0,97	LR	4,76	LR	1/5076	LR
Phase 3	-0,59	LR	3,76	LR	1/7463	LR
Phase 4	-0,48	LR	5,48	LR	1/4525	LR
Phase 5	-0,46	LR	5,47	LR	1/4545	LR
Phase 6	0,43	LR	5,55	LR	1/4386	LR
Phase 7	0,43	LR	5,52	LR	1/3663	LR
Phase 8	1,07	LR	4,56	LR	1/4785	LR
Phase 9	1,09	LR	4,49	LR	1/4255	LR
Phase 10	1,42	LR	3,40	LR	1/3135	LR
Phase 11	5,26	LR	-8,45	LR	1/1887	LR
Phase 12	6,61	LR	-8,64	LR	1/1842	LR

Table 6.13: Compressive and tensile stresses of the bridge for Hardening Soil Small Model with increased soil stiffness.

HARDENING SOIL SMALL MODEL +25% Esoil_BRIDGE				
Stage	Compressive stresses in section 3, σ_c [kN/m^2]		Tensile stresses in section 3, σ_t [kN/m^2]	
	$\sigma_{c,\ max}$	Risk Level	$\sigma_{c,\ max}$	Risk Level
Phase 1	869,10	LR	627,20	LR
Phase 2	666,20	LR	444,70	LR
Phase 3	712,70	LR	481,60	LR
Phase 4	661,00	LR	470,10	LR
Phase 5	661,60	LR	470,60	LR
Phase 6	664,80	LR	468,20	LR
Phase 7	645,60	LR	469,00	LR
Phase 8	622,70	LR	441,10	LR
Phase 9	625,50	LR	443,80	LR
Phase 10	654,20	LR	470,60	LR
Phase 11	888,70	LR	651,80	LR
Phase 12	872,00	LR	775,60	LR

Table 6.14: Horizontal and vertical displacements and angular distortion of the bridge for Hardening Soil Small Model with reduced soil stiffness.

HARDENING SOIL SMALL MODEL -25% Esoil_BRIDGE						
Stage	Horizontal displacement in section 1, u_x [mm]		Vertical displacement in section 2, u_y [mm]		Angular distortion, β [-]	
	$u_{x,max}$	Risk Level	$u_{y,max}$	Risk Level	β	Risk Level
Phase 1	1,09	LR	2,24	LR	1/4785	LR
Phase 2	-1,04	LR	6,03	LR	1/3831	LR
Phase 3	-0,50	LR	4,73	LR	1/5682	LR
Phase 4	-0,18/0,26	LR	6,79	LR	1/3497	LR
Phase 5	-0,16/0,28	LR	6,77	LR	1/3509	LR
Phase 6	1,19	LR	6,47	LR	1/3663	LR
Phase 7	1,20	LR	6,45	LR	1/6897	LR
Phase 8	2,19	LR	4,54	LR	1/4878	LR
Phase 9	2,20	LR	4,51	LR	1/11364	LR
Phase 10	2,79	LR	2,77	LR	1/1119	LR
Phase 11	8,09	LR	-12,32	IR	1/1344	LR
Phase 12	10,48	LR	-12,42	IR	1/1253	LR

Table 6.15: Compressive and tensile stresses of the bridge for Hardening Soil Small Model with reduced soil stiffness.

HARDENING SOIL SMALL MODEL -25% Esoil_BRIDGE				
Stage	Compressive stresses in section 3, σ_c [kN/m^2]		Tensile stresses in section 3, σ_t [kN/m^2]	
	$\sigma_{c,\ max}$	Risk Level	$\sigma_{c,\ max}$	Risk Level
Phase 1	867,00	LR	625,70	LR
Phase 2	644,40	LR	430,00	LR
Phase 3	696,40	LR	473,00	LR
Phase 4	636,30	LR	455,10	LR
Phase 5	636,60	LR	455,40	LR
Phase 6	618,80	LR	450,60	LR
Phase 7	619,40	LR	451,10	LR
Phase 8	606,50	LR	431,50	LR
Phase 9	607,60	LR	432,60	LR
Phase 10	642,00	LR	464,70	LR
Phase 11	883,30	LR	661,00	LR
Phase 12	869,30	LR	720,30	LR

Table 6.16: Horizontal and vertical displacements and angular distortion of the bridge for Hardening Soil Small Model with the secant pile wall made of concrete C30/37.

HARDENING SOIL SMALL MODEL– C30/37_BRIDGE						
Stage	Horizontal displacement in section 1, u_x [mm]		Vertical displacement in section 2, u_y [mm]		Angular distortion, β [-]	
	$u_{x,max}$	Risk Level	$u_{y,max}$	Risk Level	β	Risk Level
Phase 1	1,26	LR	2,59	LR	1/4926	LR
Phase 2	-1,21	LR	5,87	LR	1/4082	LR
Phase 3	-0,74	LR	4,67	LR	1/5917	LR
Phase 4	-0,66	LR	6,80	LR	1/3597	LR
Phase 5	-0,64	LR	6,78	LR	1/3623	LR
Phase 6	0,41	LR	6,92	LR	1/3460	LR
Phase 7	0,41	LR	6,89	LR	1/3497	LR
Phase 8	1,15	LR	5,72	LR	1/3759	LR
Phase 9	1,17	LR	5,64	LR	1/3831	LR
Phase 10	1,58	LR	4,27	LR	1/4831	LR
Phase 11	6,37	LR	-10,24	LR	1/1736	LR
Phase 12	8,74	LR	-10,74	LR	1/1493	LR

Table 6.17: Compressive and tensile stresses of the bridge for Hardening Soil Small Model with the secant pile wall made of concrete C30/37.

HARDENING SOIL SMALL MODEL – C30/37_BRIDGE				
Stage	Compressive stresses in section 3, σ_c [kN/m^2]		Tensile stresses in section 3, σ_t [kN/m^2]	
	$\sigma_{c,\ max}$	Risk Level	$\sigma_{c,\ max}$	Risk Level
Phase 1	864,8	LR	621,70	LR
Phase 2	654,1	LR	433,70	LR
Phase 3	703,00	LR	433,70	LR
Phase 4	672,20	LR	458,20	LR
Phase 5	647,70	LR	458,70	LR
Phase 6	630,90	LR	455,90	LR
Phase 7	631,70	LR	456,70	LR
Phase 8	609,40	LR	428,70	LR
Phase 9	612,40	LR	431,60	LR
Phase 10	644,00	LR	461,00	LR
Phase 11	892,70	LR	653,90	LR
Phase 12	879,60	LR	724,70	LR

Table 6.18: Horizontal and vertical displacements and angular distortion of the bridge for Hardening Soil Small Model with the secant pile wall made of concrete C12/16.

HARDENING SOIL SMALL MODEL– C12/16_BRIDGE						
Stage	Horizontal displacement in section 1, u_x [mm]		Vertical displacement in section 2, u_y [mm]		Angular distortion, β [-]	
	$u_{x,max}$	Risk Level	$u_{y,max}$	Risk Level	β	Risk Level
Phase 1	1,26	LR	2,59	LR	1/4926	LR
Phase 2	-1,21	LR	5,87	LR	1/4082	LR
Phase 3	-0,74	LR	4,67	LR	1/5917	LR
Phase 4	-0,66	LR	6,80	LR	1/3597	LR
Phase 5	-0,64	LR	6,78	LR	1/3623	LR
Phase 6	0,99	LR	6,91	LR	1/3472	LR
Phase 7	9,37	LR	6,88	LR	1/3497	LR
Phase 8	1,21	LR	5,68	LR	1/3788	LR
Phase 9	1,23	LR	5,59	LR	1/3876	LR
Phase 10	1,64	LR	4,22	LR	1/4902	LR
Phase 11	6,44	LR	-10,59	LR	1/1667	LR
Phase 12	8,79	LR	-10,79	LR	1/1488	LR

Table 6.19: Compressive and tensile stresses of the bridge for Hardening Soil Small Model with the secant pile wall made of concrete C12/16.

HARDENING SOIL SMALL MODEL– C12/16_BRIDGE				
Stage	Compressive stresses in section 3, σ_c [kN/m^2]		Tensile stresses in section 3, σ_t [kN/m^2]	
	$\sigma_{c,\,max}$	Risk Level	$\sigma_{c,\,max}$	Risk Level
Phase 1	864,8	LR	621,70	LR
Phase 2	654,1	LR	433,70	LR
Phase 3	703,00	LR	473,20	LR
Phase 4	647,10	LR	458,30	LR
Phase 5	647,60	LR	458,70	LR
Phase 6	631,00	LR	456,90	LR
Phase 7	631,80	LR	457,60	LR
Phase 8	608,80	LR	429,40	LR
Phase 9	611,80	LR	432,20	LR
Phase 10	643,60	LR	462,00	LR
Phase 11	892,40	LR	655,10	LR
Phase 12	879,60	LR	725,90	LR

For all studied parameters the maximum values are detected in the last phase (Backfilling).

In tables below the maximum values for all models of soil and variations are collected. Moreover, the value of the Hardening Soil Model is chosen as a reference value (highlighted) and the difference in percentage is calculated between the reference value and the values obtained in the other models and variations (tabales 6.20 – 6.23).

In tables the following abbreviation are used:

- MC – Mohr-Coulomb Model
- HS – Hardening Soil Model
- HSS – Hardening Soil Small Model
- HSS_+25% – Hardening Soil Small Model with increased soil stiffness for 25%
- HSS_–25% – Hardening Soil Small Model with decreased soil stiffness for 25%
- HSS_C30/37 – Hardening Soil Small Model with the secant pile wall made of the concrete C30/37
- HSS_C12/16 – Hardening Soil Small Model with the secant pile wall made of the concrete C12/16.

Note! For all soil models the retaining wall is made of the concrete C20/25.

Table 6.20: Maximum values for horizontal displacement of the bridge.

Model	$u_{x,max}$ [mm]	% of HSS*
MC	16,60	+88,6
HS	9,10	+3,4
HSS	8,80	0,0
HSS_+25%	6,61	-24,9
HSS_-25%	10,48	+19,1
HSS_C30/37	8,74	-0,7
HSS_C12/16	8,79	-0,1

Table 6.21: Maximum values for vertical displacement of the bridge.

Model	$u_{y,max}$ [mm]	% of HSS
MC	-12,14	+12,8
HS	-10,61	-1,4
HSS	-10,76	0,0
HSS_+25%	-8,64	-19,7
HSS_-25%	-12,42	+15,4
HSS_C30/37	-10,74	-0,2
HSS_C12/16	-10,79	+0,3

* difference in percentage between the value of a given model and HSS Model

Table 6.22: Maximum values for compressive and tensile stresses of the bridge.

Model	σ_c, [kN/m^2]	% of HSS	σ_t, [kN/m^2]	% of HSS
MC	926,60	+5,4	788,50	+8,7
HS	899,10	+2,2	732,90	+1,1
HSS	879,40	0,0	725,20	0,0
HSS_+25%	872,00	-0,8	775,60	+6,9
HSS_-25%	869,30	-1,1	720,30	-0,7
HSS_C30/37	879,60	0,0	724,70	-0,1
HSS_C12/16	879,60	0,0	725,90	0,1

Table 6.23: Maximum values for angular distortion of the bridge.

Model	β [-]	% of HSS
MC	1/839	+77,8
HS	1/1471	+1,5
HSS	1/1493	0,0
HSS_+25%	1/1842	-19,0
HSS_-25%	1/1253	+19,1
HSS_C30/37	1/1493	-0,1
HSS_C12/16	1/1488	+0,2

Comments on the obtained results.

Horizontal displacement of the bridge (u_x)

1) Minimum value is detected for HSS Model, equal to 8,8 mm
2) Maximum value is detected for MC Model, equal to 16,6 mm, that results for 89% higher value than for HSS Model.
3) For HS Model equal to 9,1 mm, for 3% higher value than for HSS Model.
4) For +25% E_{soil} equal to 6,61 mm, for 25% lower value than for HSS Model.
5) For -25% E_{soil} equal to 10,48 mm, for 19% higher value than for HSS Model.
6) Wall stiffness almost do not affect the results – the difference is less than 1%.

Vertical displacement of the bridge (u_y)

1) Minimum value is detected for HS Model, equal to 10,61 mm

2) Maximum value is detected for MC Model, equal to 12,42 mm, for 14,4% higher value than for HS Model.
3) For HSS Model equal to 10,76 mm, for 1,4% higher value than for HS Model.
4) For +25% E_{soil} equal to 8,64 mm, for 18,6% lower value than for HS Model.
5) For -25% E_{soil} equal to 12,42 mm, for 17,1% higher value than for HS Model.
6) Wall stiffness almost do not affect the results – the difference ranges between 1 and 2%.

Angular distortion of the bridge (β)

1) Minimum value is detected for HSS Model, equal to 1/1493
2) Maximum value is detected for MC Model, equal to 1/839, for 78% higher than for HSS Model.
3) For HS Model equal to 1/1471, for 1,5% higher value than for HSS Model.
4) For +25% E_{soil} equal to 1/1842, for 19% lower value than for HSS Model.
5) For -25% E_{soil} equal to 1/1253, for 19% higher value than for HSS Model.
6) Wall stiffness almost do not affect the results – the difference is 0,1- 0,2%.

Compressive and tensile stresses in the bridge (σ_c, σ_t)

1) Minimum value is detected for HSS Model: σ_c = 879,4 kN/m^2,
   σ_t = 725,20 kN/m^2
2) Maximum value is detected for MC Model: σ_c = 926,60 kN/m^2 is for 5,4% higher value than for HSS,
   σ_t = 778,50 kN/m^2, for 8,7% higher value than for HSS.
3) For HS Model: σ_c = 899,10 kN/m^2 is for 2,2% higher value than for HSS,
   σ_t = 778,50 kN/m^2, for 1,1% higher value than for HSS.
4) For +25% E_{soil}, -25% E_{soil} and for different wall stiffness (C30/37, C12/16) the results almost do not differ from the for HSS Model, except for +25% E_{soil}: σ_t = 775,60 kN/m^2 that results for 6,9% higher value than for HSS.

6.2.2 Piles

In figures below are represented results for the pile 1, where the soil was modelled with Hardening Soil Small Model in the last construction phase (Backfilling) for the horizontal displacement (fig. 6.6) and in phase 6 for the skin friction, where the maximum values were detected (fig. 6.7).

The entire calculation results are in Annex G2.

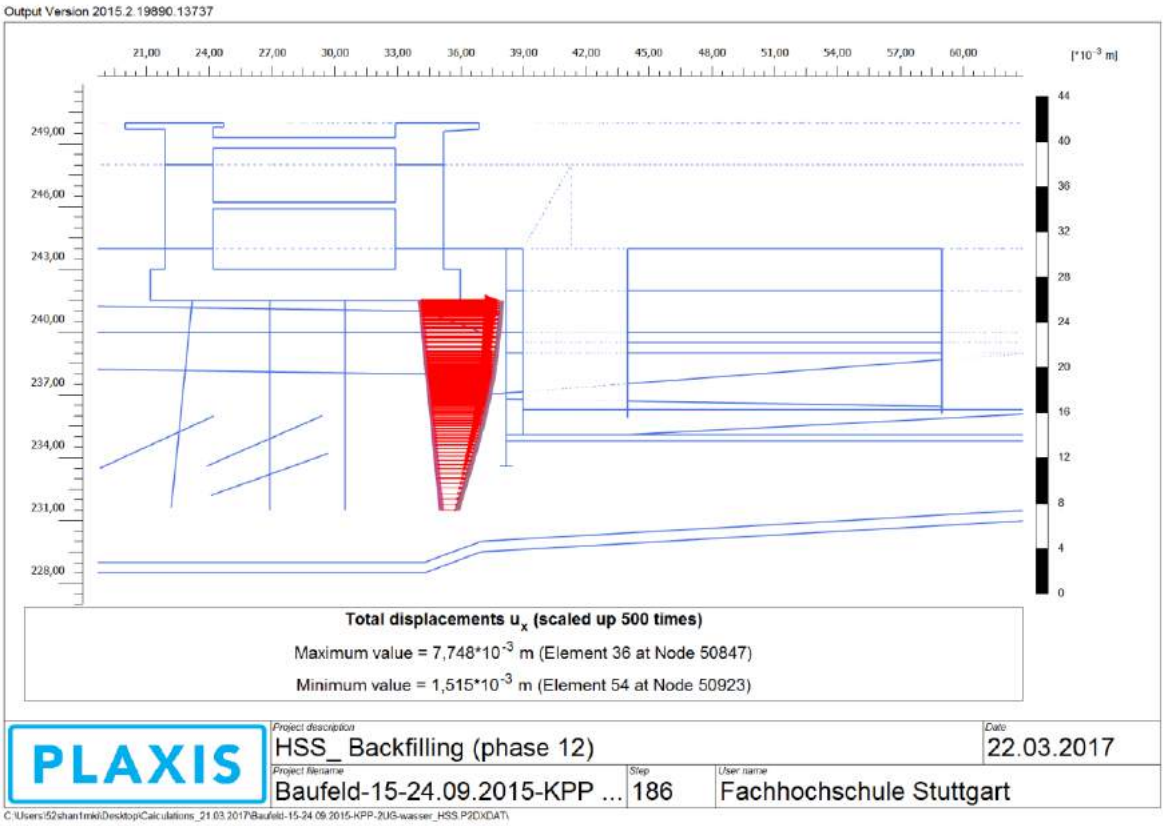

Figure 6.6: Horizontal displacement for the pile 1 in phase 12.

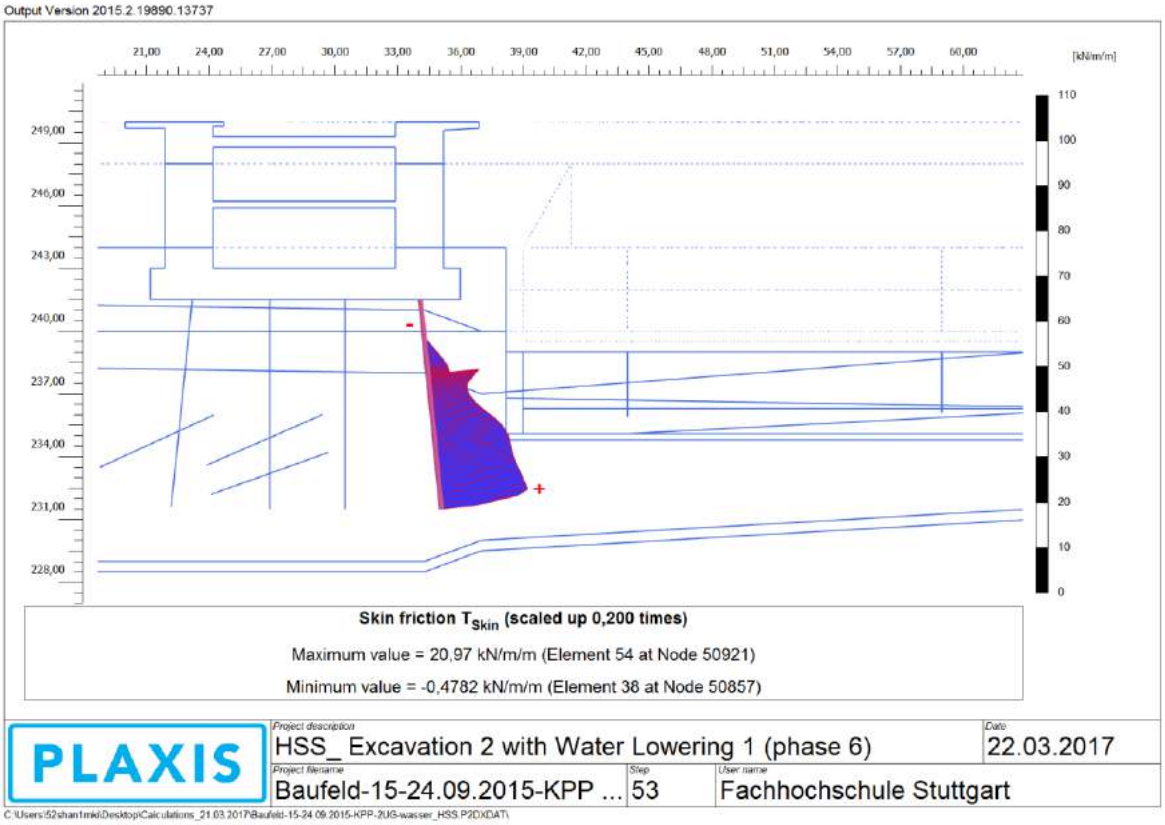

Figure 6.7: Skin friction for the pile 1 in phase 6.

The entire results for all models are represented in the tables below (tab. 6.24 – 6.30).

Table 6.24: Horizontal displacement and skin friction of the pile 1 for Mohr-Coulomb Model.

MOHR-COULOMB MODEL_PILES				
Stage	Horizontal displacement, u_x [mm]		Skin Friction, T_{skin} [kN/m^2]	
	$u_{x,max}$	Risk Level	$T_{skin,max}$	Risk Level
Phase 1	-1,00	LR	26,133	LR
Phase 2	4,20	LR	29,109	LR
Phase 3	3,95	LR	29,202	LR
Phase 4	5,81	LR	35,154	LR
Phase 5	5,87	LR	35,092	LR
Phase 6	10,23	IR	29,853	LR
Phase 7	10,07	IR	30,287	LR
Phase 8	13,66	HR	29,977	LR
Phase 9	13,59	HR	30,07	LR
Phase 10	13,73	HR	34,565	LR
Phase 11	13,13	HR	24,025	LR
Phase 12	14,80	HR	30,752	LR

Table 6.25: Horizontal displacement and skin friction of the pile 1 for Hardening Soil Model.

HARDENING SOIL MODEL_PILES				
Stage	Horizontal displacement, u_x [mm]		Skin Friction, T_{skin} [kN/m^2]	
	$u_{x,max}$	Risk Level	$T_{skin,\ max}$	Risk Level
Phase 1	0,82	LR	33,387	LR
Phase 2	-0,78/0,95	LR	38,378	LR
Phase 3	-0,43/ 0,85	LR	38,409	LR
Phase 4	1,11	LR	43,896	LR
Phase 5	1,14	LR	43,741	LR
Phase 6	2,70	LR	47,864	LR
Phase 7	2,65	LR	47,957	LR
Phase 8	4,37	LR	52,266	LR
Phase 9	4,31	LR	52,607	LR
Phase 10	4,27	LR	61,628	LR
Phase 11	6,00	LR	46,376	LR
Phase 12	8,08	IR	49,042	LR

Table 6.26: Horizontal displacement and skin friction of the pile 1 for Hardening Soil Small Model.

HARDENING SOIL SMALL MODEL_PILES				
Stage	Horizontal displacement, u_x [mm]		Skin Friction, T_{skin} [kN/m^2]	
	$u_{x,max}$	Risk Level	$T_{skin,max}$	Risk Level
Phase 1	0,93	LR	46,965	LR
Phase 2	-0,83/0,90	LR	59,148	LR
Phase 3	-0,48/0,78	LR	57,381	LR
Phase 4	-0,24/ 1,0	LR	63,674	LR
Phase 5	-0,22/ 1,0	LR	63,457	LR
Phase 6	2,30	LR	65,007	IR
Phase 7	2,3	LR	65,007	IR
Phase 8	4,00	LR	65,007	IR
Phase 9	3,90	LR	65,007	IR
Phase 10	3,80	LR	65,007	IR
Phase 11	5,50	LR	46,035	LR
Phase 12	7,75	LR	48,67	LR

Table 6.27: Horizontal displacement and skin friction of the pile1 for Hardening Soil Small Model with increased soil stiffness.

HARDENING SOIL SMALL MODEL_PILES_+25% E_{soil}				
Stage	Horizontal displacement, u_x [mm]		Skin Friction, T_{skin} [kN/m^2]	
	$u_{x,max}$	Risk Level	$T_{skin,max}$	Risk Level
Phase 1	0,73	LR	44,826	LR
Phase 2	0,73	LR	54,87	LR
Phase 3	0,63	LR	53,444	LR
Phase 4	0,83	LR	59,954	LR
Phase 5	0,84	LR	59,737	LR
Phase 6	1,88	LR	61,039	LR
Phase 7	1,87	LR	61,287	LR
Phase 8	3,28	LR	65,007	IR
Phase 9	3,24	LR	65,007	IR
Phase 10	3,18	LR	65,007	IR
Phase 11	4,53	LR	47,213	LR
Phase 12	6,61	LR	50,313	LR

Table 6.28: Horizontal displacement and skin friction of the pile 1 for Hardening Soil Small Model with reduced soil stiffness.

HARDENING SOIL SMALL MODEL_PILES_-25% E_{soil}				
Stage	Horizontal displacement, u_x [mm]		Skin Friction, T_{skin} [kN/m^2]	
	$u_{x,max}$	Risk Level	T_{skin}	Risk Level
Phase 1	0,74	LR	49,042	LR
Phase 2	1,25	LR	62,806	LR
Phase 3	1,11	LR	60,543	LR
Phase 4	1,49	LR	65,007	LR
Phase 5	1,51	LR	64,821	LR
Phase 6	3,27	LR	65,007	IR
Phase 7	3,26	LR	65,007	IR
Phase 8	5,27	LR	65,007	IR
Phase 9	5,26	LR	65,007	LR
Phase 10	5,15	LR	65,007	LR
Phase 11	6,98	LR	49,259	LR
Phase 12	9,28	IR	52,483	LR

Table 6.29: Horizontal displacement and skin friction of the pile1 for Hardening Soil Small Model with the secant pile wall made of concrete C30/37.

HARDENING SOIL SMALL MODEL_PILES_C30/37				
Stag	Horizontal displacement, u_x [mm]		Skin Friction, T_{skin} [kN/m^2]	
	$u_{x,max}$	Risk Level	T_{skin}	Risk Level
Phase 1	0,93	LR	46,97	LR
Phase 2	0,90	LR	59,15	LR
Phase 3	0,78	LR	57,38	LR
Phase 4	1,00	LR	63,55	LR
Phase 5	1,03	LR	63,36	LR
Phase 6	2,29	LR	65,01	IR
Phase 7	2,28	LR	65,01	IR
Phase 8	3,91	LR	65,01	IR
Phase 9	3,87	LR	65,01	IR
Phase 10	3,76	LR	65,01	IR
Phase 11	5,47	LR	46,04	LR
Phase 12	7,73	LR	48,79	LR

Table 6.30: Horizontal displacement and skin friction of the pile 1 for Hardening Soil Small Model with the secant pile wall made of concrete C12/16.

HARDENING SOIL SMALL MODEL_PILES_C12/16				
Stage	Horizontal displacement, u_x [mm]		Skin Friction, T_{skin} [kN/m^2]	
	$u_{x,max}$	Risk Level	T_{skin}	Risk Level
Phase 1	0,93	LR	48,05	LR
Phase 2	0,90	LR	59,15	LR
Phase 3	0,78	LR	57,38	LR
Phase 4	1,01	LR	63,77	LR
Phase 5	1,03	LR	63,55	LR
Phase 6	2,30	LR	65,01	IR
Phase 7	2,30	LR	65,01	IR
Phase 8	3,86	LR	65,01	IR
Phase 9	3,95	LR	65,01	IR
Phase 10	3,84	LR	65,01	IR
Phase 11	5,53	LR	46,00	LR
Phase 12	7,77	LR	48,55	LR

The maximum values for the horizontal displacement is detected in the last phase (Backfilling), while for the skin friction in phases 6 – 10.

In tables 6.31-6.32 the maximum values for all models of soil and variations are collected and the difference in percentage is calculated between the reference value (Hardening Soil Small Model) and the values obtained in the other models and variations.

Table 6.31: Maximum values for horizontal displacement of the pile 1.

Model	$u_{x,max}$ [mm]	% of HSS*
MC	14,80	+91,0
HS	8,08	+4,3
HSS	7,75	0,0
HSS_+25%	6,61	-14,7
HSS_-25%	9,28	+19,7
HSS_C30/37	7,73	-0,3
HSS_C12/16	7,77	0,3

Table 6.32: Maximum values for skin friction of the pile 1.

Model	T_{skin} [kN/m^2]	% of HSS
MC	35,15	-45,9
HS	61,63	-5,2
HSS	65,01	0,0
HSS_+25%	65,01	0,0
HSS_-25%	65,01	0,0
HSS_C30/37	65,01	0,0
HSS_C12/16	65,01	0,0

Comments on the obtained results

Horizontal displacement of the pile 1 (u_x)

1) Minimum value is detected for HSS Model, equal to 7,8 mm
2) Maximum value is detected for MC Model, equal to 14,8 mm, for 91% higher than for HSS Model.
3) For HS Model equal to 8,1 mm, for 4,1% higher value than for HSS Model.
4) For +25% E_{soil} equal to 6,61 mm, for 14,7% lower value than for HSS Model.
5) For -25% E_{soil} equal to 9,28 mm, for 19,7% higher value than for HSS Model.

Skin friction of the pile 1 (T_{skin})

1) The properties of the embedded piles were measured for the original soil stiffness. As we don't have the data of the load tests on pile for the +25%E_{soil} and -25%E_{soil}, we are not able to discuss about the risk evaluation of the skin friction for these options.
2) The variation of the class concrete of the retaining wall do not affect the results.

6.2.3 Secant pile wall

In the figure 6.8 is represented the horizontal displacement of the secant pile wall for the last construction phase (Backfilling), where the maximum value is detected. The soil was modelled with the Hardening Soil Small Model.

The entire calculation results are in Annex G3.

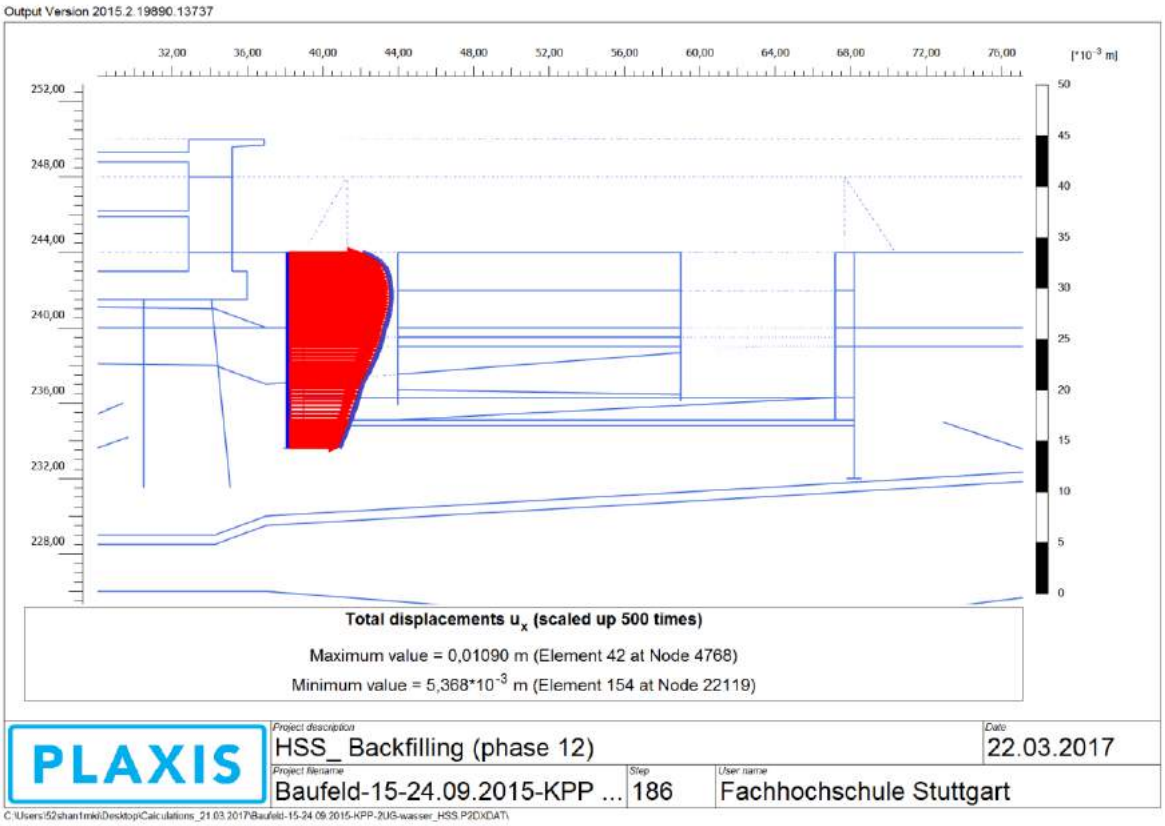

Figure 6.8: Horizontal displacement of the secant pile wall.

The entire results for all models are summarized in tables 6.33 – 6.39.

Table 6.33: Horizontal displacement of the wall for Mohr-Coulomb Model.

MOHR-COULOMB MODEL_WALL		
Stage	Horizontal displacement u_x [mm]	
	$u_{x,max}$	Risk Level
Phase 3	10,16	LR
Phase 4	14,91	HR
Phase 5	14,92	HR
Phase 6	15,62	HR
Phase 7	15,62	HR
Phase 8	15,50	HR
Phase 9	15,50	HR
Phase 10	15,50	HR
Phase 11	15,56	HR
Phase 12	23,04	HR

Table 6.34: Horizontal displacement for the wall in Hardening Soil Model.

HARDENING SOIL MODEL_WALL		
Stage	Horizontal displacement u_x [mm]	
	$u_{x,max}$	Risk Level
Phase 3	-1,87	LR
Phase 4	5,5	LR
Phase 5	5,50	LR
Phase 6	5,70	LR
Phase 7	5,70	LR
Phase 8	5,70	LR
Phase 9	5,70	LR
Phase 10	5,70	LR
Phase 11	5,70	LR
Phase 12	12,20	IR

Table 6.35: Horizontal displacement of the wall for Hardening Soil Small Model.

HARDENING SOIL SMALL MODEL_WALL		
Stage	Horizontal displacement u_x [mm]	
	$u_{x,max}$	Risk Level
Phase 3	-2,62	LR
Phase 4	4,31	LR
Phase 5	4,31	LR
Phase 6	4,90	LR
Phase 7	4,86	LR
Phase 8	4,83	LR
Phase 9	4,83	LR
Phase 10	5,20	LR
Phase 11	5,15	LR
Phase 12	10,90	IR

Table 6.36: Horizontal displacement of the wall for Hardening Soil Small Model with increased soil stiffness.

HARDENING SOIL SMALL MODEL_WALL_+25% E_{soil}		
Stage	Horizontal displacement u_x [mm]	
	$u_{x,max}$	Risk Level
Phase 3	-1,97	LR
Phase 4	3,68	LR
Phase 5	3,68	LR
Phase 6	4,10	LR
Phase 7	4,10	LR
Phase 8	4,10	LR
Phase 9	4,05	LR
Phase 10	4,36	LR
Phase 11	4,29	LR
Phase 12	9,84	LR

Table 6.37: Horizontal displacement of the wall for Hardening Soil Small Model with reduced soil stiffness.

HARDENING SOIL SMALL MODEL_WALL_-25% E_{soil}		
Stage	Horizontal displacement u_x [mm]	
	$u_{x,max}$	Risk Level
Phase 3	-3,25	LR
Phase 4	6,03	LR
Phase 5	6,03	LR
Phase 6	6,73	LR
Phase 7	6,73	LR
Phase 8	6,66	LR
Phase 9	6,66	LR
Phase 10	6,69	LR
Phase 11	6,68	LR
Phase 12	13,04	IR

Table 6.38: Horizontal displacement of the wall for Hardening Soil Small Model with the secant pile wall made of concrete C30/37.

HARDENING SOIL SMALL MODEL_WALL_C30/37		
Stage	Horizontal displacement, u_x [mm]	
	$u_{x,max}$	Risk Level
Phase 3	-2,62	LR
Phase 4	4,28	LR
Phase 5	4,28	LR
Phase 6	4,82	LR
Phase 7	4,82	LR
Phase 8	4,76	LR
Phase 9	4,76	LR
Phase 10	5,08	LR
Phase 11	5,06	LR
Phase 12	10,89	IR

Table 6.39: Horizontal displacement of the wall for Hardening Soil Small Model with the secant pile wall made of concrete C12/16.

HARDENING SOIL SMALL MODEL_WALL_C12/16		
Stage	Horizontal displacement u_x [mm]	
	$u_{x,max}$	Risk Level
Phase 3	-2,62	LR
Phase 4	4,33	LR
Phase 5	4,33	LR
Phase 6	4,90	LR
Phase 7	4,90	LR
Phase 8	4,89	LR
Phase 9	4,89	LR
Phase 10	5,26	LR
Phase 11	5,24	LR
Phase 12	10,90	IR

The maximum values are detected in the last phase (Backfilling) and collected in table 6.40. Also the difference in percentage is calculated respect to the reference value (HSS Model).

Table 6.40: Maximum values for horizontal displacement of the wall.

Model	$u_{x,max}$ [mm]	% of HSS*
MC	23,04	+111,4
HS	12,20	+11,9
HSS	10,90	0,0
HSS_+25%	9,84	-9,7
HSS_-25%	13,04	+19,6
HSS_C30/37	10,89	-0,1
HSS_C12/16	10,90	0,0

Comments on the obtained results

Horizontal displacement of the wall (u_x)

1) Minimum value is detected for HSS Model, equal to 10,9 mm
2) Maximum value is detected for MC Model, equal to 23 mm, for 111% higher than for HSS Model.
3) For HS Model equal to 12,2 mm, for 12% higher value than for HSS Model.
4) For +25% E_{soil} equal to 9,84 mm, for 9,7% lower value than for HSS Model.
5) For -25% E_{soil} equal to 13 mm, for 19,6% higher value than for HSS Model.
6) Wall stiffness do not affect much the results – the difference is 0,1%.

6.2.4 Hotel

In figures below are represented results for the hotel, where the soil was modelled with Hardening Soil Small Model, in the last construction phase (Backfilling) for the vertical displacement and stresses (fig. 6.9, 6.11 and 6.12) and for the phase 11 for the horizontal displacement (fig. 6.10), where the maximum values were detected.

The entire calculation results are in Annex G4.

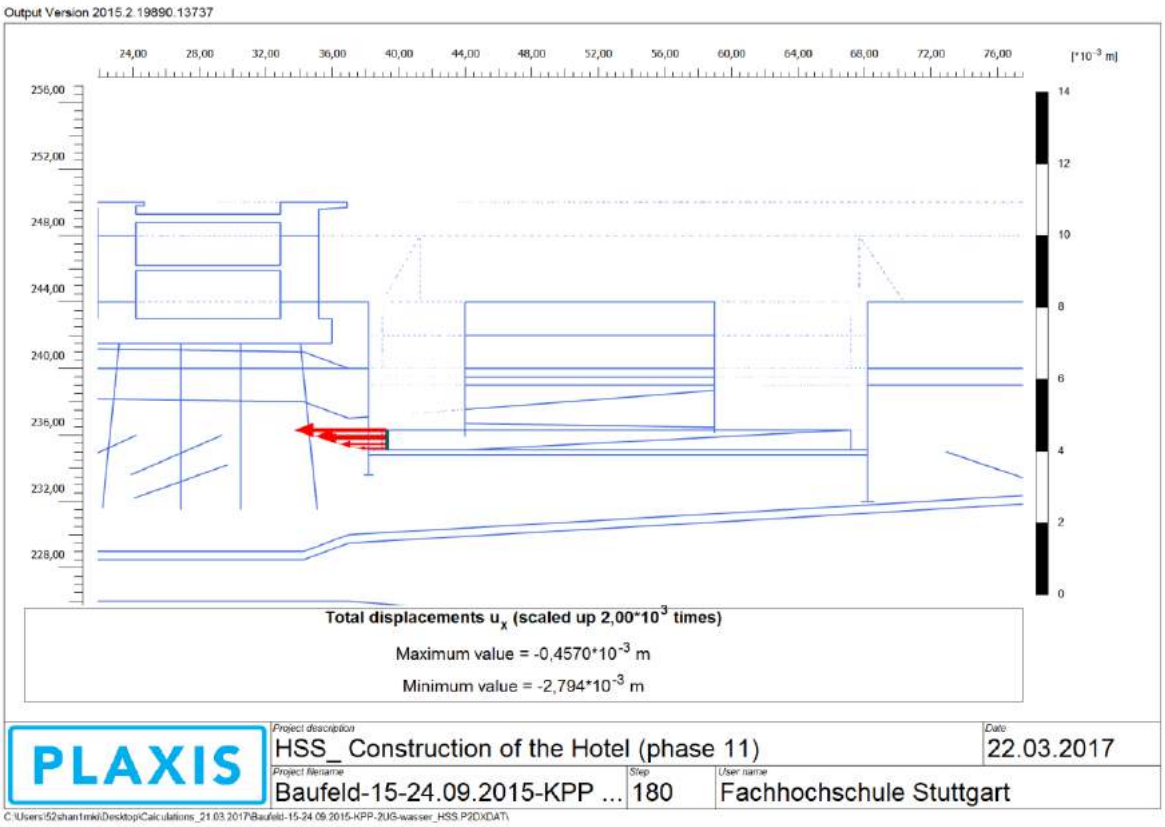

Figure 6.9: Horizontal displacement for the hotel in section 1 in phase 11.

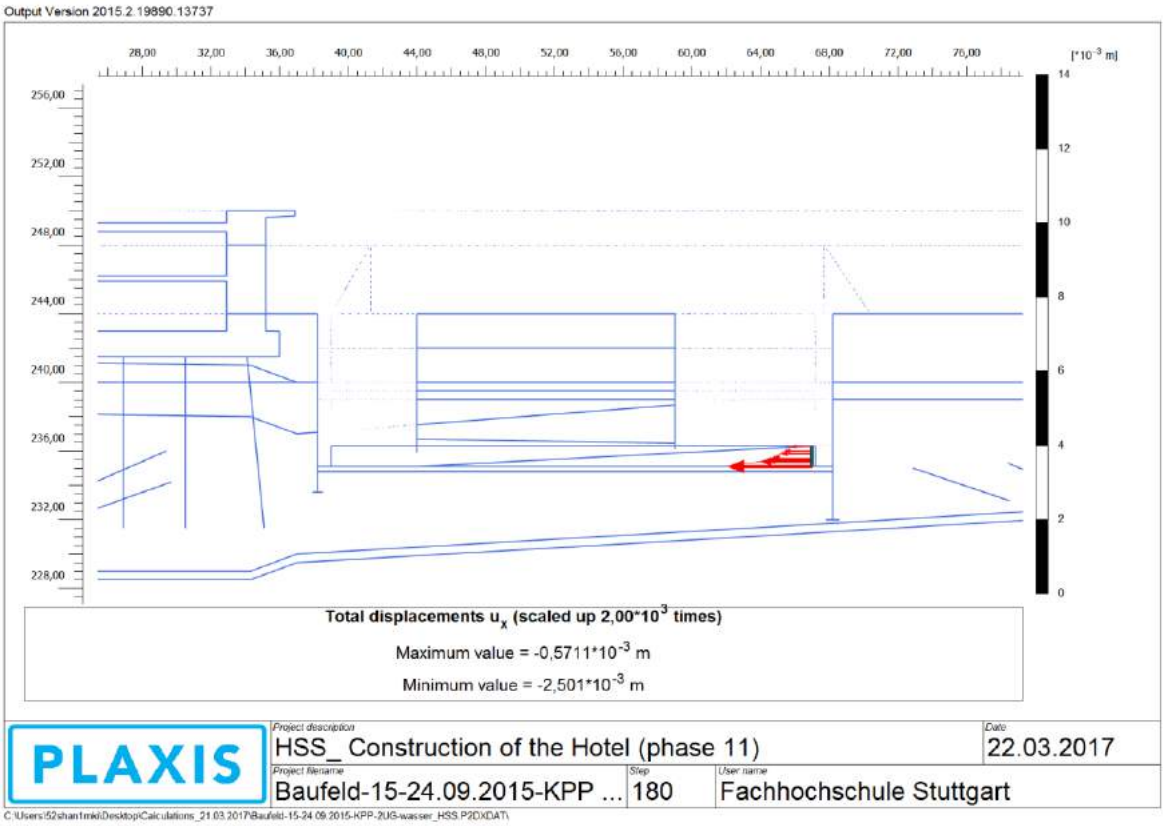

Figure 6.10: Horizontal displacement for the hotel in section 2 in phase 11.

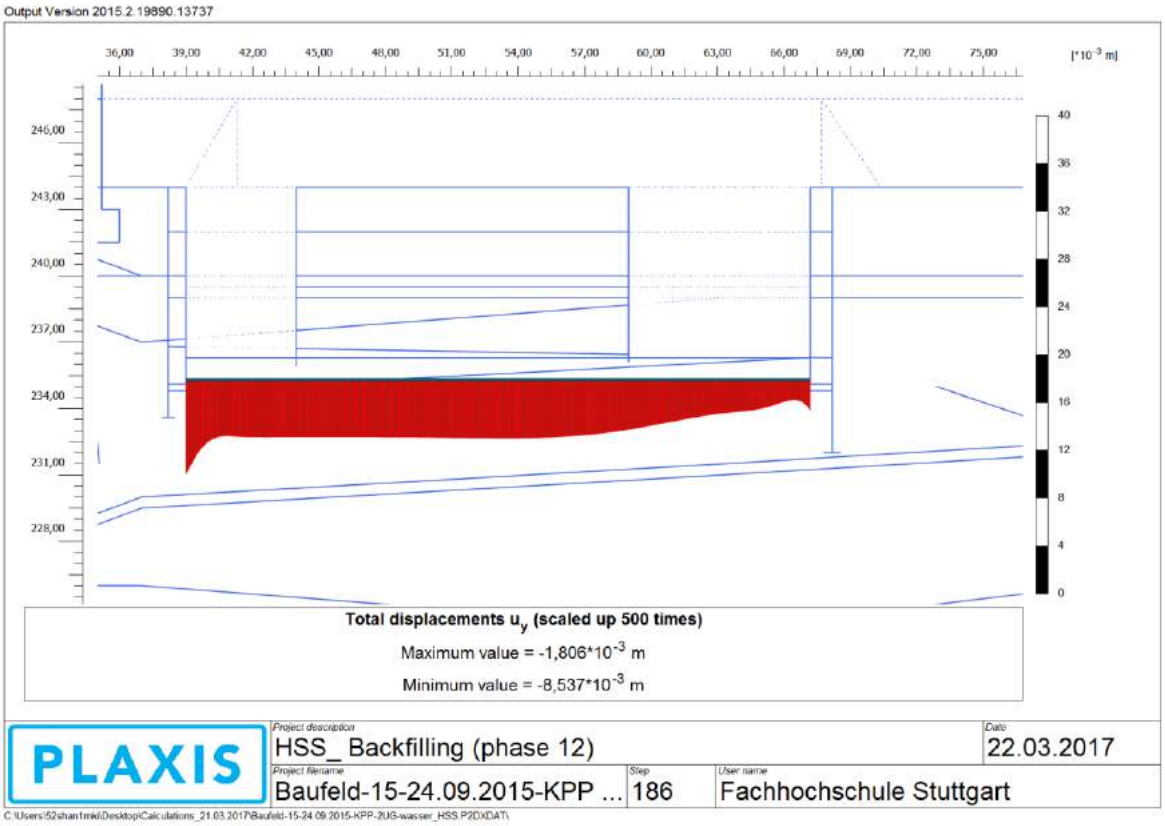

Figure 6.11: Vertical displacement for the hotel in section 3 in phase 12.

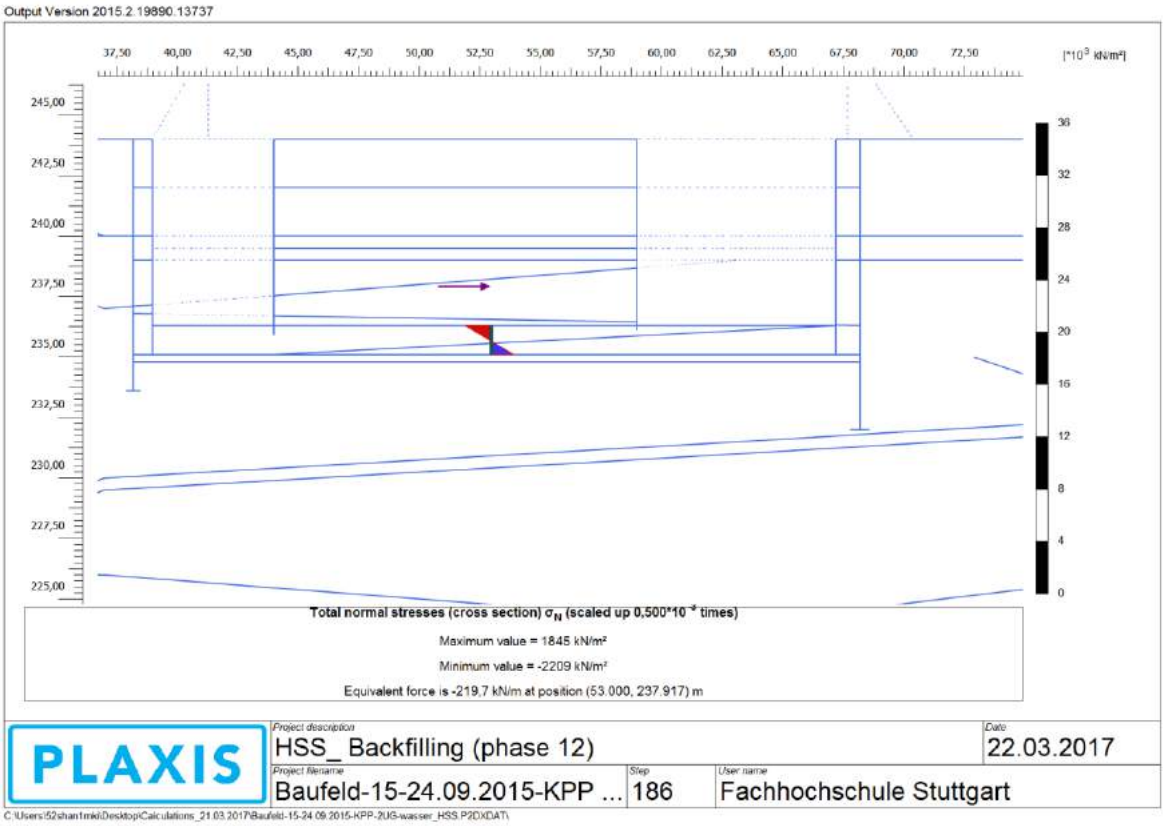

Figure 6.12: Compressive and tensile stresses for the hotel in section 4 in phase 11.

The entire results for all models are summarized in tables 6.41 – 6.50.

Table 6.41: Horizontal and vertical displacements and angular distortion of the hotel for Mohr-Coulomb Model.

MOHR-COULOMB MODEL_HOTEL							
Stage	Horizontal displacement, $u_{x,max}$ [mm]			Vertical displacement, u_y [mm]		Angular distortion, β [-]	
	Section 1	Section 2	Risk Level	$u_{y,max}$	Risk Level	β	Risk Level
Phase 11	-2,05/ 2,8	-7,5	HR	-16,01	HR	1/917	LR
Phase 12	5,52	-4,83	HR	-20,05	HR	1/979	LR

Table 6.42: Compressive and tensile stresses of the hotel for Mohr-Coulomb Model.

MOHR-COULOMB MODEL_HOTEL				
Stage	Compressive stresses, σ_c [kN/m^2]		Tensile stresses, σ_t [kN/m^2]	
	$\sigma_{c,\ max}$	Risk Level	$\sigma_{t,\ max}$	Risk Level
Phase 11	3150,0	LR	3255,0	HR
Phase 12	3200,0	LR	3281,0	HR

Table 6.43: Horizontal and vertical displacements and angular distortion of the hotel for Hardening Soil Model.

HARDENING SOIL MODEL_HOTEL							
Stage	Horizontal displacement, $u_{x,max}$ [mm]			Vertical displacement, u_y [mm]		Angular distortion, β [-]	
	Section 1	Section 2	Risk Level	$u_{y,max}$	Risk Level	β	Risk Level
Phase 11	-2,6	-2,25	LR	-6,70	LR	1/4132	LR
Phase 12	-1,26/ 1,07	-0,91/ 0,74	LR	-8,70	IR	1/4651	LR

Table 6.44: Compressive and tensile stresses in the hotel for Hardening Soil Model.

HARDENING SOIL MODEL_HOTEL				
Stage	Compressive stresses, σ_c [kN/m^2]		Tensile stresses, σ_t [kN/m^2]	
	$\sigma_{c,\ max}$	Risk Level	$\sigma_{t,\ max}$	Risk Level
Phase 11	2108,0	LR	1833,0	LR
Phase 12	2245,0	LR	1873,0	LR

Table 6.45: Horizontal and vertical displacements and angular distortion of the hotel for Hardening Soil Small Model.

HARDENING SOIL SMALL MODEL_HOTEL							
Stage	Horizontal displacement, $u_{x,max}$ [mm]			Vertical displacement, u_y [mm]		Angular distortion, β [-]	
	Section 1	Section 2	Risk Level	$u_{y,max}$	Risk Level	β	Risk Level
Phase 11	-2,8	-2,5	LR	-6,55	LR	1/4132	LR
Phase 12	-1,48/ 0,86	-1,2/ 0,63	LR	-8,50	LR	1/4065	LR

Table 6.46: Compressive and tensile stresses in the hotel for Hardening Soil Small Model.

HARDENING SOIL SMALL MODEL_HOTEL				
Stage	Compressive stresses, σ_c [kN/m^2]		Tensile stresses, σ_t [kN/m^2]	
	$\sigma_{c,max}$	Risk Level	$\sigma_{t,max}$	Risk Level
Phase 11	2069,0	LR	1795,0	LR
Phase 12	2209,0	LR	1645,0	LR

Table 6.47: Horizontal and vertical displacements and angular distortion of the hotel for Hardening Soil Small Model with increased soil stiffness.

HARDENING SOIL SMALL MODEL+25% E_{soil}_HOTEL							
Stage	Horizontal displacement, $u_{x,max}$ [mm]			Vertical displacement, u_y [mm]		Angular distortion, β [-]	
	Section 1	Section 2	Risk Level	$u_{y,max}$	Risk Level	β	Risk Level
Phase 11	-2,00	-1,94	LR	-4,65	LR	1/5376	LR
Phase 12	-1/ 0,83	-0,5	LR	-6,37	LR	1/5263	LR

Table 6.48: Compressive and tensile stresses in the hotel for Hardening Soil Small Model with increased soil stiffness.

HARDENING SOIL SMALL MODEL+25% E_{soil}_HOTEL				
Stage	Compressive stresses, σ_c [kN/m^2]		Tensile stresses, σ_t [kN/m^2]	
	$\sigma_{c,max}$	Risk Level	$\sigma_{t,max}$	Risk Level
Phase 11	1886,0	LR	1558,0	LR
Phase 12	2016,0	LR	1603,0	LR

Table 6.49: Horizontal and vertical displacements and angular distortion of the hotel in Hardening Soil Small Model with reduced soil stiffness.

HARDENING SOIL SMALL MODEL-25% E_{soil}_HOTEL							
Stage	Horizontal displacement, $u_{x,max}$ [mm]			Vertical displacement, u_y [mm]		Angular distortion, β [-]	
	Section 1	Section 2	Risk Level	$u_{y,max}$	Risk Level	β	Risk Level
Phase 11	-2,52	-3,96	IR	-8,53	IR	1/3484	LR
Phase 12	-0,88/ 1,6	-2,34	LR	-2,71	LR	1/3436	LR

Table 6.50: Compressive and tensile stresses in the hotel for Hardening Soil Small Model with reduced soil stiffness.

HARDENING SOIL SMALL MODEL-25% E_{soil}_HOTEL				
Stage	Compressive stresses, σ_c [kN/m^2]		Tensile stresses, σ_t [kN/m^2]	
	$\sigma_{c,max}$	Risk Level	$\sigma_{t,max}$	Risk Level
Phase 11	2162,0	LR	1980,0	LR
Phase 12	2282,0	LR	2008,0	LR

Table 6.51: Horizontal and vertical displacements and angular distortion of the hotel for Hardening Soil Small Model with the secant pile wall made of concrete C30/37.

HARDENING SOIL SMALL MODEL - C30/37_HOTEL							
Stage	Horizontal displacement, $u_{x,max}$ [mm]			Vertical displacement, u_y [mm]		Angular distortion, β [-]	
	Section 1	Section 2	Risk Level	$u_{y,max}$	Risk Level	β	Risk Level
Phase 11	-2,83	-2,53	LR	-6,55	LR	1/4132	LR
Phase 12	-1,5/ 0,81	-1,21/ 0,63	LR	-8,54	IR	1/4717	LR

Table 6.52: Compressive and tensile stresses in the hotel for Hardening Soil Small Model with the secant pile wall made of concrete C30/37.

HARDENING SOIL SMALL MODEL - C30/37_HOTEL				
Stage	Compressive stresses, σ_c [kN/m^2]		Tensile stresses, σ_t [kN/m^2]	
	$\sigma_{c,max}$	Risk Level	$\sigma_{t,max}$	Risk Level
Phase 11	2068,0	LR	1795,0	LR
Phase 12	2209,0	LR	1844,0	LR

Table 6.53: Horizontal and vertical displacements and angular distortion of the hotel in Hardening Soil Small Model with the secant pile wall made of concrete C12/16.

HARDENING SOIL SMALL MODEL – C12/16_HOTEL							
Stage	Horizontal displacement, $u_{x,max}$ [mm]			Vertical displacement, u_y [mm]		Angular distortion, β [-]	
	Section 1	Section 2	Risk Level	$u_{y,max}$	Risk Level	β	Risk Level
Phase 11	-2,74	-2,51	LR	-6,54	LR	1/4149	LR
Phase 12	-1,44/ 0,92	-0,62	LR	-8,54	IR	1/4082	LR

Table 6.54: Compressive and tensile stresses in the hotel for Hardening Soil Small Model with the secant pile wall made of concrete C12/16.

HARDENING SOIL SMALL MODEL – C12/16_HOTEL				
Stage	Compressive stresses, σ_c [kN/m^2]		Tensile stresses, σ_t [kN/m^2]	
	$\sigma_{c,max}$	Risk Level	$\sigma_{t,max}$	Risk Level
Phase 11	2067,0	LR	1793,0	LR
Phase 12	2206,0	LR	1843,0	LR

The maximum values are collected in tables 6.55 - 6.58. Also the difference in percentage is calculated of a given value respect to the value of reference (HSS Model).

Table 6.55: Maximum values for horizontal displacement of the hotel.

Model	Section 1		Section 2	
	$u_{x,max}$ [mm]	% of HSS	$u_{x,max}$ [mm]	% of HSS
MC	5,52	-	-7,5	+66,7
HS	-2,6	-7,7	-2,25	-11,1
HSS	-2,8	0,0	-2,5	0,0
HSS_+25%	-2,00	-40,0	-1,94	-28,9
HSS_-25%	-2,52	-11,1	-3,96	+36,9
HSS_C30/37	-2,83	1,1	-2,53	+1,2
HSS_C12/16	-2,74	-2,2	-2,51	+0,4

Table 6.56: Maximum values for vertical displacement of the hotel.

Model	$u_{y,max}$ [mm]	% of HSS
MC	-20,16	+137,2
HS	-8,70	+2,4
HSS	-8,50	0,0
HSS_+25%	-6,37	-25,1
HSS_-25%	-10,68	+25,6
HSS_C30/37	-8,54	+0,5
HSS_C12/16	-8,54	+0,5

Table 6.57: Maximum values for angular distortion of the hotel.

Model	β [-]	% of HSS
MC	1/917	+543,6
HS	1/4132	-1,6
HSS	1/4065	0,0
HSS_+25%	1/5263	-22,7
HSS_-25%	1/3436	+18,4
HSS_C30/37	1/4132	-1,6
HSS_C12/16	1/4082	-0,2

Table 6.58: Maximum values for compressive and tensile stresses of the hotel.

Model	σ_c, [kN/m^2]	% of HSS	σ_t, [kN/m^2]	% HSS
MC	3200,00	+35,3	3281,00	+45,3
HS	2108,00	+1,9	1833,00	+2,1
HSS	2069,00	0,0	1795,00	0,0
HSS_+25%	1886,00	-9,7	1558,00	-15,2
HSS_-25%	2162,00	+4,3	1980,00	+9,3
HSS_C30/37	2068,00	0,0	1795,00	0,0
HSS_C12/16	2067,00	-0,1	1793,00	-0,1

Comments on the obtained results

Vertical displacement of the hotel (u_y)

1) Minimum value is detected for HSS Model, equal to 8,5 mm

2) Maximum value is detected for MC Model, equal to 20,16 mm, for 137,2% higher value than for HSS Model.
3) For HS Model equal to 8,7 mm, for 2,4% higher value than for HSS Model.
4) For +25% E_{soil} equal to 6,37 mm, for 25% lower value than for HSS Model.
5) For -25% E_{soil} equal to 10,68 mm, for 25,6% higher value than for HSS Model.
6) Wall stiffness almost do not affect the results – the difference results 0,5%.

Horizontal displacement of the hotel (u_x)

Basement moves to the left in phase of construction (phase 11) about 2-3 mm, but return to the original position after backfilling in phase 12.

Angular distortion of the hotel (β)

1) Minimum value is detected for HS Model, equal to 1/4132.
2) For HSS Model equal to 1/4065, for 1,6% higher value than for HS Model.
3) Maximum value is detected for MC Model, equal to 1/917, that results much higher than for HSS Model.
4) For +25% E_{soil} equal to 1/5263, for 22,7% lower value than for HSS Model.
5) For -25% E_{soil} equal to 1/3436, for 18,4% higher value than for HSS Model.
6) Wall stiffness affects little the results – the difference is 0,2- 1,6%.

Compressive and tensile stresses in the hotel (σ_c, σ_t)

1) Minimum value is detected for HSS Model: σ_c = 2069,0 kN/m^2, σ_t = 1795,0 kN/m^2
2) Maximum value is detected for MC Model: σ_c = 2108,0 kN/m^2 is for 35,3% higher than for HSS;
   σ_t = 1833,0 kN/m^2, for 45,3% higher value than for HSS.
3) For HS Model: σ_c = 2108,0 kN/m^2 is for 1,9% higher value than for HSS,
   σ_t = 1833,0 kN/m^2, for 2,1% higher value than for HSS.
4) For +25% E_{soil}: σ_c = 1886,0 kN/m^2 is for 9,7% lower value than for HSS,
   σ_t = 1558,0 kN/m^2, for 15,2% lower value than for HSS.
5) For -25% E_{soil}: σ_c = 2162,0 kN/m^2 is for 4,3% higher value than for HSS,
   σ_t = 1980,0 kN/m^2, for 9,3% higher value than for HSS.
6) For different wall stiffness (C30/37, C12/16) the results do not differ from the for HSS Model.

6.2.5 Soil capacity

In figure 6.13 are represented results for bearing capacity of soil under the hotel basement, where the soil was modelled with Hardening Soil Small Model, in the last construction phase (Backfilling).

The entire calculation results are in Annex G5 are summarized in tables 6.42 – 6.50.

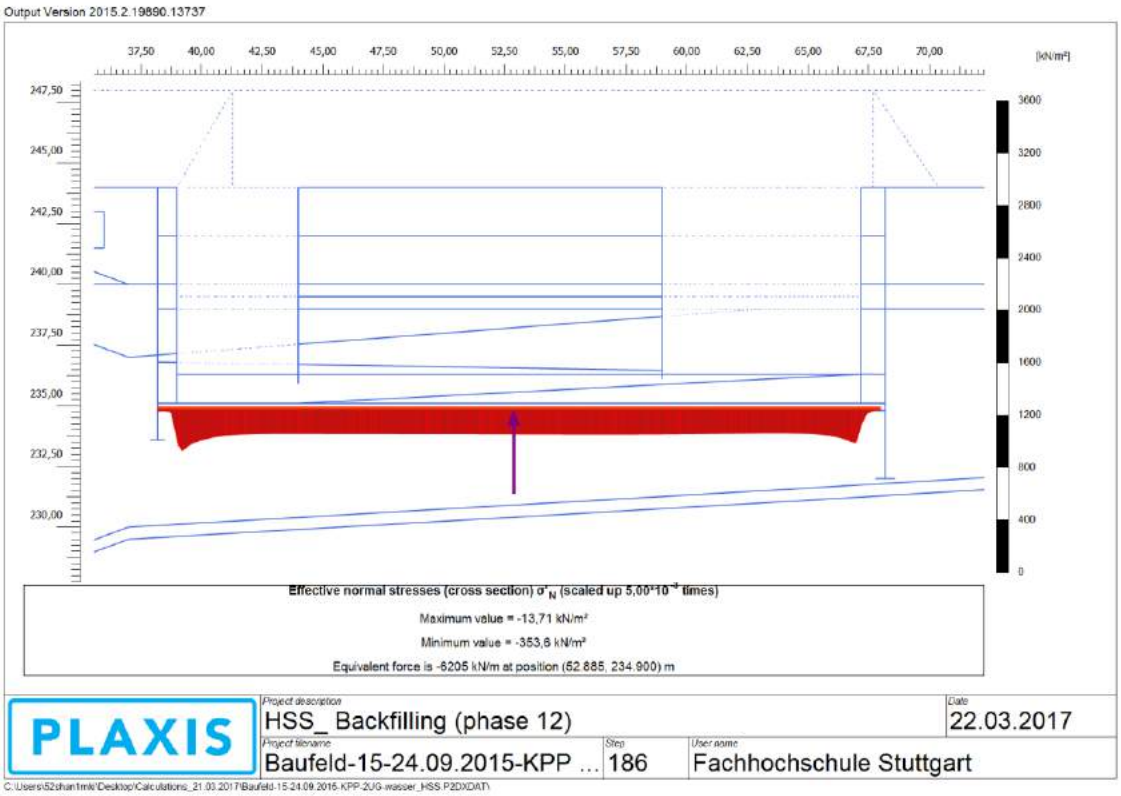

Figure 6.13: Bearing capacity of soil under the hotel basement in phase 12.

Table 6.59: Bearing capacity of soil for Mohr-Coulomb Model.

MOHR-COULOMB MODEL_SOIL						
Stage	Bearing capacity, q_{max} [kN/m^2]					
	Section 1	Risk Level	Section 2	Risk Level	Section 3	Risk Level
Phase 11	-389,9	HR	-202,6	LR	-339,8	HR
Phase 12	-402,9	HR	-203,9	LR	-336,3	HR

Table 6.60: Bearing capacity of soil for Hardening Soil Model.

HARDENING SOIL MODEL_SOIL						
Stage	Bearing capacity, q_{max} [kN/m^2]					
	Section 1	Risk Level	Section 2	Risk Level	Section 3	Risk Level
Phase 11	-341,2	HR	-215,0	LR	-278,4	HR
Phase 12	-370,6	HR	-215,4	LR	-292,8	HR

Table 6.61: Bearing capacity of soil for Hardening Soil Small Model.

HARDENING SOIL SMALL MODEL_SOIL						
Stage	Bearing capacity, q_{max} [kN/m^2]					
	Section 1	Risk Level	Section 2	Risk Level	Section 3	Risk Level
Phase 11	-341,8	HR	-214,0	LR	-277,2	HR
Phase 12	-356,6	HR	-215,7	LR	-292,6	HR

Table 6.62: Bearing capacity of soil for Hardening Soil Small Model with increased soil stiffness.

HARDENING SOIL SMALL MODEL+25% E_{soil}_SOIL						
Stage	Bearing capacity, q_{max} [kN/m^2]					
	Section 1	Risk Level	Section 2	Risk Level	Section 3	Risk Level
Phase 11	-339,00	HR	-216,55	LR	-270,35	HR
Phase 12	-366,47	HR	-217,44	LR	-288,57	HR

Table 6.63: Bearing capacity of soil for Hardening Soil Small Model with reduced soil stiffness.

HARDENING SOIL SMALL MODEL-25% E_{soil}_SOIL						
Stage	Bearing capacity, q_{max} [kN/m^2]					
	Section 1	Risk Level	Section 2	Risk Level	Section 3	Risk Level
Phase 11	-339,52	HR	-212,33	LR	-278,89	HR
Phase 12	-354,74	HR	-213,63	LR	-291,51	HR

Table 6.64: Bearing capacity of soil for Hardening Soil Small Model with the secant pile wall made of concrete C30/37.

HARDENING SOIL SMALL MODEL - C30/37_SOIL						
Stage	Bearing capacity, q_{max} [kN/m^2]					
	Section 1	Risk Level	Section 2	Risk Level	Section 3	Risk Level
Phase 11	-340,80	HR	-214,00	LR	-276,50	HR
Phase 12	-355,82	HR	-215,07	LR	-292,17	HR

Table 6.65: Bearing capacity of soil for Hardening Soil Small Model with the secant pile wall made of concrete C12/16.

HARDENING SOIL SMALL MODEL – C12/16_SOIL						
Stage	Bearing capacity, q_{max} [kN/m^2]					
	Section 1	Risk Level	Section 2	Risk Level	Section 3	Risk Level
Phase 11	-339,13	HR	-214,00	LR	-276,03	HR
Phase 12	-354,12	HR	-215,06	LR	-291,64	HR

The maximum values are collected in table 6.66. Also the difference in percentage is calculated respect to the reference value (HSS Model).

Table 6.66: Maximum values for bearing capacity of soil.

Phase 12	Section 1		Section 2		Section 3	
	q [kN/m^2]	% of HSS	q [kN/m^2]	% HSS	q [kN/m^2]	% HSS
MC	-402,90	+11,5	-203,90	-5,8	-336,30	+13,0
HS	-370,60	+3,8	-215,41	-0,1	-292,80	+0,1
HSS	-356,60	0,0	-215,70	0,0	-292,60	0,0
HSS_+25%	-366,47	+2,7	-217,44	0,8	-288,57	-1,4
HSS_-25%	-354,74	-0,5	-213,63	-1,0	-291,51	-0,4
HSS_C30/37	-355,82	-0,2	-215,07	-0,3	-292,17	-0,1
HSS_C12/16	-354,12	-0,7	-215,06	-0,3	-291,64	-0,3

Comments on the obtained results

Bearing capacity of soil (q)

1) In section 1 and section 3 the bearing capacity exceeds the allowable value of 180 kN/m^2 in all models.
2) In section 2 the bearing capacity do not exceed the allowable value of 240 kN/m^2 in all models.
3) Results differs very little for HS and HSS Models, as well as for +25% E_{soil}, -25% E_{soil}, C30/37 and C12/16.
4) For HSS Model:

   Section 1: q = -356,60 kN/m^2

   Section 2: q = -215,70 kN/m^2

   Section 3: q = -292,60 kN/m^2

5) MC Model gives considerably different results from HSS Model:
   Section 1: q = -402,90 kN/m^2 that for 13% higher value than for HSS Model.
   Section 2: q = -203,90 kN/m^2 that for 5,5% lower value than for HSS Model.
   Section 3: q = -336,30 kN/m^2 that for 15% higher value than for HSS Model.

6.3 Summary of the obtained results

1) Horizontal displacements, u_x, settlements, u_y and angular distortion, β change with the soil model (Mohr-Coulomb, Hardening Soil or Hardening Soil Small) and the soil stiffness ($E_{50}^{ref}, E_{oed}^{ref}, E_{ur}^{ref}$).
2) Compressive, σ_c and tensile stresses, σ_t and bearing capacity of soil, q are less affected by soil model or soil stiffness.
3) Stiffness of the retaining walls (C20/25- original, C30/37, C12/16) affects less the investigated parameters for the present study case.
4) Increment in stiffness of soil for 25% shows considerably smaller values: less deformation and distortion compare to the original stiffness.
5) Reduce in stiffness of soil for 25% shows considerably bigger values: more deformation and distortion compare to the original stiffness.
6) Hardening Soil and Hardening Soil Small models shows almost same results.
7) Mohr-Coulomb model gives considerably higher results compare to the Hardening Soil model for displacements: more than eighty percent for displacements and distortion values, while for stresses no more than forty five percent.

CONCLUSIONS

With rapid infrastructure construction and urban development, there has been an increasing demand for utilization of underground spaces which give rise to a large number of excavation projects. Deep excavation has the potential to cause unfavorable effects on nearby ground as well as structures and facilities around it. With increasing number of excavations constructed in congested urban areas, it is necessary not only to ensure the safety of the excavation, but to minimize ground and wall displacements and hence to guarantee the serviceability of adjacent properties. Any severe damage to the nearby utilities probably lead to economic losses and complicated conflicts among owners, constructors and the public. That is why it is very important to estimate the possible level of risks during the geotechnical operations and the construction process.

The concepts of safety, risk and hazard scenarios are defined and mainly commented in two Eurocodes: EN 1990 “Basis of structural design” and EN 1001-1-7 “Eurocode 1-Actions on structures-Part 1-7: general actions-Accidental actions”.

The high risk for geotechnical design is first of all connected with the engineer’s ability to realistically model the behavior soils and of a geological environment due to the changes caused by new constructions activity.

Nowadays it is difficult to imagine the geotechnical design without use of special softwares based on the numerical modelling. In many cases the complexity of geological structure and questions related to the ground water flow, as well as the non-linearity of soil behavior presents a lot of challenge for geotechnical engineers. The choose of not appropriate soil model may lead to not precise prediction of soil movement such as settlements, displacements, distortions and generated stresses, hence, may lead to serious

consequences, in the worst case to collapses. It is well known that material parameters of geomaterials scatter within a considerable range. It is also very important to choose the "right" soil parameters on base of the *in situ* and laboratory tests.

In this work there was proposed and described some risk scenario for deep foundation. The qualitative and quantitative impact of risk scenarios was shown in a case study.

The risk criterions recommended in this master thesis are based on qualitative and quantitative uncertainties of the design methods and follow the parameters that control them. These parameters (soil behavior, stiffness of soil, material properties of soil structure, deformation of structures, etc.) have an important influence to the design specifications. The application of these findings in the design needs further research in the context of different geotechnical design.

The study case presents the construction of the multistorey hotel in the congested urban area of Stuttgart. The contraction requires the excavation of 8 m depth. The simulation was made in FEM software PLAXIS 2D 2015. Changing soil model, soil stiffness and the stiffness of the retaining wall which some of the necessary parameters for risk evaluation were applied in PLAXIS calculations. For the case study the soil was modelled with Mohr-Coulomb, Hardening Soil and Hardening Soil Small Strain models. Then, in Hardening Soil Small Model the soil stiffness of all layers was reduced for one quarter of the original value, was increased for one quarter of the original value, the stiffness of the secant pile wall was reduced using the concrete of low class C12/16 and increased using the high class concrete C30/37.

The obtained results show that the displacement parameters such as horizontal and vertical displacements and angular distortion change considerably with the soil model and soil stiffness, meanwhile the stiffness of the retaining wall give a small difference for this case study. Stresses such as compressive and tensile stresses and bearing capacity undergo less changes than displacement parameters regarded to the soil models and soil and wall stiffnesses. The Mohr- Coulomb models gives considerably higher values for the parameters regarding the risk evaluation compare to the Hardening Soil Model, while the difference between values for Hardening Soil and Hardening Soil Small model are relatively small.

To be most effective regarding the determination and evaluation of risk scenarios, the next sequence should be followed:

- Real Process description of the geotechnical issue.

- Qualitative Risk analysis by meaning of identifications of: hazards, scenarios and consequences.

- Quantification Risk evaluation and consequences.

- Risk acceptance or mitigating measures.

The natural task of geotechnical engineers is to decrease this risk with the help of the new design and construction methods utilizing all new findings in our activities.

REFERENCES

[1] Hillson, D. A. “What is risk? Towards a common definition”. Inform journal of the UK Institute of Risk Management, April 2002

[2] Stacey, T.R. Design as a Strategic Issue, Proc. 2nd Int. Seminar on Strategic vsTactical Approaches in Mining. Perth, Australian Centre for Geomechanics, Section 4, 2006

[3] Einstein, H.H.,Baecher, G.B. Probabilistic and statistical methods in engineering geology.Rock Mechanics, Vol. 4, 1984

[4] Baecher, G.B., and Christian, J.T. Reliability andStatistics in Geotechnical Engineering. John Wiley &Sons Ltd., Chichester, West Sussex, UK, 2003

[5] Brown, D.H. First language acquisition. Principles of language and teaching, 5th Ed. Pearson ESL

[6] Douglas, J., Noy, E. A. Building Surveys and Reports, 4th Edition.A John Wiley & Sons, Ltd., Publication

[7] Bond, A.J., Schuppener, B., Scarpelli, G., Orr, T.L.L: Eurocode 7. Geotechnical design worked examples, Report EUR 26227 EN

[8] Chai, J., Chen W.F., Duan, L. "Shallow Foundations"*Bridge Engineering Handbook.*Ed. Boca Raton: CRC Press, 2000

[9] Bentler, D.J. Finite element analysis of deep excavations. Master-thesis, Virginia Polytechnic Institute, August 1998

[10] GouwTjie-Liong, Ir., Eng, M. ChFC, Geotechnical-Failure-Can-it-Be-Prevented? International Symposium on sustainable Geosynthetics and Green Technology for Climate Change (SGCC2011)

[11] Ghorbani, M., Sharifzadeh M., Yasrobi S., Daiyan, M. Geotechnical, structural and geodetic measurements for conventional tunneling hazards in urban areas – The case of Niayesh road tunnel project. Tunneling and underground space technology 31, 2012

[12] Leca, E., New, B. Settlements induced by tunneling in soft ground. Tunneling and underground space technology 22, 2007

[13] Mayring, P. Einführung in die qualitative Sozialforschung: eine Anleitung zum qualitativen Denken,Weinheim, 2002

[14] Aliaga, M., Gunderson, B. Interactive Statistics, Saddle River, 2000

[15] Idowu Temitope, Ezekiel Research Methodology retrieved from https://www.academia.edu/15209462/Qualitative_and_Quantitative_research_approaches, 2012

[16] Ou, C.Y. Deep Excavation: Theory and Practice. Taylor&Francis Group, London, UK, 2006

[17] Clough, G.W. and O´Rourke, T.D. Construction induced settlements of in situ walls, Design and Performance of Earth Retaining Structures.ASCE Special Publication, №25, 1990

[18] Schmidt, H. H., Buchmaier, R. F., Vogt-Breyer, C. Grundlagen der Geotechnik. 4. Auflage, Springer Vieweg, 2013

[19] Hsieh, P. G. Prediction of Ground Movements Caused by Deep Excavation in Clay, PhD Dissertation, Department of Construction Engineering, National Taiwan University of Science and Technology, 1999

[20] Elkady T. 'Effect of Excavation-induced Movements on Adjacent Piles', Proceedings of the 18th international conference on soil mechanics and geotechnical engineering, Paris (707), 2013.

[21] Dhatrak, A I., Kulkarni, S. Effect of Deep Excavation Adjacent to Pile Structure. International Journal of Innovative Research in Science, Engineering and Technology, Vol. 5, 2016

[22] Kempfert, H.G., Gebreselassie, B. Excavations and Foundations in Soft Soils. Springer-Verlag Berlin Heidelberg, 2006

[23] Duncan, J.M., Wright S.G. Soil Strength and Slope Stability. John Wiley & Sons, Inc., 2005

[24] Atkinson, J.H. An introduction to the mechanics of soils and foundations. McGraw-Hill Book Company Europe, 1993

[25] Janbu, N. Slopes and excavations in normally and lightly overconsolidated clays.Proc. 9th ICSMFE, Tokyo, 1977

[26] Atkinson, J. H., Sallfors, G. Experimental determination of soil properties. In Proc. 10th ECSMFE, 3, 1998

[27] Material Models Manual Plaxis, 2015

[28] Obrzud, R.F. On the use of the Hardening Soil Small Strain model in geotechnical practice, In Numerics in Geotechnics and Structures, Elmepress Int, Lausanne, 2010

[29] Truty, A. Hardening soil model with small strain stiffness. Technical Report 080901,Zace Services Ltd., Lausanne, 2008

[30] Potts, D.M., Zdravković, L. Finite Element Analysis in Geotechnical Engineering: Theory, Thomas Telford Limited, 1999

[31] Addenbrooke, T., Potts, D., and Puzrin, A. The influence of pre-failure soil stiffness onthe numerical analysis of the tunnel construction. Géotechnique, 47(3), 2010

[32] Schanz, T., Vermeer, P., Bonier, P. Formulation and verification of the Hardening Soil model. In Beyond 2000 in Computational Geotechnics. Balkema, Rotterdam, 1999

[33] Duncan, J.M., Chang, C.-Y. Nonlinear analysis of stress and strain in soils. Journal of the Soil Mechanics and Foundations Division ASCE, (96, SM 5), 1963

[34] Ohde, J. Grundbaumechanik. Bd. III. Hütte, 1951

[35] Rowe, P. W. The stress-dilatancy relation for static equilibrium of an assembly of particles in contact. In Proc. Roy. Soc. A., № 269, 1962

[36] Schanz, T., Vermeer, P.A. Angles of friction and dilatancy of sand. Geotechnique, 48, 1996

[37] Eurocode 2: Design of concrete structures (2004), CEN

[38] Benz, T. Small-Strain Stiffness of Soils and its Numerical Consequences. PhD thesis, Universität Stuttgart, 2006

[39] Lafleur, J., Silvestri, V., Asselin, R., Soulie, M. Behaviour of test excavation in soft champlain sea clay. Canadian Geotechnical Journal, 25, 1998

[40] Kondner, R.L. Hyperbolic stress-strain response: cohesive soils. Journal of the Soil Mechanics and Foundations Division ASCE, (89, SM 1), 1963

[41] Alpan, I. The geotechnical properties of soils. Earth-Science Reviews, №6, 1970

[42] Gouw, T. L. Common Mistakes on the Application of Plaxis 2D in Analysing Excavation Problems. International Journal of Applied Engineering Research, Vol. 9, № 21, 2014

[43] Brinkgreeve, R.B.J., Shen, R.F. Structural Elements & Modelling Excavations in Plaxis, Power Point Presentation File, Delf, Netherlands, 2011

[44] Sluis, J., Witteveen, B. Plaxis Bulletin, Autumn issue 2013.

[45] Empfehlungen des Arbeitskreises "Baugruben"- EA "Baugruben", 5. Auflage. Ernst & Sohn GmbH & Co, 2012

LIST OF NOTATIONS AND ABREVIATIONS

Chapter 1

e_a – active earth pressure (kN/m^2)

e_p – passive earth pressure (kN/m^2)

K_a – coefficient of active earth pressure (-)

K_p – coefficient of passive earth pressure (-)

σ_v' – effective vertical pressure (kN/m^2)

c' – cohesion intercept in Mohr-Coulomb failure criterion (kPa)

Chapter 2

ρ – settlement, (mm)

ρ_a – settlement in the serviceability limit state (mm)

q_a – load in serviceability limit state (kN/m^2)

q_c – load in ultimate limit state (kN/m^2)

q – bearing capacity of the soil (kN/m^2)

τ_s – shear stresses along the shaft of piles (kN/m^2)

q_b – normal stresses at base of piles (kN/m^2)

L_f – load factor (-)

w – width of visible cracks in the buildings (mm)

u_x – horizontal displacement (mm)

s – total settlements (mm)

β – angular distortion (-)

σ_c – compressive stress (kN/m^2)

σ_t – tensile stress (kN/m^2)

H – height of the wall (m)

E – Young's modulus (kN/m^2)

I – inertia moment (m^4)

A – cross-section area (m^2)

η – factor of safety (-)

Chapter 3

u_e – excess pore water pressure (kPa)

u_i – pore pressure immediately after construction (kPa)

u_c – steady state pore pressure (kPa)

φ' – angle of friction (◦)

s_u – undrained strength (kPa)

Chapter 4

ULS – ultimate limit state analysis (-)

SLS – serviceability limit state analysis (-)

e – voids ratio

H – excavation depth (m)

ε – strain (-)

ε^e – elastic strain (-)

ε^p, ε^{ps}, ε^{pc} – plastic strain, shear hardening part of plastic strain, compression hardening part of plastic strain (-)

ε_v, ε_v^{pc}, ε_v^{ps} – volumetric strain, shear hardening part of plastic volumetric strain, compression hardening part of plastic volumetric strain (-)

ν' – Poisson's ratio (-)

ν_{ur} – Poisson's ratio of unloading/ reloading (-)

$\underline{D}^e$ – Elastic material stiffness matrix (-)

f, f^c, f^s – yield function, compression yield function, shear yield function (-)

g, g^c, g^s – plastic potential function, plastic potential function for shear hardening, plastic potential function for compression hardening (-)

λ, λ^c, λ – plastic multiplier, plastic multiplier for shear hardening, plastic multiplier for compression hardening (-)

τ_n – shear stress (kN/m^2)

G – shear modulus (kN/m^2)

G_0 – initial shear modulus (kN/m^2)

γ – shear strain (-)

γ^p – plastic shear strain (-)

$\gamma_{0,7}$ – shear strain level at 70% of G_0 (-)

m – exponent of the power low (-)

E – Young's modulus (kN/m^2)

E_{oed} – oedometer modulus (kN/m^2)

E_{50}^{ref} – triaxial stiffness modulus at the reference confining pressure p^{ref} (kN/m^2)

E_{oed}^{ref} – oedometer stiffness modulus at the reference confining pressure p^{ref} (kN/m^2)

E_{ur}^{ref} – unloading/ reloading stiffness modulus at the reference confining pressure p^{ref} (kN/m^2)

p^{ref} – reference pressure (kN/m^2)

q – deviatoric stress (kN/m^2)

q_a – asymptotic failure stress (kN/m^2)

q_f – ultimate deviatoric stress (kN/m^2)

R_f – failure ratio (-)

σ_f' – normal effective stresses on the failure plane (kN/m^2)

σ_t' – tension strength (kN/m^2)

σ_1' – major effective principal stress (kN/m^2)

σ_3' – minor effective principal stress (kN/m^2)

σ_1 – major total principal stress (kN/m^2)

σ_3 – minor total principal stress (kN/m^2)

φ' – angle of friction (◦)

φ_p – failure angle of friction(◦)

φ_{cv} – critical state angle of friction (◦)

φ_m – mobilized angle of friction (◦)

ψ – dilatancy angel (◦)

ψ_m – mobilized angle of dilatancy(◦)

M – stress ratio at failure (-)

p_p – preconsolidation stress (kN/m^2)

H^s – shear hardening modulus (kN/m^2)

H^c – compression hardening modulus (kN/m^2)

Chapter 5

LR – low risk level

IR – intermediate risk level

HR – high risk level

I_c – consistency index (-)

k_f – permeability coefficient of soil (m/s)

E_s – compressibility modulus (kN/m^2)

σ_v – axial stress (kN/m^2)

ε_a – axial strain (-)

L – distance of influence (m)

L – pile length (m)

s – depth of the groundwater lowering (m)

s – pile head settlements (m)

R_d – pile resistance (kN)

R_{inter} – interface factor/ friction reduction factor (-)

δ – angle of friction between structure and soil (◦)

T_{skin} – lateral skin friction (kN/m^2)

LIST OF FIGURES

LIST OF TABLES

ANNEXES

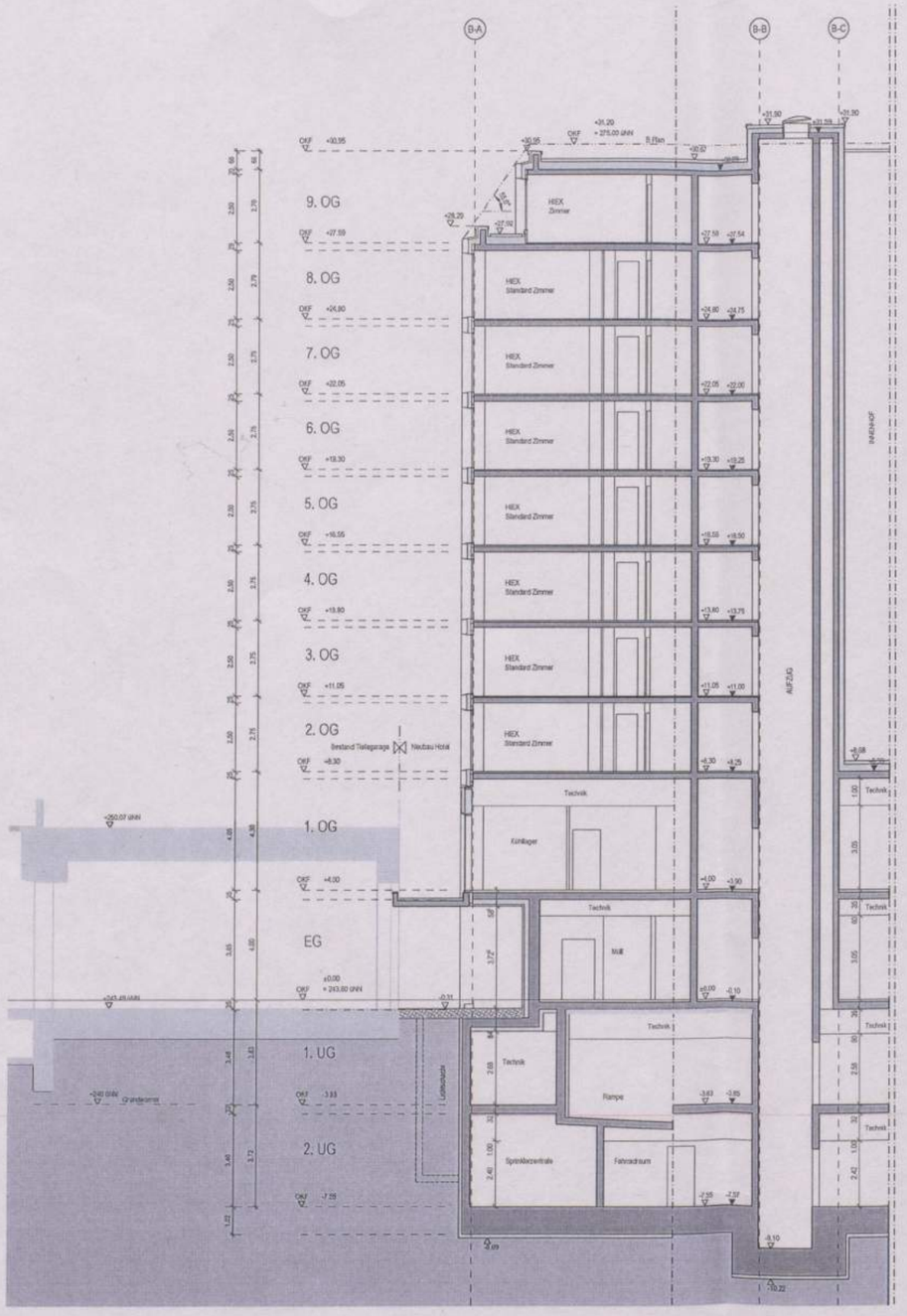

INDEX	DATUM	ÄNDERUNG		
A	13.07.2015	ergänzter Planstand	HNYP	

VERFASSER	LPH	PLANART	GESCHOSS	INHALT	STATUS	INDEX
ARC	4	SN	BB	SBB	F	A

PROJEKT

Stuttgart Europaviertel
Hotel Stuttgart Baufeld 15

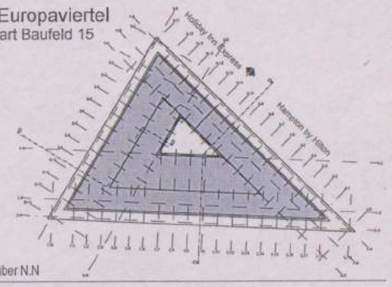

N

±0.00 = 243.80 m über N.N

AUFTRAGGEBER
Objektgesellschaft Hotelprojekt Stuttgart
Wolframstraße GmbH & Co. KG
Steinmessen 12 | 75086 Bröckerfeld | DATUM 13.05.2015 | UNTERSCHRIFT

ARCHITEKT
Eike Becker_Architekten
Gesellschaft von Architekten mbH
Charlottenstraße 4 | 10969 Berlin
Tel.: +49 (0) 30 25 93 74 - 0 | DATUM 13.05.2015 | UNTERSCHRIFT

PROJEKTSTEUERER
ASTO Communal Projekt GmbH
Am Neuen Markt 15 | 99448 Kranichfeld | T: 036450- 438 15 | m.caprani@astopark.de

STATIK
R&P RUFFERT
Ingenieurgesellschaft mbH
Schmidtstedter Straße 25-25 | 99084 Erfurt
T: 03 61 - 59 08 7 - 0 | info.erfurt@ruffert-ingenieure.de

HAUSTECHNIK
IGIV Ingenieure GmbH
Göltzsstraße 18 | 70825 Korntal-Münchingen
T: 07 11 - 83 95 05 - 0 | mhoneck@igiv-ingenieure.de

BRANDSCHUTZ
Heister + Ronkartz
Weserstraße 3 | 41836 Hückelhoven
T: 0 24 33 - 9 51 71 - 0 | info@heister-ronkartz.de

BAUPHYSIK
W&W Bauphysik GbR
Wiesenfeldstraße 65 | 71087 Leubsdorf
T: 0 71 95 - 95 03 - 64 | mail@wwbauphysik.de

PHASE
Genehmigungsplanung

MAßSTAB
1:100

PLANINHALT
Schnitt BB

ERSTELLT 13.05.2015 | GEZ.V. eb_a

PLANGRÖSSE A1 | PROJEKT-NR. 475

VERFASSER	LPH	PLANART	GESCHOSS	INHALT	STATUS	INDEX
ARC	4	SN	BB	SBB	F	A

Annex A2

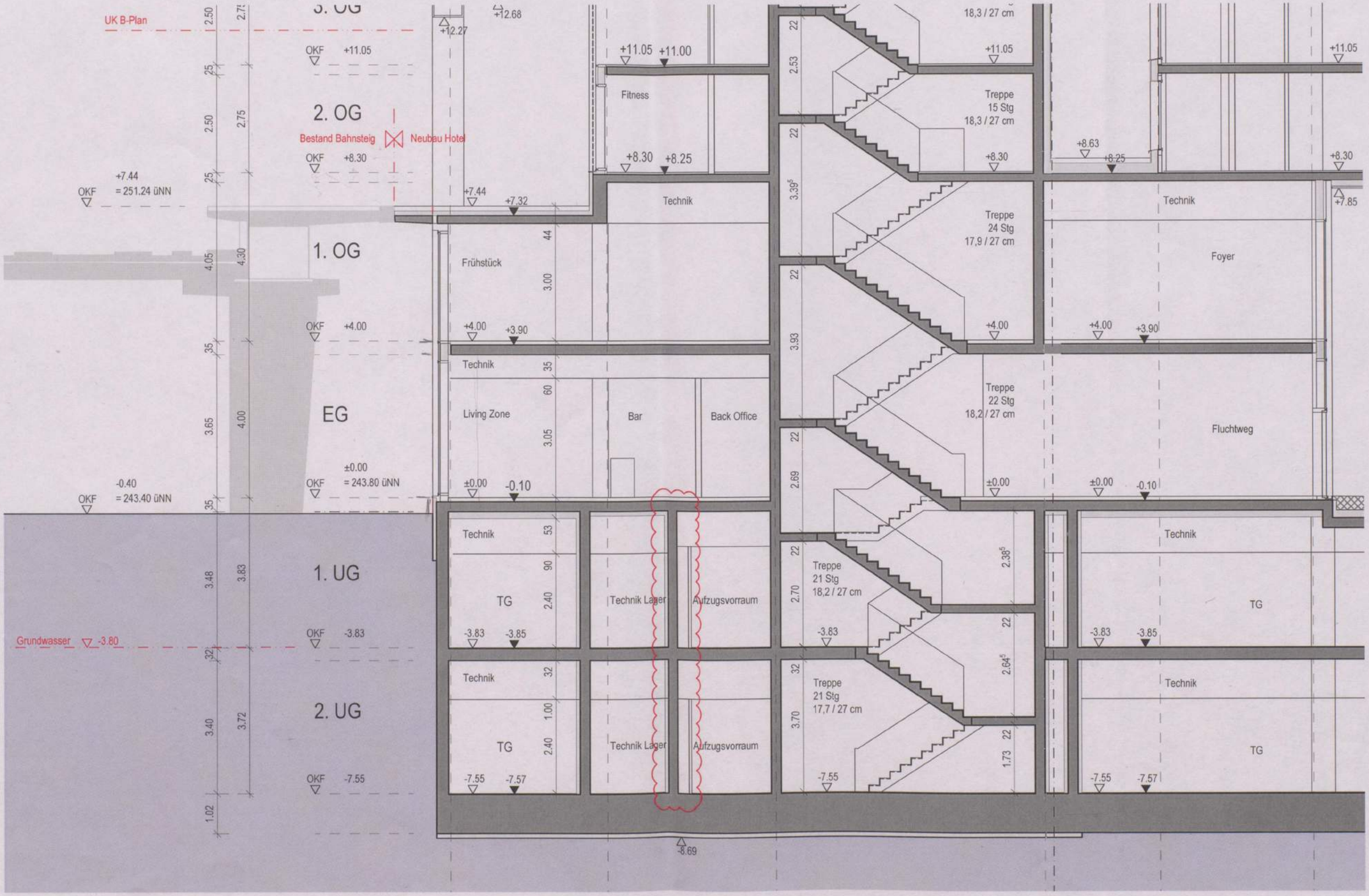
UK B-Plan
3. OG
OKF +11.05
2. OG
Bestand Bahnsteig
Neubau Hotel
OKF +8.30
+7.44
OKF = 251.24 üNN
1. OG
OKF +4.00
EG
±0.00
OKF = 243.80 üNN
-0.40
OKF = 243.40 üNN
1. UG
Grundwasser -3.80
OKF -3.83
2. UG
OKF -7.55
+12.27
+12.68
+11.05 +11.00
Fitness
+8.30 +8.25
Technik
+7.44
+7.32
Frühstück
+4.00 +3.90
Technik
Living Zone
Bar
Back Office
±0.00 -0.10
Technik
TG
Technik Lager
Aufzugsvorraum
-3.83 -3.85
Technik
TG
Technik Lager
Aufzugsvorraum
-7.55 -7.57
-8.69
18,3 / 27 cm
+11.05
Treppe
15 Stg
18,3 / 27 cm
+8.30
Treppe
24 Stg
17,9 / 27 cm
+4.00
Treppe
22 Stg
18,2 / 27 cm
±0.00
Treppe
21 Stg
18,2 / 27 cm
-3.83
Treppe
21 Stg
17,7 / 27 cm
-7.55
+8.63
+8.25
+4.00 +3.90
±0.00 -0.10
+11.05
+8.30
+7.85
Technik
Foyer
Fluchtweg
Technik
TG
-3.83 -3.85
Technik
TG
-7.55 -7.57

Annex A3

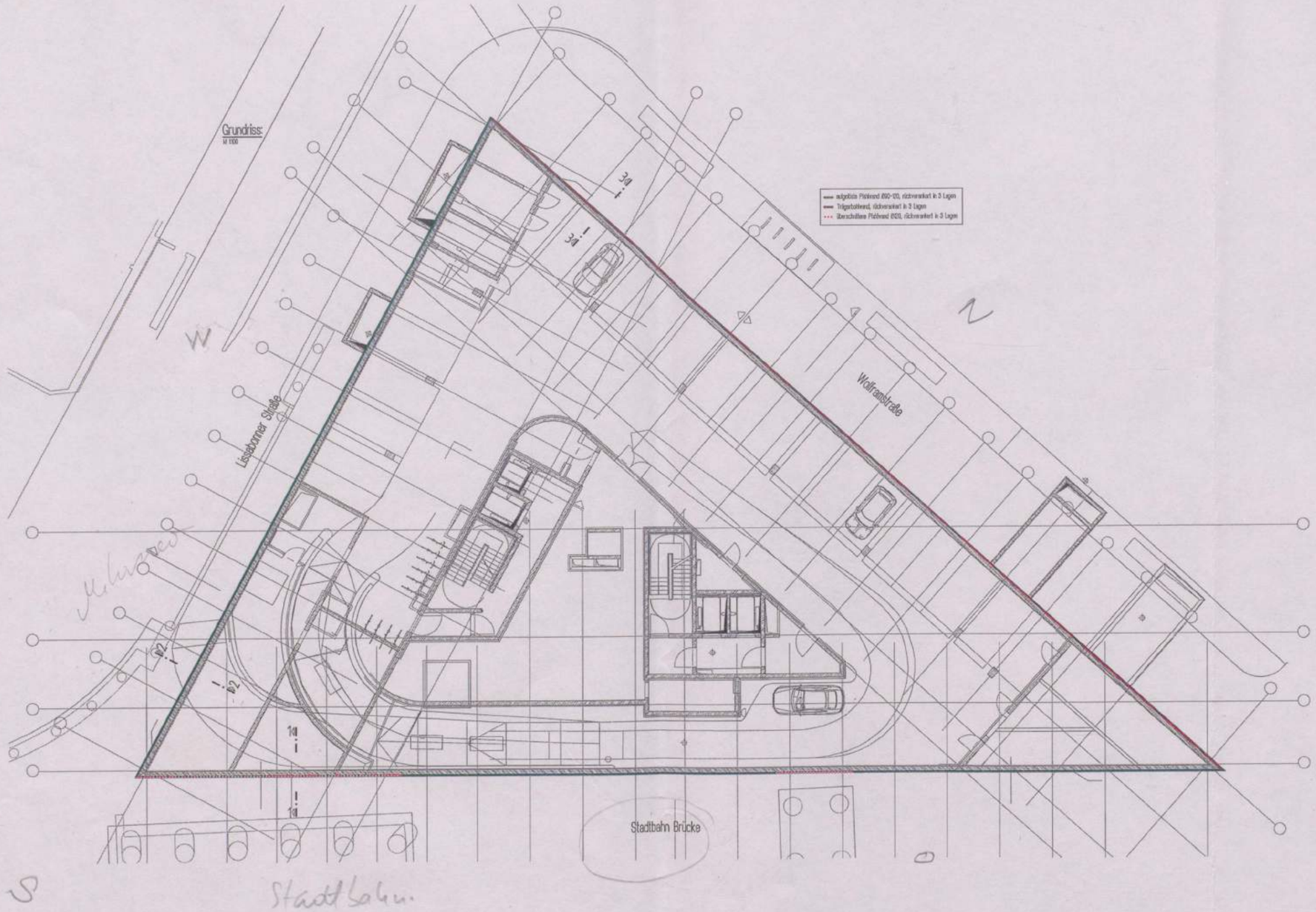
Grundriss
M 1:100
Lissabonner Straße
Wolframstraße
Stadtbahn Brücke
Stadtbahn

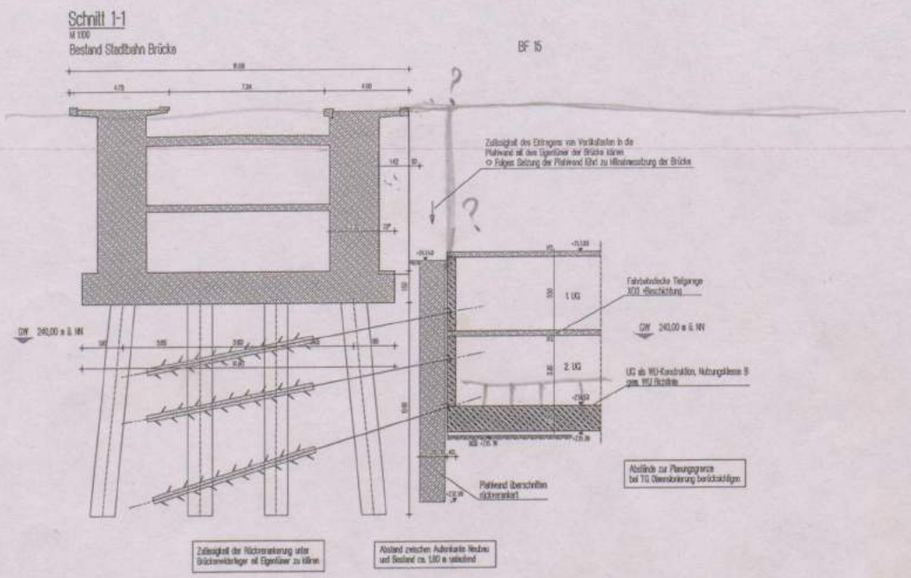
Schnitt 1-1
M 1:100
Bestand Stadtbahn Brücke
BF 15
1.UG
2.UG

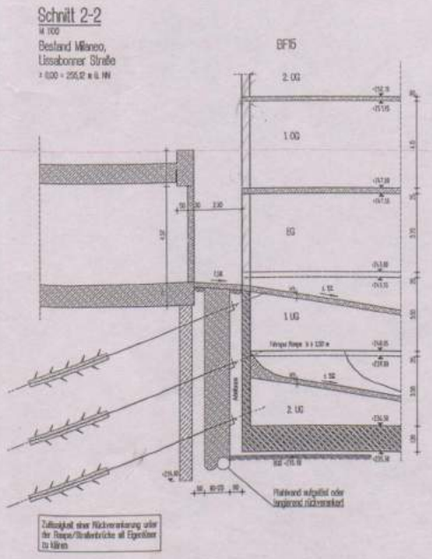
Schnitt 2-2
M 1:100
Bestand Milaneo,
Lissabonner Straße
BF15
2.OG
1.OG
EG
1.UG
2.UG

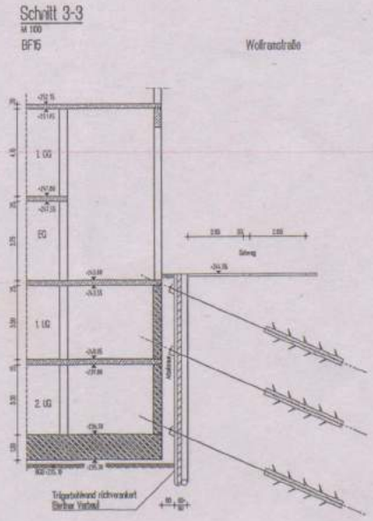
Schnitt 3-3
M 1:100
BF15
Wolframstraße
1.OG
EG
1.UG
2.UG

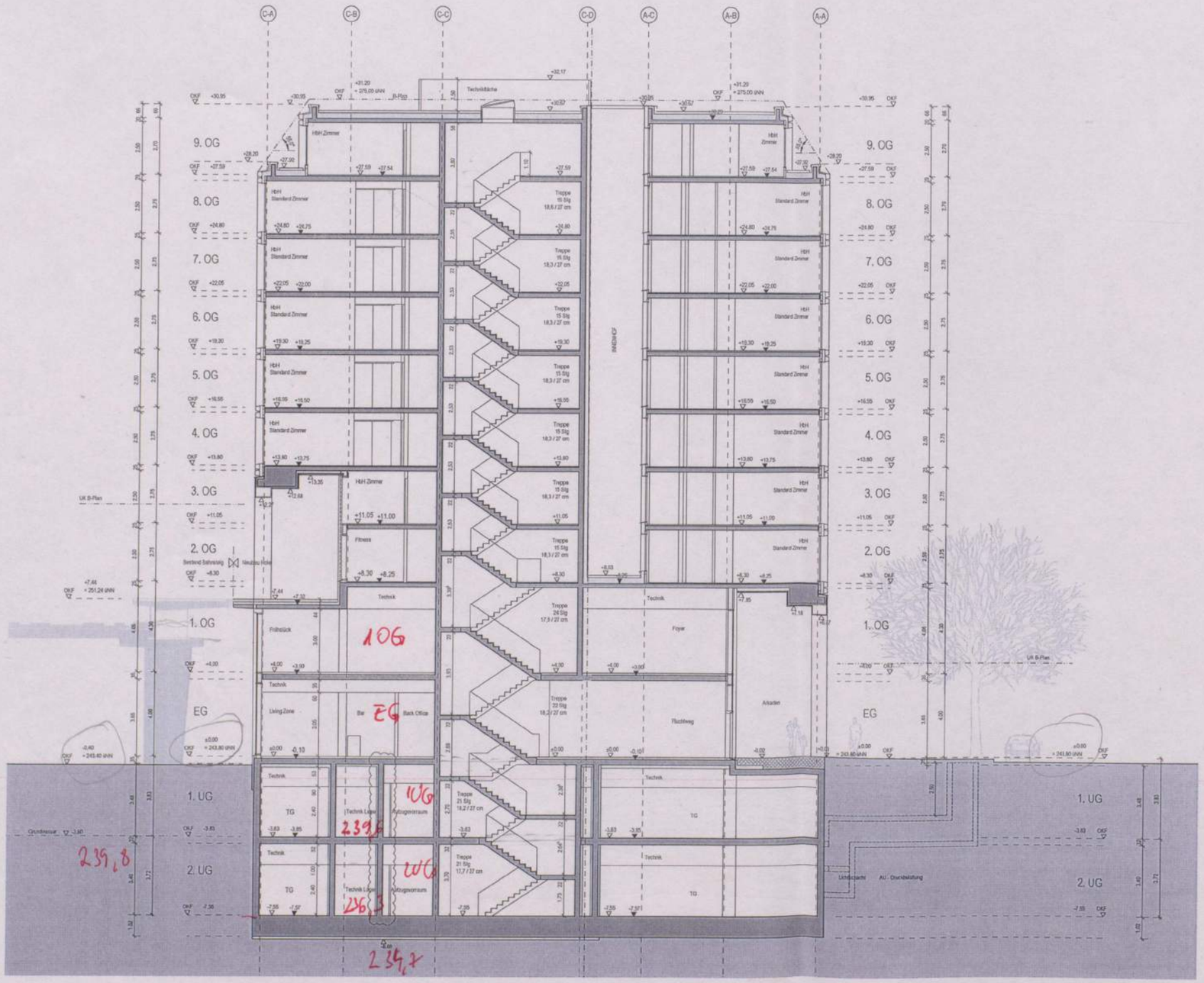

INDEX	DATUM	ÄNDERUNG	BEARB.	GEPR.
A	13.07.2015	ergänzter Planstand	HVP	

VERFASSER	LFN	PLANART	GESCHOSS	INHALT	STATUS	INDEX
ARC	4	SN	AA	SAA	F	A

PROJEKT

Stuttgart Europaviertel
Hotel Stuttgart Baufeld 15

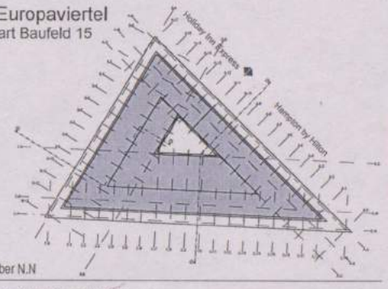

N

±0.00 = 243,80 m über N.N

AUFTRAGGEBER
Objektgesellschaft Hotelprojekt Stuttgart
Wolframstraße GmbH & Co. KG
Steinmeisen 12 | 76646 Bruchsal | DATUM 15.05.2015 | UNTERSCHRIFT

ARCHITEKT
Eike Becker_Architekten
Gesellschaft von Architekten mbH
Charlottenstraße 4 | 10969 Berlin
Tel.: +49 (0) 30 25 93 74 - 0 | DATUM 13.05.2015 | UNTERSCHRIFT

PROJEKTSTEUERER
ASTO Communal Projekt GmbH
Am Neuen Markt 15 | 99448 Kranichfeld | T: 036450- 438 15 | m.caprani@astopark.de

STATIK
R&P RUFFERT
Ingenieurgesellschaft mbH
Schmidstedter Straße 23-25 | 99084 Erfurt
T: 03 61 - 59 06 7 - 0 | info.erfurt@ruffert-ingenieure.de

HAUSTECHNIK
IGV Ingenieure GmbH
Gottbisstraße 16 | 70825 Korntal-Münchingen
T: 07 11 - 83 95 05 - 0 | mhoesel@igv-ingenieure.de

BRANDSCHUTZ
Heister + Ronkartz
Wiesenstraße 3 | 41836 Hückelhoven
T: 0 24 33 - 9 51 71 - 0 | info@heister-ronkartz.de

BAUPHYSIK
W&W Bauphysik GbR
Wiesenstraße 69 | 71397 Leutenbach
T: 0 71 95 - 95 03 - 04 | mail@wwbauphysik.de

PHASE
Genehmigungsplanung

MASSSTAB
1:100

PLANINHALT
Schnitt AA

ERSTELLT
13.05.2015

GEZ. V.
eb_a

PLANGRÖSSE
A1

PROJEKT-NR.
475

VERFASSER	LFN	PLANART	GESCHOSS	INHALT	STATUS	INDEX
ARC	4	SN	AA	SAA	F	A

Annex B1

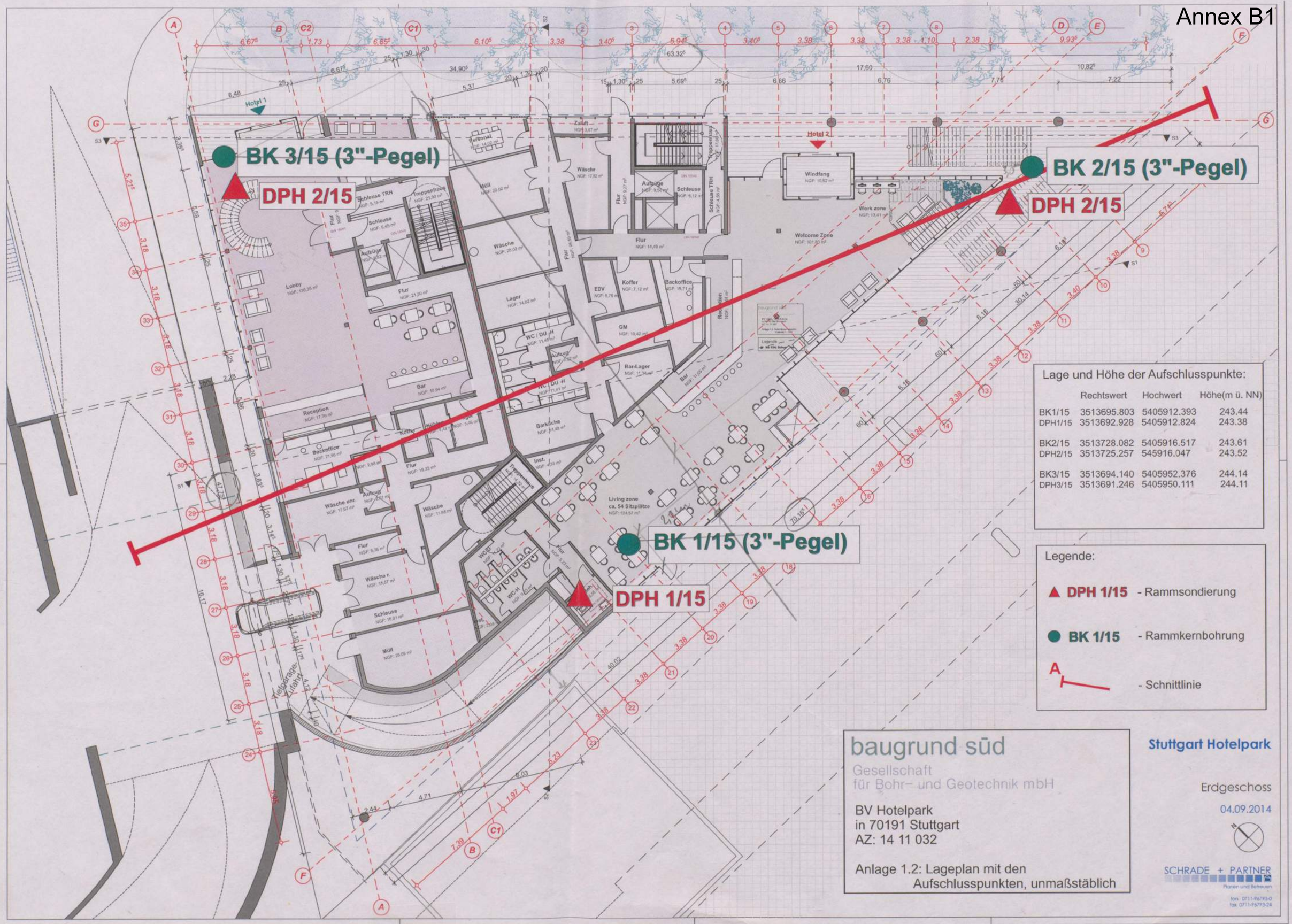

Lage und Höhe der Aufschlusspunkte:

	Rechtswert	Hochwert	Höhe(m ü. NN)
BK1/15	3513695.803	5405912.393	243.44
DPH1/15	3513692.928	5405912.824	243.38
BK2/15	3513728.082	5405916.517	243.61
DPH2/15	3513725.257	545916.047	243.52
BK3/15	3513694.140	5405952.376	244.14
DPH3/15	3513691.246	5405950.111	244.11

Legende:

▲ DPH 1/15 - Rammsondierung

● BK 1/15 - Rammkernbohrung

A - Schnittlinie

baugrund süd
Gesellschaft
für Bohr- und Geotechnik mbH

BV Hotelpark
in 70191 Stuttgart
AZ: 14 11 032

Anlage 1.2: Lageplan mit den Aufschlusspunkten, unmaßstäblich

Stuttgart Hotelpark

Erdgeschoss

04.09.2014

SCHRADE + PARTNER
Planen und Betreuen
tel. 0711-96793-0
fax 0711-96793-24

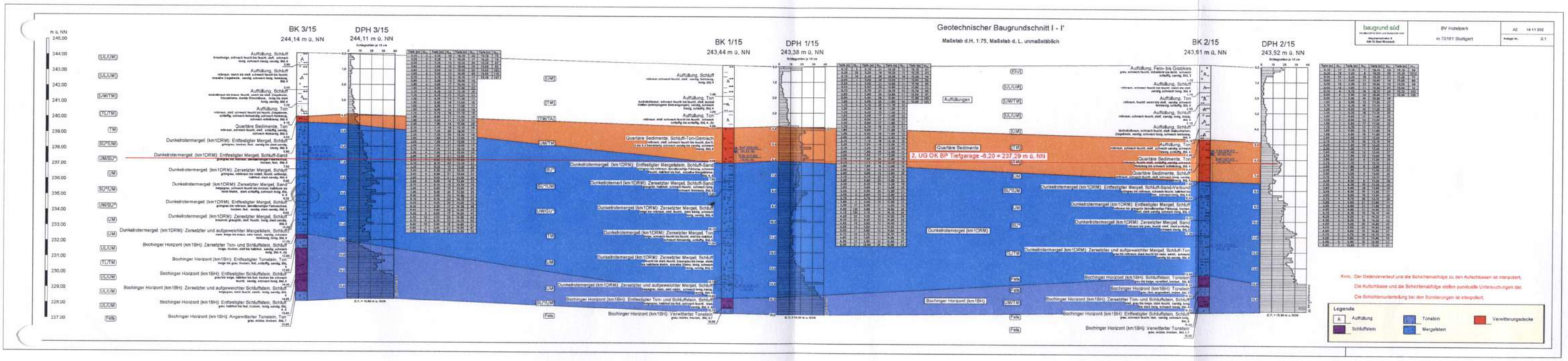
Geotechnischer Baugrundschnitt I - I'
Maßstab d.H. 1:75, Maßstab d. L. unmaßstäblich
BK 3/15
244,14 m ü. NN
DPH 3/15
244,11 m ü. NN
BK 1/15
243,44 m ü. NN
DPH 1/15
243,38 m ü. NN
BK 2/15
243,61 m ü. NN
DPH 2/15
243,52 m ü. NN
m ü. NN
Auffüllungen
Quartäre Sedimente
2. UG OK BP Tiefgarage -8,20 = 237,29 m ü. NN
Dunkelrotermergel (km1DRM)
Bochinger Horizont (km1BH)
Anm.: Der Geländeverlauf und die Schichtenabfolge zu den Aufschlüssen ist interpoliert.
Die Aufschlüsse und die Schichtenabfolge stellen punktuelle Untersuchungen dar.
Die Schichtenunterteilung bei den Sondierungen ist interpoliert.
Legende
Auffüllung
Schluffstein
Tonstein
Mergelstein
Verwitterungsdecke
baugrund süd
BV Hotelpark
in 70191 Stuttgart

Ge

Ma

BK 1/15

243,44 m ü. NN

DPH 1/15

243,38 m ü. NN

Schlagzahlen je 10 cm

n]	N_{10}	Tiefe [m]	N_{10}
	20	15.10	75
	17	15.20	79
	20	15.30	87
	20	15.40	93
	20	15.50	102
	20	15.60	115
	17	15.70	137
	16		
	17		
	22		
	15		
	13		
	11		
	15		
	13		
	19		
	19		
	19		
	19		
	20		
	18		
	11		
	10		
	10		
	13		
	15		
	18		
	20		
	23		
	29		
	27		
	22		
	25		
	32		
	29		
	23		
	25		
	26		
	25		
	23		
	29		
	32		
	38		
	42		
	45		
	49		
	52		
	61		
	67		
	73		

[UM] **Auffüllung, Schluff**
rotbraun,schwach feucht, steif, sandig, feinkiesig, tonig, bkl. 4

2.00

[TM] **Auffüllung, Ton**
dunkelrotbraun, schwach feucht bis feucht, steif, dunkel Stellen (anthopogene Beimengungen), sandig, schwach kiesig, schluffig, Bkl. 4

3.00

TM/TA **Auffüllung, Ton**
rotbraun, steif, schwach feucht bis feucht, schwach schluffig bis schluffig, Bkl. 4, (5)

4.00

UM/TM **Quartäre Sedimente, Schluff-Ton-Gemisch**
rotbraun, steif, schwach feucht bis feucht, (bei 5, 2 bis 5,3 Sandstein), schwach sandig bis sandig, schwach kiesig, Bkl. 4

5.40 (238.04) (03.02.15)
5.62 (237.82) (18.02.15)

6.00

SU* **Dunkelrotermergel: (km1DRM): Entfestigter Mergelstein, Schluff**
grüngrau bis rotbraun: lamellenartige Färbung, schwach feucht, halbfest bis fest, stark sandig, einzelne Mergelsteine, Bkl. 4, 6

7.50

SU*/UM **Dunkelrotemerl (km1DRM): Zersetzter Mergel, Schluff-Sand**
graugrün, halbfest, schwach feucht, schwach tonig, schwach feinkiesig, Bkl. 4

8.00

UM/GU* **Dunkelrotemergel (km1DRM): Zersetzter Mergel, Schluff**
beige bis rotbraun, steif, feucht, stark kiesig, schwach tonig, sandig, Bkl. 4

10.70

TM **Dunkelrotemergel (km1DRM): Zersetzter Mergel, Ton**
beige, schwach feucht bis feucht, steif bis halbfest, schwach feinsandig, schluffig, Bkl. 4

11.50

UM **Dunkelrotemergel (km1DRM): Zersetzter Mergel, Schluff**
feucht bis sterk feucht, braungrau bis beige, steife bis halbfeste Matrix, einzelne Steine, tonig, schwach kiesig, sandig, Bkl. 4

14.10

UM **Dunkelrotemergel (km1DRM): Zersetzter und aufgeweichter Mergel, Schluff**
beigegrau, nass, sehr weich, schwach tonig/kiesig, sandig, Bkl. 4

14.20 (229.14) (03.02.15)

15.00

SU*/UM **Bochinger Horizont (km1BH): Entfestigter Ton- und Schluffstein, Schluff**
beigegrau, halbfest bis fest, schwach feucht, stark sandig, Bkl. 4, 6

15.70

Fels **Bochinger Horizont (km1BH): Verwitterter Tonstein**
grau, mürbe, trocken, Bkl. 6,7

16.00

E.T. = 16,00 m u. GOK

Tiefe [m]	N_{10}	Tiefe [m]	N_{10}	Tiefe [m]	N_{10}	Tiefe [m]	N_{10}
0.10	4	5.10	21	10.10	12	15.10	47
0.20	20	5.20	19	10.20	12	15.20	49
0.30	10	5.30	28	10.30	10	15.30	56
0.40	3	5.40	20	10.40	11	15.40	58
0.50	3	5.50	21	10.50	11	15.50	66
0.60	2	5.60	20	10.60	12	15.60	72
0.70	2	5.70	21	10.70	12	15.70	88
0.80	2	5.80	24	10.80	11	15.80	97
0.90	2	5.90	26	10.90	11	15.90	109
1.00	2	6.00	22	11.00	14	16.00	125
1.10	2	6.10	22	11.10	12		
1.20	1	6.20	18	11.20	13		
1.30	2	6.30	19	11.30	13		
1.40	2	6.40	17	11.40	12		
1.50	3	6.50	17	11.50	13		
1.60	3	6.60	17	11.60	11		
1.70	3	6.70	16	11.70	11		
1.80	4	6.80	17	11.80	12		
1.90	4	6.90	18	11.90	13		
2.00	4	7.00	18	12.00	12		
2.10	6	7.10	18	12.10	15		
2.20	7	7.20	19	12.20	13		
2.30	6	7.30	18	12.30	12		
2.40	7	7.40	18	12.40	14		
2.50	7	7.50	17	12.50	12		
2.60	7	7.60	14	12.60	15		
2.70	7	7.70	18	12.70	15		
2.80	8	7.80	16	12.80	16		
2.90	8	7.90	13	12.90	18		
3.00	7	8.00	13	13.00	20		
3.10	7	8.10	23	13.10	21		
3.20	7	8.20	25	13.20	23		
3.30	7	8.30	23	13.30	19		
3.40	7	8.40	21	13.40	20		
3.50	8	8.50	20	13.50	21		
3.60	8	8.60	19	13.60	23		
3.70	9	8.70	19	13.70	23		
3.80	8	8.80	18	13.80	23		
3.90	17	8.90	17	13.90	23		
4.00	126	9.00	15	14.00	39		
4.10	100	9.10	14	14.10	24		
4.20	22	9.20	15	14.20	26		
4.30	23	9.30	13	14.30	32		
4.40	19	9.40	12	14.40	27		
4.50	18	9.50	11	14.50	33		
4.60	17	9.60	12	14.60	34		
4.70	18	9.70	11	14.70	35		
4.80	18	9.80	11	14.80	30		
4.90	19	9.90	10	14.90	37		
5.00	21	10.00	24	15.00	42		

Quart

2. UG OK BP

Dunkelrot

Bochinger

Annex B2-2

baugrund süd Gesellschaft für Bohr- und Geotechnik mbH Maybachstraße 5 88410 Bad Wurzach	BV Hotelpark in 70191 Stuttgart	AZ 14 11 032 Anlage Nr. 2.1

BK 2/15

243,61 m ü. NN

DPH 2/15

243,52 m ü. NN

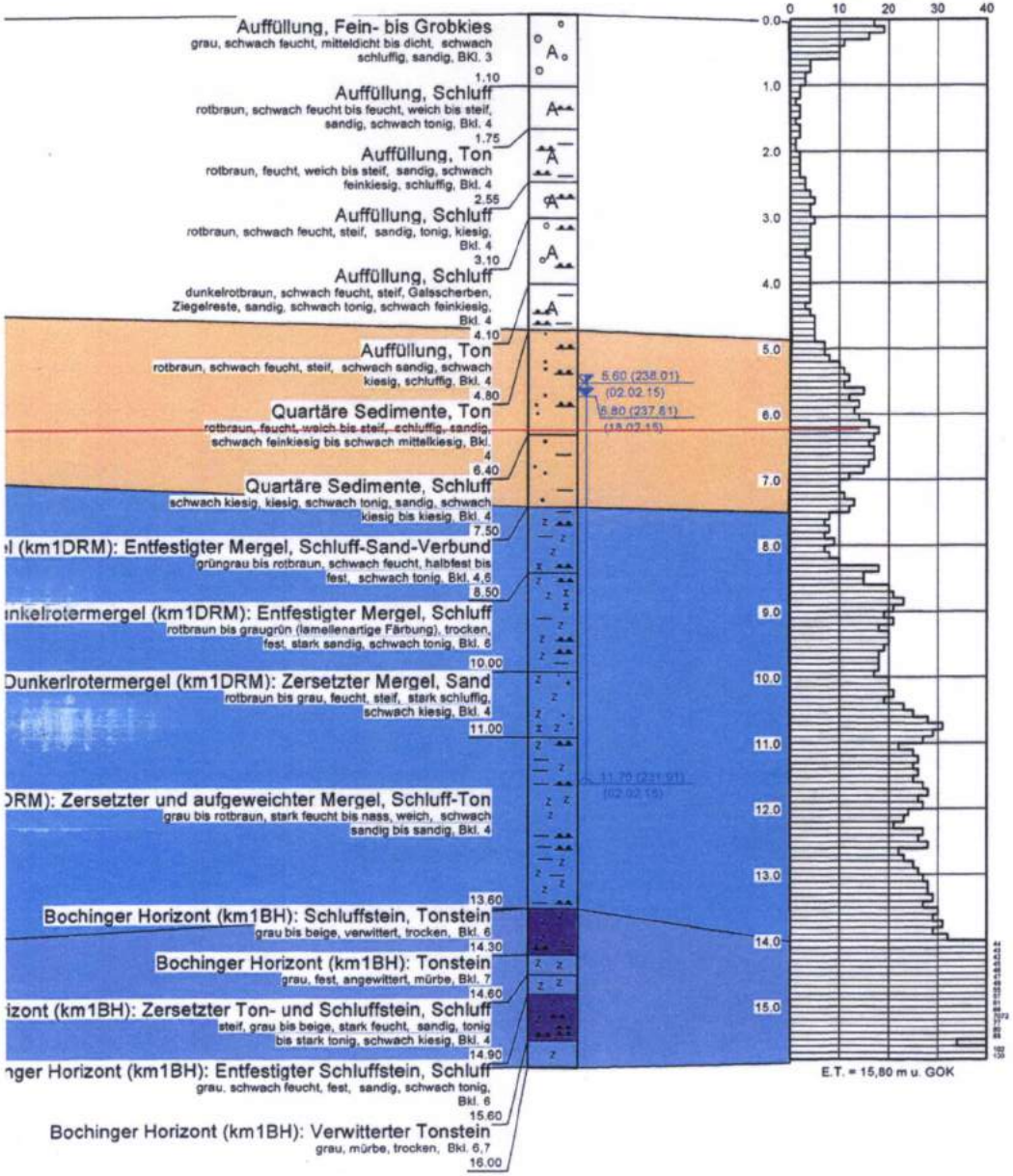

Tiefe [m]	N_{10}	Tiefe [m]	N_{10}	Tiefe [m]	N_{10}	Tiefe [m]	N_{10}
0.10	17	5.10	7	10.10	20	15.10	66
0.20	19	5.20	8	10.20	20	15.20	7072
0.30	16	5.30	10	10.30	21	15.30	77
0.40	11	5.40	11	10.40	19	15.40	80
0.50	10	5.50	12	10.50	23	15.50	88
0.60	10	5.60	11	10.60	25	15.60	34
0.70	4	5.70	15	10.70	28	15.70	102
0.80	4	5.80	12	10.80	31	15.80	120
0.90	3	5.90	14	10.90	29		
1.00	3	6.00	13	11.00	27		
1.10	2	6.10	14	11.10	22		
1.20	2	6.20	16	11.20	25		
1.30	1	6.30	18	11.30	26		
1.40	2	6.40	17	11.40	25		
1.50	2	6.50	16	11.50	26		
1.60	1	6.60	17	11.60	25		
1.70	2	6.70	17	11.70	27		
1.80	2	6.80	16	11.80	28		
1.90	1	6.90	15	11.90	26		
2.00	1	7.00	12	12.00	27		
2.10	2	7.10	10	12.10	24		
2.20	2	7.20	10	12.20	23		
2.30	2	7.30	11	12.30	21		
2.40	2	7.40	13	12.40	27		
2.50	3	7.50	12	12.50	26		
2.60	3	7.60	8	12.60	28		
2.70	4	7.70	7	12.70	22		
2.80	5	7.80	8	12.80	23		
2.90	4	7.90	7	12.90	25		
3.00	4	8.00	9	13.00	26		
3.10	5	8.10	7	13.10	27		
3.20	4	8.20	8	13.20	28		
3.30	4	8.30	10	13.30	28		
3.40	4	8.40	18	13.40	29		
3.50	4	8.50	15	13.50	27		
3.60	3	8.60	15	13.60	30		
3.70	4	8.70	20	13.70	29		
3.80	4	8.80	21	13.80	31		
3.90	4	8.90	23	13.90	29		
4.00	4	9.00	21	14.00	32		
4.10	4	9.10	19	14.10	44		
4.20	4	9.20	21	14.20	43		
4.30	4	9.30	18	14.30	42		
4.40	3	9.40	20	14.40	45		
4.50	4	9.50	20	14.50	46		
4.60	5	9.60	19	14.60	47		
4.70	5	9.70	18	14.70	49		
4.80	5	9.80	18	14.80	55		
4.90	5	9.90	18	14.90	57		
5.00	7	10.00	17	15.00	61		

Anm.: Der Geländeverlauf und die Schichtenabfolge zu den Aufschlüssen ist interpoliert.

Die Aufschlüsse und die Schichtenabfolge stellen punktuelle Untersuchungen dar.

Die Schichtenunterteilung bei den Sondierungen ist interpoliert.

Legende

- A — Auffüllung
- Tonstein
- Verwitterungsdecke
- Schluffstein
- Mergelstein

Annex B2-2

Geotechnischer Baugrundschnitt I - I'

Maßstab d.H. 1:75, Maßstab d. L. unmaßstäblich

baugrund süd
Gesellschaft für Bohr- und Geotechnik mbH
Maybachstraße 5
88410 Bad Wurzach

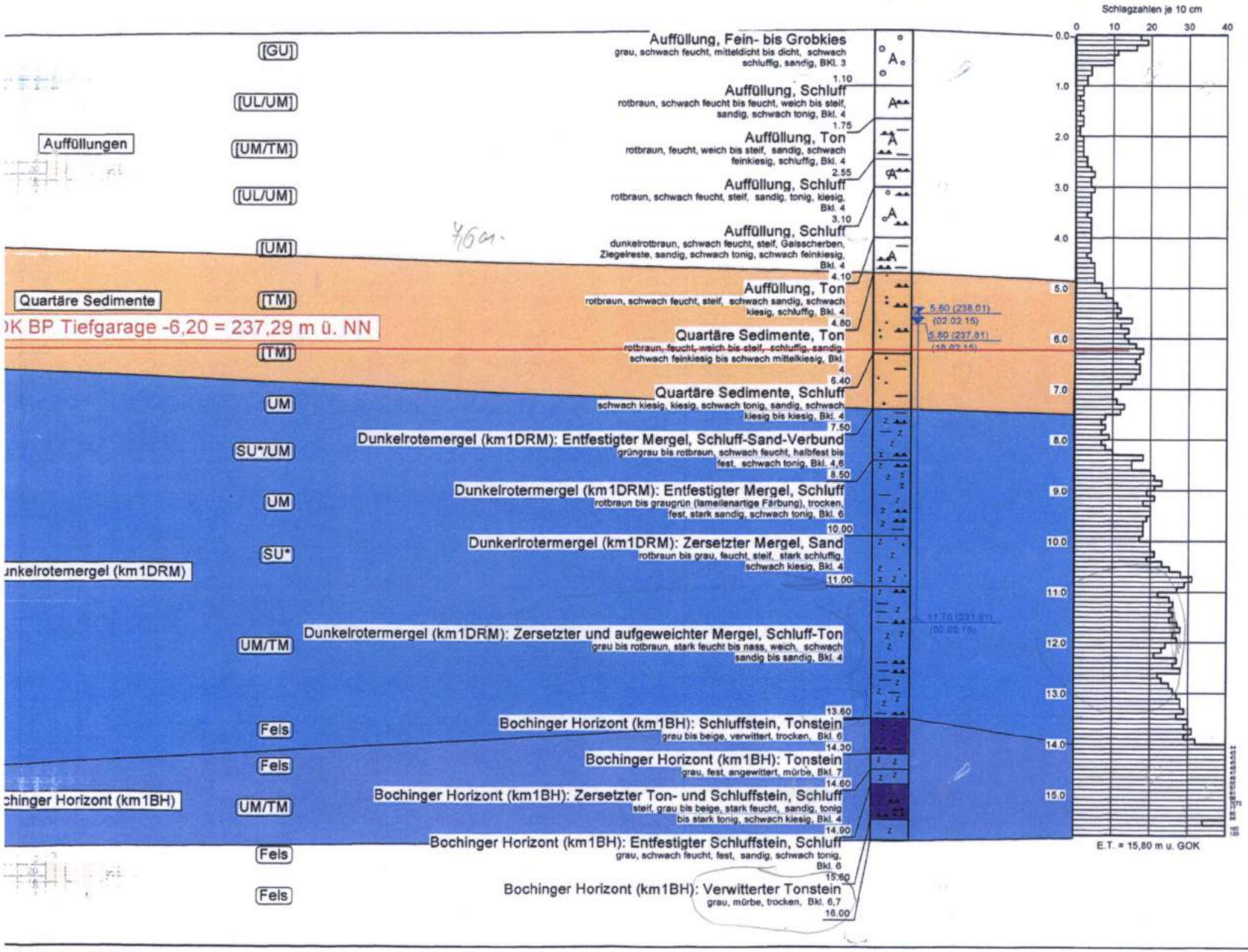

Tiefe [m]	N_{10}	Tiefe [m]	N_{10}	Tiefe [m]	N_{10}	Tiefe [m]	N_{10}
0.10	17	5.10	7	10.10	20	15.10	66
0.20	19	5.20	8	10.20	20	15.20	7072
0.30	16	5.30	10	10.30	21	15.30	77
0.40	11	5.40	11	10.40	19	15.40	80
0.50	10	5.50	12	10.50	23	15.50	86
0.60	10	5.60	11	10.60	25	15.60	34
0.70	4	5.70	15	10.70	28	15.70	102
0.80	4	5.80	12	10.80	31	15.80	120
0.90	3	5.90	14	10.90	29		
1.00	3	6.00	13	11.00	27		
1.10	2	6.10	14	11.10	22		
1.20	2	6.20	16	11.20	25		
1.30	1	6.30	18	11.30	26		
1.40	2	6.40	17	11.40	25		
1.50	2	6.50	16	11.50	26		
1.60	1	6.60	17	11.60	25		
1.70	2	6.70	17	11.70	27		
1.80	2	6.80	16	11.80	28		
1.90	1	6.90	15	11.90	26		
2.00	1	7.00	12	12.00	27		
2.10	2	7.10	10	12.10	24		
2.20	2	7.20	10	12.20	23		
2.30	2	7.30	11	12.30	21		
2.40	2	7.40	13	12.40	27		
2.50	3	7.50	12	12.50	26		
2.60	3	7.60	8	12.60	28		
2.70	4	7.70	7	12.70	22		
2.80	5	7.80	8	12.80	23		
2.90	4	7.90	7	12.90	25		
3.00	4	8.00	9	13.00	26		
3.10	5	8.10	7	13.10	27		
3.20	4	8.20	8	13.20	28		
3.30	4	8.30	10	13.30	28		
3.40	4	8.40	18	13.40	29		
3.50	4	8.50	16	13.50	27		
3.60	3	8.60	15	13.60	30		
3.70	4	8.70	20	13.70	29		
3.80	4	8.80	21	13.80	31		
3.90	4	8.90	23	13.90	29		
4.00	4	9.00	21	14.00	32		
4.10	4	9.10	19	14.10	44		
4.20	4	9.20	21	14.20	43		
4.30	4	9.30	18	14.30	42		
4.40	3	9.40	20	14.40	45		
4.50	4	9.50	20	14.50	46		
4.60	5	9.60	19	14.60	47		
4.70	5	9.70	18	14.70	49		
4.80	5	9.80	18	14.80	55		
4.90	5	9.90	18	14.90	57		
5.00	7	10.00	17	15.00	61		

Anm.: Der Geländeverlauf und die Sc

Die Aufschlüsse und die Schic

Die Schichtenunterteilung bei

Legende

A Auffüllung

Schluffstein

Annex B2-2

BK 3/15

244,14 m ü. NN

DPH 3/15

244,11 m ü. NN

Schlagzahlen je 10 cm

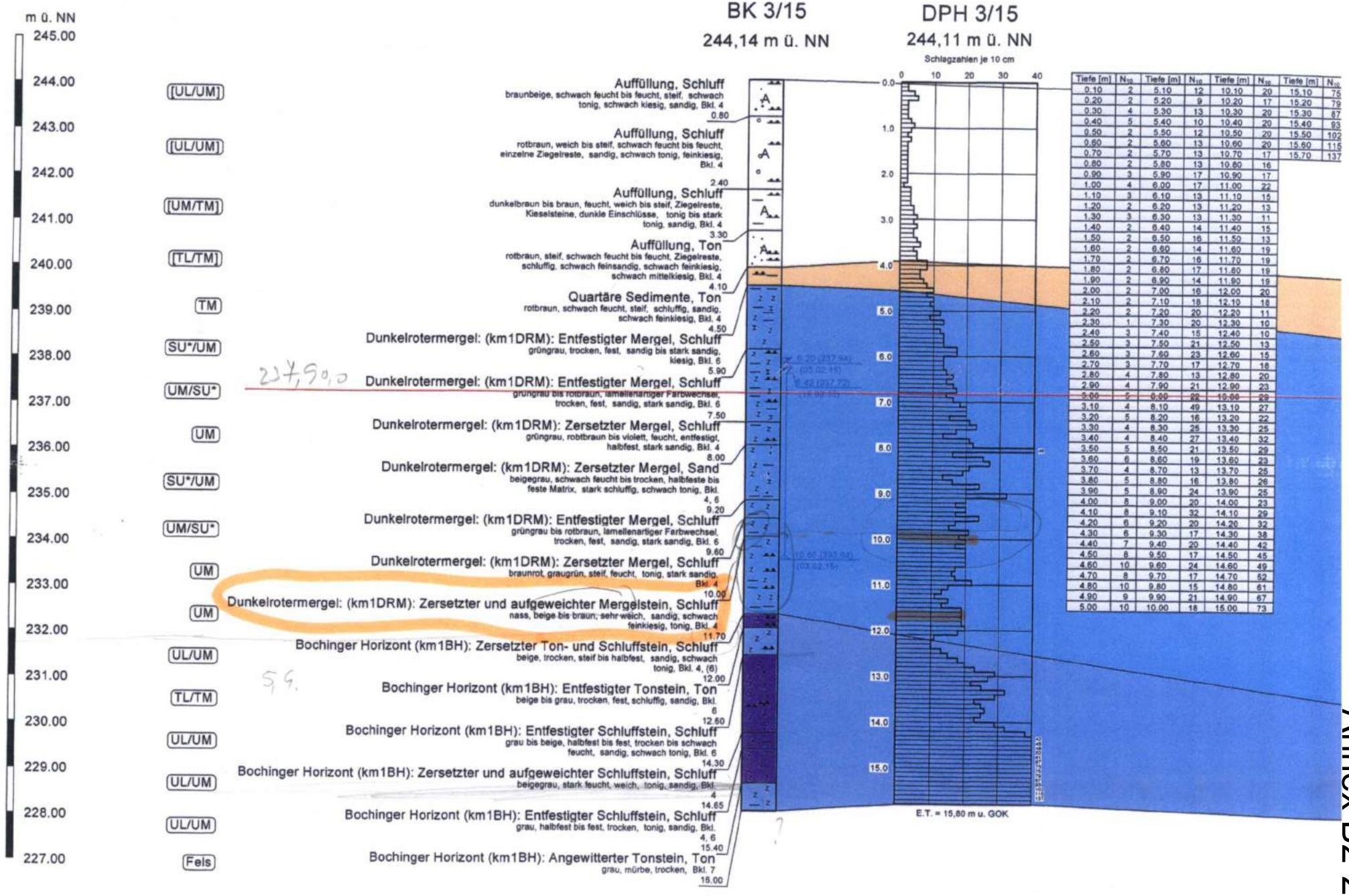

Tiefe [m]	N_{10}	Tiefe [m]	N_{10}	Tiefe [m]	N_{10}	Tiefe [m]	N_{10}
0.10	2	5.10	12	10.10	20	15.10	75
0.20	2	5.20	9	10.20	17	15.20	79
0.30	4	5.30	13	10.30	20	15.30	87
0.40	5	5.40	10	10.40	20	15.40	93
0.50	2	5.50	12	10.50	20	15.50	102
0.60	2	5.60	13	10.60	20	15.60	115
0.70	2	5.70	13	10.70	17	15.70	137
0.80	2	5.80	13	10.80	16		
0.90	3	5.90	17	10.90	17		
1.00	4	6.00	17	11.00	22		
1.10	3	6.10	13	11.10	15		
1.20	2	6.20	13	11.20	13		
1.30	3	6.30	13	11.30	11		
1.40	2	6.40	14	11.40	15		
1.50	2	6.50	16	11.50	13		
1.60	2	6.60	14	11.60	19		
1.70	2	6.70	16	11.70	19		
1.80	2	6.80	17	11.80	19		
1.90	2	6.90	14	11.90	19		
2.00	2	7.00	16	12.00	20		
2.10	2	7.10	18	12.10	18		
2.20	2	7.20	20	12.20	11		
2.30	1	7.30	20	12.30	10		
2.40	3	7.40	15	12.40	10		
2.50	3	7.50	21	12.50	13		
2.60	3	7.60	23	12.60	15		
2.70	3	7.70	17	12.70	16		
2.80	4	7.80	13	12.80	20		
2.90	4	7.90	21	12.90	23		
~~3.00~~	~~5~~	~~8.00~~	~~22~~	~~13.00~~	~~29~~		
3.10	4	8.10	49	13.10	27		
3.20	5	8.20	16	13.20	22		
3.30	4	8.30	25	13.30	25		
3.40	4	8.40	27	13.40	32		
3.50	5	8.50	21	13.50	29		
3.60	6	8.60	19	13.60	23		
3.70	4	8.70	13	13.70	25		
3.80	5	8.80	16	13.80	26		
3.90	5	8.90	24	13.90	25		
4.00	8	9.00	20	14.00	23		
4.10	8	9.10	32	14.10	29		
4.20	6	9.20	20	14.20	32		
4.30	6	9.30	17	14.30	38		
4.40	7	9.40	20	14.40	42		
4.50	8	9.50	17	14.50	45		
4.60	10	9.60	24	14.60	49		
4.70	8	9.70	17	14.70	52		
4.80	10	9.80	15	14.80	61		
4.90	9	9.90	21	14.90	67		
5.00	10	10.00	18	15.00	73		

BK 1/15: Tiefe 0,0 – 4,0 m u. GOK

BK 1/15: Tiefe 4,0 – 10,0 m u. GOK

BK 1/15: Tiefe 10,0 – 16,0 m u. GOK

BK 2/15: Tiefe 0,0 – 4,0 m u. GOK

BK 2/15: Tiefe 4,0 – 8,0 m u. GOK

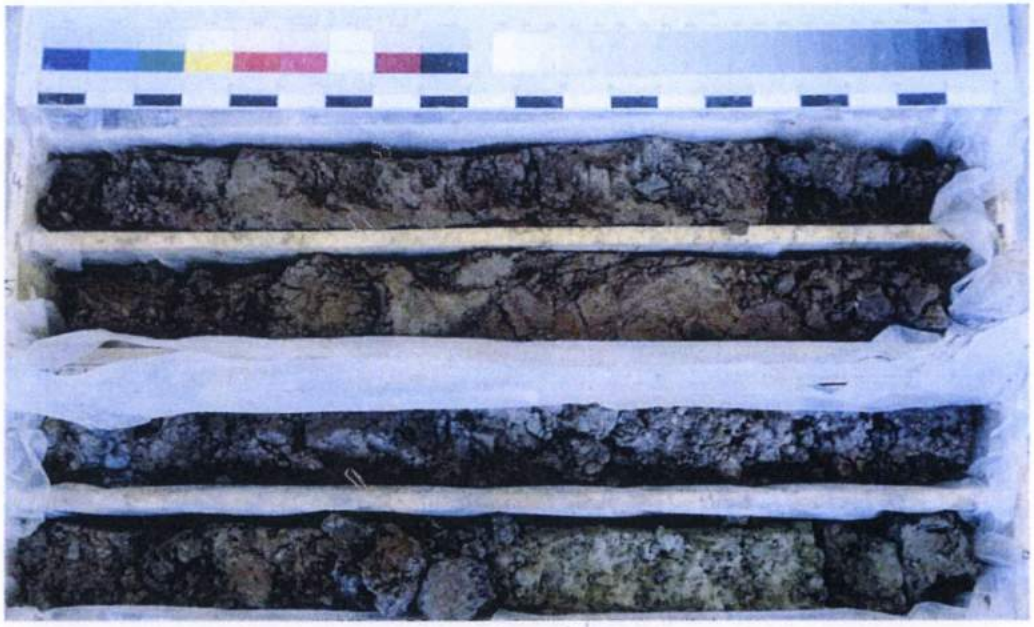

BK 2/15: Tiefe 8,0 – 12,0 m u. GOK

BK 2/15: Tiefe 12,0 – 16,0 m u. GOK

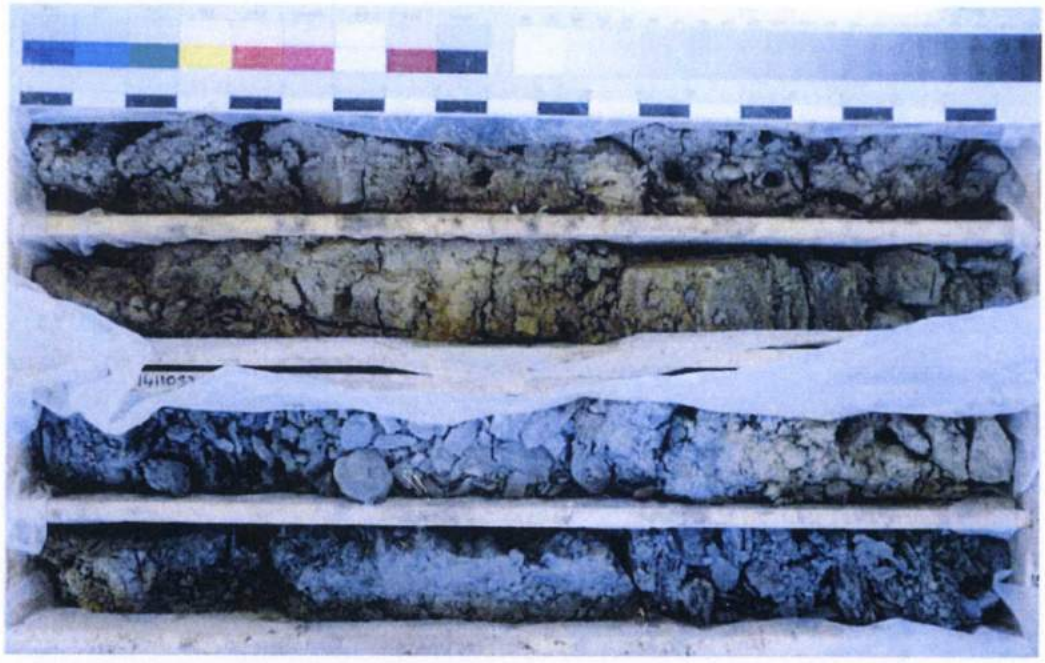

BK 3/15: Tiefe 0,0 – 4,0 m u. GOK

BK 3/15: Tiefe 4,0 – 8,0 m u. GOK

BK 3/15: Tiefe 8,0 – 12,0 m u. GOK

BK 3/15: Tiefe 12,0 – 16,0 m u. GOK

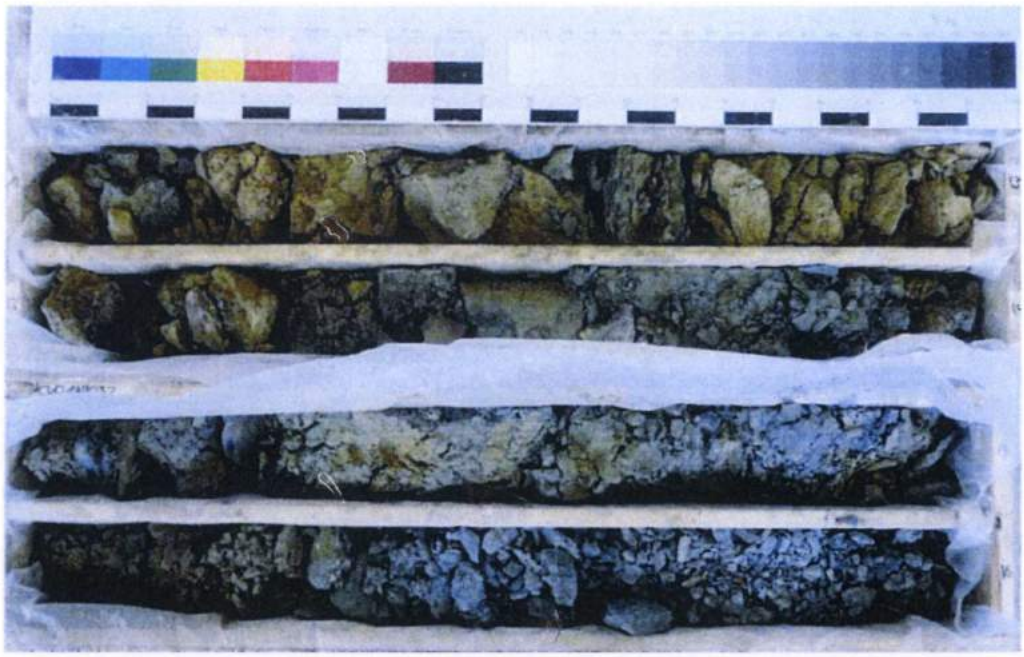

BauGrund Süd
ErdEnergieManagement GmbH
Maybachstraße 5
88410 Bad Wurzach

Projekt :	Hotelpark Wolframstraße, 70191 Stuttgart
Projektnr.:	AZ 14 11 032
Anlage :	2.2
Maßstab :	1: 75 / 1: 20

Pegelausbau

BK1/15

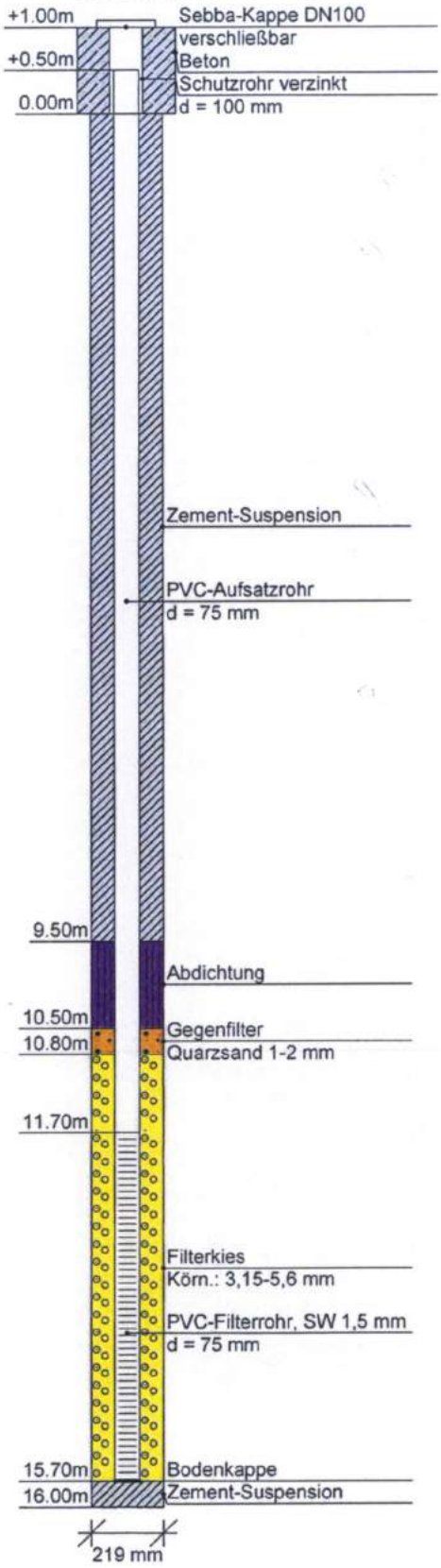

DC

BauGrund Süd
ErdEnergieManagement GmbH
Maybachstraße 5
88410 Bad Wurzach

Projekt :	Hotelpark Wolframstraße, 70191 Stuttgart
Projektnr.:	AZ 14 11 032
Anlage :	2.3
Maßstab :	1: 75 / 1: 20

Pegelausbau

BK2/15

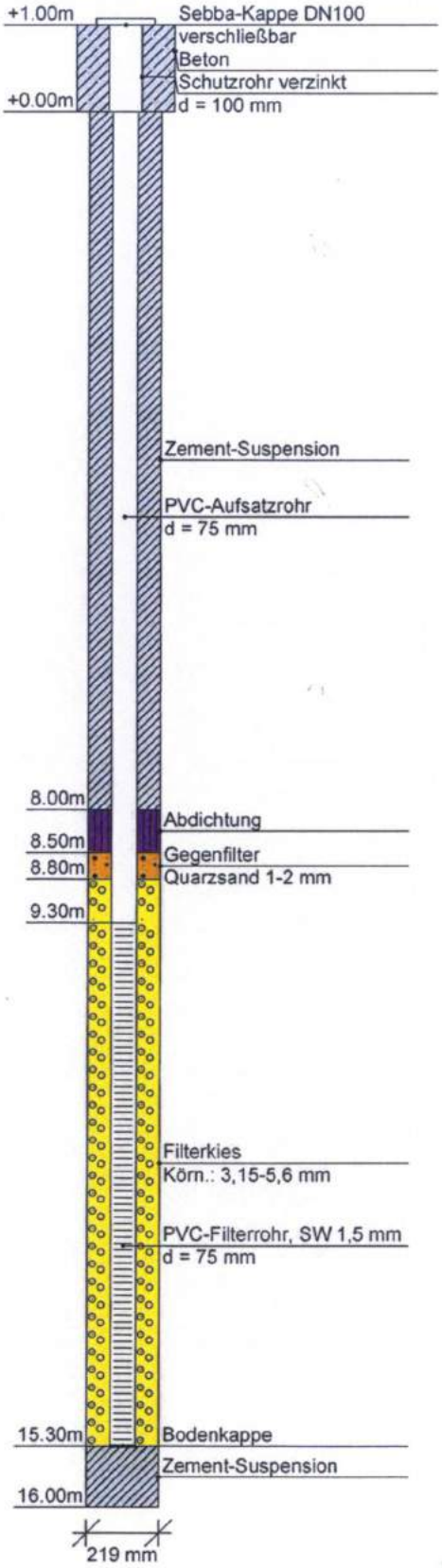

DC

BauGrund Süd
ErdEnergieManagement GmbH
Maybachstraße 5
88410 Bad Wurzach

Projekt :	Hotelpark Wolframstraße, 70191 Stuttgart
Projektnr.:	AZ 14 11 032
Anlage :	2.4
Maßstab :	1: 75 / 1: 20

Pegelausbau

BK3/15

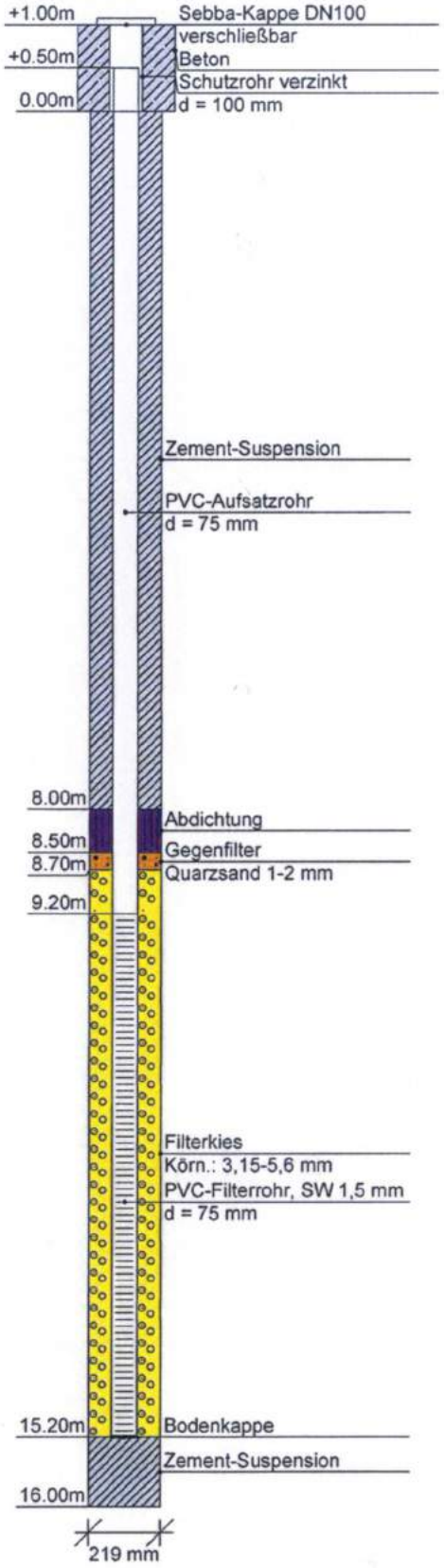

DC

baugrund süd
Gesellschaft für Bohr- und Geotechnik
Maybachstraße 5, 88410 Bad Wurzach

Anlage 4.1

Wassergehaltsbestimmung nach DIN 18121

BV Hotelpark in 70191 Stuttgart
AZ 14 11 032

Bohrung Nr.	BK 2/14				
Prüfungsnummer	1	2	3	4	5
Entnahmetiefe [m]	2,0	4,0	6,0	8,0	10,0
Behälter Gewicht [g]	112,41	113,14	112,99	112,9	112,63
Probe feucht + Behälter [g]	349,86	411,74	306,56	435,62	410,91
Probe trocken + Behälter [g]	304,19	348	275,77	380,91	358,98
Wassergehalt w [%]	23,81	27,14	18,92	20,41	21,08

Bohrung Nr.	BK 2/14		
Prüfungsnummer	6	7	8
Entnahmetiefe [m]	12,0	13,0	14,0
Behälter Gewicht [g]	112,68	112,75	113,05
Probe feucht + Behälter [g]	306,09	443,26	353,75
Probe trocken + Behälter [g]	273,75	391,73	322,73
Wassergehalt w [%]	20,08	18,47	14,79

BauGrund Süd Gesellschaft für Bohr-und Geotechnik mbH Maybachstraße 5 88410 Bad Wurzach Bearbeiter: DV Datum: 18.02.2015	**Körnungslinie** BV Hotelpark in 70191 Stuttgart	Prüfungsnummer: 1 Probe entnommen am: 12.02.2015 Art der Entnahme: gestört Arbeitsweise: Siebung und Schlämmung

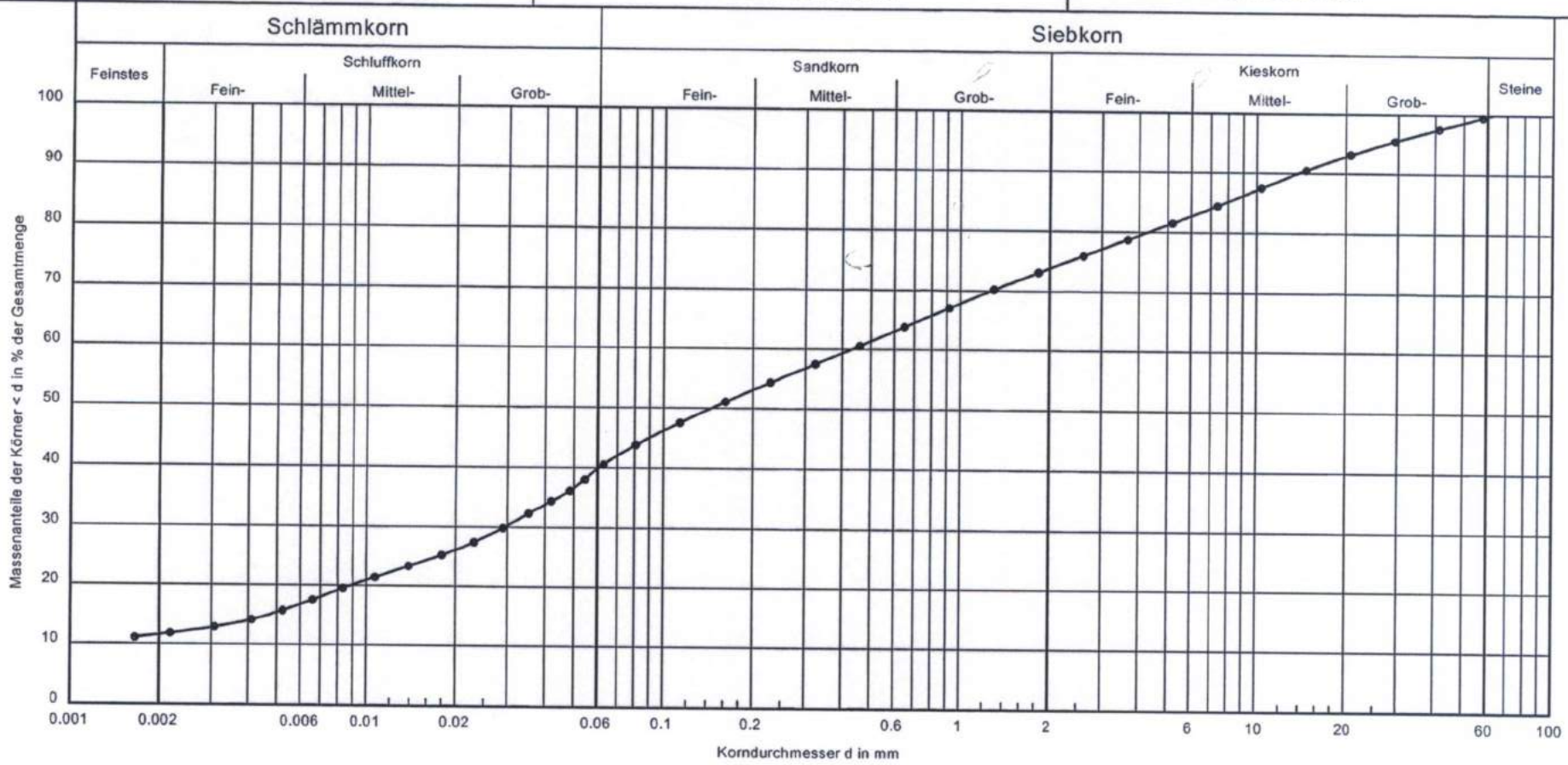

Bezeichnung:	●——●	Nach DIN 4022: 1. Sand, schluffig, kiesig (S, u, g, t') schwach tonig	Bericht: AZ 14 11 032 Anlage: 4.2
Bodenart:	S, u, t', fg', mg', gg'		
Tiefe:	6,0 - 7,0		
U/Cc	-/-		
Entnahmestelle:	BK 1/15		
k [m/s] (Mallet):	$6.9 \cdot 10^{-8}$		
T/U/S/G [%]:	11.5/28.3/34.0/25.9		

Annex C

BauGrund Süd Gesellschaft für Bohr-und Geotechnik mbH Maybachstraße 5 88410 Bad Wurzach Bearbeiter: DV Datum: 18.02.2015	**Körnungslinie** BV Hotelpark in 70191 Stuttgart	Prüfungsnummer: 1 Probe entnommen am: 12.02.2015 Art der Entnahme: gestört Arbeitsweise: Siebung und Schlämmung

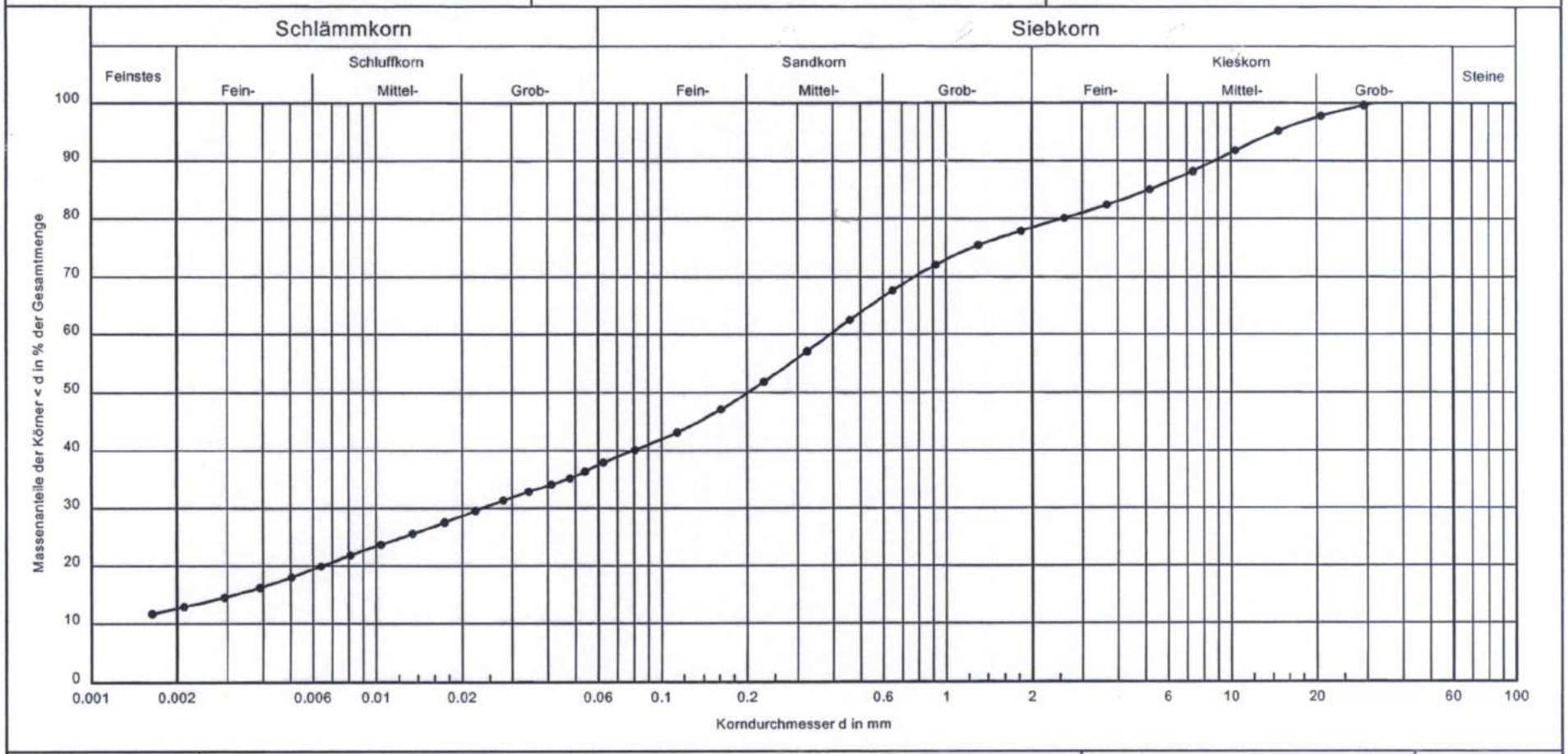

Bezeichnung:	●——●	Nach DIN 4022:	Bericht:
Bodenart:	S, u, t', fg', mg'	1. Sand, schluffig, kiesig (S, u, g, t')	AZ 14 11 032
Tiefe:	7,5 - 7,8	schwach tonig	Anlage:
U/Cc	-/-		4.3
Entnahmestelle:	BK 2/15		
k [m/s] (Mallet):	$3.3 \cdot 10^{-8}$		
T/U/S/G [%]:	12.6/24.9/40.9/21.5		

Annex C

BauGrund Süd Gesellschaft für Bohr-und Geotechnik mbH Maybachstraße 5 88410 Bad Wurzach Bearbeiter: DV Datum: 18.02.2015	**Körnungslinie** BV Hotelpark in 70191 Stuttgart	Prüfungsnummer: 1 Probe entnommen am: 12.02.2015 Art der Entnahme: gestört Arbeitsweise: Siebung und Schlämmung

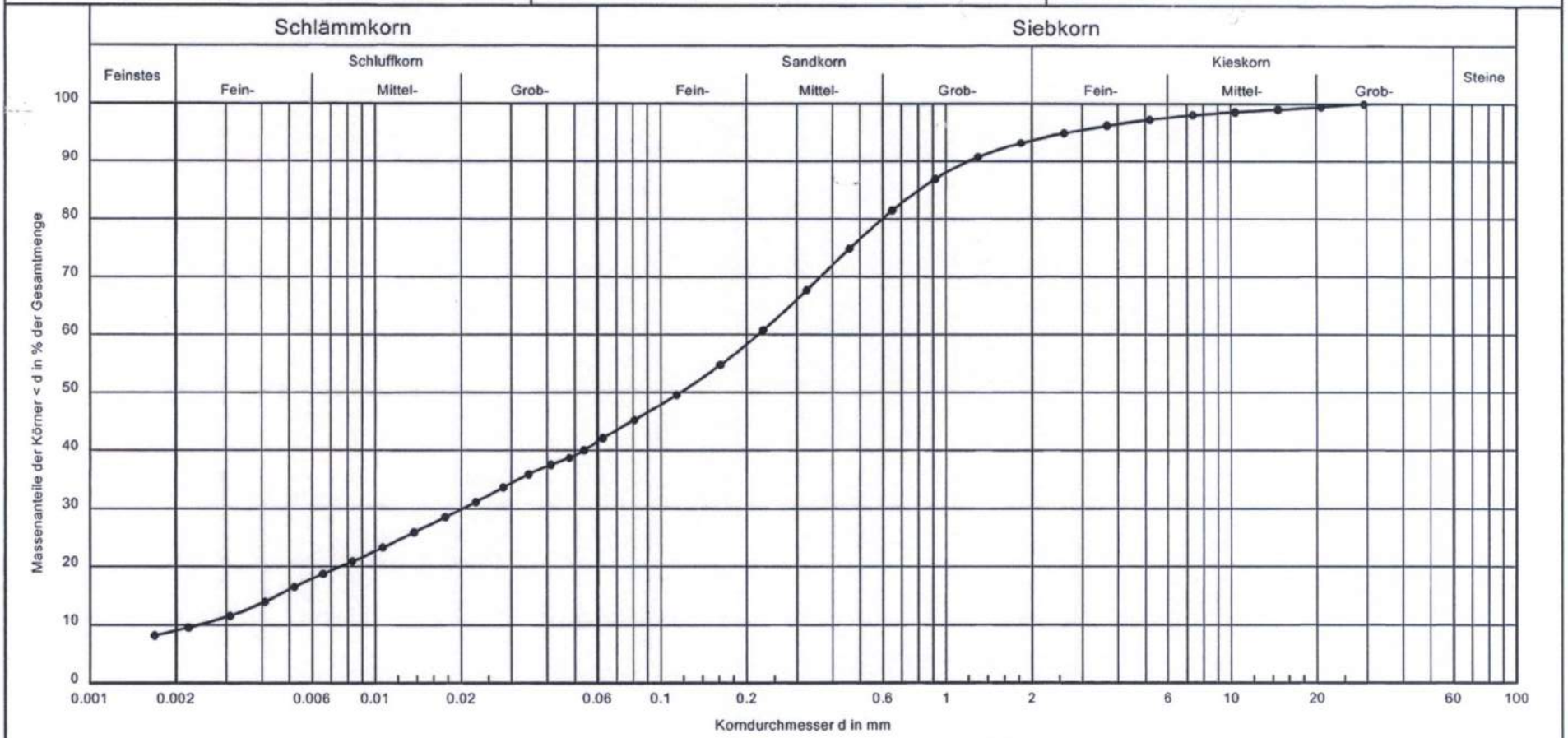

Bezeichnung:		Nach DIN 4022:	Bericht:
Bodenart:	S, ū, t', g'	1. Sand, stark schluffig (S, u*, t', g')	AZ 14 11 032
Tiefe:	6,0 - 7	schwach tonig, schwach kiesig	Anlage:
U/Cc	91.5/0		4.4
Entnahmestelle:	BK 3/1		
k [m/s] (Mallet):	4.7 · 1		
T/U/S/G [%]:	9.0/32.5/52 .4		

Annex C

PLAXIS Report

Annex D

1.1 Materials - Soil and interfaces - HS small (1/2)

Identification		**Fill**	**Fließerde**	**Dunkelrote Mergel-stark**	**DRM-weich**	**Bochinger Horizont**
Identification number		1	2	3	4	5
Drainage type		Drained	Drained	Drained	Drained	Drained
Colour						
Comments						
γ_{unsat}	kN/m³	18,00	20,00	20,00	19,00	22,00
γ_{sat}	kN/m³	18,00	20,00	21,00	20,00	23,00
Dilatancy cut-off		No	No	No	No	No
e_{init}		0,5000	0,5000	0,5000	0,5000	0,5000
e_{min}		0,000	0,000	0,000	0,000	0,000
e_{max}		999,0	999,0	999,0	999,0	999,0
Rayleigh α		0,000	0,000	0,000	0,000	0,000
Rayleigh β		0,000	0,000	0,000	0,000	0,000
E_{50}^{ref}	kN/m²	6000	10,00E3	35,00E3	15,00E3	50,00E3
E_{oed}^{ref}	kN/m²	6000	10,00E3	35,00E3	15,00E3	50,00E3
E_{ur}^{ref}	kN/m²	18,00E3	30,00E3	105,0E3	45,00E3	150,0E3
power (m)		0,6000	0,7000	0,6000	0,7000	0,6500
Use alternatives		No	No	No	No	No
C_c		0,05750	0,03450	9,857E-3	0,02300	6,900E-3
C_s		0,01725	0,01035	2,957E-3	6,900E-3	2,070E-3

Annex D

Identification		Fill	Fließerde	Dunkelrote Mergel-stark	DRM-weich	Bochinger Horizont
e_{init}		0,5000	0,5000	0,5000	0,5000	0,5000
c_{ref}	kN/m²	3,000	8,000	15,00	5,000	45,00
φ (phi)	°	27,00	25,00	25,00	27,50	25,00
ψ (psi)	°	0,000	0,000	0,000	0,000	0,000
$\gamma_{0.7}$		0,01000E-3	0,01000E-3	1,000E-6	0,01000E-3	1,000E-6
G_0^{ref}	kN/m²	30,00E3	48,00E3	131,0E3	55,00E3	120,0E3
Set to default values		No	No	No	No	No
v_{ur}		0,2000	0,2000	0,2000	0,2000	0,2000
p_{ref}	kN/m²	100,0	100,0	100,0	100,0	100,0
K_0^{nc}		0,5460	0,5774	0,5774	0,5383	0,5774
c_{inc}	kN/m²/m	0,000	0,000	0,000	0,000	0,000
y_{ref}	m	0,000	0,000	0,000	0,000	0,000
R_f		0,9000	0,9000	0,9000	0,9000	0,9000
Tension cut-off		Yes	Yes	Yes	Yes	Yes
Tensile strength	kN/m²	2,000	0,000	0,000	0,000	0,000
Undrained behaviour		Standard	Standard	Standard	Standard	Standard
Skempton-B		0,9866	0,9866	0,9866	0,9866	0,9866
v_u		0,4950	0,4950	0,4950	0,4950	0,4950
$K_{w,ref}$ / n	kN/m²	737,5E3	1,229E6	4,302E6	1,844E6	6,146E6
Failure criterion		Mohr-Coulomb	Mohr-Coulomb	Mohr-Coulomb	Mohr-Coulomb	Mohr-Coulomb
Strength		Manual	Manual	Manual	Manual	Manual
R_{inter}		0,7000	0,7000	0,7000	0,7000	0,9000

Identification		Fill	Fließerde	Dunkelrote Mergel-stark	DRM-weich	Bochinger Horizont
Consider gap closure		Yes	Yes	Yes	Yes	Yes
δ_{inter}		0,000	0,000	0,000	0,000	0,000
R	m² K/kW	0,000	0,000	0,000	0,000	0,000
K_0 determination		Manual	Manual	Manual	Manual	Manual
$K_{0,x} = K_{0,z}$		Yes	Yes	Yes	Yes	Yes
$K_{0,x}$		0,5460	0,5774	0,4000	0,4000	0,4000
$K_{0,z}$		0,5460	0,5774	0,4000	0,4000	0,4000
OCR		1,000	1,000	1,000	1,000	1,000
POP	kN/m²	0,000	0,000	0,000	0,000	0,000
Data set		Standard	Standard	Standard	Standard	Standard
Type		Coarse	Medium	Fine	Very fine	Medium
< 2 µm	%	10,00	19,00	46,00	74,00	19,00
2 µm - 50 µm	%	13,00	41,00	26,00	11,00	41,00
50 µm - 2 mm	%	77,00	40,00	28,00	15,00	40,00
Set to default values		Yes	Yes	Yes	Yes	Yes
k_x	m/day	0,6000	0,1206	0,2480	0,1500	0,1206
k_y	m/day	0,6000	0,1206	0,2480	0,1500	0,1206
$-\psi_{unsat}$	m	10,00E3	10,00E3	10,00E3	10,00E3	10,00E3
e_{init}		0,5000	0,5000	0,5000	0,5000	0,5000
S_s	1/m	0,000	0,000	0,000	0,000	0,000
c_k		1,000E15	1,000E15	1,000E15	1,000E15	1,000E15
c_s	kJ/t/K	0,000	0,000	0,000	0,000	0,000

Identification		Fill	Fließerde	Dunkelrote Mergel-stark	DRM-weich	Bochinger Horizont
λ_s	kW/m/K	0,000	0,000	0,000	0,000	0,000
ρ_s	t/m³	0,000	0,000	0,000	0,000	0,000
Solid thermal expansion		Linear	Linear	Linear	Linear	Linear
α_x	1/K	0,000	0,000	0,000	0,000	0,000
α_y	1/K	0,000	0,000	0,000	0,000	0,000
α_z	1/K	0,000	0,000	0,000	0,000	0,000
D_v	m²/day	0,000	0,000	0,000	0,000	0,000
f_{Tv}		0,000	0,000	0,000	0,000	0,000
Unfrozen water content		No	No	No	No	No

1.2 Materials - Soil and interfaces - HS small (2/2)

Identification		Grundgispschichten	Grenzdolomit	Fill_Embankment
Identification number		6	7	10
Drainage type		Drained	Drained	Drained
Colour				
Comments				
γ_{unsat}	kN/m³	22,00	23,00	18,00
γ_{sat}	kN/m³	22,00	23,00	18,00
Dilatancy cut-off		No	No	No
e_{init}		0,5000	0,5000	0,5000
e_{min}		0,000	0,000	0,000
e_{max}		999,0	999,0	999,0
Rayleigh α		0,000	0,000	0,000
Rayleigh β		0,000	0,000	0,000
E_{50}^{ref}	kN/m²	35,00E3	80,00E3	6000
E_{oed}^{ref}	kN/m²	35,00E3	80,00E3	6000
E_{ur}^{ref}	kN/m²	105,0E3	160,0E3	18,00E3
power (m)		0,6000	0,2000	0,6000
Use alternatives		No	No	No

Identification		Grundgispschichten	Grenzdolomit	Fill_Embankment
C_c		9,857E-3	4,312E-3	0,05750
C_s		2,957E-3	1,941E-3	0,01725
e_{init}		0,5000	0,5000	0,5000
c_{ref}	kN/m²	25,00	50,00	10,00
φ (phi)	°	25,00	25,00	27,00
ψ (psi)	°	0,000	0,000	0,000
$\gamma_{0.7}$		10,00	1,000E-6	0,01000E-3
G_0^{ref}	kN/m²	131,0E3	164,0E3	30,00E3
Set to default values		No	No	No
v_{ur}		0,2000	0,2000	0,2000
p_{ref}	kN/m²	100,0	100,0	100,0
K_0^{nc}		0,5774	0,5770	0,5460
c_{inc}	kN/m²/m	0,000	0,000	0,000
y_{ref}	m	0,000	0,000	0,000
R_f		0,9000	0,9000	0,9000
Tension cut-off		Yes	Yes	Yes
Tensile strength	kN/m²	0,000	0,000	3,000
Undrained behaviour		Standard	Standard	Standard
Skempton-B		0,9866	0,9866	0,9866

Identification		Grundgispschichten	Grenzdolomit	Fill_Embankment
v_u		0,4950	0,4950	0,4950
$K_{w,ref}$ / n	kN/m²	4,302E6	6,556E6	737,5E3
Failure criterion		Mohr-Coulomb	Mohr-Coulomb	Mohr-Coulomb
Strength		Manual	Manual	Manual
R_{inter}		0,9000	0,9000	0,7000
Consider gap closure		Yes	Yes	Yes
δ_{inter}		0,000	0,000	0,000
R	m² K/kW	0,000	0,000	0,000
K_0 determination		Manual	Manual	Manual
$K_{0,x} = K_{0,z}$		Yes	Yes	Yes
$K_{0,x}$		0,4000	0,4000	0,5460
$K_{0,z}$		0,4000	0,4000	0,5460
OCR		1,000	1,000	1,000
POP	kN/m²	0,000	0,000	0,000
Data set		Standard	Standard	Standard
Type		Fine	Fine	Coarse
< 2 µm	%	46,00	46,00	10,00
2 µm - 50 µm	%	26,00	26,00	13,00
50 µm - 2 mm	%	28,00	28,00	77,00

Identification		Grundgispschichten	Grenzdolomit	Fill_Embankment
Set to default values		Yes	Yes	Yes
k_x	m/day	0,2480	0,2480	0,6000
k_y	m/day	0,2480	0,2480	0,6000
$-\psi_{unsat}$	m	10,00E3	10,00E3	10,00E3
e_{init}		0,5000	0,5000	0,5000
S_s	1/m	0,000	0,000	0,000
c_k		1,000E15	1,000E15	1,000E15
c_s	kJ/t/K	0,000	0,000	0,000
λ_s	kW/m/K	0,000	0,000	0,000
ρ_s	t/m³	0,000	0,000	0,000
Solid thermal expansion		Linear	Linear	Linear
α_x	1/K	0,000	0,000	0,000
α_y	1/K	0,000	0,000	0,000
α_z	1/K	0,000	0,000	0,000
D_v	m²/day	0,000	0,000	0,000
f_{Tv}		0,000	0,000	0,000
Unfrozen water content		No	No	No

2.1 Materials - Soil and interfaces - Hardening soil (1/2)

Identification		Auffüllung	Fließerde	Dunkelrote Mergel-stark	DRM-weich	Bochinger Horizont
Identification number		1	2	3	4	5
Drainage type		Drained	Drained	Drained	Drained	Drained
Colour						
Comments						
γ_{unsat}	kN/m³	18,00	20,00	20,00	19,00	22,00
γ_{sat}	kN/m³	18,00	20,00	21,00	20,00	23,00
Dilatancy cut-off		No	No	No	No	No
e_{init}		0,5000	0,5000	0,5000	0,5000	0,5000
e_{min}		0,000	0,000	0,000	0,000	0,000
e_{max}		999,0	999,0	999,0	999,0	999,0
Rayleigh α		0,000	0,000	0,000	0,000	0,000
Rayleigh β		0,000	0,000	0,000	0,000	0,000
E_{50}^{ref}	kN/m²	5000	8000	32,00E3	15,00E3	45,00E3
E_{oed}^{ref}	kN/m²	5000	8000	32,00E3	15,00E3	45,00E3
E_{ur}^{ref}	kN/m²	15,00E3	24,00E3	96,00E3	45,00E3	135,0E3
power (m)		0,6000	0,7000	0,6000	0,7000	0,6500
Use alternatives		No	No	No	No	No
C_c		0,06900	0,04312	0,01078	0,02300	7,667E-3
C_s		0,02070	0,01294	3,234E-3	6,900E-3	2,300E-3

Identification		Auffüllung	Fließerde	Dunkelrote Mergel-stark	DRM-weich	Bochinger Horizont
e_{init}		0,5000	0,5000	0,5000	0,5000	0,5000
c_{ref}	kN/m²	3,000	8,000	15,00	5,000	45,00
φ (phi)	°	27,00	25,00	25,00	27,50	25,00
ψ (psi)	°	0,000	0,000	0,000	0,000	0,000
Set to default values		No	No	No	No	No
v_{ur}		0,2000	0,2000	0,2000	0,2000	0,2000
p_{ref}	kN/m²	100,0	100,0	100,0	100,0	100,0
K_0^{nc}		0,5460	0,5774	0,5774	0,5383	0,5774
c_{inc}	kN/m²/m	0,000	0,000	0,000	0,000	0,000
y_{ref}	m	0,000	0,000	0,000	0,000	0,000
R_f		0,9000	0,9000	0,9000	0,9000	0,9000
Tension cut-off		Yes	Yes	Yes	Yes	Yes
Tensile strength	kN/m²	2,000	0,000	0,000	0,000	0,000
Undrained behaviour		Standard	Standard	Standard	Standard	Standard
Skempton-B		0,9866	0,9866	0,9866	0,9866	0,9866
v_u		0,4950	0,4950	0,4950	0,4950	0,4950
$K_{w,ref}$ / n	kN/m²	614,6E3	983,3E3	3,933E6	1,844E6	5,531E6
Strength		Manual	Manual	Manual	Manual	Manual
R_{inter}		0,7000	0,7000	0,7000	0,7000	0,9000
Consider gap closure		Yes	Yes	Yes	Yes	Yes
δ_{inter}		0,000	0,000	0,000	0,000	0,000
R	m² K/kW	0,000	0,000	0,000	0,000	0,000

Identification		Auffüllung	Fließerde	Dunkelrote Mergel-stark	DRM-weich	Bochinger Horizont
K_0 determination		Manual	Manual	Manual	Manual	Manual
$K_{0,x} = K_{0,z}$		Yes	Yes	Yes	Yes	Yes
$K_{0,x}$		0,5460	0,5774	0,4000	0,4000	0,4000
$K_{0,z}$		0,5460	0,5774	0,4000	0,4000	0,4000
OCR		1,000	1,000	1,000	1,000	1,000
POP	kN/m²	0,000	0,000	0,000	0,000	0,000
Data set		Standard	Standard	Standard	Standard	Standard
Type		Coarse	Medium	Fine	Very fine	Medium
< 2 µm	%	10,00	19,00	46,00	74,00	19,00
2 µm - 50 µm	%	13,00	41,00	26,00	11,00	41,00
50 µm - 2 mm	%	77,00	40,00	28,00	15,00	40,00
Set to default values		Yes	Yes	Yes	Yes	Yes
k_x	m/day	0,6000	0,1206	0,2480	0,1500	0,1206
k_y	m/day	0,6000	0,1206	0,2480	0,1500	0,1206
$-\psi_{unsat}$	m	10,00E3	10,00E3	10,00E3	10,00E3	10,00E3
e_{init}		0,5000	0,5000	0,5000	0,5000	0,5000
S_s	1/m	0,000	0,000	0,000	0,000	0,000
c_k		1,000E15	1,000E15	1,000E15	1,000E15	1,000E15
c_s	kJ/t/K	0,000	0,000	0,000	0,000	0,000
λ_s	kW/m/K	0,000	0,000	0,000	0,000	0,000
ρ_s	t/m³	0,000	0,000	0,000	0,000	0,000
Solid thermal expansion		Linear	Linear	Linear	Linear	Linear

Identification		Auffüllung	Fließerde	Dunkelrote Mergel-stark	DRM-weich	Bochinger Horizont
α_x	1/K	0,000	0,000	0,000	0,000	0,000
α_y	1/K	0,000	0,000	0,000	0,000	0,000
α_z	1/K	0,000	0,000	0,000	0,000	0,000
D_v	m²/day	0,000	0,000	0,000	0,000	0,000
f_{Tv}		0,000	0,000	0,000	0,000	0,000
Unfrozen water content		No	No	No	No	No

2.2 Materials - Soil and interfaces - Hardening soil (2/2)

Identification		Grundgispschichten	Grenzdolomit	Auffüllung Boeschung
Identification number		6	7	10
Drainage type		Drained	Drained	Drained
Colour				
Comments				
γ_{unsat}	kN/m³	22,00	23,00	18,00
γ_{sat}	kN/m³	22,00	23,00	18,00
Dilatancy cut-off		No	No	No
e_{init}		0,5000	0,5000	0,5000
e_{min}		0,000	0,000	0,000
e_{max}		999,0	999,0	999,0
Rayleigh α		0,000	0,000	0,000
Rayleigh β		0,000	0,000	0,000
E_{50}^{ref}	kN/m²	32,00E3	75,00E3	5000
E_{oed}^{ref}	kN/m²	32,00E3	75,00E3	5000
E_{ur}^{ref}	kN/m²	96,00E3	150,0E3	15,00E3
power (m)		0,6000	0,2000	0,6000

Identification		Grundgispschichten	Grenzdolomit	Auffüllung Boeschung
Use alternatives		No	No	No
C_c		0,01078	4,600E-3	0,06900
C_s		3,234E-3	2,070E-3	0,02070
e_{init}		0,5000	0,5000	0,5000
c_{ref}	kN/m²	25,00	50,00	10,00
φ (phi)	°	25,00	25,00	27,00
ψ (psi)	°	0,000	0,000	0,000
Set to default values		No	No	No
v_{ur}		0,2000	0,2000	0,2000
p_{ref}	kN/m²	100,0	100,0	100,0
K_0^{nc}		0,5774	0,5774	0,5460
c_{inc}	kN/m²/m	0,000	0,000	0,000
y_{ref}	m	0,000	0,000	0,000
R_f		0,9000	0,9000	0,9000
Tension cut-off		Yes	Yes	Yes
Tensile strength	kN/m²	0,000	0,000	3,000
Undrained behaviour		Standard	Standard	Standard
Skempton-B		0,9866	0,9866	0,9866
v_u		0,4950	0,4950	0,4950

Identification		Grundgispschichten	Grenzdolomit	Auffüllung Boeschung
$K_{w,ref}$ / n	kN/m²	3,933E6	6,146E6	614,6E3
Strength		Manual	Manual	Manual
R_{inter}		0,9000	0,9000	0,7000
Consider gap closure		Yes	Yes	Yes
δ_{inter}		0,000	0,000	0,000
R	m² K/kW	0,000	0,000	0,000
K_0 determination		Manual	Manual	Manual
$K_{0,x} = K_{0,z}$		Yes	Yes	Yes
$K_{0,x}$		0,4000	0,4000	0,5460
$K_{0,z}$		0,4000	0,4000	0,5460
OCR		1,000	1,000	1,000
POP	kN/m²	0,000	0,000	0,000
Data set		Standard	Standard	Standard
Type		Fine	Fine	Coarse
< 2 µm	%	46,00	46,00	10,00
2 µm - 50 µm	%	26,00	26,00	13,00
50 µm - 2 mm	%	28,00	28,00	77,00
Set to default values		Yes	Yes	Yes
k_x	m/day	0,2480	0,2480	0,6000

Identification		Grundgispschichten	Grenzdolomit	Auffüllung Boeschung
k_y	m/day	0,2480	0,2480	0,6000
$-\psi_{unsat}$	m	10,00E3	10,00E3	10,00E3
e_{init}		0,5000	0,5000	0,5000
S_s	1/m	0,000	0,000	0,000
c_k		1,000E15	1,000E15	1,000E15
c_s	kJ/t/K	0,000	0,000	0,000
λ_s	kW/m/K	0,000	0,000	0,000
ρ_s	t/m³	0,000	0,000	0,000
Solid thermal expansion		Linear	Linear	Linear
α_x	1/K	0,000	0,000	0,000
α_y	1/K	0,000	0,000	0,000
α_z	1/K	0,000	0,000	0,000
D_v	m²/day	0,000	0,000	0,000
f_{Tv}		0,000	0,000	0,000
Unfrozen water content		No	No	No

3.1 Materials - Soil and interfaces - Mohr-Coulomb (1/2)

Identification		Fill	Fließerde	Dunkelrote Mergel-stark	DRM-weich	Bochinger Horizont
Identification number		1	2	3	4	5
Drainage type		Drained	Drained	Drained	Drained	Drained
Colour						
Comments						
γ_{unsat}	kN/m³	18,00	20,00	20,00	19,00	22,00
γ_{sat}	kN/m³	18,00	20,00	21,00	20,00	23,00
Dilatancy cut-off		No	No	No	No	No
e_{init}		0,5000	0,5000	0,5000	0,5000	0,5000
e_{min}		0,000	0,000	0,000	0,000	0,000
e_{max}		999,0	999,0	999,0	999,0	999,0
Rayleigh α		0,000	0,000	0,000	0,000	0,000
Rayleigh β		0,000	0,000	0,000	0,000	0,000
E	kN/m²	5000	8000	32,00E3	15,00E3	45,00E3
ν (nu)		0,3000	0,2800	0,2500	0,2800	0,2500
G	kN/m²	1923	3125	12,80E3	5859	18,00E3
E_{oed}	kN/m²	6731	10,23E3	38,40E3	19,18E3	54,00E3
c_{ref}	kN/m²	3,000	8,000	15,00	5,000	45,00
φ (phi)	°	27,00	25,00	25,00	27,50	25,00
ψ (psi)	°	0,000	0,000	0,000	0,000	0,000

Identification		Fill	Fließerde	Dunkelrote Mergel-stark	DRM-weich	Bochinger Horizont
V_s	m/s	32,37	39,15	79,24	55,00	89,59
V_p	m/s	60,57	70,83	137,2	99,50	155,2
Set to default values		No	Yes	Yes	Yes	Yes
E_{inc}	kN/m²/m	0,000	0,000	0,000	0,000	0,000
y_{ref}	m	0,000	0,000	0,000	0,000	0,000
c_{inc}	kN/m²/m	0,000	0,000	0,000	0,000	0,000
y_{ref}	m	0,000	0,000	0,000	0,000	0,000
Tension cut-off		Yes	Yes	Yes	Yes	Yes
Tensile strength	kN/m²	2,000	0,000	0,000	0,000	0,000
Undrained behaviour		Standard	Standard	Standard	Standard	Standard
Skempton-B		0,9783	0,9805	0,9833	0,9805	0,9833
v_u		0,4950	0,4950	0,4950	0,4950	0,4950
$K_{w,ref}$ / n	kN/m²	187,5E3	305,4E3	1,254E6	572,6E3	1,764E6
Strength		Manual	Manual	Manual	Manual	Manual
R_{inter}		0,7000	0,7000	0,7000	0,7000	0,9000
Consider gap closure		Yes	Yes	Yes	Yes	Yes
δ_{inter}		0,000	0,000	0,000	0,000	0,000
R	m² K/kW	0,000	0,000	0,000	0,000	0,000
K_0 determination		Automatic	Automatic	Manual	Manual	Manual
$K_{0,x} = K_{0,z}$		Yes	Yes	Yes	Yes	Yes
$K_{0,x}$		0,5460	0,5774	0,4000	0,4000	0,4000
$K_{0,z}$		0,5460	0,5774	0,4000	0,4000	0,4000

Identification		Fill	Fließerde	Dunkelrote Mergel-stark	DRM-weich	Bochinger Horizont
Data set		Standard	Standard	Standard	Standard	Standard
Type		Coarse	Medium	Fine	Very fine	Medium
< 2 µm	%	10,00	19,00	46,00	74,00	19,00
2 µm - 50 µm	%	13,00	41,00	26,00	11,00	41,00
50 µm - 2 mm	%	77,00	40,00	28,00	15,00	40,00
Set to default values		Yes	Yes	Yes	Yes	Yes
k_x	m/day	0,6000	0,1206	0,2480	0,1500	0,1206
k_y	m/day	0,6000	0,1206	0,2480	0,1500	0,1206
$-\psi_{unsat}$	m	10,00E3	10,00E3	10,00E3	10,00E3	10,00E3
e_{init}		0,5000	0,5000	0,5000	0,5000	0,5000
S_s	1/m	0,000	0,000	0,000	0,000	0,000
c_k		1,000E15	1,000E15	1,000E15	1,000E15	1,000E15
c_s	kJ/t/K	0,000	0,000	0,000	0,000	0,000
λ_s	kW/m/K	0,000	0,000	0,000	0,000	0,000
ρ_s	t/m³	0,000	0,000	0,000	0,000	0,000
Solid thermal expansion		Linear	Linear	Linear	Linear	Linear
α_x	1/K	0,000	0,000	0,000	0,000	0,000
α_y	1/K	0,000	0,000	0,000	0,000	0,000
α_z	1/K	0,000	0,000	0,000	0,000	0,000
D_v	m²/day	0,000	0,000	0,000	0,000	0,000
f_{Tv}		0,000	0,000	0,000	0,000	0,000
Unfrozen water content		No	No	No	No	No

3.2 Materials - Soil and interfaces - Mohr-Coulomb (2/2)

Identification		Grundgispschichten	Grenzdolomit	Fill_Embankment	Sauberkeits und Kiesfilter
Identification number		6	7	10	11
Drainage type		Drained	Drained	Drained	Drained
Colour					
Comments					
γ_{unsat}	kN/m³	22,00	23,00	18,00	18,00
γ_{sat}	kN/m³	22,00	23,00	18,00	21,00
Dilatancy cut-off		No	No	No	No
e_{init}		0,5000	0,5000	0,5000	0,5000
e_{min}		0,000	0,000	0,000	0,000
e_{max}		999,0	999,0	999,0	999,0
Rayleigh α		0,000	0,000	0,000	0,000
Rayleigh β		0,000	0,000	0,000	0,000
E	kN/m²	32,00E3	75,00E3	5000	100,0E3
v (nu)		0,2500	0,2000	0,3000	0,3000
G	kN/m²	12,80E3	31,25E3	1923	38,46E3
E_{oed}	kN/m²	38,40E3	83,33E3	6731	134,6E3

Identification		Grundgispschichten	Grenzdolomit	Fill_Embankment	Sauberkeits und Kiesfilter
c_{ref}	kN/m²	25,00	50,00	10,00	1,000
φ (phi)	°	25,00	25,00	27,00	37,50
ψ (psi)	°	0,000	0,000	0,000	0,000
V_s	m/s	75,55	115,5	32,37	144,8
V_p	m/s	130,9	188,5	60,57	270,9
Set to default values		Yes	Yes	No	Yes
E_{inc}	kN/m²/m	0,000	0,000	0,000	0,000
y_{ref}	m	0,000	0,000	0,000	0,000
c_{inc}	kN/m²/m	0,000	0,000	0,000	0,000
y_{ref}	m	0,000	0,000	0,000	0,000
Tension cut-off		Yes	Yes	Yes	Yes
Tensile strength	kN/m²	0,000	0,000	3,000	0,000
Undrained behaviour		Standard	Standard	Standard	Standard
Skempton-B		0,9833	0,9866	0,9783	0,9783
v_u		0,4950	0,4950	0,4950	0,4950
$K_{w,ref}$ / n	kN/m²	1,254E6	3,073E6	187,5E3	3,750E6
Strength		Manual	Manual	Manual	Rigid
R_{inter}		0,9000	0,9000	0,7000	1,000
Consider gap closure		Yes	Yes	Yes	Yes

Identification		Grundgispschichten	Grenzdolomit	Fill_Embankment	Sauberkeits und Kiesfilter
δ_{inter}		0,000	0,000	0,000	0,000
R	m² K/kW	0,000	0,000	0,000	0,000
K_0 determination		Manual	Manual	Automatic	Automatic
$K_{0,x} = K_{0,z}$		Yes	Yes	Yes	Yes
$K_{0,x}$		0,4000	0,4000	0,5460	0,3912
$K_{0,z}$		0,4000	0,4000	0,5460	0,3912
Data set		Standard	Standard	Standard	Standard
Type		Fine	Fine	Coarse	Coarse
< 2 µm	%	46,00	46,00	10,00	10,00
2 µm - 50 µm	%	26,00	26,00	13,00	13,00
50 µm - 2 mm	%	28,00	28,00	77,00	77,00
Set to default values		Yes	Yes	Yes	Yes
k_x	m/day	0,2480	0,2480	0,6000	0,6000
k_y	m/day	0,2480	0,2480	0,6000	0,6000
$-\psi_{unsat}$	m	10,00E3	10,00E3	10,00E3	10,00E3
e_{init}		0,5000	0,5000	0,5000	0,5000
S_s	1/m	0,000	0,000	0,000	0,000
c_k		1,000E15	1,000E15	1,000E15	1,000E15
c_s	kJ/t/K	0,000	0,000	0,000	0,000

Identification		Grundgispschichten	Grenzdolomit	Fill_Embankment	Sauberkeits und Kiesfilter
λ_s	kW/m/K	0,000	0,000	0,000	0,000
ρ_s	t/m³	0,000	0,000	0,000	0,000
Solid thermal expansion		Linear	Linear	Linear	Linear
α_x	1/K	0,000	0,000	0,000	0,000
α_y	1/K	0,000	0,000	0,000	0,000
α_z	1/K	0,000	0,000	0,000	0,000
D_v	m²/day	0,000	0,000	0,000	0,000
f_{Tv}		0,000	0,000	0,000	0,000
Unfrozen water content		No	No	No	No

4 Materials - Soil and interfaces - Linear elastic

Identification		Railway Bridge	Building Stiffness	Backfill Material	Basement Hotel
Identification number		8	9	12	13
Drainage type		Non-porous	Non-porous	Drained	Non-porous
Colour					
Comments					
γ_{unsat}	kN/m³	25,00	0,000	24,00	0,000
γ_{sat}	kN/m³	25,00	0,000	24,00	0,000
Dilatancy cut-off		No	No	No	No
e_{init}		0,5000	0,5000	0,5000	0,5000
e_{min}		0,000	0,000	0,000	0,000
e_{max}		999,0	999,0	999,0	999,0
Rayleigh α		0,000	0,000	0,000	0,000
Rayleigh β		0,000	0,000	0,000	0,000
E	kN/m²	37,00E6	150,0E3	29,96E6	30,00E6
v (nu)		0,2000	0,2000	0,2000	0,2000
G	kN/m²	15,42E6	62,50E3	12,48E6	12,50E6
E_{oed}	kN/m²	41,11E6	166,7E3	33,29E6	33,33E6
V_s	m/s	2460	0,000	2259	0,000

Identification		Railway Bridge	Building Stiffness	Backfill Material	Basement Hotel
V_p	m/s	4016	0,000	3689	0,000
Set to default values		Yes	Yes	Yes	Yes
E_{inc}	kN/m²/m	0,000	0,000	0,000	0,000
y_{ref}	m	0,000	0,000	0,000	0,000
Undrained behaviour		Standard	Standard	Standard	Standard
Skempton-B		0,9866	0,9866	0,9866	0,9866
v_u		0,4950	0,4950	0,4950	0,4950
$K_{w,ref}$ / n	kN/m²	1,516E9	6,146E6	1,228E9	1,229E9
Strength		Manual	Rigid	Rigid	Rigid
R_{inter}		0,8000	1,000	1,000	1,000
Consider gap closure		Yes	Yes	Yes	Yes
δ_{inter}		0,000	0,000	0,000	0,000
R	m² K/kW	0,000	0,000	0,000	0,000
K_0 determination		Automatic	Automatic	Automatic	Automatic
$K_{0,x} = K_{0,z}$		Yes	Yes	Yes	Yes
$K_{0,x}$		1,000	1,000	0,5460	1,000
$K_{0,z}$		1,000	1,000	0,5460	1,000
Data set		Standard	Standard	Standard	Standard
Type		Coarse	Coarse	Coarse	Coarse

Identification		Railway Bridge	Building Stiffness	Backfill Material	Basement Hotel
< 2 µm	%	10,00	10,00	10,00	10,00
2 µm - 50 µm	%	13,00	13,00	13,00	13,00
50 µm - 2 mm	%	77,00	77,00	77,00	77,00
Set to default values		No	No	Yes	No
k_x	m/day	0,000	0,000	0,6000	0,000
k_y	m/day	0,000	0,000	0,6000	0,000
$-\psi_{unsat}$	m	10,00E3	10,00E3	10,00E3	10,00E3
e_{init}		0,5000	0,5000	0,5000	0,5000
S_s	1/m	0,000	0,000	0,000	0,000
c_k		1,000E15	1,000E15	1,000E15	1,000E15
c_s	kJ/t/K	0,000	0,000	0,000	0,000
λ_s	kW/m/K	0,000	0,000	0,000	0,000
ρ_s	t/m³	0,000	0,000	0,000	0,000
Solid thermal expansion		Linear	Linear	Linear	Linear
α_x	1/K	0,000	0,000	0,000	0,000
α_y	1/K	0,000	0,000	0,000	0,000
α_z	1/K	0,000	0,000	0,000	0,000
D_v	m²/day	0,000	0,000	0,000	0,000
f_{Tv}		0,000	0,000	0,000	0,000

5 Materials - Soil and interfaces - Mohr-Coulomb

Identification		**Sauberkeits und Kiesfilter**
Identification number		11
Drainage type		Drained
Colour		
Comments		
γ_{unsat}	kN/m³	18,00
γ_{sat}	kN/m³	21,00
Dilatancy cut-off		No
e_{init}		0,5000
e_{min}		0,000
e_{max}		999,0
Rayleigh α		0,000
Rayleigh β		0,000
E	kN/m²	100,0E3
v (nu)		0,3000
G	kN/m²	38,46E3
E_{oed}	kN/m²	134,6E3
c_{ref}	kN/m²	1,000

Identification		**Sauberkeits und Kiesfilter**
φ (phi)	°	37,50
ψ (psi)	°	0,000
V_s	m/s	144,8
V_p	m/s	270,9
Set to default values		Yes
E_{inc}	kN/m²/m	0,000
y_{ref}	m	0,000
c_{inc}	kN/m²/m	0,000
y_{ref}	m	0,000
Tension cut-off		Yes
Tensile strength	kN/m²	0,000
Undrained behaviour		Standard
Skempton-B		0,9783
v_u		0,4950
$K_{w,ref}$ / n	kN/m²	3,750E6
Strength		Rigid
R_{inter}		1,000
Consider gap closure		Yes
δ_{inter}		0,000

Identification		**Sauberkeits und Kiesfilter**
R	m² K/kW	0,000
K_0 determination		Automatic
$K_{0,x} = K_{0,z}$		Yes
$K_{0,x}$		0,3912
$K_{0,z}$		0,3912
Data set		Standard
Type		Coarse
< 2 µm	%	10,00
2 µm - 50 µm	%	13,00
50 µm - 2 mm	%	77,00
Set to default values		Yes
k_x	m/day	0,6000
k_y	m/day	0,6000
$-\psi_{unsat}$	m	10,00E3
e_{init}		0,5000
S_s	1/m	0,000
c_k		1,000E15
c_s	kJ/t/K	0,000
λ_s	kW/m/K	0,000

Identification		**Sauberkeits und Kiesfilter**
ρ_s	t/m³	0,000
Solid thermal expansion		Linear
α_x	1/K	0,000
α_y	1/K	0,000
α_z	1/K	0,000
D_v	m²/day	0,000
f_{Tv}		0,000
Unfrozen water content		No

5 Materials - Plates -

Identification		Secant Pile Wall	Soldier Pile Wall	Roof-Hotel	Walls-Hotel	Foot
Identification number		1	2	3	4	5
Comments						
Colour						
Material type		Elastic	Elastic	Elastic	Elastic	Elastic
Isotropic		Yes	Yes	Yes	Yes	Yes
End bearing		No	No	No	No	Yes
EA_1	kN/m	33,00E6	1,443E6	12,00E6	15,00E6	33,00E6
EA_2	kN/m	33,00E6	1,443E6	12,00E6	15,00E6	33,00E6
EI	kN m²/m	3,320E6	23,97E3	160,0E3	312,5E3	5,000E6
d	m	1,099	0,4465	0,4000	0,5000	1,348
w	kN/m/m	16,00	0,6000	0,000	0,000	16,000
v (nu)		0,2000	0,1500	0,2000	0,2000	0,2000
Rayleigh α		0,000	0,000	0,000	0,000	0,000
Rayleigh β		0,000	0,000	0,000	0,000	0,000
Identification number		1	2	3	4	5
c	kJ/t/K	0,000	0,000	0,000	0,000	0,000
λ	kW/m/K	0,000	0,000	0,000	0,000	0,000

Identification		Secant Pile Wall	Soldier Pile Wall	Roof-Hotel	Walls-Hotel	Foot
ρ	t/m³	0,000	0,000	0,000	0,000	0,000
α	1/K	0,000	0,000	0,000	0,000	0,000

6 Materials - Embedded beam row -

Identification		**Piles-Bridge**
Identification number		1
Comments		
Colour		
E	kN/m²	30,00E6
γ	kN/m³	25,00
Pile type		Predefined
Predefined pile type		Massive circular pile
Diameter	m	1,200
A	m²	1,131
I_3	m⁴	0,1018
I_2	m⁴	0,1018
Rayleigh α		0,000
Rayleigh β		0,000
Axial skin resistance		Linear
$T_{skin, start, max}$	kN/m	65,00
$T_{skin, end, max}$	kN/m	65,00
F_{max}	kN	1500

Identification		**Piles-Bridge**
Identification number		1
Comments		
Colour		
Material type		Elastic
E	kN/m²	30,00E6
γ	kN/m³	25,00
Pile type		Predefined
Predefined pile type		Massive circular pile
Diameter	m	1,200
A	m²	1,131
I	m⁴	0,1018
$L_{spacing}$	m	3,100
Rayleigh α		0,000
Rayleigh β		0,000
Axial skin resistance		Linear
$T_{skin, start, max}$	kN/m	65,00
$T_{skin, end, max}$	kN/m	65,00
Lateral skin resistance		Unlimited
F_{max}	kN	1500

Identification	Piles-Bridge
Default values	Yes
Axial stiffness factor	1,227
Lateral stiffness factor	1,227
Base stiffness factor	12,27
Identification number	1

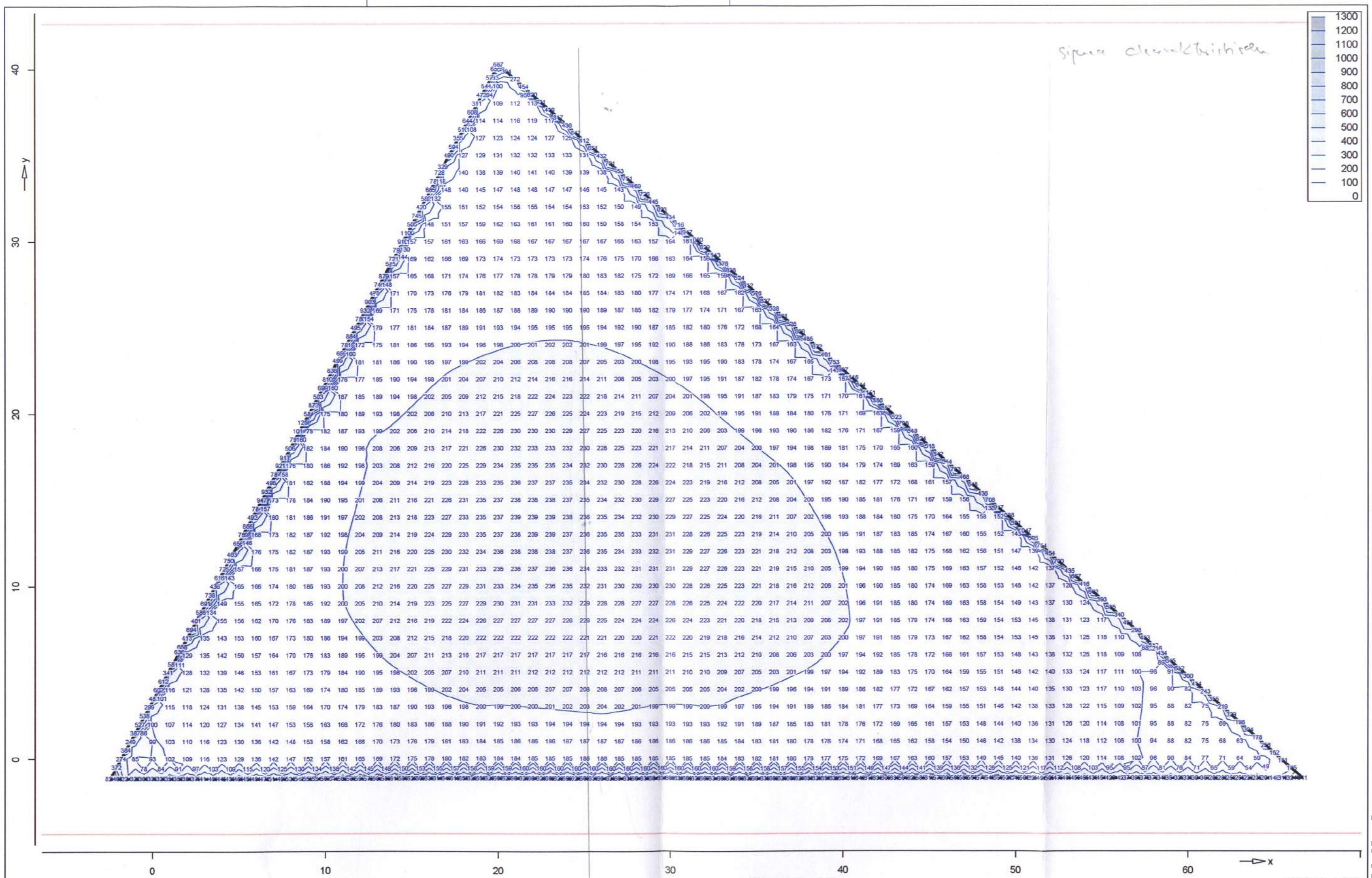

Spurre elektrisch

Flächenpressungen

Lagerkraft in z-Richtung in [kN/m²]

Maßstab: 1:200

lastkombinationsweise dargestellt
aus Lastkombination LK-1
Max = 1259 (Kn. 1611), Min = 49 (Kn. 1725), Step = 100

Auftragsnr.		Seite
P1719	R&P RUFFERT Ingenieurgesellschaft mbH Beratende Ingenieure	
Pos.		MicroFe 2015.031
BP01-N2		

Annex E

Pfahlwiderstands-Setzungsdiagramm für

Bohrpfahlgründung im Gipskeuper - Bochinger Horizont

baugrund süd Gesellschaft für Bohr- und Geotechnik Maybachstraße 5 88410 Bad Wurzach	BV Hotelpark in 70191 Stuttgart	AZ 14 11 032 Anlage 8.1

Boden	q_b [MN/m²]	$c_{u,k}$ [kN/m²]	$q_{b,k,01}$ [MN/m²]	$q_{b,k,02}$ [MN/m²]	$q_{b,k,10}$ [MN/m²]	$q_{s,k}$ [MN/m²]	Bezeichnung
	0.0	150.0	0.600	0.700	1.200	0.0500	Gipskeuper: Dunkelrotermergel
	0.0	100.0	0.350	0.450	0.800	0.0389	Gipskeuper:Dunkelrotermergel
	0.0	200.0	0.775	0.950	1.400	0.0575	Gipskeuper: Blochinger Horizont
	0.0	150.0	0.600	0.700	1.200	0.0500	Gipskeuper: Grundgipsschichten

System

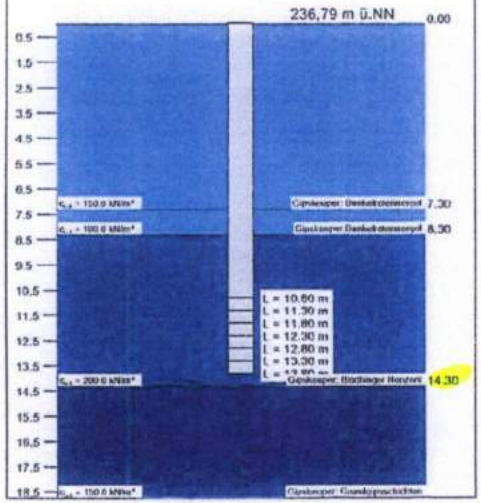

D [m]	Länge [m]	R_k [MN]	R_d [MN]	$R_{E,k}$ [MN]	zul V [MN]	s [cm]
1.200	10.80	3.643	2.602	1.826	1.826	1.07
1.200	11.30	3.728	2.663	1.869	1.869	1.08
1.200	11.80	3.813	2.723	1.911	1.911	1.10
1.200	12.30	3.898	2.784	1.954	1.954	1.12
1.200	12.80	3.982	2.845	1.996	1.996	1.14
1.200	13.30	4.067	2.905	2.039	2.039	1.15
1.200	13.80	4.152	2.966	2.081	2.081	1.17

zul V = $R_{E,k}$ = R_k / ($\gamma_P \cdot \gamma_{G,Q}$) = R_k / (1.400 · 1.425) = R_k / 2.00 [$\gamma_{G,Q}$ = 1.425]

Bohrpfahl

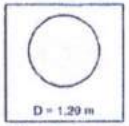

Berechnungsgrundlagen γ_P = 1.40
Baugrundschichtung gem. BK1/15 γ_G = 1.35
Norm: EC 7 γ_Q = 1.50
Bohrpfahl Anteil Veränderliche Lasten = 0.500
Verhältniswert (min, max) = 0.00 $\gamma_{G,Q}$ = 0.500 · γ_Q + (1 - 0.500) · γ_G
Interpolation Mantelreibung: $\gamma_{G,Q}$ = 1.425
bei q_b < 7.5 MN/m² deaktiviert — Zul V
bei $c_{u,k}$ < 60 kN/m² deaktiviert — Setzung
Pfahldurchmesser = 1.200 m

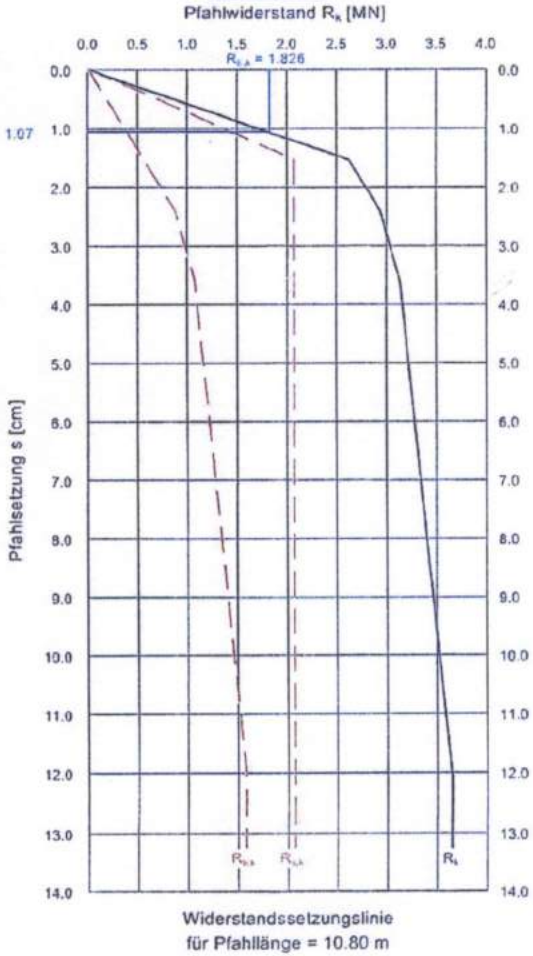

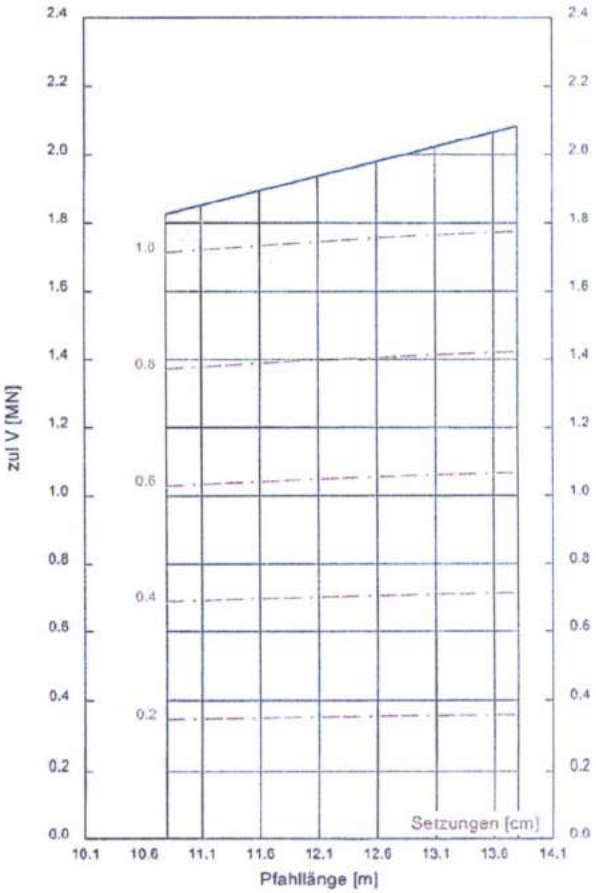

Annex F

Annex G:

Results FE - Calculations in Plaxis

HSS_Bridge_ Horizontal Displacement, u_x

Output Version 2015.2.19890.13737

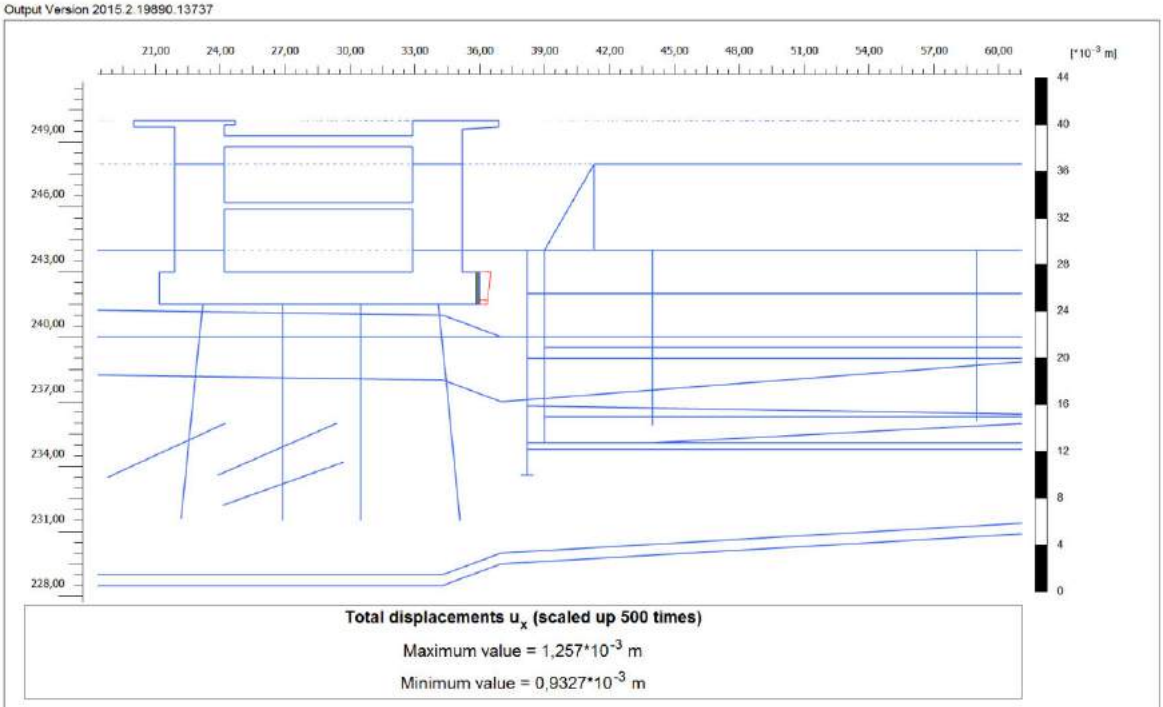

PLAXIS

Project description: HSS_ „Wish in Place“ Bridge (phase 1)

Date: 22.03.2017

Project filename: Baufeld-15-24.09.2015-KPP ... | Step: 7 | User name: Fachhochschule Stuttgart

C:\Users\52shan1mki\Desktop\Calculations_21.03.2017\Baufeld-15-24.09.2015-KPP-2UG-wasser_HSS.P2DXDAT\

Output Version 2015.2.19890.13737

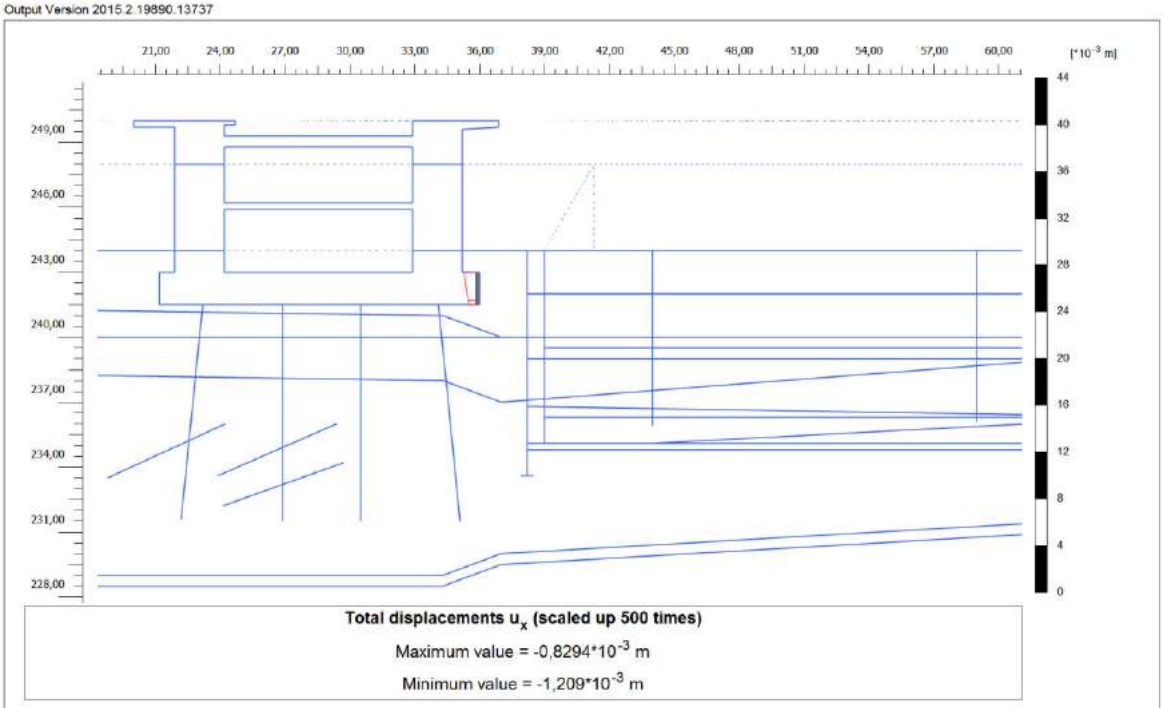

PLAXIS

Project description: HSS_Preliminary Excavation (phase 2)

Date: 22.03.2017

Project filename: Baufeld-15-24.09.2015-KPP ... | Step: 18 | User name: Fachhochschule Stuttgart

C:\Users\52shan1mki\Desktop\Calculations_21.03.2017\Baufeld-15-24.09.2015-KPP-2UG-wasser_HSS.P2DXDAT\

Output Version 2015.2.19890.13737

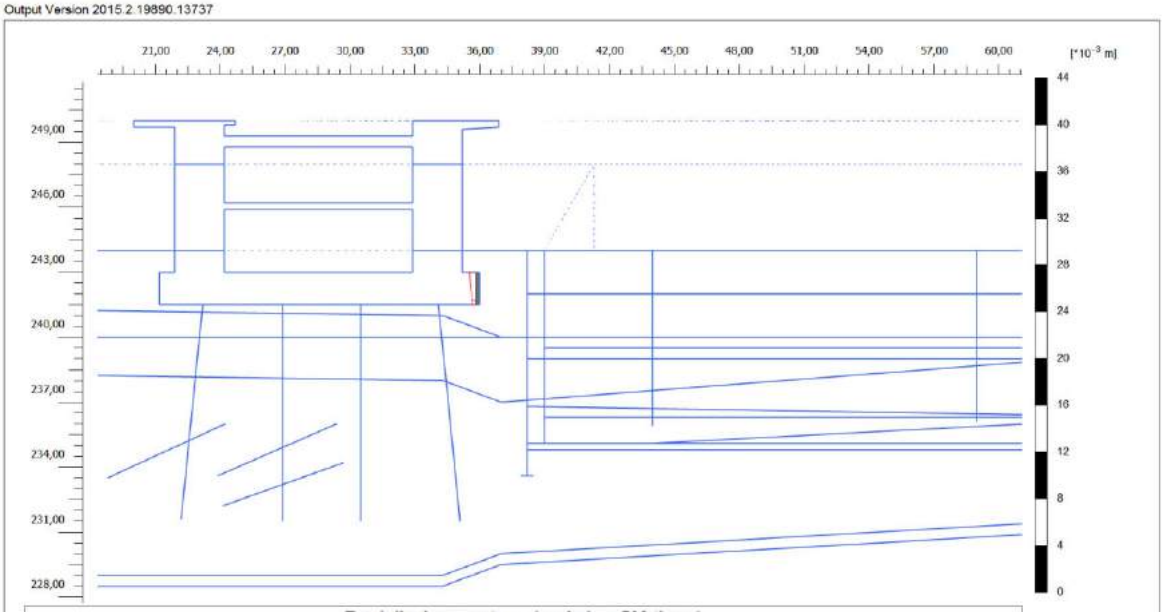

Total displacements u_x (scaled up 500 times)

Maximum value = $-0{,}4833*10^{-3}$ m

Minimum value = $-0{,}7429*10^{-3}$ m

PLAXIS	Project description: HSS_ Installation of the Retaining Walls (phase 3)		Date: 22.03.2017
	Project filename: Baufeld-15-24.09.2015-KPP ...	Step: 24	User name: Fachhochschule Stuttgart

C:\Users\52shan1mki\Desktop\Calculations_21.03.2017\Baufeld-15-24.09.2015-KPP-2UG-wasser_HSS.P2DXDAT\

Output Version 2015.2.19890.13737

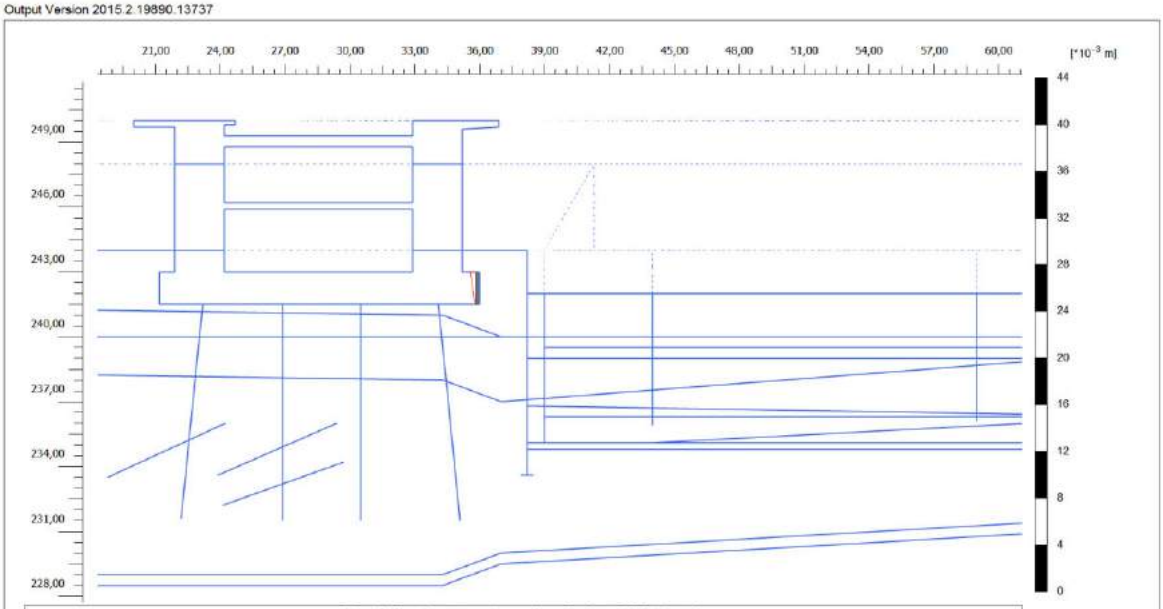

Total displacements u_x (scaled up 500 times)

Maximum value = $-0{,}2360*10^{-3}$ m

Minimum value = $-0{,}6583*10^{-3}$ m

PLAXIS	Project description: HSS_ Excavation 1 (phase 4)		Date: 22.03.2017
	Project filename: Baufeld-15-24.09.2015-KPP ...	Step: 34	User name: Fachhochschule Stuttgart

C:\Users\52shan1mki\Desktop\Calculations_21.03.2017\Baufeld-15-24.09.2015-KPP-2UG-wasser_HSS.P2DXDAT\

Output Version 2015.2.19890.13737

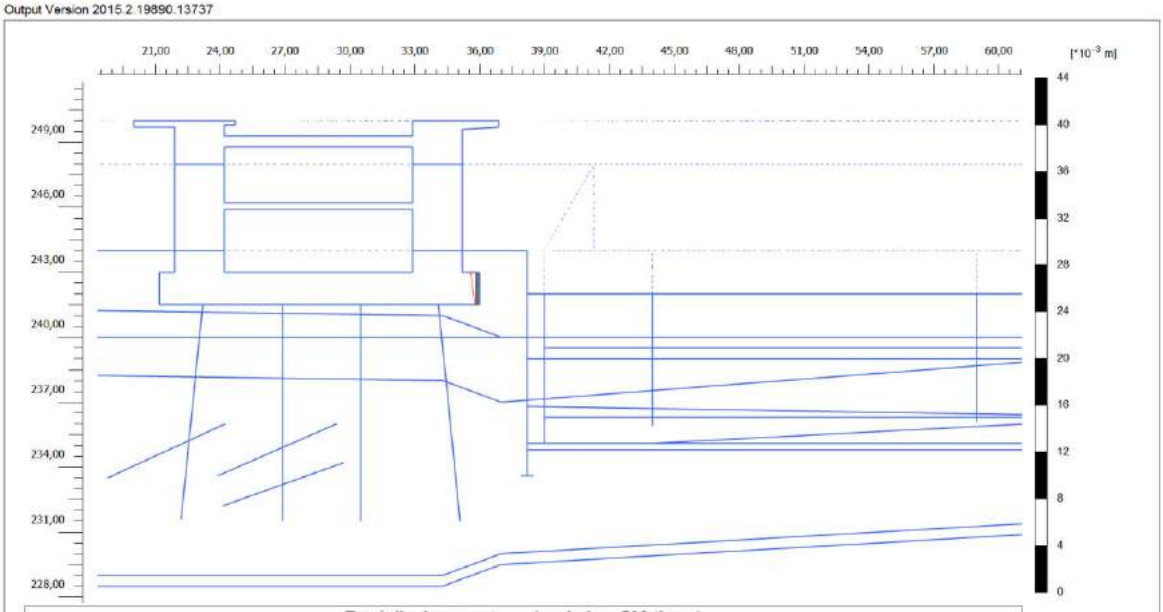

Total displacements u_x (scaled up 500 times)

Maximum value = $-0{,}2206*10^{-3}$ m

Minimum value = $-0{,}6415*10^{-3}$ m

PLAXIS	Project description		Date
	HSS_Instalation of the Strut 1 (phase 5)		22.03.2017
	Project filename: Baufeld-15-24.09.2015-KPP ...	Step: 42	User name: Fachhochschule Stuttgart

C:\Users\52shan1mki\Desktop\Calculations_21.03.2017\Baufeld-15-24.09.2015-KPP-2UG-wasser_HSS.P2DXDAT\

Output Version 2015.2.19890.13737

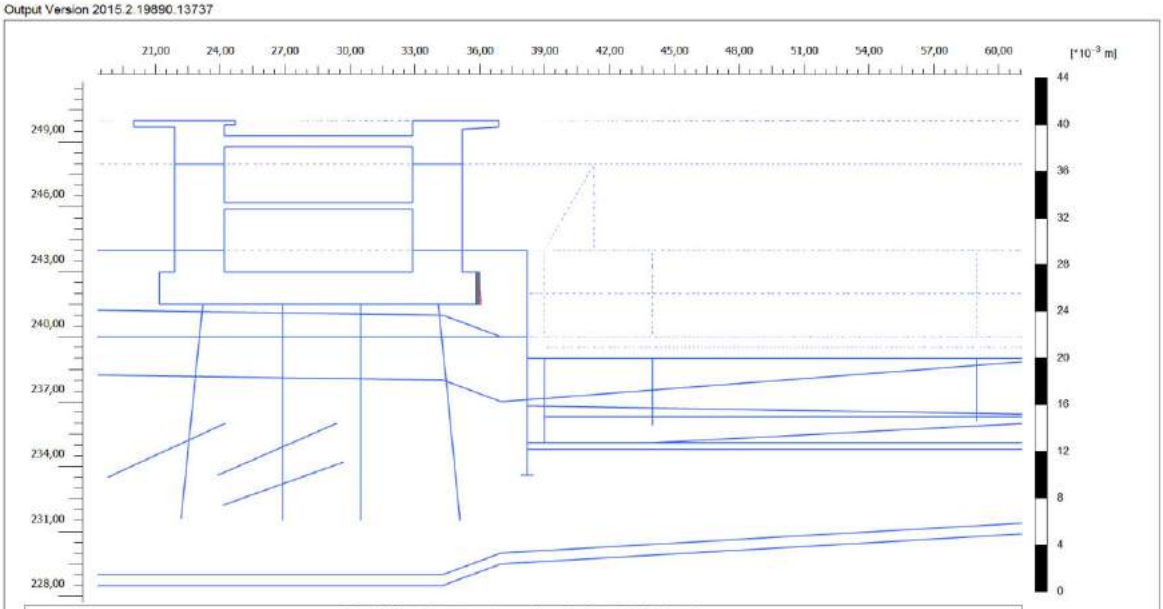

Total displacements u_x (scaled up 500 times)

Maximum value = $0{,}4279*10^{-3}$ m

Minimum value = $-0{,}01307*10^{-3}$ m

PLAXIS	Project description		Date
	HSS_ Excavation 2 with Water Lowering 1 (phase 6)		22.03.2017
	Project filename: Baufeld-15-24.09.2015-KPP ...	Step: 53	User name: Fachhochschule Stuttgart

C:\Users\52shan1mki\Desktop\Calculations_21.03.2017\Baufeld-15-24.09.2015-KPP-2UG-wasser_HSS.P2DXDAT\

Output Version 2015.2.19890.13737

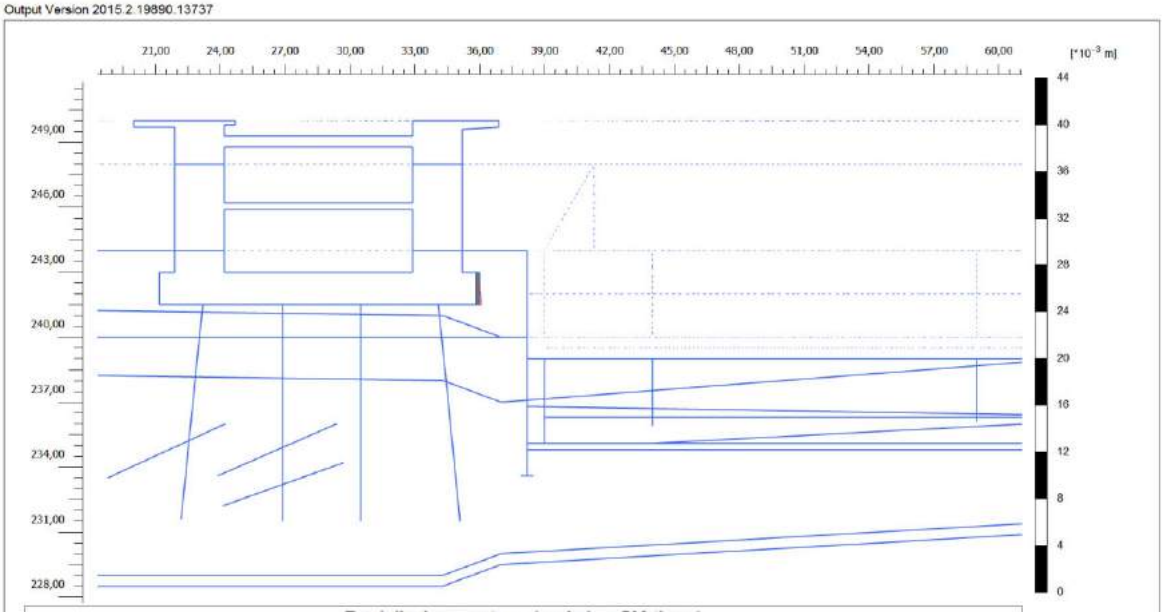

Total displacements u_x (scaled up 500 times)

Maximum value = $0{,}4340 \cdot 10^{-3}$ m

Minimum value = $-4{,}583 \cdot 10^{-6}$ m

PLAXIS	Project description		Date
	HSS_Instalation of the Strut 2 (phase 7)		22.03.2017
	Project filename	Step	User name
	Baufeld-15-24.09.2015-KPP ...	106	Fachhochschule Stuttgart

C:\Users\52shan1mki\Desktop\Calculations_21.03.2017\Baufeld-15-24.09.2015-KPP-2UG-wasser_HSS.P2DXDAT\

Output Version 2015.2.19890.13737

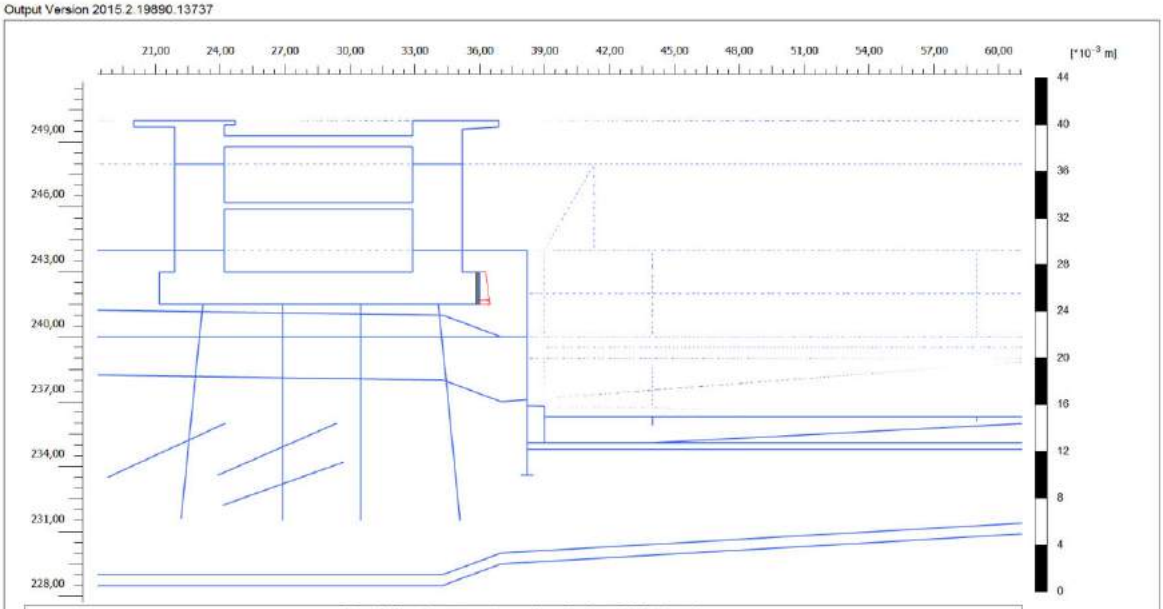

Total displacements u_x (scaled up 500 times)

Maximum value = $1{,}178 \cdot 10^{-3}$ m

Minimum value = $0{,}7716 \cdot 10^{-3}$ m

PLAXIS	Project description		Date
	HSS_ Excavation 3 with Water Lowering 2 (phase 8)		22.03.2017
	Project filename	Step	User name
	Baufeld-15-24.09.2015-KPP ...	116	Fachhochschule Stuttgart

C:\Users\52shan1mki\Desktop\Calculations_21.03.2017\Baufeld-15-24.09.2015-KPP-2UG-wasser_HSS.P2DXDAT\

Output Version 2015.2.19890.13737

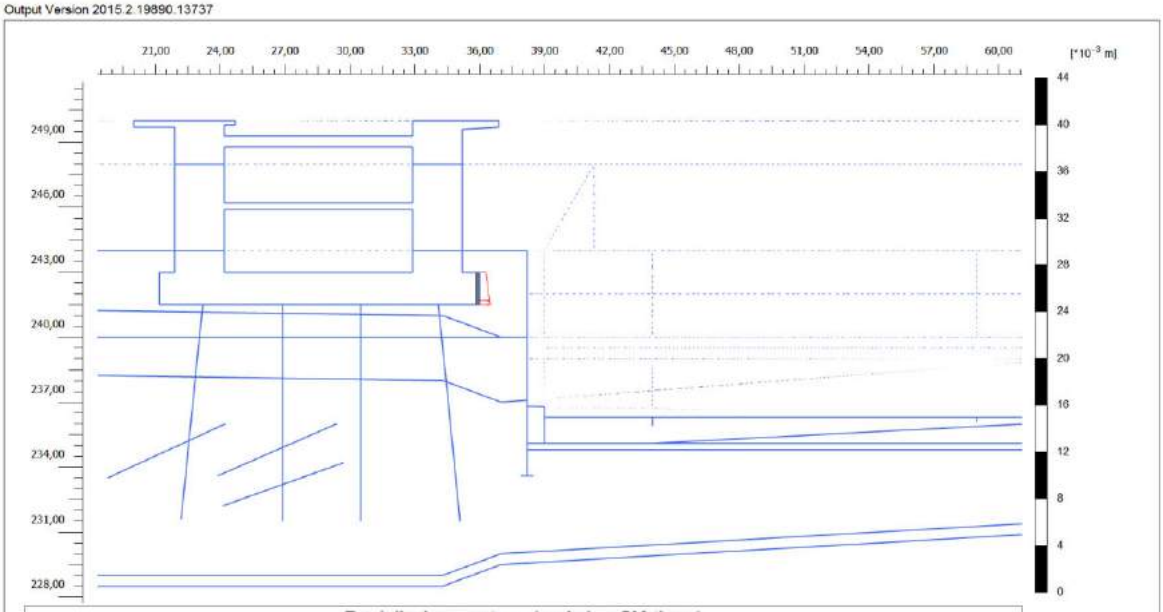

Total displacements u_x (scaled up 500 times)

Maximum value = $1{,}198 \cdot 10^{-3}$ m

Minimum value = $0{,}7991 \cdot 10^{-3}$ m

PLAXIS	Project description		Date
	HSS_Instalation of the Strut 3 (phase 9)		22.03.2017
	Project filename	Step	User name
	Baufeld-15-24.09.2015-KPP ...	162	Fachhochschule Stuttgart

C:\Users\52shan1mki\Desktop\Calculations_21.03.2017\Baufeld-15-24.09.2015-KPP-2UG-wasser_HSS.P2DXDAT\

Output Version 2015.2.19890.13737

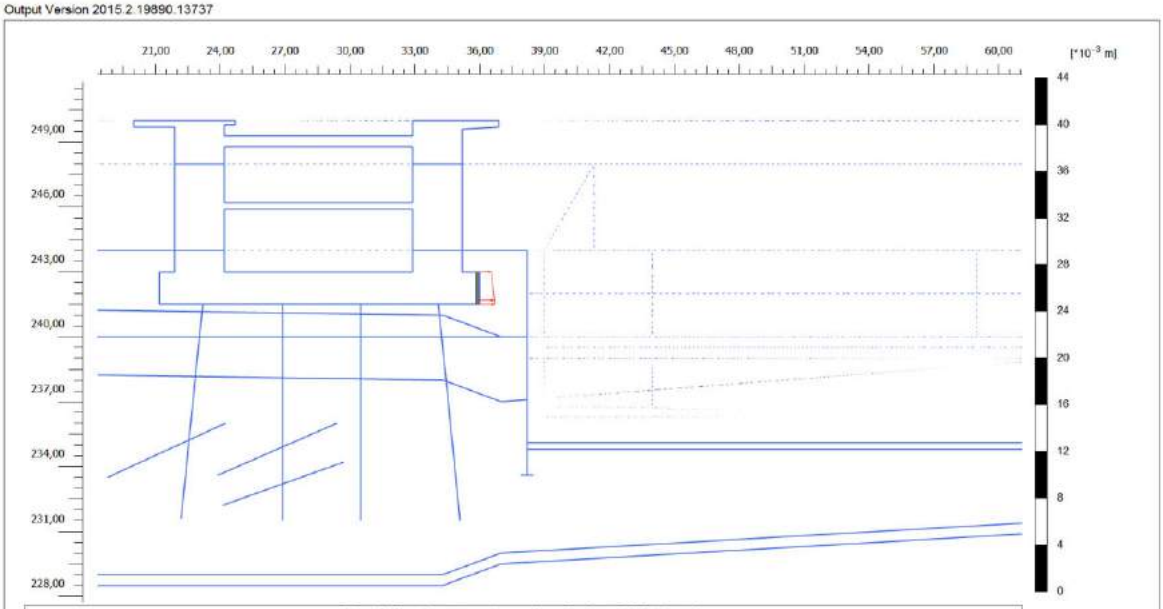

Total displacements u_x (scaled up 500 times)

Maximum value = $1{,}607 \cdot 10^{-3}$ m

Minimum value = $1{,}293 \cdot 10^{-3}$ m

PLAXIS	Project description		Date
	HSS_ Last Excavation with Water Lowering 3 (phase 10)		22.03.2017
	Project filename	Step	User name
	Baufeld-15-24.09.2015-KPP ...	172	Fachhochschule Stuttgart

C:\Users\52shan1mki\Desktop\Calculations_21.03.2017\Baufeld-15-24.09.2015-KPP-2UG-wasser_HSS.P2DXDAT\

Output Version 2015.2.19890.13737

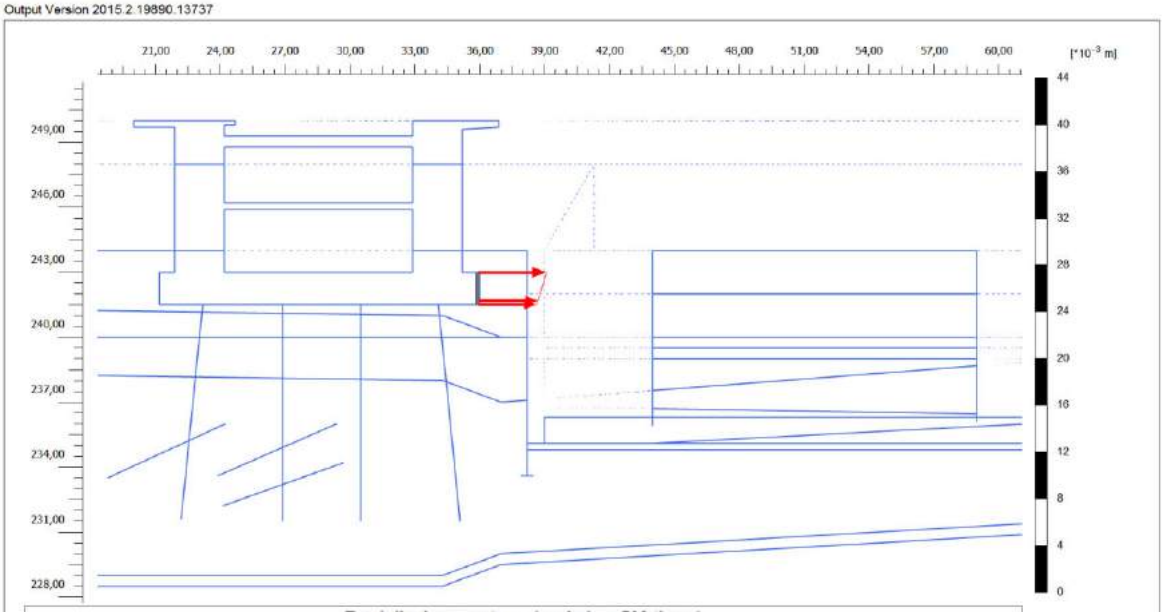

Total displacements u_x (scaled up 500 times)

Maximum value = $6{,}399 \cdot 10^{-3}$ m

Minimum value = $5{,}494 \cdot 10^{-3}$ m

PLAXIS	Project description: HSS_ Construction of the Hotel (phase 11)		Date: 22.03.2017
	Project filename: Baufeld-15-24.09.2015-KPP ...	Step: 180	User name: Fachhochschule Stuttgart

C:\Users\52shan1mki\Desktop\Calculations_21.03.2017\Baufeld-15-24.09.2015-KPP-2UG-wasser_HSS.P2DXDAT\

Output Version 2015.2.19890.13737

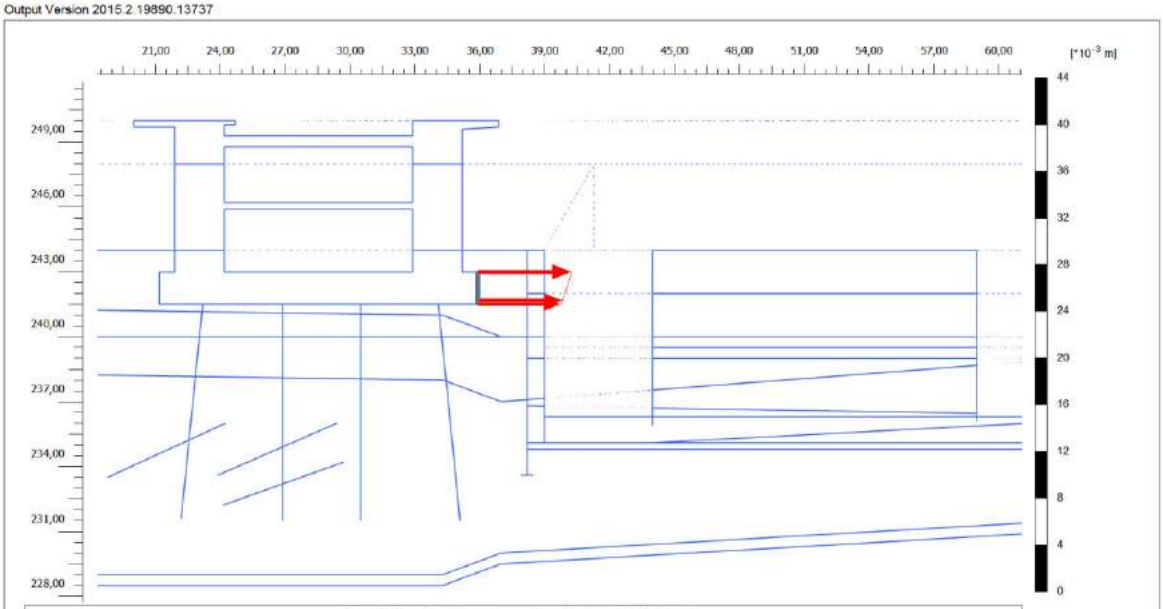

Total displacements u_x (scaled up 500 times)

Maximum value = $8{,}760 \cdot 10^{-3}$ m

Minimum value = $7{,}746 \cdot 10^{-3}$ m

PLAXIS	Project description: HSS_ Backfilling (phase 12)		Date: 22.03.2017
	Project filename: Baufeld-15-24.09.2015-KPP ...	Step: 186	User name: Fachhochschule Stuttgart

C:\Users\52shan1mki\Desktop\Calculations_21.03.2017\Baufeld-15-24.09.2015-KPP-2UG-wasser_HSS.P2DXDAT\

HSS_Bridge_ Vertical Displacement, u_y

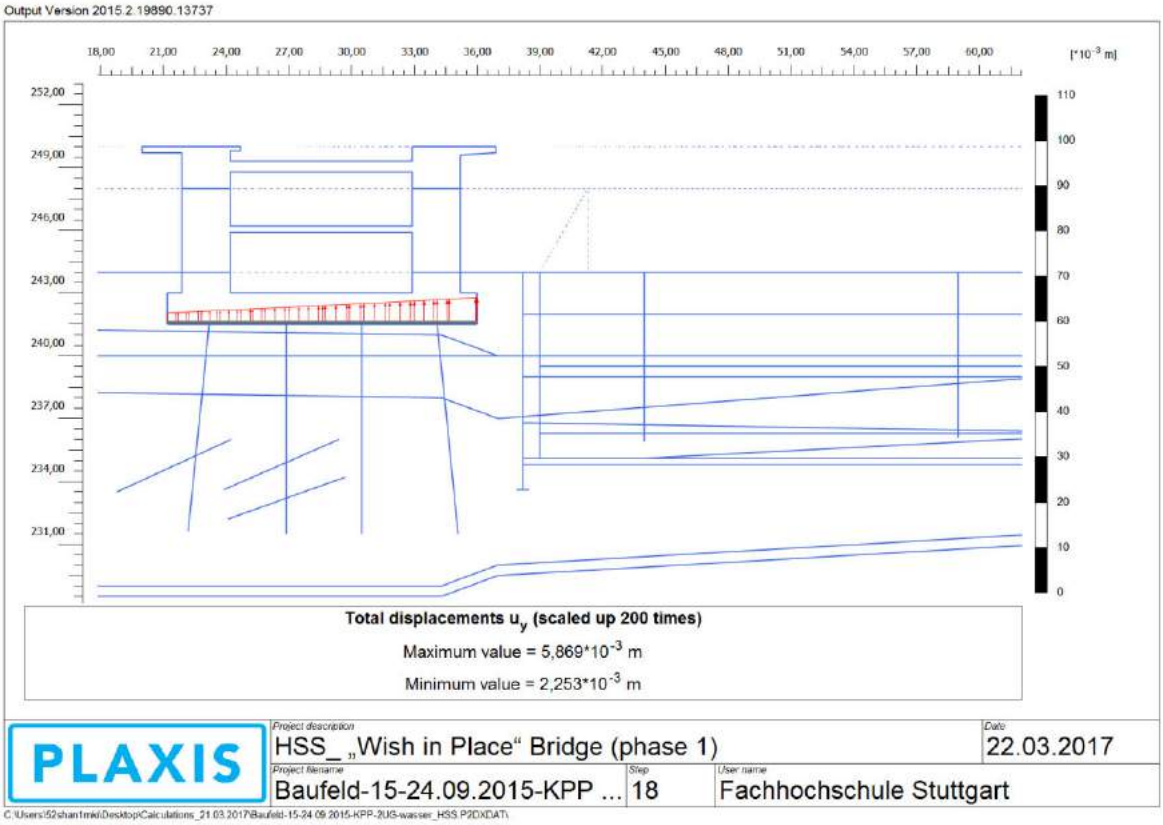

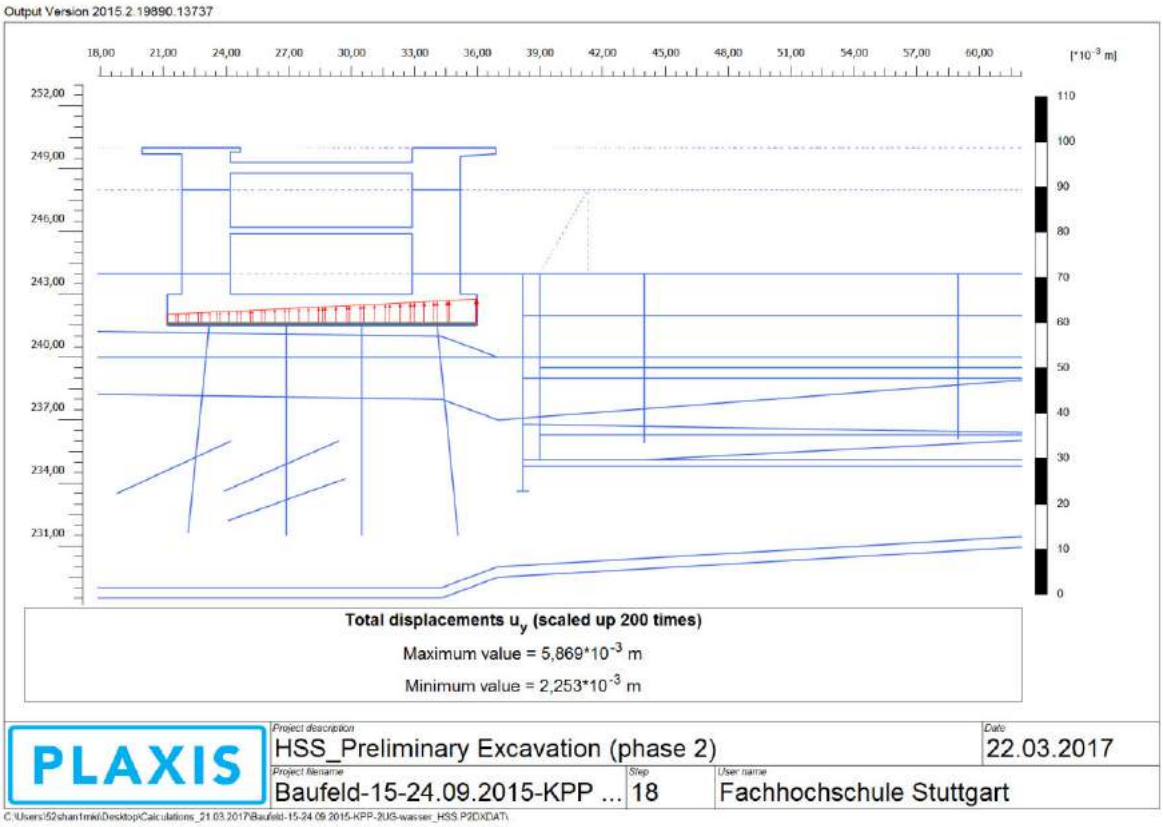

Output Version 2015.2.19890.13737

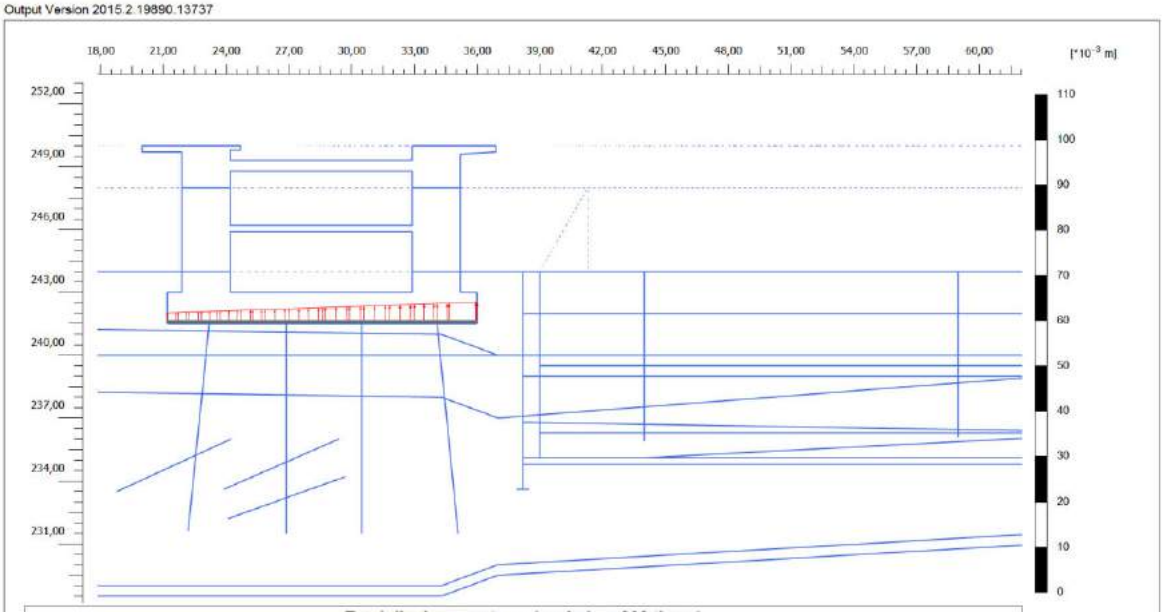

Total displacements u_y (scaled up 200 times)

Maximum value = $4{,}686 \cdot 10^{-3}$ m

Minimum value = $2{,}167 \cdot 10^{-3}$ m

PLAXIS	Project description: HSS_ Installation of the Retaining Walls (phase 3)		Date: 22.03.2017
	Project filename: Baufeld-15-24.09.2015-KPP ...	Step: 24	User name: Fachhochschule Stuttgart

C:\Users\52shan1mki\Desktop\Calculations_21.03.2017\Baufeld-15-24.09.2015-KPP-2UG-wasser_HSS.P2DXDAT\

Output Version 2015.2.19890.13737

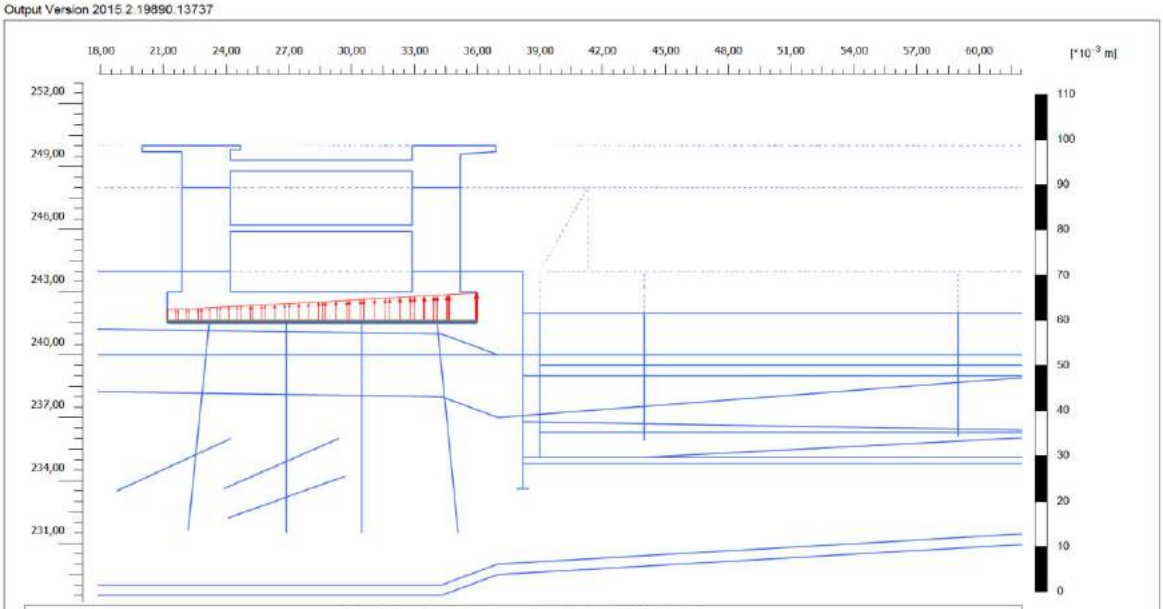

Total displacements u_y (scaled up 200 times)

Maximum value = $6{,}795 \cdot 10^{-3}$ m

Minimum value = $2{,}692 \cdot 10^{-3}$ m

PLAXIS	Project description: HSS_ Excavation 1 (phase 4)		Date: 22.03.2017
	Project filename: Baufeld-15-24.09.2015-KPP ...	Step: 34	User name: Fachhochschule Stuttgart

C:\Users\52shan1mki\Desktop\Calculations_21.03.2017\Baufeld-15-24.09.2015-KPP-2UG-wasser_HSS.P2DXDAT\

Output Version 2015.2.19890.13737

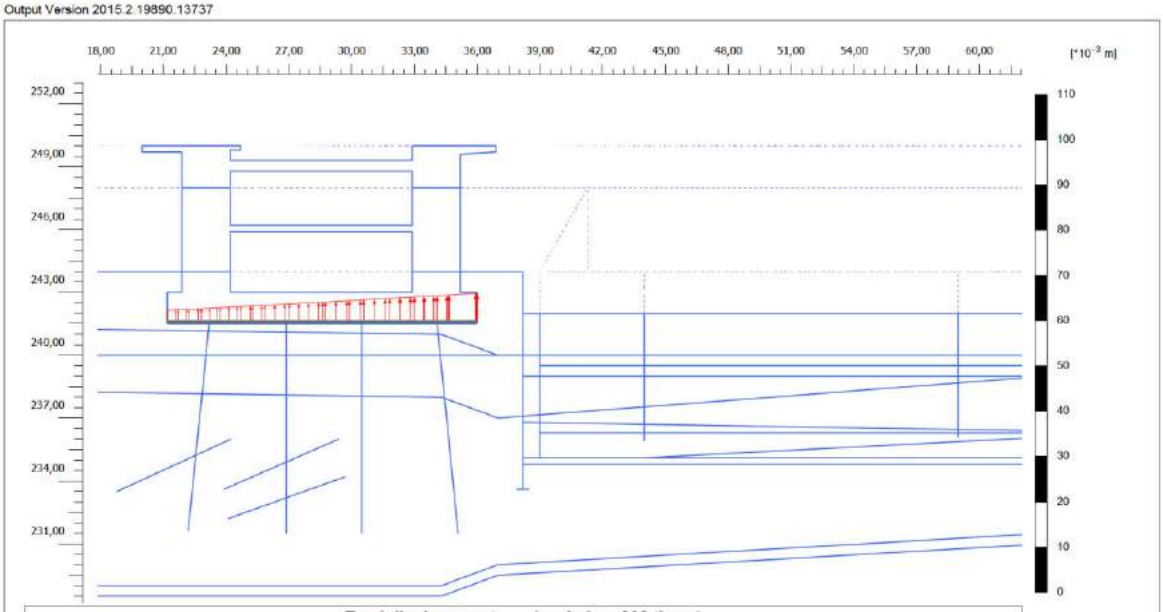

Total displacements u_y (scaled up 200 times)

Maximum value = $6{,}780 \cdot 10^{-3}$ m

Minimum value = $2{,}691 \cdot 10^{-3}$ m

PLAXIS	Project description		Date
	HSS_Instalation of the Strut 1 (phase 5)		22.03.2017
	Project filename	Step	User name
	Baufeld-15-24.09.2015-KPP ...	42	Fachhochschule Stuttgart

C:\Users\52shan1mki\Desktop\Calculations_21.03.2017\Baufeld-15-24.09.2015-KPP-2UG-wasser_HSS.P2DXDAT\

Output Version 2015.2.19890.13737

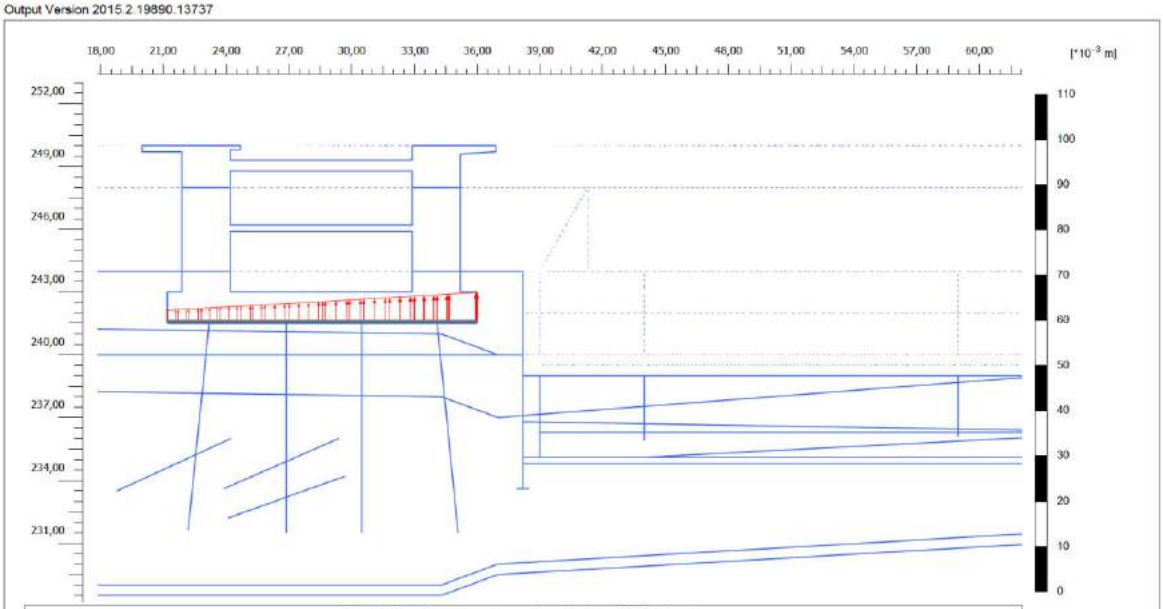

Total displacements u_y (scaled up 200 times)

Maximum value = $6{,}910 \cdot 10^{-3}$ m

Minimum value = $2{,}649 \cdot 10^{-3}$ m

PLAXIS	Project description		Date
	HSS_ Excavation 2 with Water Lowering 1 (phase 6)		22.03.2017
	Project filename	Step	User name
	Baufeld-15-24.09.2015-KPP ...	53	Fachhochschule Stuttgart

C:\Users\52shan1mki\Desktop\Calculations_21.03.2017\Baufeld-15-24.09.2015-KPP-2UG-wasser_HSS.P2DXDAT\

Output Version 2015.2.19890.13737

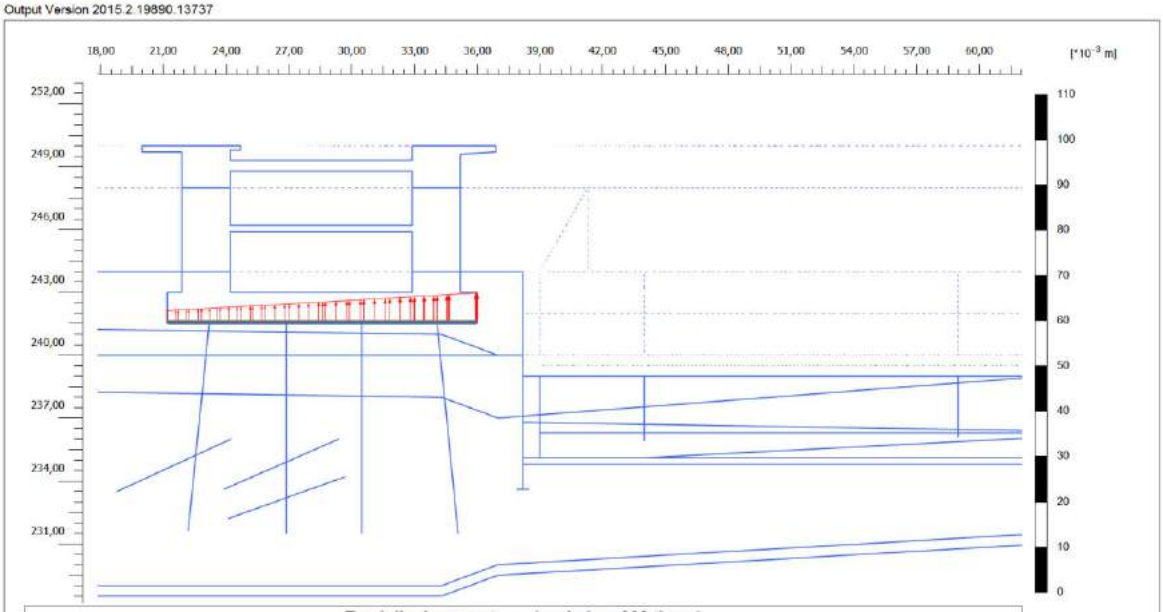

PLAXIS	Project description: HSS_Instalation of the Strut 2 (phase 7)		Date: 22.03.2017
	Project filename: Baufeld-15-24.09.2015-KPP ...	Step: 106	User name: Fachhochschule Stuttgart

C:\Users\52shan1mki\Desktop\Calculations_21.03.2017\Baufeld-15-24.09.2015-KPP-2UG-wasser_HSS.P2DXDAT\

Output Version 2015.2.19890.13737

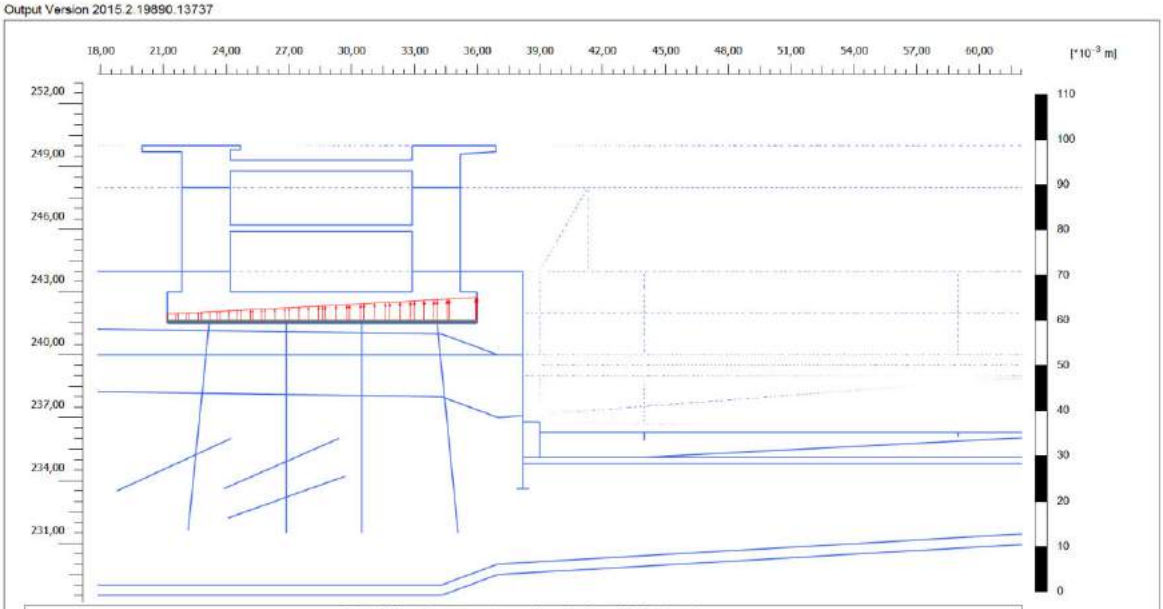

PLAXIS	Project description: HSS_ Excavation 3 with Water Lowering 2 (phase 8)		Date: 22.03.2017
	Project filename: Baufeld-15-24.09.2015-KPP ...	Step: 116	User name: Fachhochschule Stuttgart

C:\Users\52shan1mki\Desktop\Calculations_21.03.2017\Baufeld-15-24.09.2015-KPP-2UG-wasser_HSS.P2DXDAT\

Output Version 2015.2.19890.13737

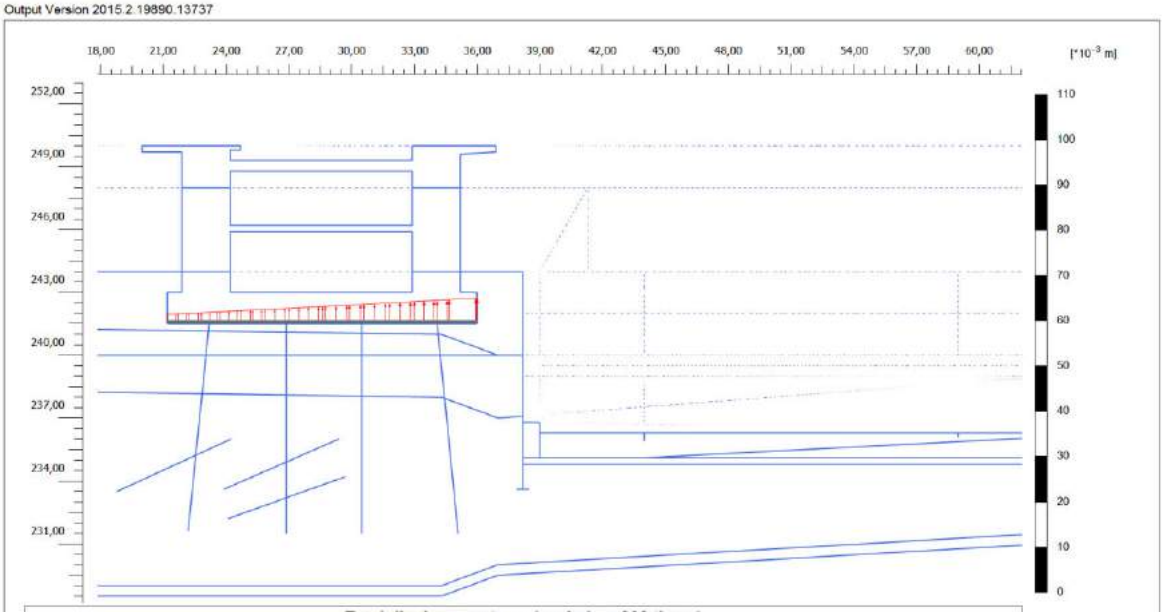

Total displacements u_y (scaled up 200 times)

Maximum value = $5{,}614 \cdot 10^{-3}$ m

Minimum value = $1{,}777 \cdot 10^{-3}$ m

PLAXIS	Project description: HSS_Instalation of the Strut 3 (phase 9)		Date: 22.03.2017
	Project filename: Baufeld-15-24.09.2015-KPP ...	Step: 162	User name: Fachhochschule Stuttgart

C:\Users\52shan1mki\Desktop\Calculations_21.03.2017\Baufeld-15-24.09.2015-KPP-2UG-wasser_HSS.P2DXDAT\

Output Version 2015.2.19890.13737

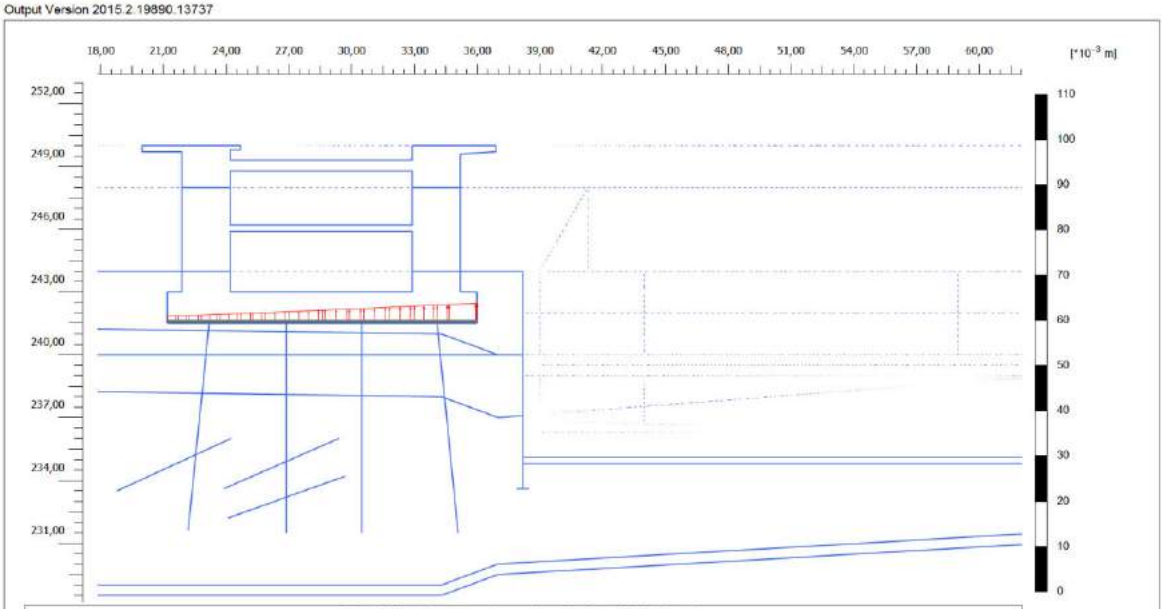

Total displacements u_y (scaled up 200 times)

Maximum value = $4{,}256 \cdot 10^{-3}$ m

Minimum value = $1{,}207 \cdot 10^{-3}$ m

PLAXIS	Project description: HSS_ Last Excavation with Water Lowering 3 (phase 10)		Date: 22.03.2017
	Project filename: Baufeld-15-24.09.2015-KPP ...	Step: 172	User name: Fachhochschule Stuttgart

C:\Users\52shan1mki\Desktop\Calculations_21.03.2017\Baufeld-15-24.09.2015-KPP-2UG-wasser_HSS.P2DXDAT\

Output Version 2015.2.19890.13737

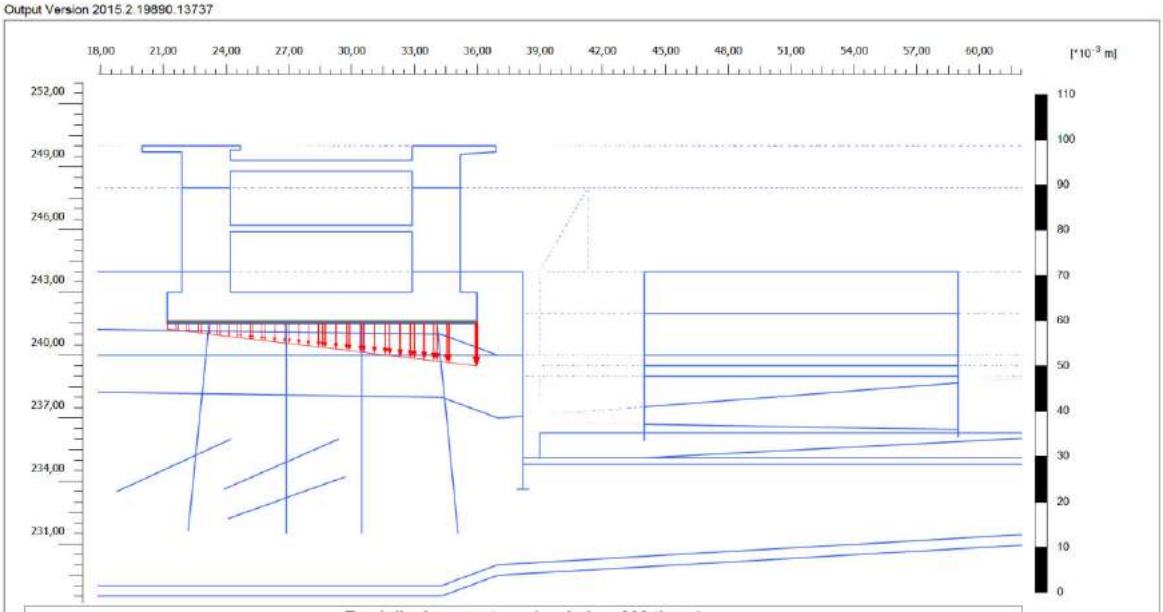

Total displacements u_y (scaled up 200 times)

Maximum value = $-1{,}717*10^{-3}$ m

Minimum value = -0,01056 m

PLAXIS	Project description: HSS_ Construction of the Hotel (phase 11)		Date: 22.03.2017
	Project filename: Baufeld-15-24.09.2015-KPP ...	Step: 180	User name: Fachhochschule Stuttgart

C:\Users\52shan1mki\Desktop\Calculations_21.03.2017\Baufeld-15-24.09.2015-KPP-2UG-wasser_HSS.P2DXDAT\

Output Version 2015.2.19890.13737

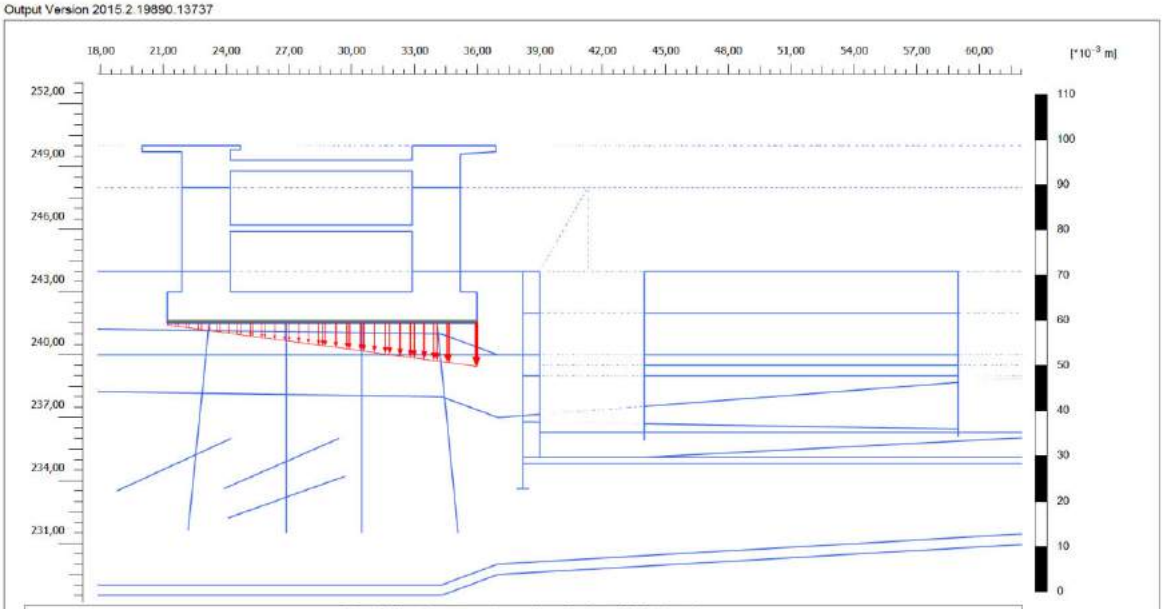

Total displacements u_y (scaled up 200 times)

Maximum value = $-0{,}8397*10^{-3}$ m

Minimum value = -0,01076 m

PLAXIS	Project description: HSS_ Backfilling (phase 12)		Date: 22.03.2017
	Project filename: Baufeld-15-24.09.2015-KPP ...	Step: 186	User name: Fachhochschule Stuttgart

C:\Users\52shan1mki\Desktop\Calculations_21.03.2017\Baufeld-15-24.09.2015-KPP-2UG-wasser_HSS.P2DXDAT\

HSS_Bridge_Stresses

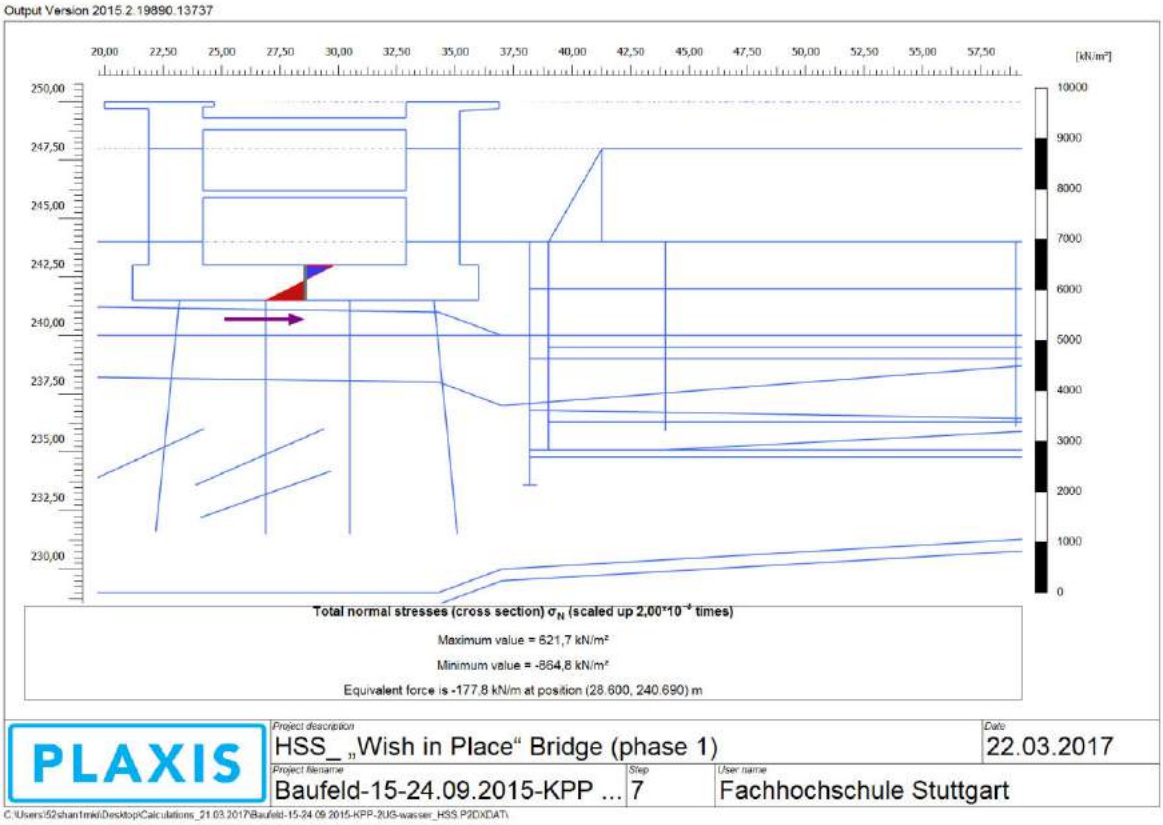

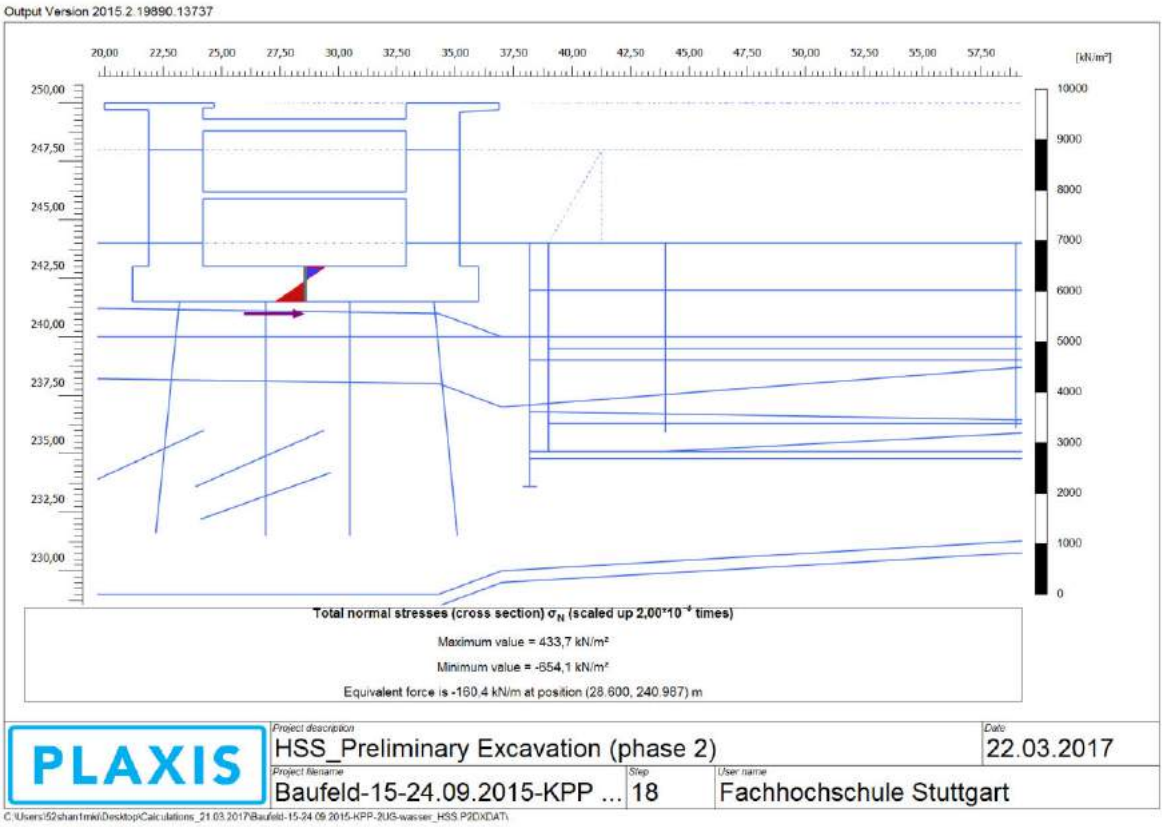

Output Version 2015.2.19890.13737

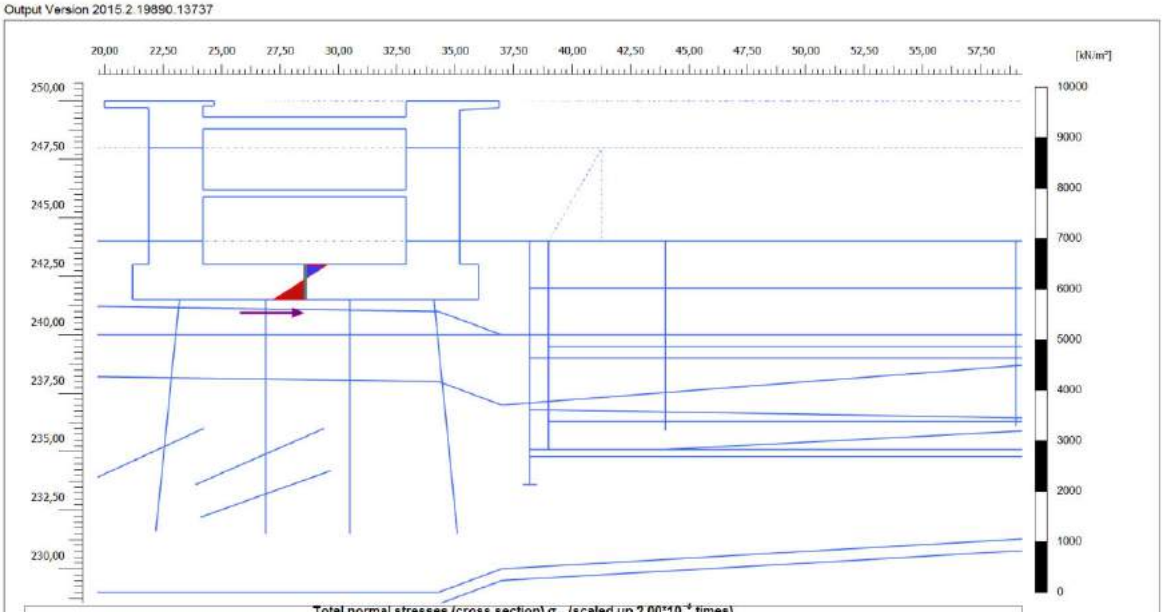

PLAXIS	Project description: HSS_ Installation of the Retaining Walls (phase 3)		Date: 22.03.2017
	Project filename: Baufeld-15-24.09.2015-KPP ...	Step: 24	User name: Fachhochschule Stuttgart

C:\Users\52shan1mki\Desktop\Calculations_21.03.2017\Baufeld-15-24.09.2015-KPP-2UG-wasser_HSS.P2DXDAT\

Output Version 2015.2.19890.13737

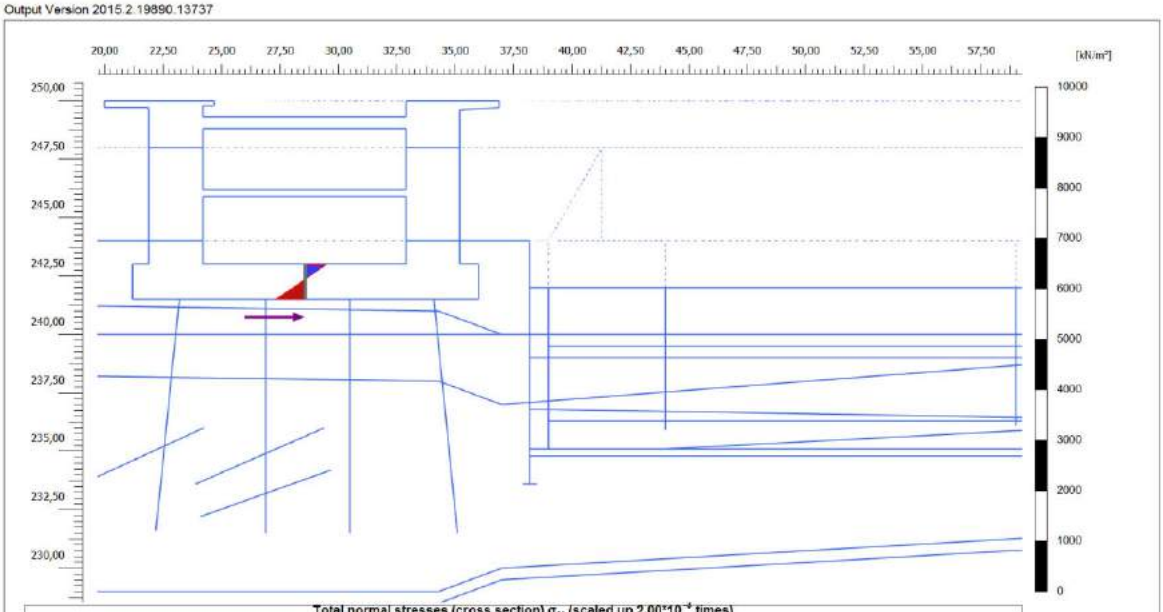

PLAXIS	Project description: HSS_ Excavation 1 (phase 4)		Date: 22.03.2017
	Project filename: Baufeld-15-24.09.2015-KPP ...	Step: 34	User name: Fachhochschule Stuttgart

C:\Users\52shan1mki\Desktop\Calculations_21.03.2017\Baufeld-15-24.09.2015-KPP-2UG-wasser_HSS.P2DXDAT\

Output Version 2015.2.19890.13737

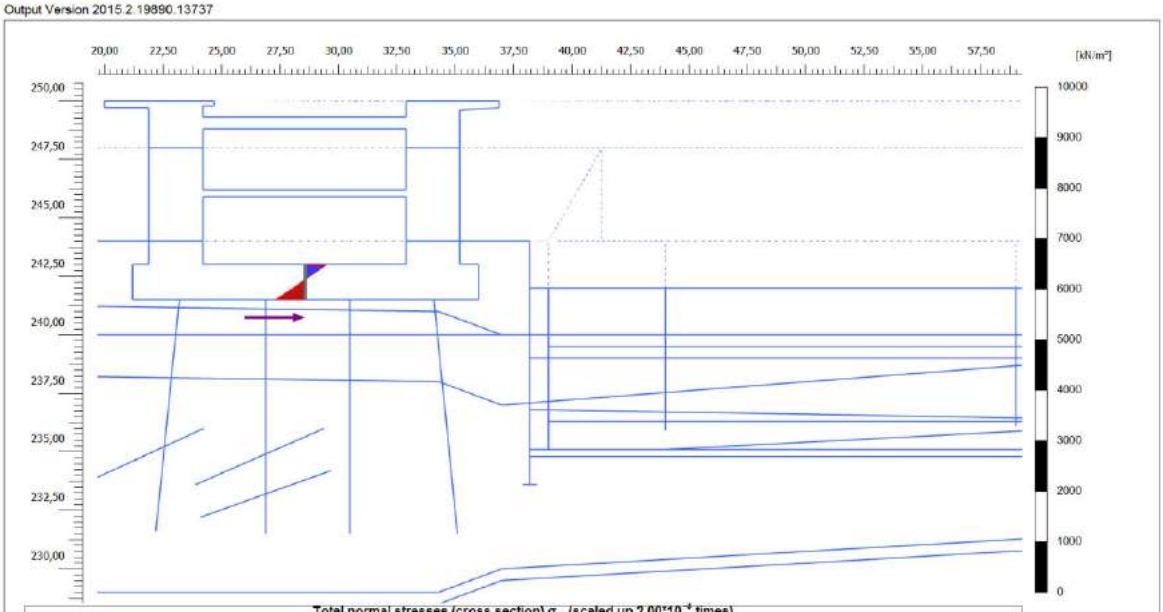

PLAXIS	Project description: HSS_Instalation of the Strut 1 (phase 5)		Date: 22.03.2017
	Project filename: Baufeld-15-24.09.2015-KPP ...	Step: 42	User name: Fachhochschule Stuttgart

C:\Users\52shan1mki\Desktop\Calculations_21.03.2017\Baufeld-15-24.09.2015-KPP-2UG-wasser_HSS.P2DXDAT\

Output Version 2015.2.19890.13737

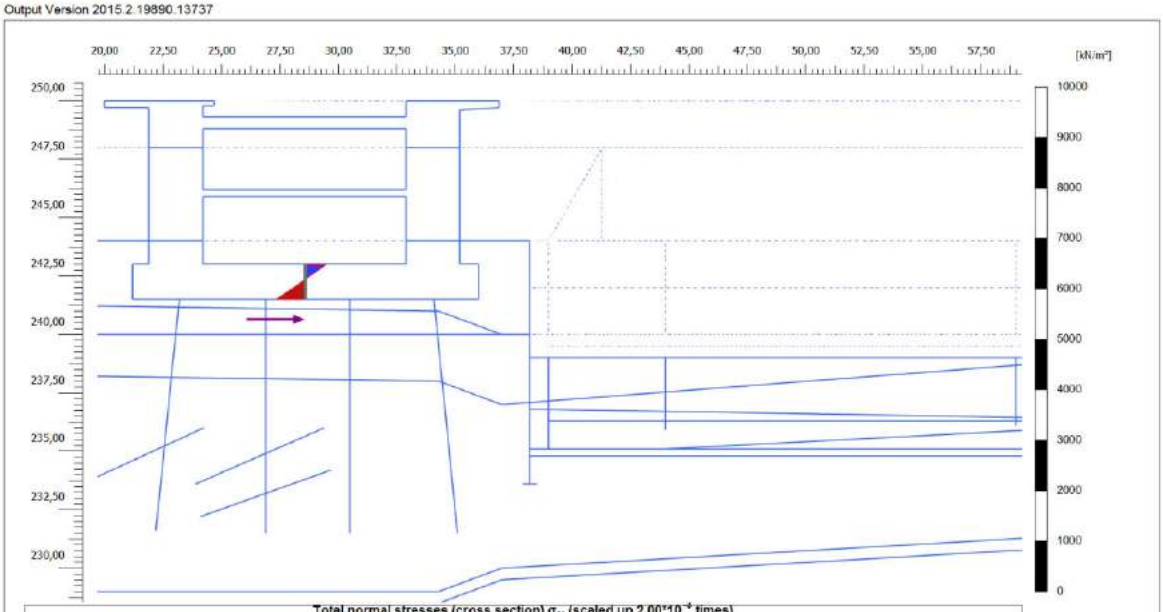

PLAXIS	Project description: HSS_ Excavation 2 with Water Lowering 1 (phase 6)		Date: 22.03.2017
	Project filename: Baufeld-15-24.09.2015-KPP ...	Step: 53	User name: Fachhochschule Stuttgart

C:\Users\52shan1mki\Desktop\Calculations_21.03.2017\Baufeld-15-24.09.2015-KPP-2UG-wasser_HSS.P2DXDAT\

Output Version 2015.2.19890.13737

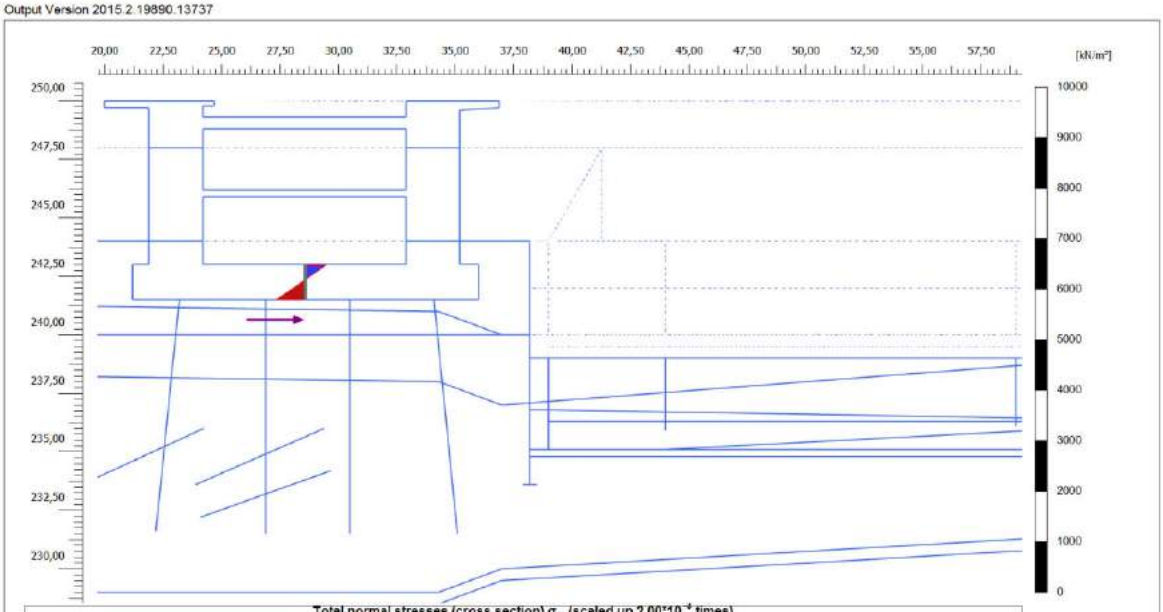

PLAXIS	Project description: HSS_Instalation of the Strut 2 (phase 7)		Date: 22.03.2017
	Project filename: Baufeld-15-24.09.2015-KPP ...	Step: 106	User name: Fachhochschule Stuttgart

C:\Users\52shan1mki\Desktop\Calculations_21.03.2017\Baufeld-15-24.09.2015-KPP-2UG-wasser_HSS.P2DXDAT\

Output Version 2015.2.19890.13737

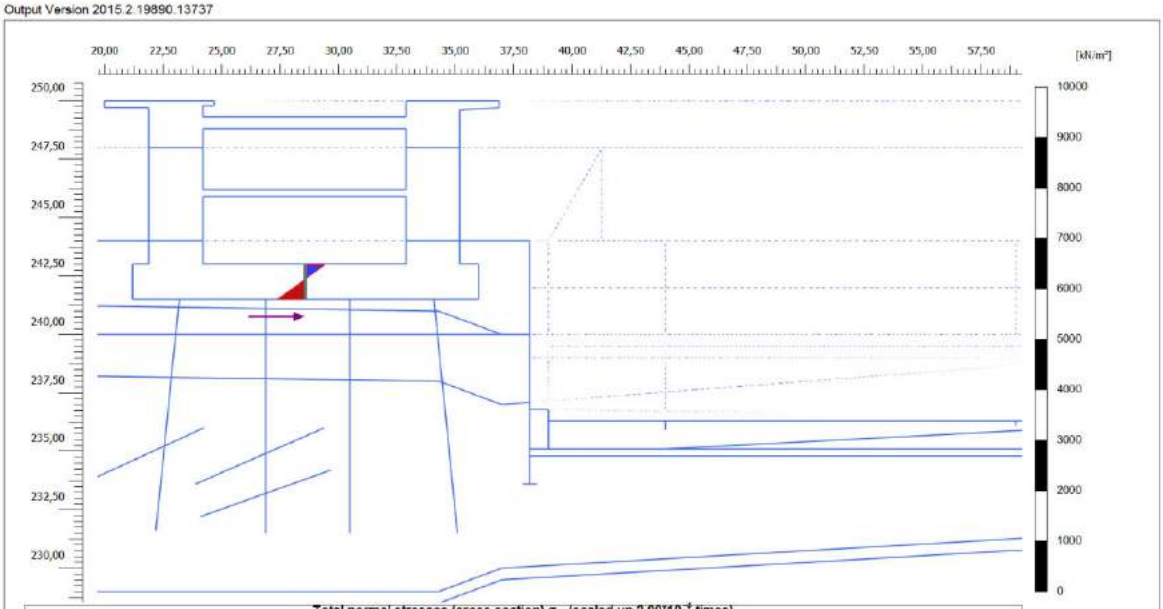

PLAXIS	Project description: HSS_ Excavation 3 with Water Lowering 3 (phase 8)		Date: 22.03.2017
	Project filename: Baufeld-15-24.09.2015-KPP ...	Step: 116	User name: Fachhochschule Stuttgart

C:\Users\52shan1mki\Desktop\Calculations_21.03.2017\Baufeld-15-24.09.2015-KPP-2UG-wasser_HSS.P2DXDAT\

Output Version 2015.2.19890.13737

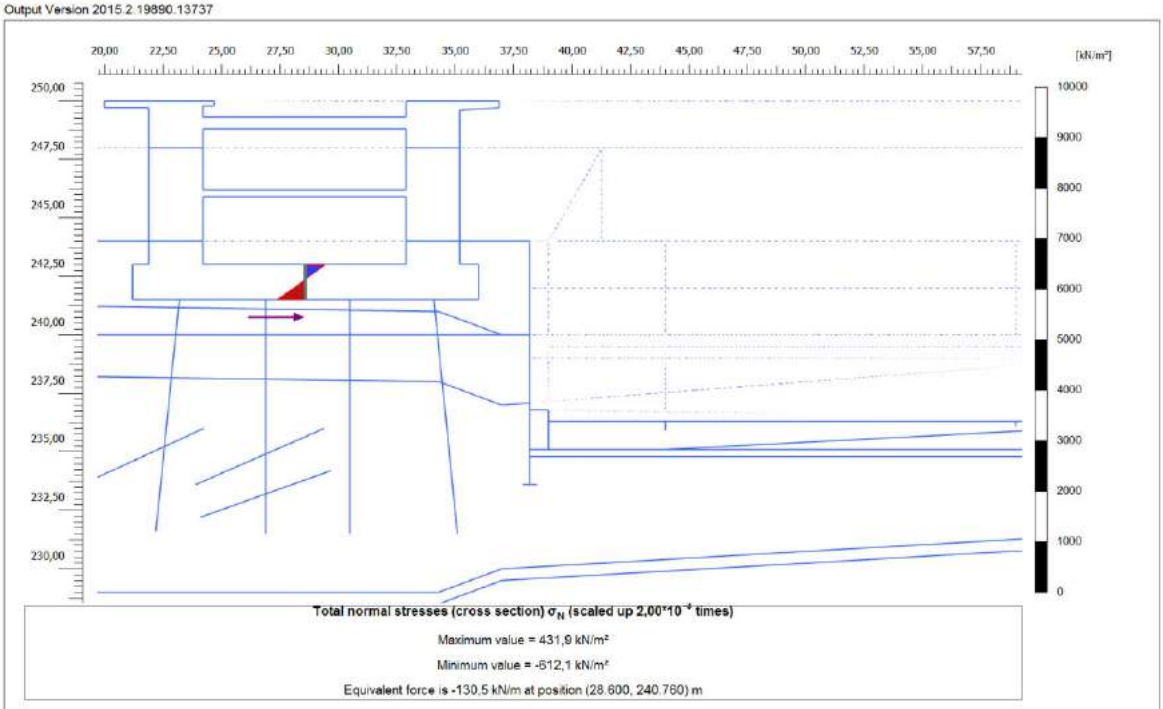

PLAXIS	Project description: HSS_Instalation of the Strut 3 (phase 9)		Date: 22.03.2017
	Project filename: Baufeld-15-24.09.2015-KPP ...	Step: 162	User name: Fachhochschule Stuttgart

C:\Users\52shan1mki\Desktop\Calculations_21.03.2017\Baufeld-15-24.09.2015-KPP-2UG-wasser_HSS.P2DXDAT\

Output Version 2015.2.19890.13737

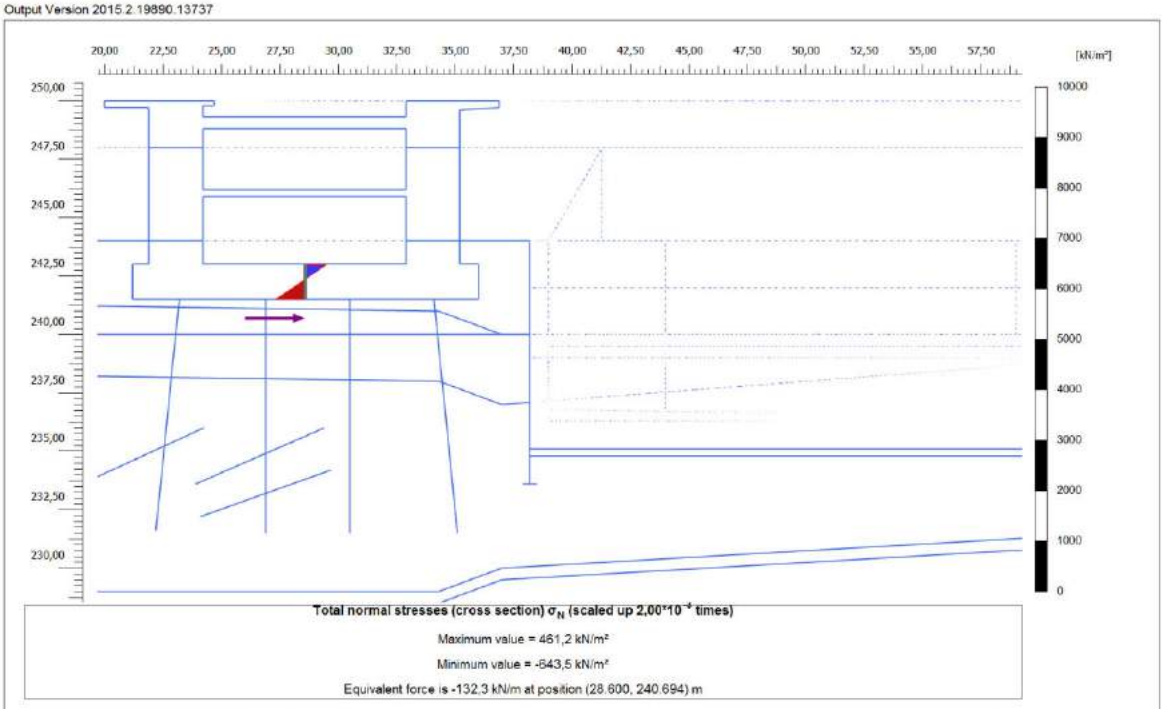

PLAXIS	Project description: HSS_ Last Excavation with Water Lowering 3 (phase 10)		Date: 22.03.2017
	Project filename: Baufeld-15-24.09.2015-KPP ...	Step: 172	User name: Fachhochschule Stuttgart

C:\Users\52shan1mki\Desktop\Calculations_21.03.2017\Baufeld-15-24.09.2015-KPP-2UG-wasser_HSS.P2DXDAT\

Output Version 2015.2.19890.13737

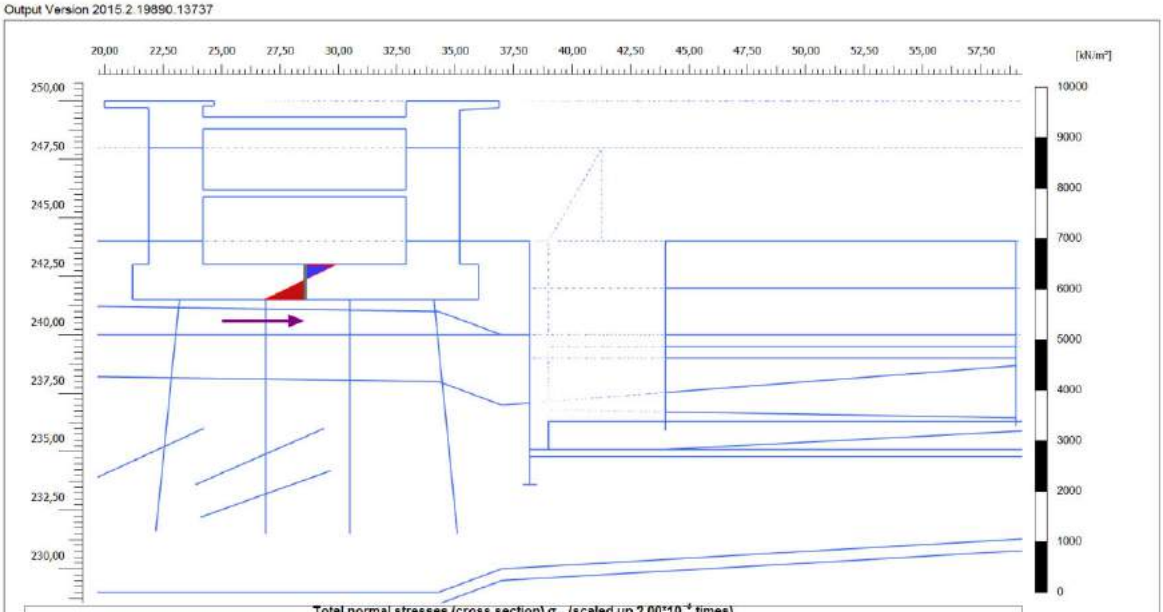

Total normal stresses (cross section) σ_N (scaled up $2{,}00 \cdot 10^{-4}$ times)

Maximum value = 854,3 kN/m²

Minimum value = -892,2 kN/m²

Equivalent force is -174,7 kN/m at position (28.600, 240.598) m

PLAXIS	Project description: HSS_Construction of the Hotel (phase 11)		Date: 22.03.2017
	Project filename: Baufeld-15-24.09.2015-KPP ...	Step: 180	User name: Fachhochschule Stuttgart

C:\Users\52shan1mki\Desktop\Calculations_21.03.2017\Baufeld-15-24.09.2015-KPP-2UG-wasser_HSS.P2DXDAT\

Output Version 2015.2.19890.13737

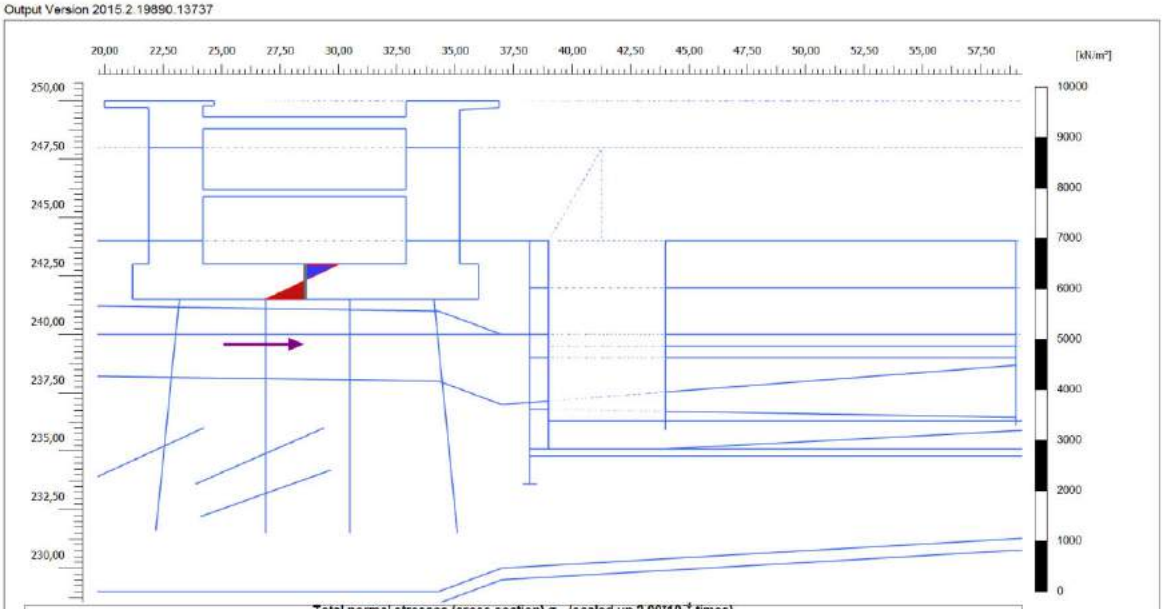

Total normal stresses (cross section) σ_N (scaled up $2{,}00 \cdot 10^{-4}$ times)

Maximum value = 725,2 kN/m²

Minimum value = -879,4 kN/m²

Equivalent force is -112,2 kN/m at position (28.600, 239.579) m

PLAXIS	Project description: HSS_Backfilling (phase 12)		Date: 22.03.2017
	Project filename: Baufeld-15-24.09.2015-KPP ...	Step: 186	User name: Fachhochschule Stuttgart

C:\Users\52shan1mki\Desktop\Calculations_21.03.2017\Baufeld-15-24.09.2015-KPP-2UG-wasser_HSS.P2DXDAT\

HSS_Piles_Horizontal Displacement, u_x

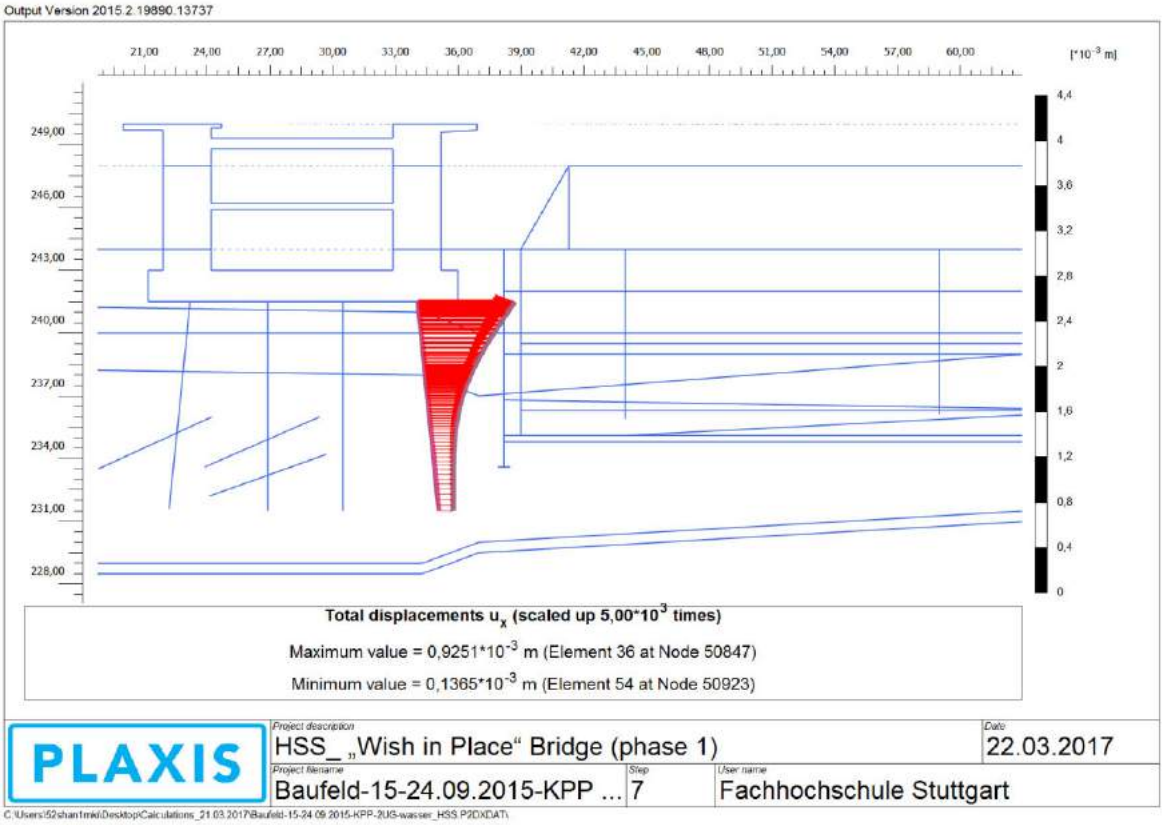

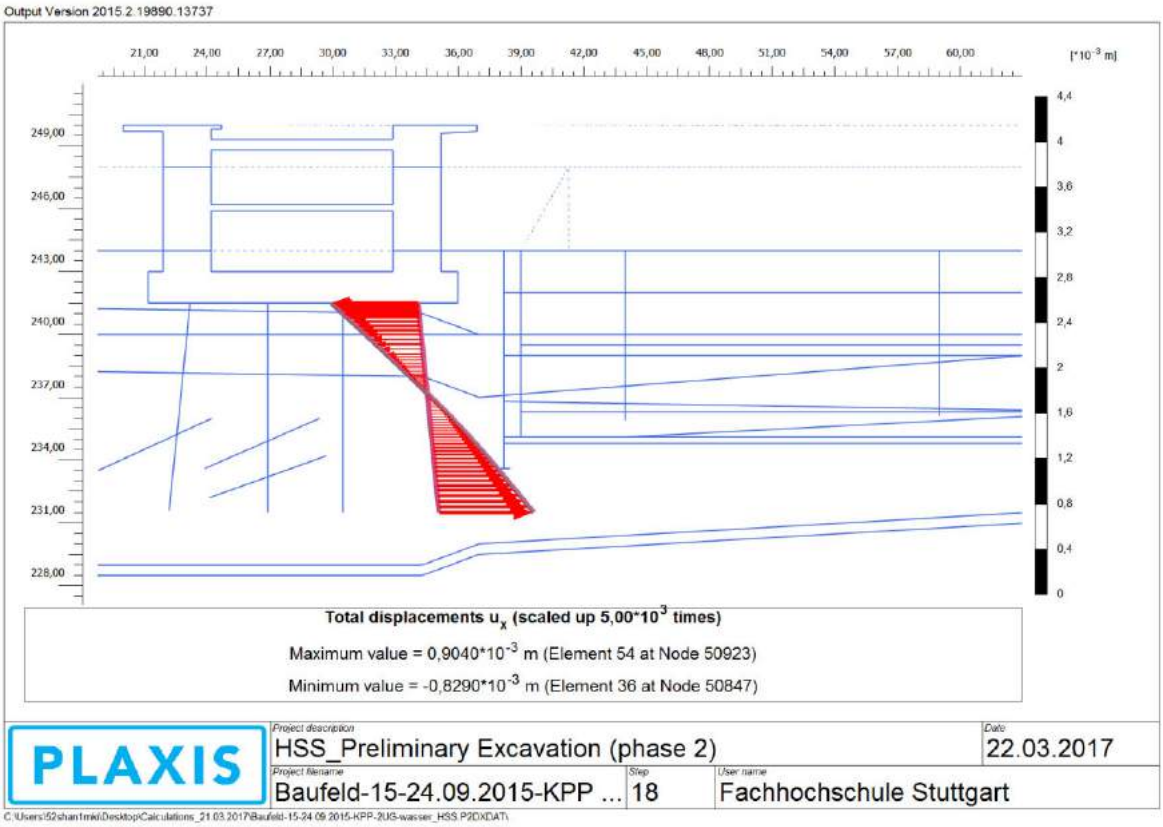

Output Version 2015.2.19890.13737

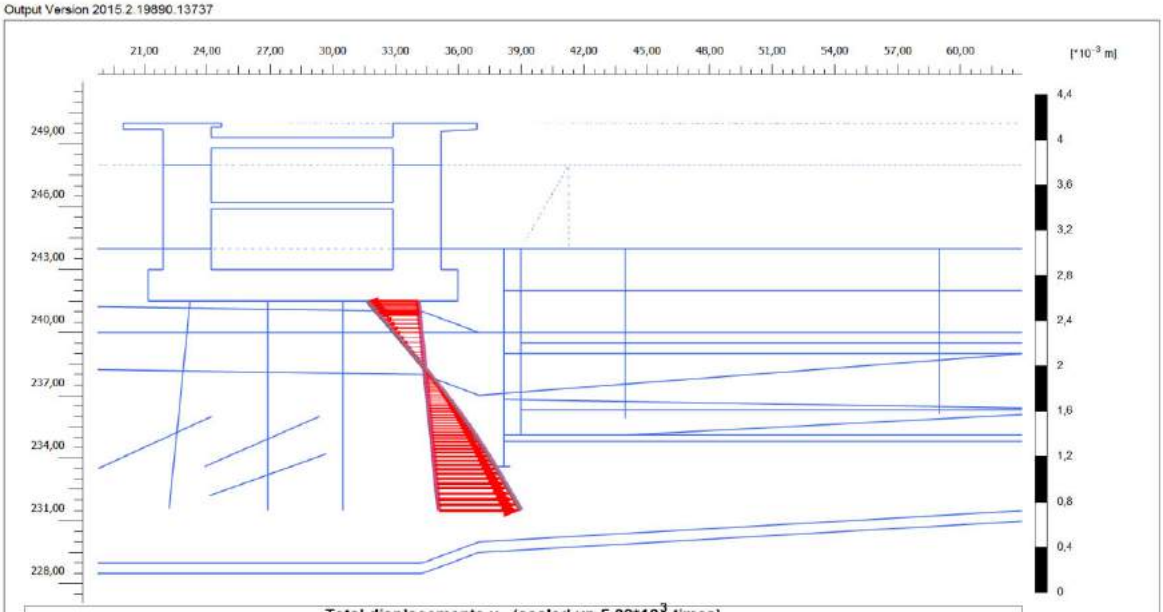

Total displacements u_x (scaled up $5{,}00*10^3$ times)

Maximum value = $0{,}7824*10^{-3}$ m (Element 54 at Node 50923)

Minimum value = $-0{,}4818*10^{-3}$ m (Element 36 at Node 50847)

PLAXIS	Project description: HSS_ Installation of the Retaining Walls (phase 3)		Date: 22.03.2017
	Project filename: Baufeld-15-24.09.2015-KPP ...	Step: 24	User name: Fachhochschule Stuttgart

C:\Users\52shan1mki\Desktop\Calculations_21.03.2017\Baufeld-15-24.09.2015-KPP-2UG-wasser_HSS.P2DXDAT\

Output Version 2015.2.19890.13737

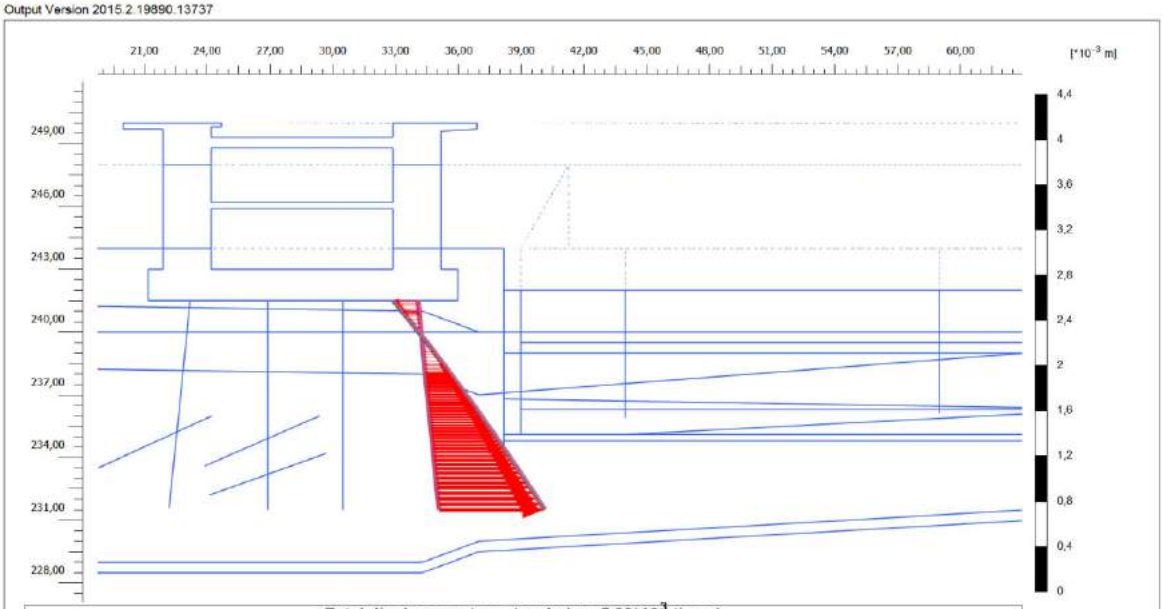

Total displacements u_x (scaled up $5{,}00*10^3$ times)

Maximum value = $1{,}010*10^{-3}$ m (Element 54 at Node 50923)

Minimum value = $-0{,}2358*10^{-3}$ m (Element 36 at Node 50847)

PLAXIS	Project description: HSS_ Excavation 1 (phase 4)		Date: 22.03.2017
	Project filename: Baufeld-15-24.09.2015-KPP ...	Step: 34	User name: Fachhochschule Stuttgart

C:\Users\52shan1mki\Desktop\Calculations_21.03.2017\Baufeld-15-24.09.2015-KPP-2UG-wasser_HSS.P2DXDAT\

Output Version 2015.2.19890.13737

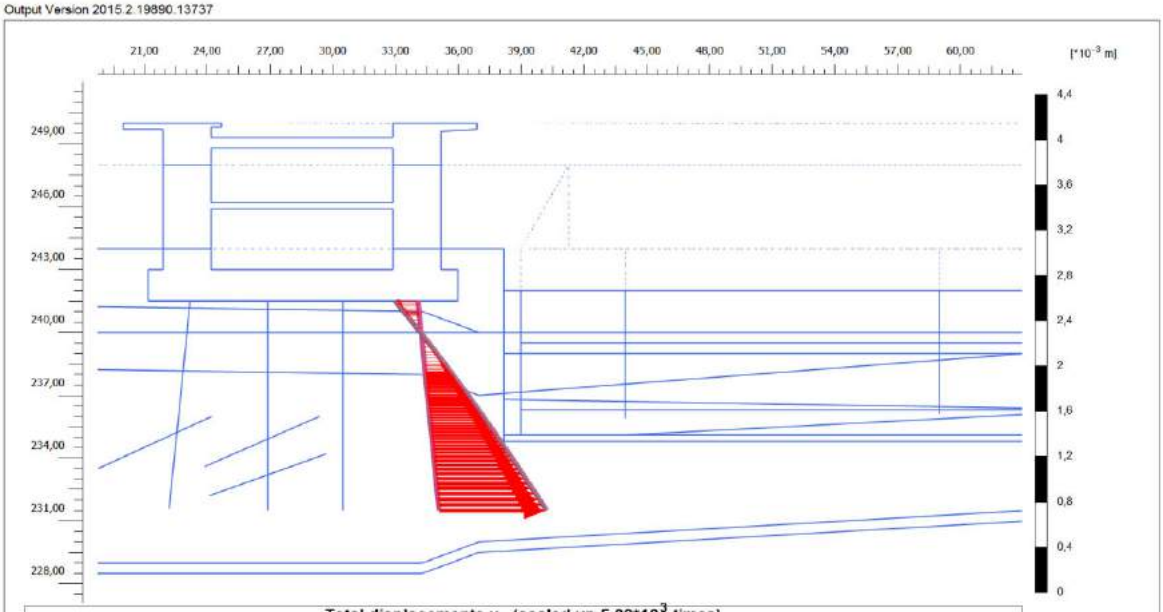

Total displacements u_x (scaled up $5{,}00*10^3$ times)

Maximum value = $1{,}029*10^{-3}$ m (Element 54 at Node 50923)

Minimum value = $-0{,}2203*10^{-3}$ m (Element 36 at Node 50847)

PLAXIS	Project description: HSS_Instalation of the Strut 1 (phase 5)		Date: 22.03.2017
	Project filename: Baufeld-15-24.09.2015-KPP ...	Step: 42	User name: Fachhochschule Stuttgart

C:\Users\52shan1mki\Desktop\Calculations_21.03.2017\Baufeld-15-24.09.2015-KPP-2UG-wasser_HSS.P2DXDAT\

Output Version 2015.2.19890.13737

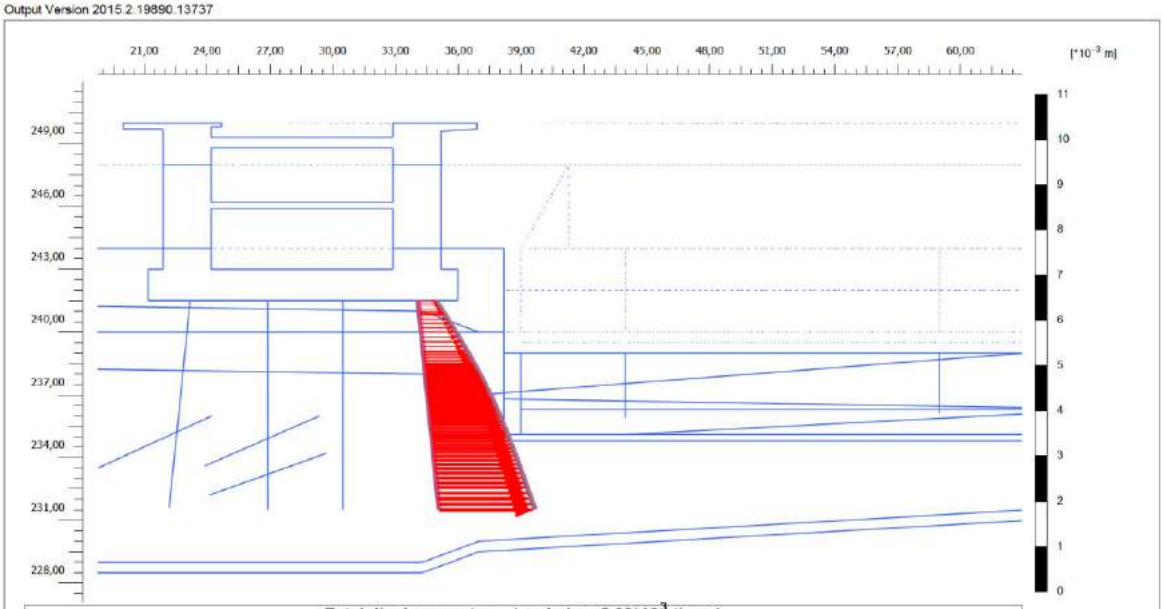

Total displacements u_x (scaled up $2{,}00*10^3$ times)

Maximum value = $2{,}294*10^{-3}$ m (Element 54 at Node 50923)

Minimum value = $0{,}4282*10^{-3}$ m (Element 36 at Node 50847)

PLAXIS	Project description: HSS_ Excavation 2 with Water Lowering 1 (phase 6)		Date: 22.03.2017
	Project filename: Baufeld-15-24.09.2015-KPP ...	Step: 53	User name: Fachhochschule Stuttgart

C:\Users\52shan1mki\Desktop\Calculations_21.03.2017\Baufeld-15-24.09.2015-KPP-2UG-wasser_HSS.P2DXDAT\

Output Version 2015.2.19890.13737

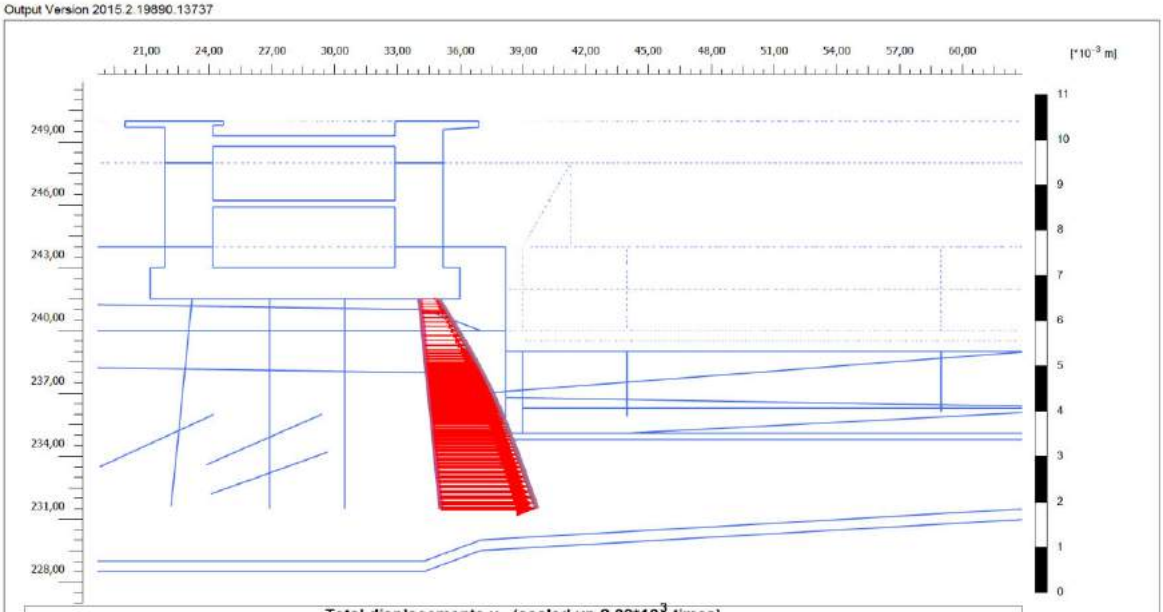

Total displacements u_x (scaled up $2{,}00*10^3$ times)

Maximum value = $2{,}286*10^{-3}$ m (Element 54 at Node 50923)

Minimum value = $0{,}4343*10^{-3}$ m (Element 36 at Node 50847)

PLAXIS	Project description: HSS_Instalation of the Strut 2 (phase 7)		Date: 22.03.2017
	Project filename: Baufeld-15-24.09.2015-KPP ...	Step: 106	User name: Fachhochschule Stuttgart

C:\Users\52shan1mki\Desktop\Calculations_21.03.2017\Baufeld-15-24.09.2015-KPP-2UG-wasser_HSS.P2DXDAT\

Output Version 2015.2.19890.13737

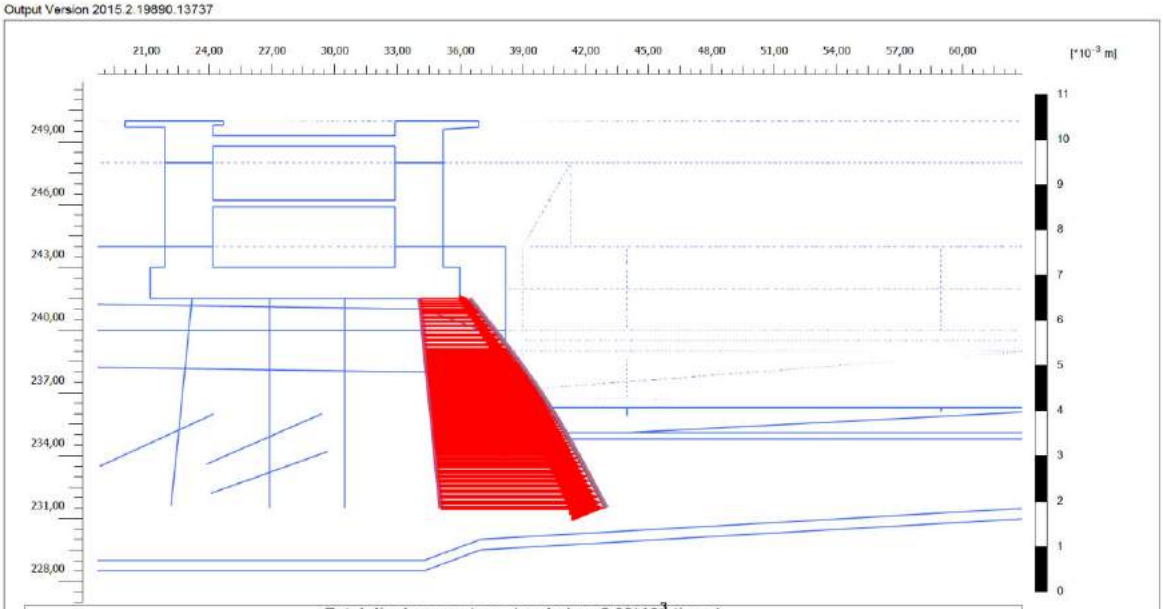

Total displacements u_x (scaled up $2{,}00*10^3$ times)

Maximum value = $3{,}950*10^{-3}$ m (Element 54 at Node 50923)

Minimum value = $1{,}179*10^{-3}$ m (Element 36 at Node 50847)

PLAXIS	Project description: HSS_ Excavation 3 with Water Lowering 2 (phase 8)		Date: 22.03.2017
	Project filename: Baufeld-15-24.09.2015-KPP ...	Step: 116	User name: Fachhochschule Stuttgart

C:\Users\52shan1mki\Desktop\Calculations_21.03.2017\Baufeld-15-24.09.2015-KPP-2UG-wasser_HSS.P2DXDAT\

Output Version 2015.2.19890.13737

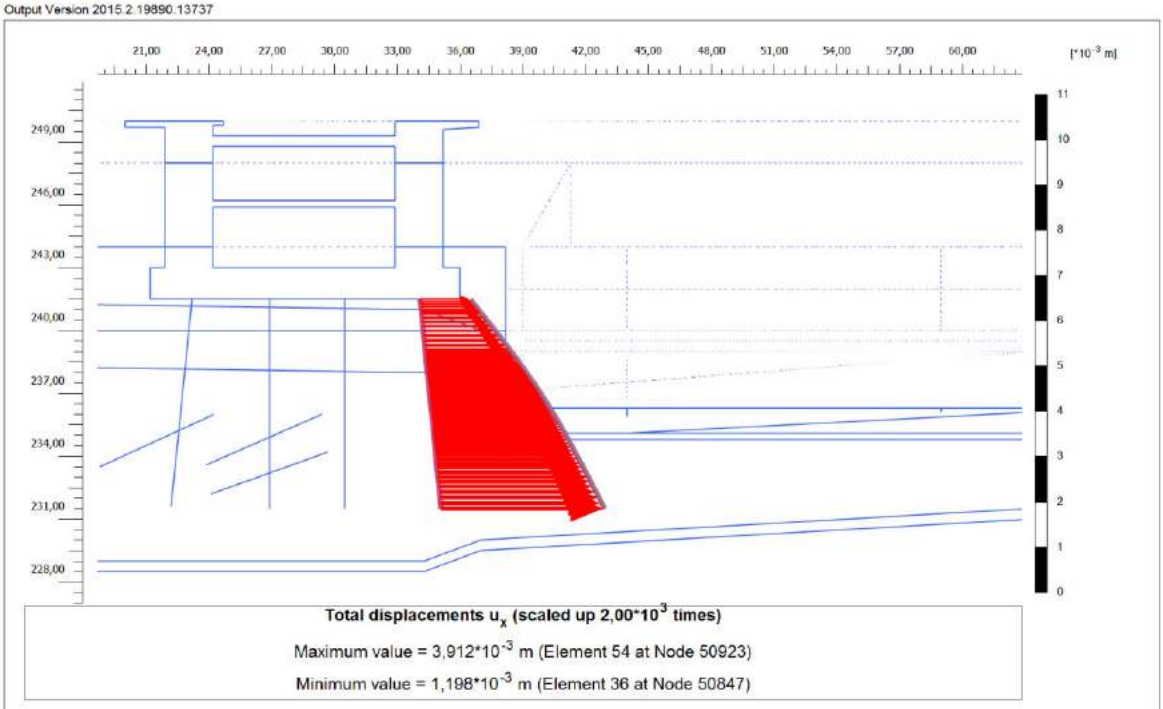

PLAXIS	Project description: HSS_Instalation of the Strut 3 (phase 9)		Date: 22.03.2017
	Project filename: Baufeld-15-24.09.2015-KPP ...	Step: 162	User name: Fachhochschule Stuttgart

C:\Users\52shan1mki\Desktop\Calculations_21.03.2017\Baufeld-15-24.09.2015-KPP-2UG-wasser_HSS.P2DXDAT\

Output Version 2015.2.19890.13737

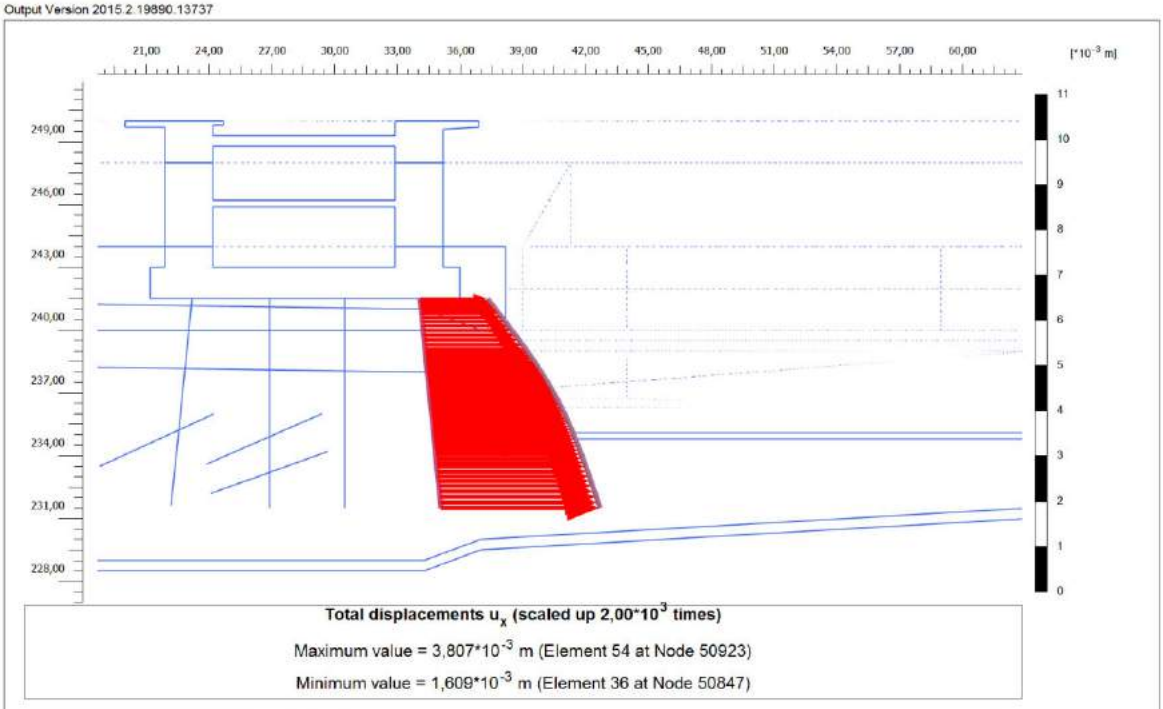

PLAXIS	Project description: HSS_ Last Excavation with Water Lowering 3 (phase 10)		Date: 22.03.2017
	Project filename: Baufeld-15-24.09.2015-KPP ...	Step: 172	User name: Fachhochschule Stuttgart

C:\Users\52shan1mki\Desktop\Calculations_21.03.2017\Baufeld-15-24.09.2015-KPP-2UG-wasser_HSS.P2DXDAT\

Output Version 2015.2.19890.13737

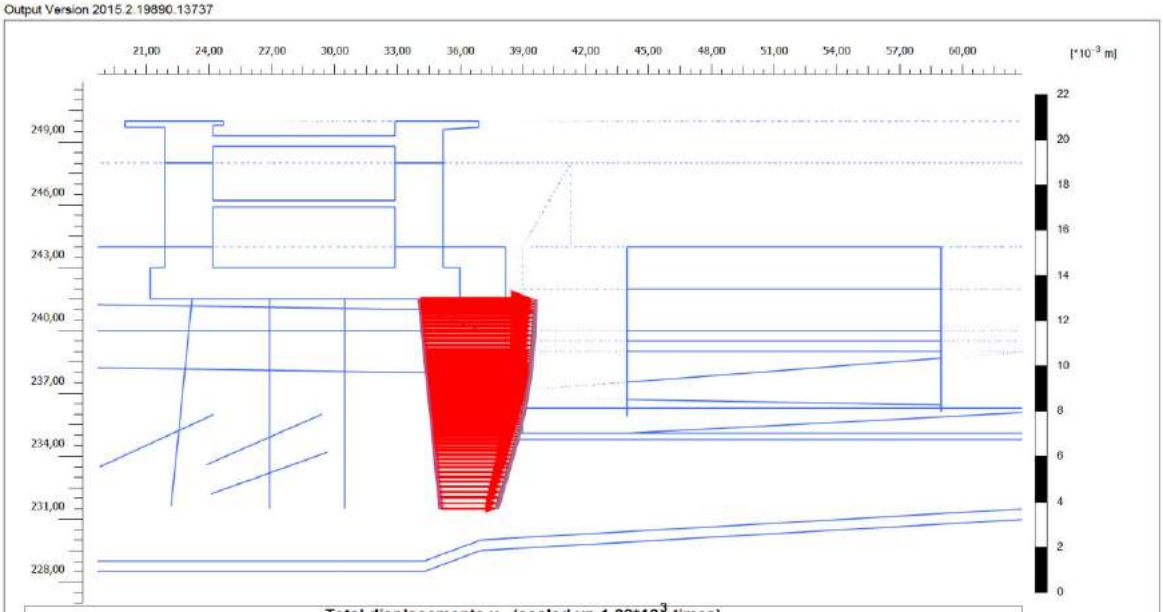

Total displacements u_x (scaled up $1{,}00*10^3$ times)

Maximum value = $5{,}498*10^{-3}$ m (Element 36 at Node 50847)

Minimum value = $2{,}666*10^{-3}$ m (Element 54 at Node 50923)

PLAXIS	Project description: HSS_ Construction of the Hotel (phase 11)		Date: 22.03.2017
	Project filename: Baufeld-15-24.09.2015-KPP ...	Step: 180	User name: Fachhochschule Stuttgart

C:\Users\52shan1mki\Desktop\Calculations_21.03.2017\Baufeld-15-24.09.2015-KPP-2UG-wasser_HSS.P2DXDAT\

Output Version 2015.2.19890.13737

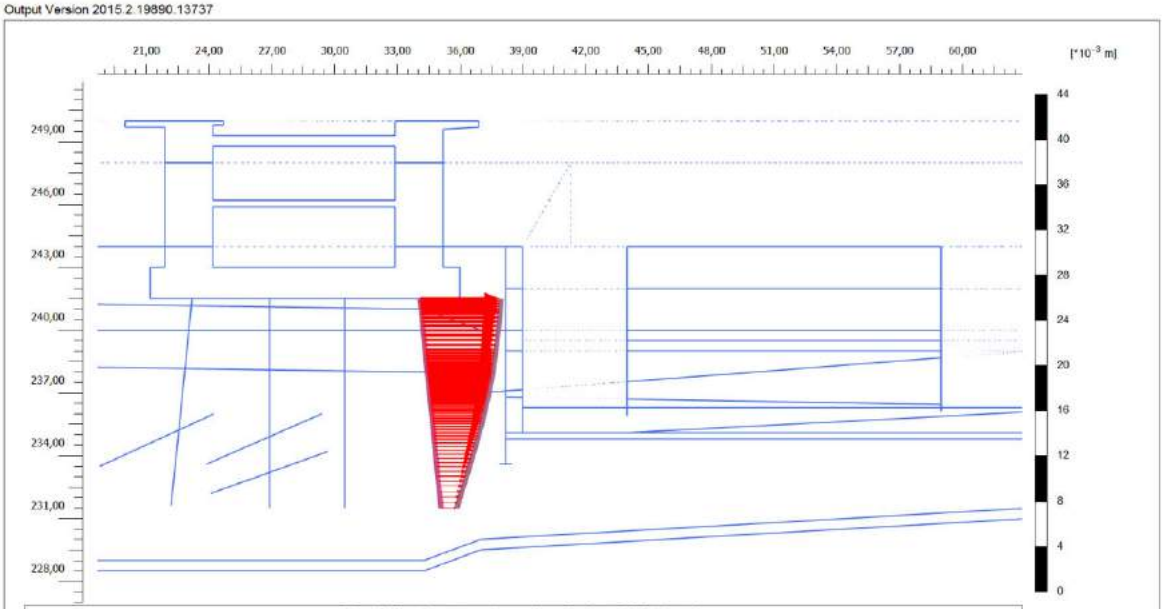

Total displacements u_x (scaled up 500 times)

Maximum value = $7{,}748*10^{-3}$ m (Element 36 at Node 50847)

Minimum value = $1{,}515*10^{-3}$ m (Element 54 at Node 50923)

PLAXIS	Project description: HSS_ Backfilling (phase 12)		Date: 22.03.2017
	Project filename: Baufeld-15-24.09.2015-KPP ...	Step: 186	User name: Fachhochschule Stuttgart

C:\Users\52shan1mki\Desktop\Calculations_21.03.2017\Baufeld-15-24.09.2015-KPP-2UG-wasser_HSS.P2DXDAT\

HSS_Piles_Skin Friction

Output Version 2015.2.19890.13737

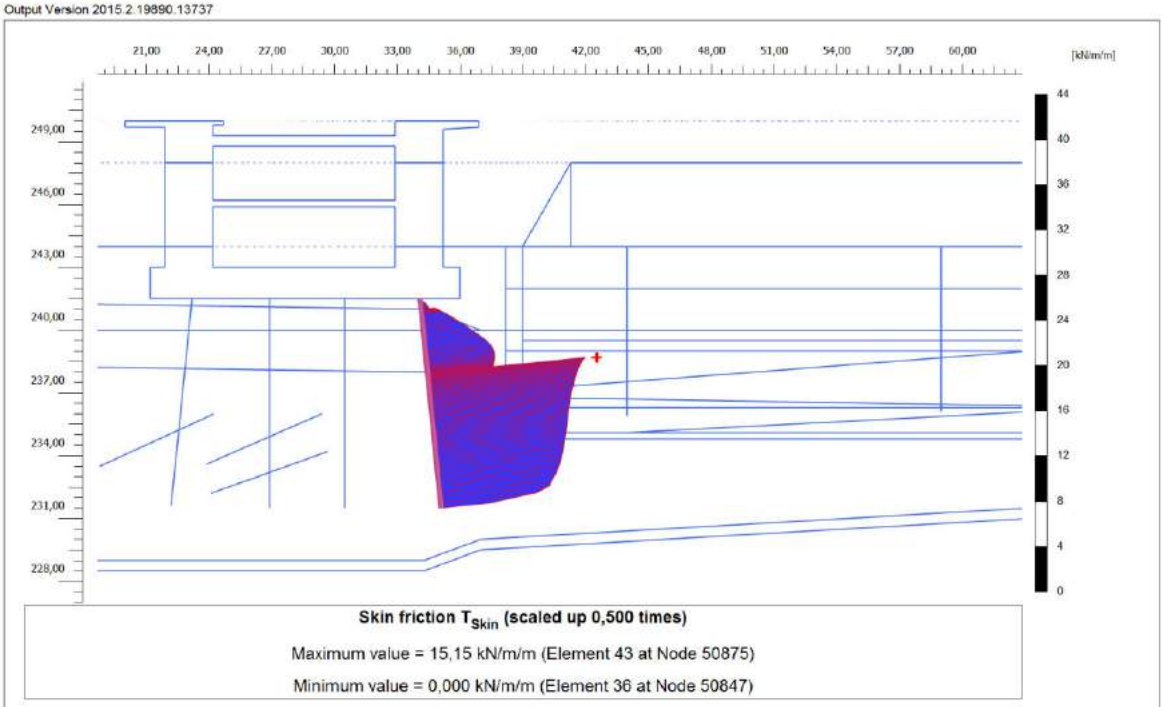

PLAXIS	Project description: HSS_ „Wish in Place“ Bridge (phase 1)		Date: 22.03.2017
	Project filename: Baufeld-15-24.09.2015-KPP ...	Step: 7	User name: Fachhochschule Stuttgart

C:\Users\52shan1mki\Desktop\Calculations_21.03.2017\Baufeld-15-24.09.2015-KPP-2UG-wasser_HSS.P2DXDAT\

Output Version 2015.2.19890.13737

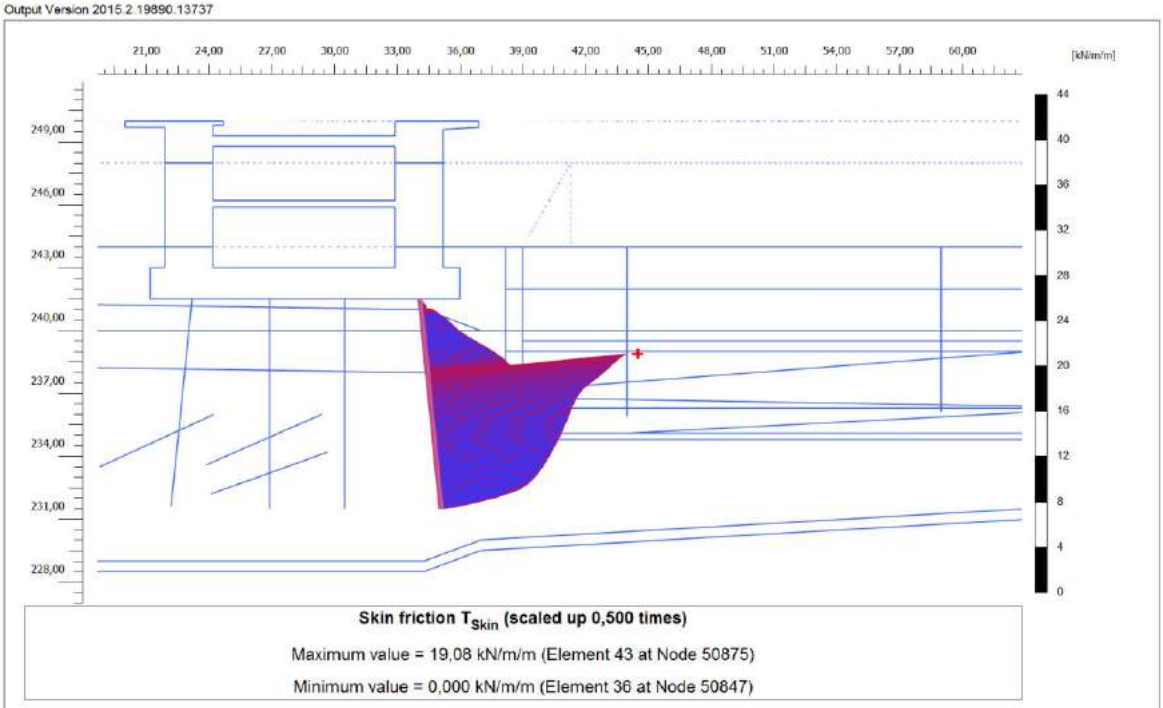

PLAXIS	Project description: HSS_Preliminary Excavation (phase 2)		Date: 22.03.2017
	Project filename: Baufeld-15-24.09.2015-KPP ...	Step: 18	User name: Fachhochschule Stuttgart

C:\Users\52shan1mki\Desktop\Calculations_21.03.2017\Baufeld-15-24.09.2015-KPP-2UG-wasser_HSS.P2DXDAT\

Output Version 2015.2.19890.13737

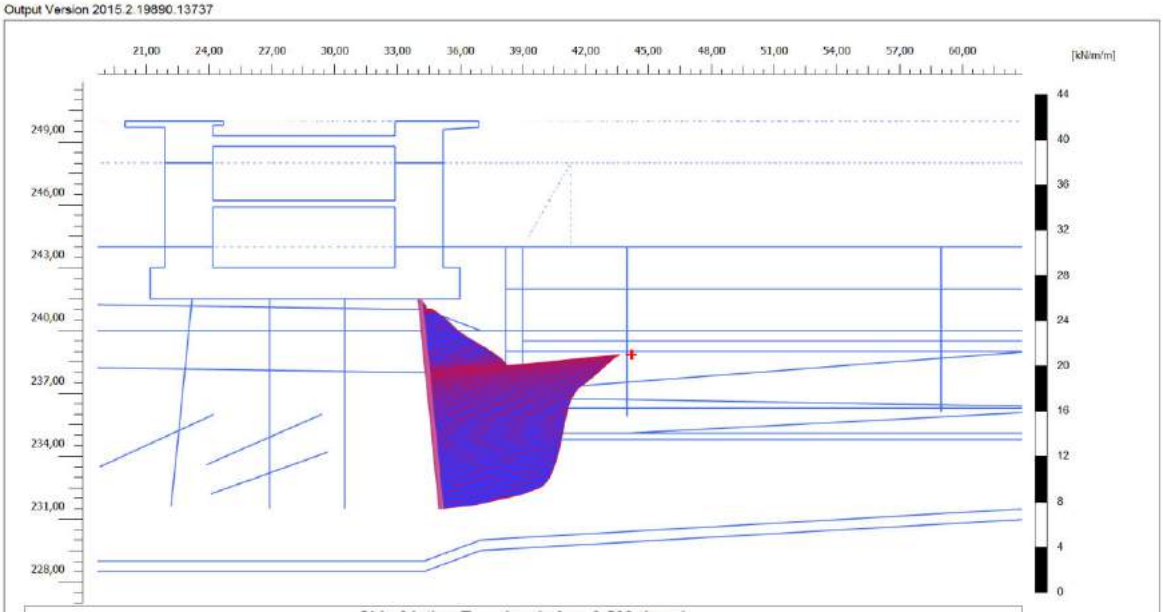

Skin friction T_{Skin} (scaled up 0,500 times)

Maximum value = 18,51 kN/m/m (Element 43 at Node 50875)

Minimum value = 0,000 kN/m/m (Element 36 at Node 50847)

PLAXIS	Project description: HSS_ Installation of the Retaining Walls (phase 3)		Date: 22.03.2017
	Project filename: Baufeld-15-24.09.2015-KPP ...	Step: 24	User name: Fachhochschule Stuttgart

C:\Users\52shan1mki\Desktop\Calculations_21.03.2017\Baufeld-15-24.09.2015-KPP-2UG-wasser_HSS.P2DXDAT\

Output Version 2015.2.19890.13737

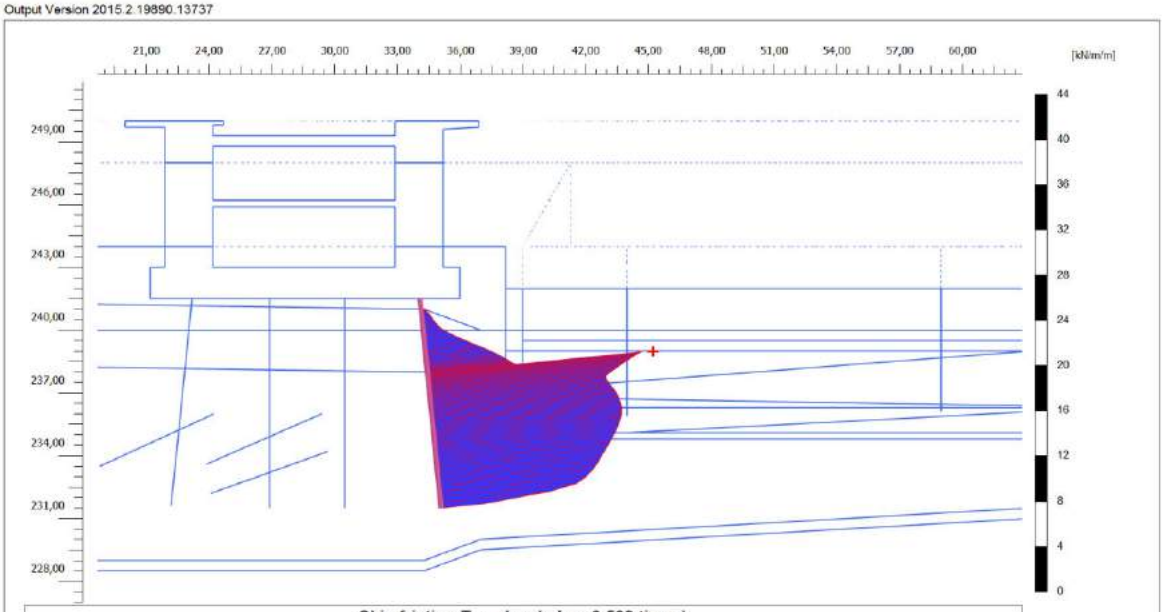

Skin friction T_{Skin} (scaled up 0,500 times)

Maximum value = 20,54 kN/m/m (Element 43 at Node 50875)

Minimum value = 0,000 kN/m/m (Element 36 at Node 50847)

PLAXIS	Project description: HSS_ Excavation 1 (phase 4)		Date: 22.03.2017
	Project filename: Baufeld-15-24.09.2015-KPP ...	Step: 34	User name: Fachhochschule Stuttgart

C:\Users\52shan1mki\Desktop\Calculations_21.03.2017\Baufeld-15-24.09.2015-KPP-2UG-wasser_HSS.P2DXDAT\

Output Version 2015.2.19890.13737

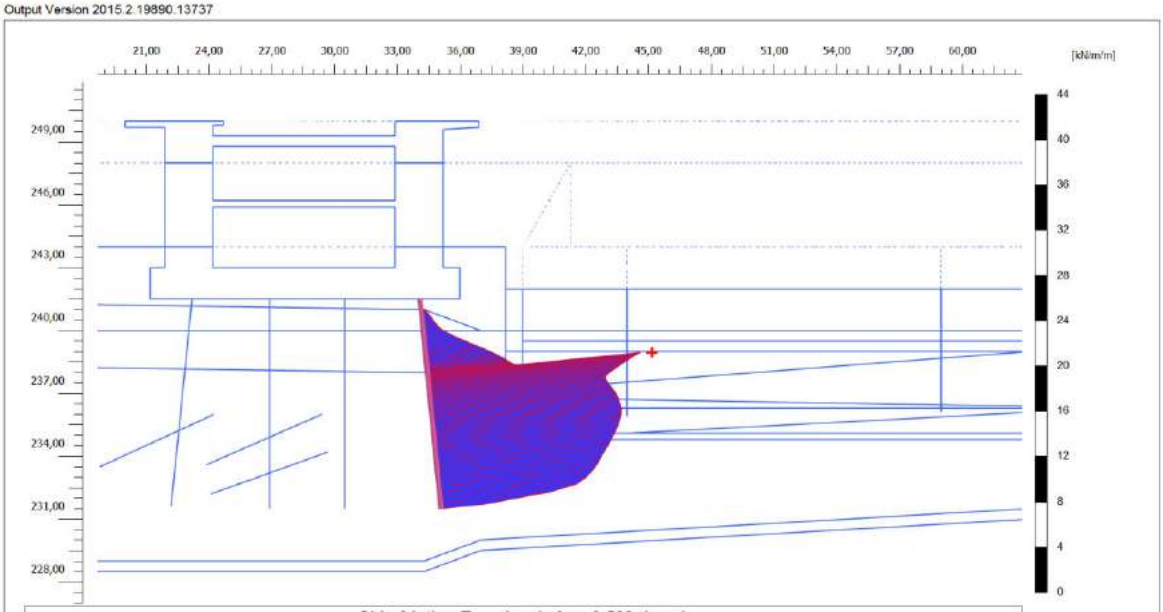

Skin friction T_{Skin} (scaled up 0,500 times)

Maximum value = 20,47 kN/m/m (Element 43 at Node 50875)

Minimum value = 0,000 kN/m/m (Element 36 at Node 50847)

PLAXIS	Project description: HSS_Instalation of the Strut 1 (phase 5)		Date: 22.03.2017
	Project filename: Baufeld-15-24.09.2015-KPP ...	Step: 42	User name: Fachhochschule Stuttgart

C:\Users\52shan1mki\Desktop\Calculations_21.03.2017\Baufeld-15-24.09.2015-KPP-2UG-wasser_HSS.P2DX\DAT\

Output Version 2015.2.19890.13737

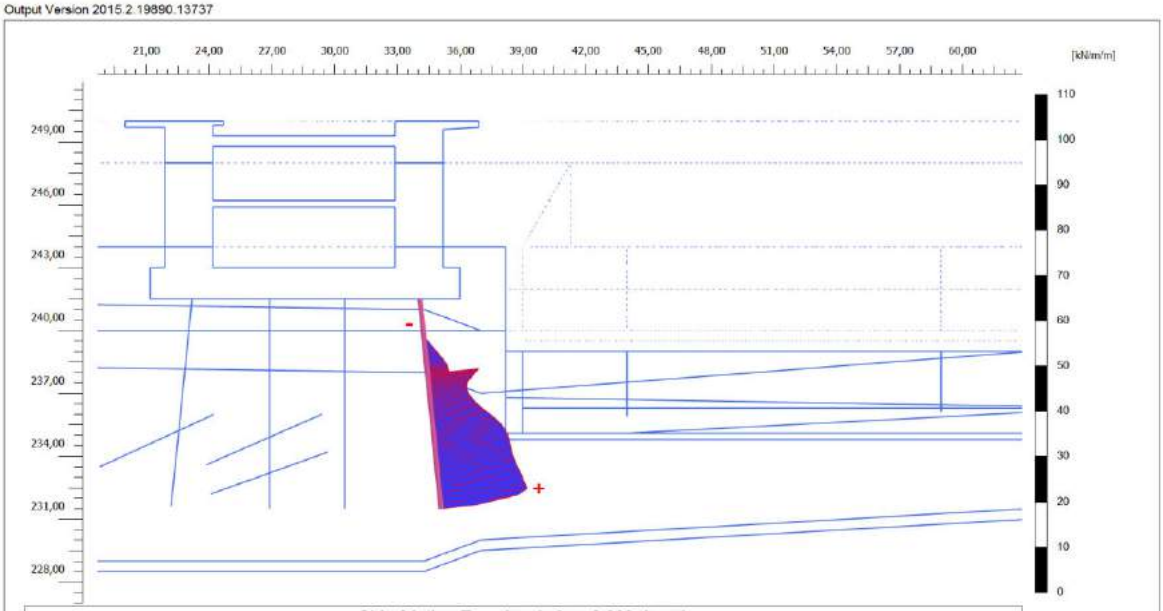

Skin friction T_{Skin} (scaled up 0,200 times)

Maximum value = 20,97 kN/m/m (Element 54 at Node 50921)

Minimum value = -0,4782 kN/m/m (Element 38 at Node 50857)

PLAXIS	Project description: HSS_ Excavation 2 with Water Lowering 1 (phase 6)		Date: 22.03.2017
	Project filename: Baufeld-15-24.09.2015-KPP ...	Step: 53	User name: Fachhochschule Stuttgart

C:\Users\52shan1mki\Desktop\Calculations_21.03.2017\Baufeld-15-24.09.2015-KPP-2UG-wasser_HSS.P2DX\DAT\

Output Version 2015.2.19890.13737

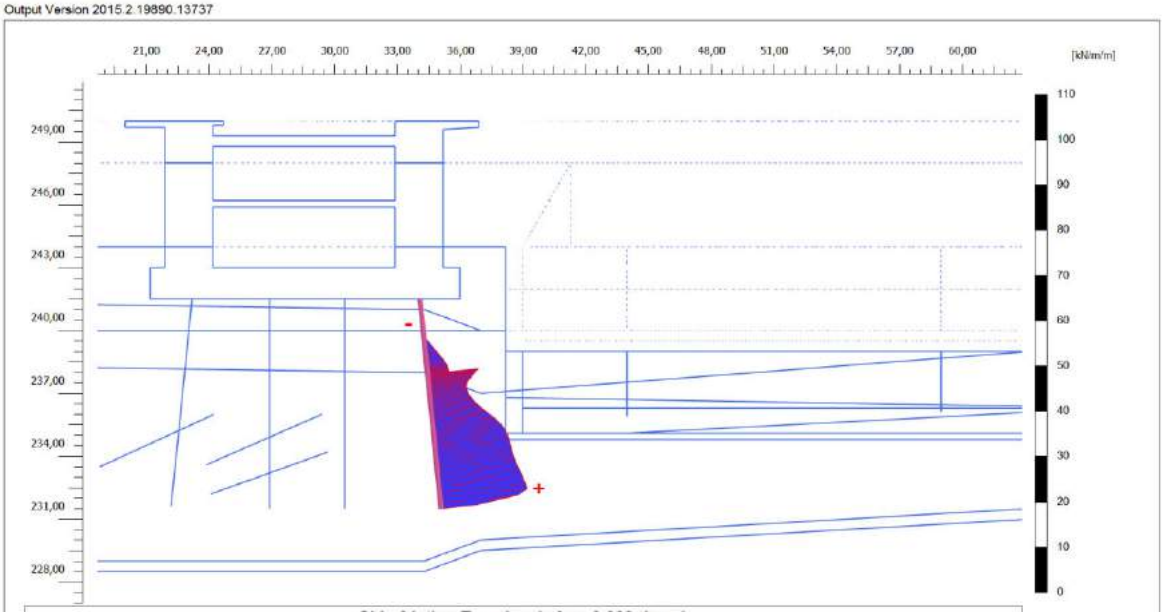

Skin friction T_{Skin} (scaled up 0,200 times)

Maximum value = 20,97 kN/m/m (Element 54 at Node 50921)

Minimum value = -0,4892 kN/m/m (Element 38 at Node 50857)

PLAXIS	Project description		Date
	HSS_Instalation of the Strut 2 (phase 7)		22.03.2017
	Project filename	Step	User name
	Baufeld-15-24.09.2015-KPP ...	106	Fachhochschule Stuttgart

C:\Users\52shan1mki\Desktop\Calculations_21.03.2017\Baufeld-15-24.09.2015-KPP-2UG-wasser_HSS.P2DXDAT\

Output Version 2015.2.19890.13737

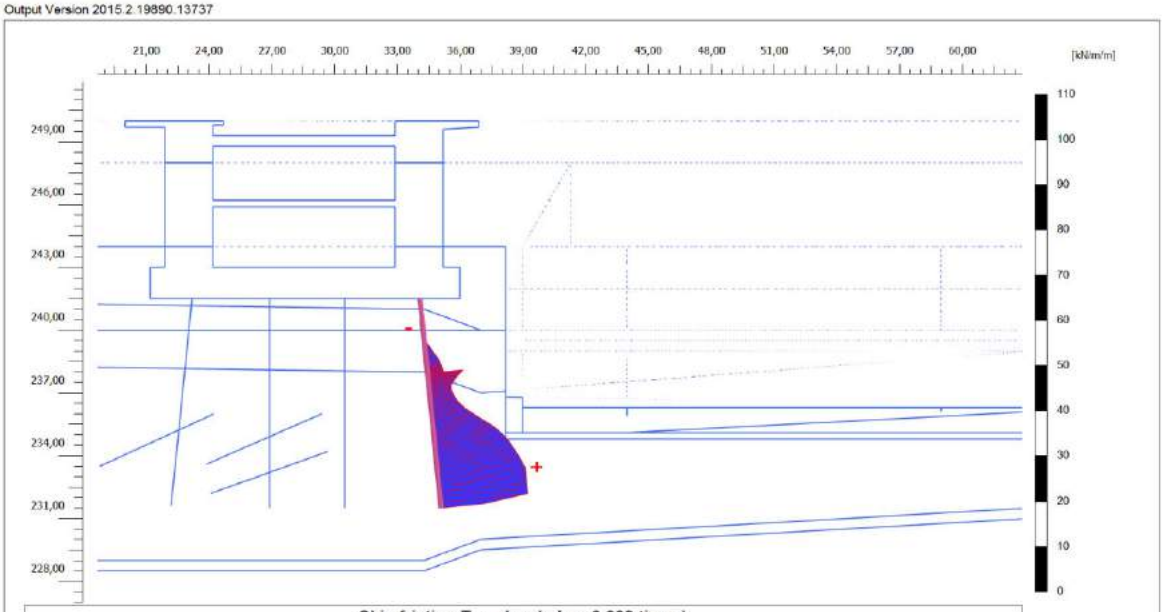

Skin friction T_{Skin} (scaled up 0,200 times)

Maximum value = 20,97 kN/m/m (Element 53 at Node 50917)

Minimum value = -0,6384 kN/m/m (Element 38 at Node 50858)

PLAXIS	Project description		Date
	HSS_ Excavation 3 with Water Lowering 2 (phase 8)		22.03.2017
	Project filename	Step	User name
	Baufeld-15-24.09.2015-KPP ...	116	Fachhochschule Stuttgart

C:\Users\52shan1mki\Desktop\Calculations_21.03.2017\Baufeld-15-24.09.2015-KPP-2UG-wasser_HSS.P2DXDAT\

Output Version 2015.2.19890.13737

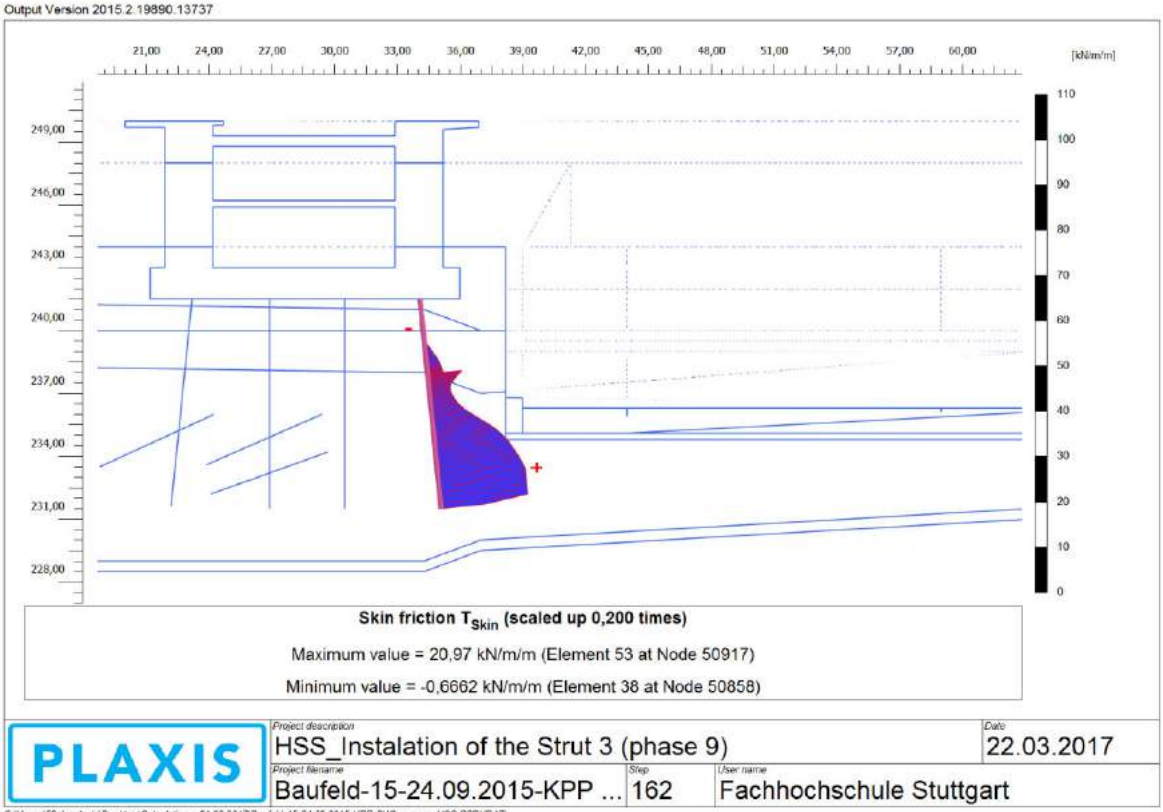

PLAXIS	Project description: HSS_Instalation of the Strut 3 (phase 9)		Date: 22.03.2017
	Project filename: Baufeld-15-24.09.2015-KPP ...	Step: 162	User name: Fachhochschule Stuttgart

C:\Users\52shan1mki\Desktop\Calculations_21.03.2017\Baufeld-15-24.09.2015-KPP-2UG-wasser_HSS.P2DXDAT\

Output Version 2015.2.19890.13737

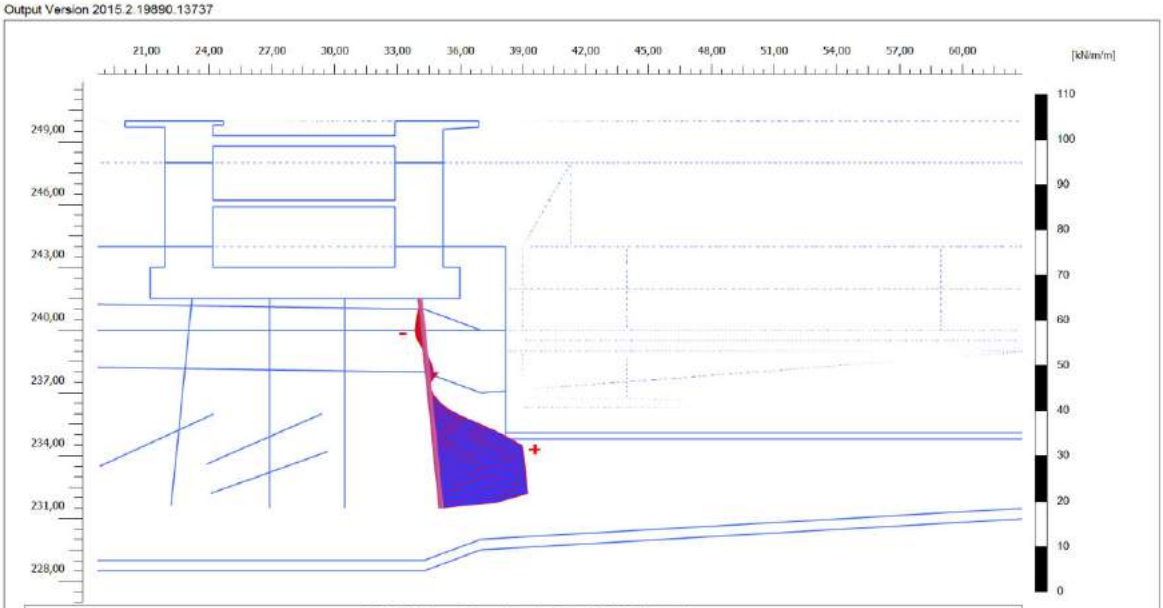

PLAXIS	Project description: HSS_ Last Excavation with Water Lowering 3 (phase 10)		Date: 22.03.2017
	Project filename: Baufeld-15-24.09.2015-KPP ...	Step: 172	User name: Fachhochschule Stuttgart

C:\Users\52shan1mki\Desktop\Calculations_21.03.2017\Baufeld-15-24.09.2015-KPP-2UG-wasser_HSS.P2DXDAT\

Output Version 2015.2.19890.13737

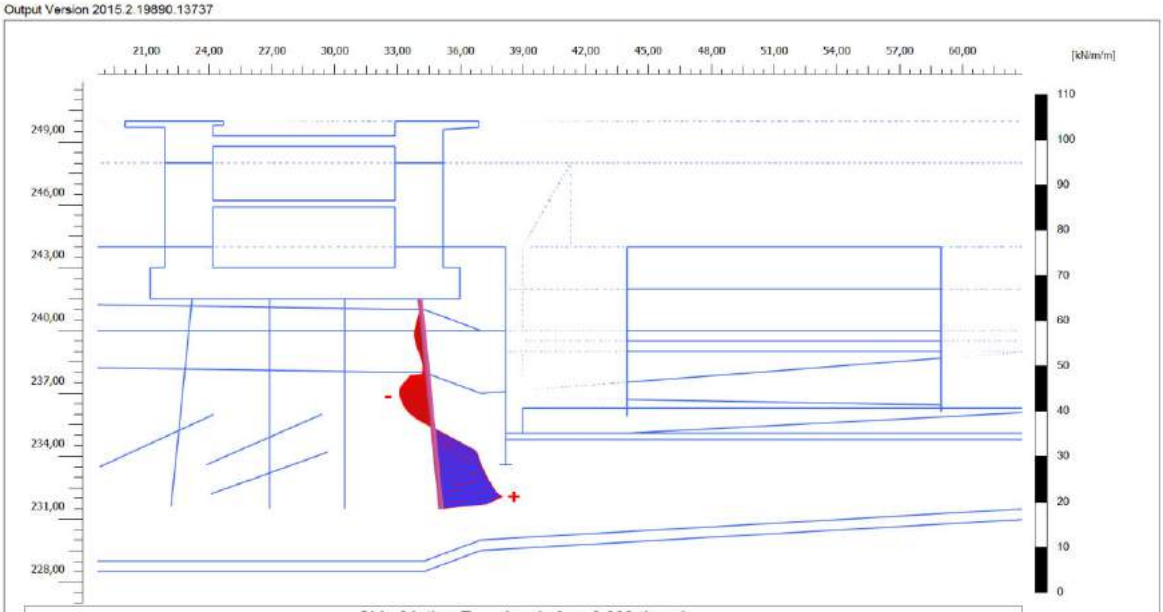

Skin friction T_{Skin} (scaled up 0,200 times)

Maximum value = 14,85 kN/m/m (Element 54 at Node 50922)

Minimum value = -7,048 kN/m/m (Element 46 at Node 50888)

PLAXIS	Project description: HSS_ Construction of the Hotel (phase 11)		Date: 22.03.2017
	Project filename: Baufeld-15-24.09.2015-KPP ...	Step: 180	User name: Fachhochschule Stuttgart

C:\Users\52shan1mki\Desktop\Calculations_21.03.2017\Baufeld-15-24.09.2015-KPP-2UG-wasser_HSS.P2DXDAT\

Output Version 2015.2.19890.13737

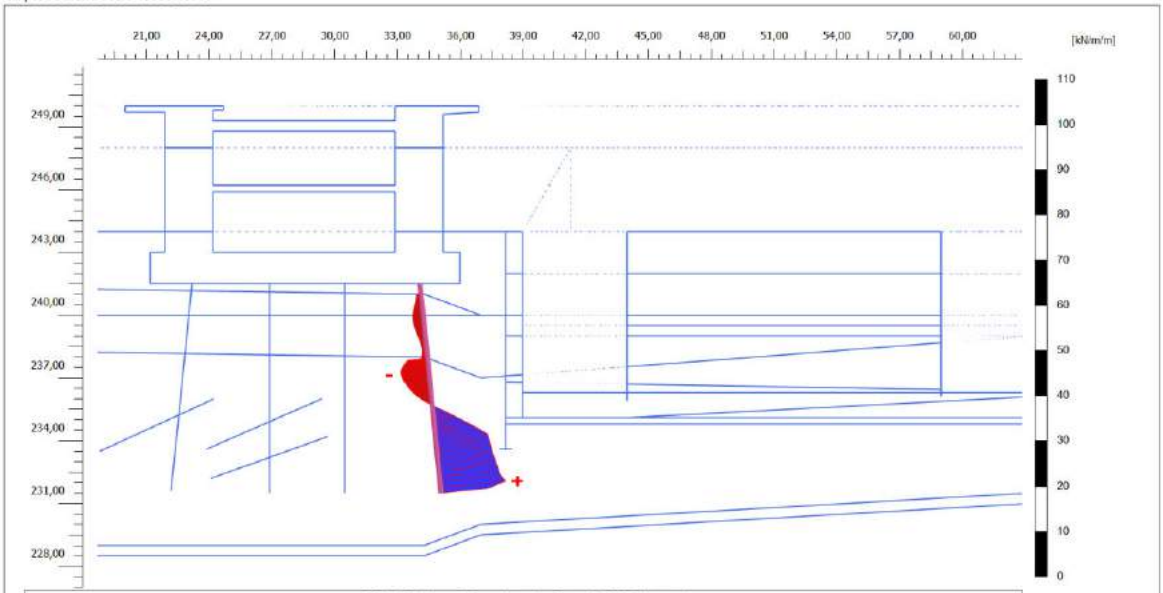

Skin friction T_{Skin} (scaled up 0,200 times)

Maximum value = 15,69 kN/m/m (Element 54 at Node 50922)

Minimum value = -6,670 kN/m/m (Element 45 at Node 50885)

PLAXIS	Project description: HSS_ Backfilling (phase 12)		Date: 22.03.2017
	Project filename: Baufeld-15-24.09.2015-KPP ...	Step: 186	User name: Fachhochschule Stuttgart

C:\Users\52shan1mki\Desktop\Calculations_21.03.2017\Baufeld-15-24.09.2015-KPP-2UG-wasser_HSS.P2DXDAT\

HHS_Wall_Horizontal Displacement, u_x

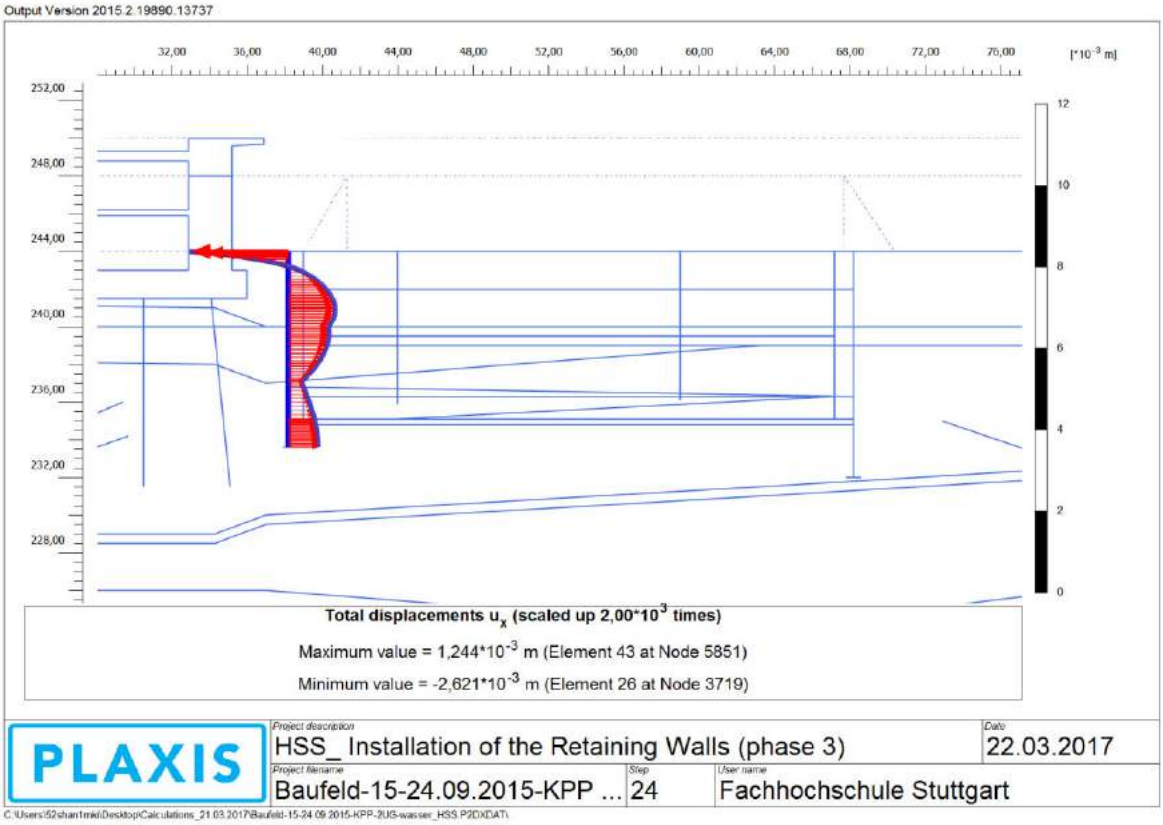

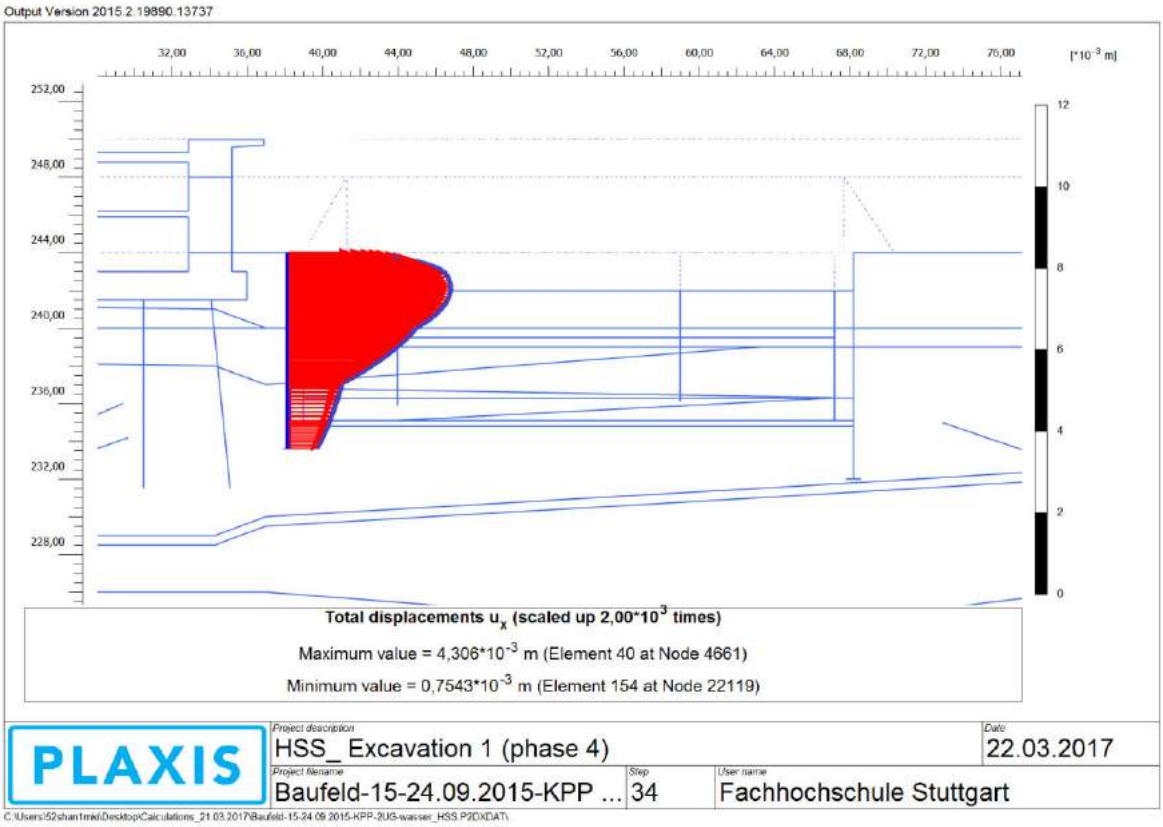

Output Version 2015.2.19890.13737

Total displacements u_x (scaled up $2{,}00*10^3$ times)

Maximum value = $4{,}309*10^{-3}$ m (Element 40 at Node 4661)

Minimum value = $0{,}7832*10^{-3}$ m (Element 154 at Node 22119)

PLAXIS	Project description: HSS_Instalation of the Strut 1 (phase 5)		Date: 22.03.2017
	Project filename: Baufeld-15-24.09.2015-KPP ...	Step: 42	User name: Fachhochschule Stuttgart

C:\Users\52shan1mki\Desktop\Calculations_21.03.2017\Baufeld-15-24.09.2015-KPP-2UG-wasser_HSS.P2DXDAT\

Output Version 2015.2.19890.13737

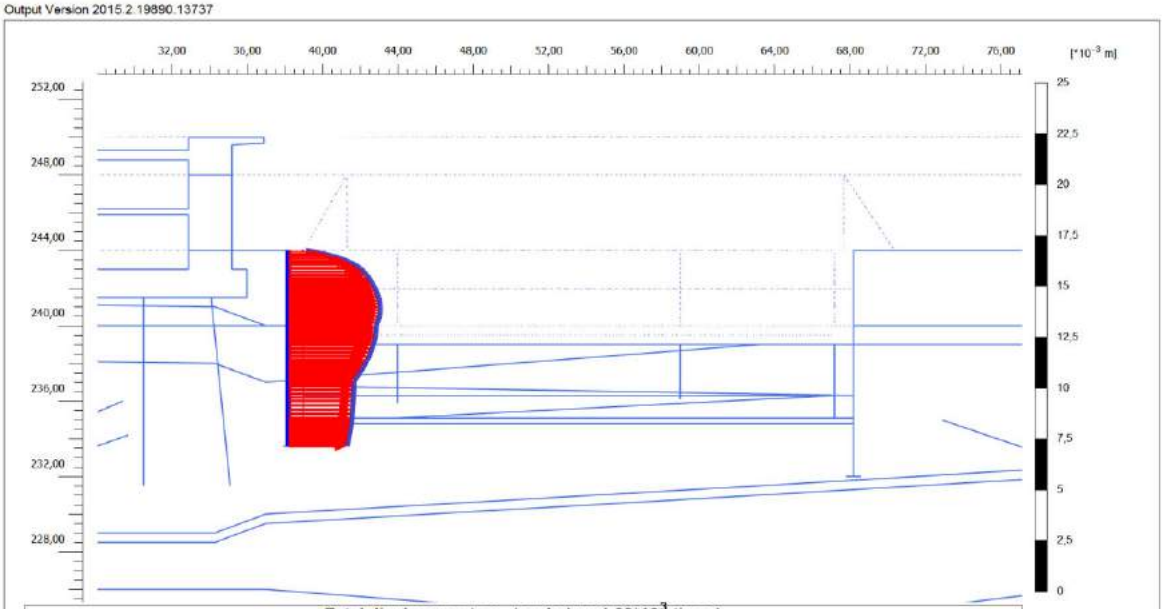

Total displacements u_x (scaled up $1{,}00*10^3$ times)

Maximum value = $4{,}862*10^{-3}$ m (Element 43 at Node 5852)

Minimum value = $0{,}9162*10^{-3}$ m (Element 26 at Node 3719)

PLAXIS	Project description: HSS_ Excavation 2 with Water Lowering 1 (phase 6)		Date: 22.03.2017
	Project filename: Baufeld-15-24.09.2015-KPP ...	Step: 53	User name: Fachhochschule Stuttgart

C:\Users\52shan1mki\Desktop\Calculations_21.03.2017\Baufeld-15-24.09.2015-KPP-2UG-wasser_HSS.P2DXDAT\

Output Version 2015.2.19890.13737

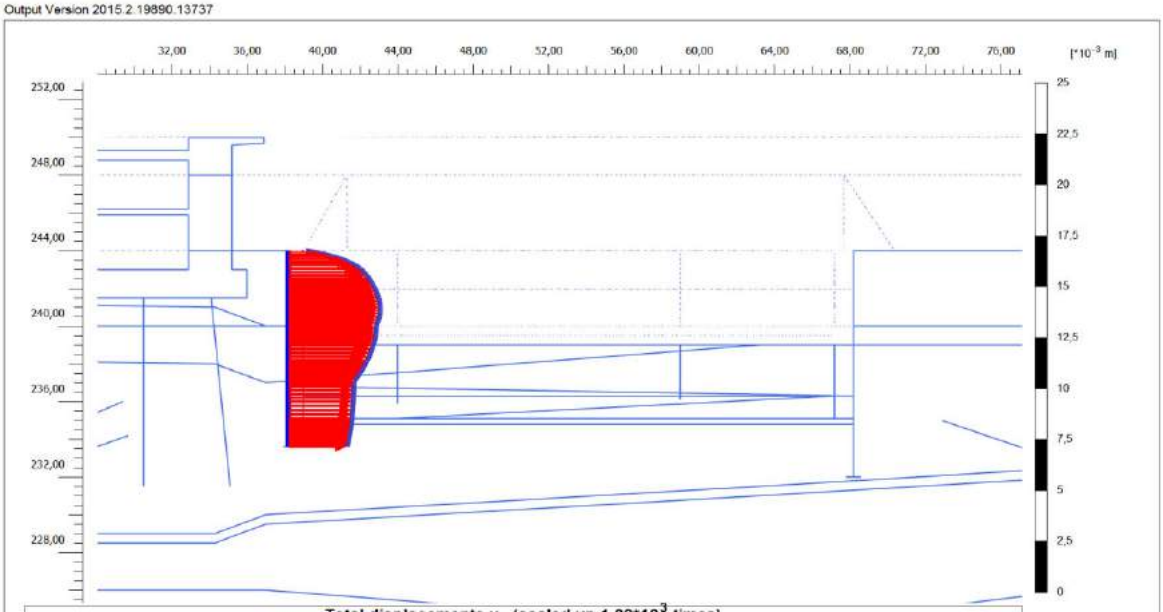

Total displacements u_x (scaled up $1{,}00*10^3$ times)

Maximum value = $4{,}862*10^{-3}$ m (Element 43 at Node 5852)

Minimum value = $0{,}9163*10^{-3}$ m (Element 26 at Node 3719)

PLAXIS	Project description: HSS_Instalation of the Strut 2 (phase 7)		Date: 22.03.2017
	Project filename: Baufeld-15-24.09.2015-KPP ...	Step: 106	User name: Fachhochschule Stuttgart

C:\Users\52shan1mki\Desktop\Calculations_21.03.2017\Baufeld-15-24.09.2015-KPP-2UG-wasser_HSS.P2DXDAT\

Output Version 2015.2.19890.13737

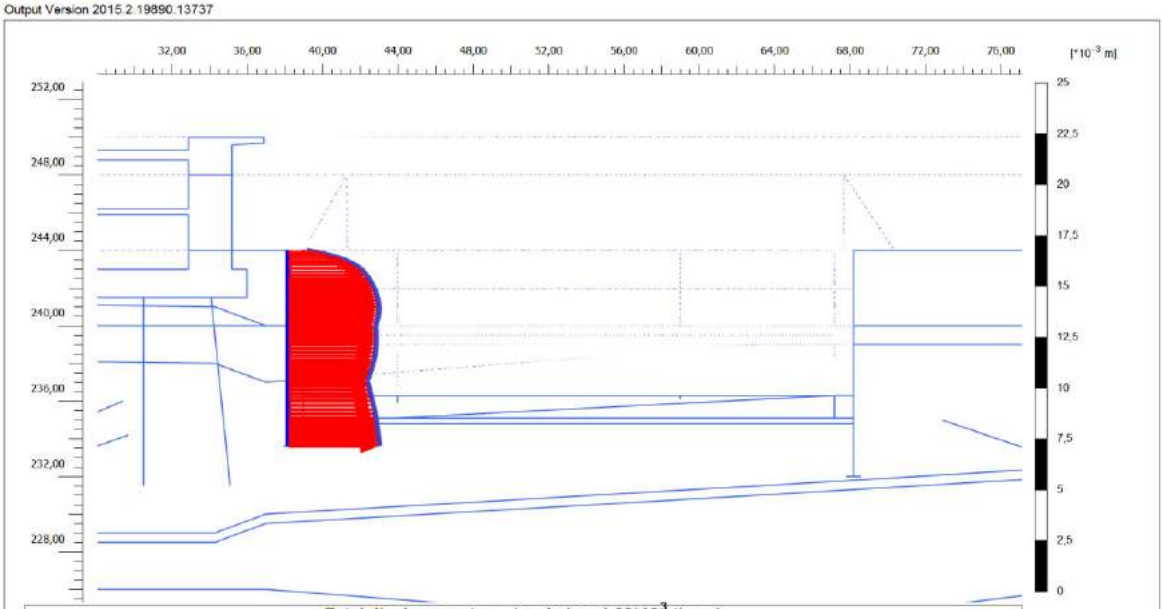

Total displacements u_x (scaled up $1{,}00*10^3$ times)

Maximum value = $4{,}827*10^{-3}$ m (Element 154 at Node 22119)

Minimum value = $0{,}9531*10^{-3}$ m (Element 26 at Node 3719)

PLAXIS	Project description: HSS_ Excavation 3 with Water Lowering 2 (phase 8)		Date: 22.03.2017
	Project filename: Baufeld-15-24.09.2015-KPP ...	Step: 116	User name: Fachhochschule Stuttgart

C:\Users\52shan1mki\Desktop\Calculations_21.03.2017\Baufeld-15-24.09.2015-KPP-2UG-wasser_HSS.P2DXDAT\

Output Version 2015.2.19890.13737

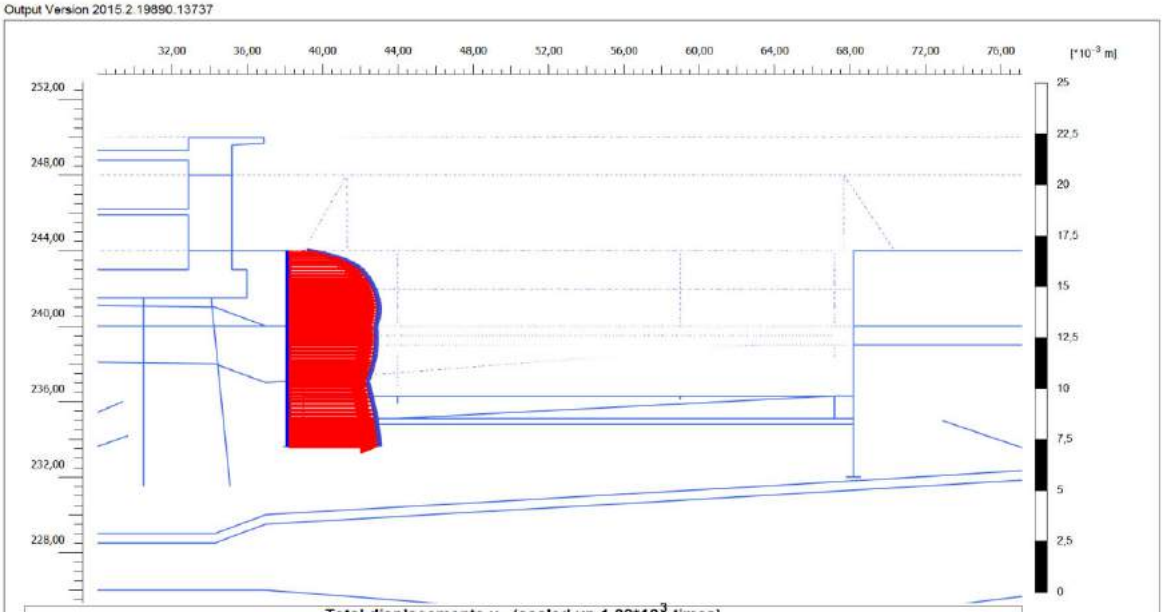

Total displacements u_x (scaled up 1,00*10^3 times)

Maximum value = 4,829*10^{-3} m (Element 154 at Node 22119)

Minimum value = 0,9532*10^{-3} m (Element 26 at Node 3719)

PLAXIS	Project description: HSS_Instalation of the Strut 3 (phase 9)		Date: 22.03.2017
	Project filename: Baufeld-15-24.09.2015-KPP ...	Step: 162	User name: Fachhochschule Stuttgart

C:\Users\52shan1mki\Desktop\Calculations_21.03.2017\Baufeld-15-24.09.2015-KPP-2UG-wasser_HSS.P2DXDAT\

Output Version 2015.2.19890.13737

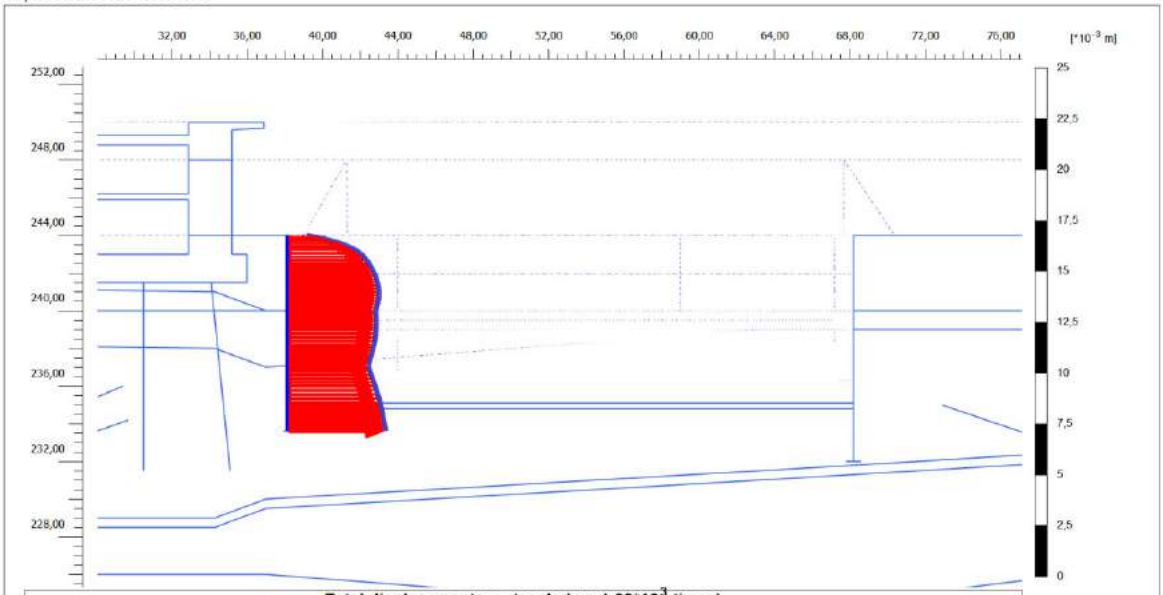

Total displacements u_x (scaled up 1,00*10^3 times)

Maximum value = 5,166*10^{-3} m (Element 154 at Node 22119)

Minimum value = 0,9595*10^{-3} m (Element 26 at Node 3719)

PLAXIS	Project description: HSS_ Last Excavation with Water Lowering 3 (phase 10)		Date: 22.03.2017
	Project filename: Baufeld-15-24.09.2015-KPP ...	Step: 172	User name: Fachhochschule Stuttgart

C:\Users\52shan1mki\Desktop\Calculations_21.03.2017\Baufeld-15-24.09.2015-KPP-2UG-wasser_HSS.P2DXDAT\

Output Version 2015.2.19890.13737

Total displacements u_x (scaled up $1{,}00*10^3$ times)

Maximum value = $5{,}145*10^{-3}$ m (Element 154 at Node 22119)

Minimum value = $0{,}9725*10^{-3}$ m (Element 26 at Node 3719)

PLAXIS	Project description: HSS_ Construction of the Hotel (phase 11)		Date: 22.03.2017
	Project filename: Baufeld-15-24.09.2015-KPP ...	Step: 180	User name: Fachhochschule Stuttgart

C:\Users\52shan1mki\Desktop\Calculations_21.03.2017\Baufeld-15-24.09.2015-KPP-2UG-wasser_HSS.P2DXDAT\

Output Version 2015.2.19890.13737

Total displacements u_x (scaled up 500 times)

Maximum value = 0,01090 m (Element 42 at Node 4768)

Minimum value = $5{,}368*10^{-3}$ m (Element 154 at Node 22119)

PLAXIS	Project description: HSS_ Backfilling (phase 12)		Date: 22.03.2017
	Project filename: Baufeld-15-24.09.2015-KPP ...	Step: 186	User name: Fachhochschule Stuttgart

C:\Users\52shan1mki\Desktop\Calculations_21.03.2017\Baufeld-15-24.09.2015-KPP-2UG-wasser_HSS.P2DXDAT\

HSS_Hotel_Vertical displacement, u_y

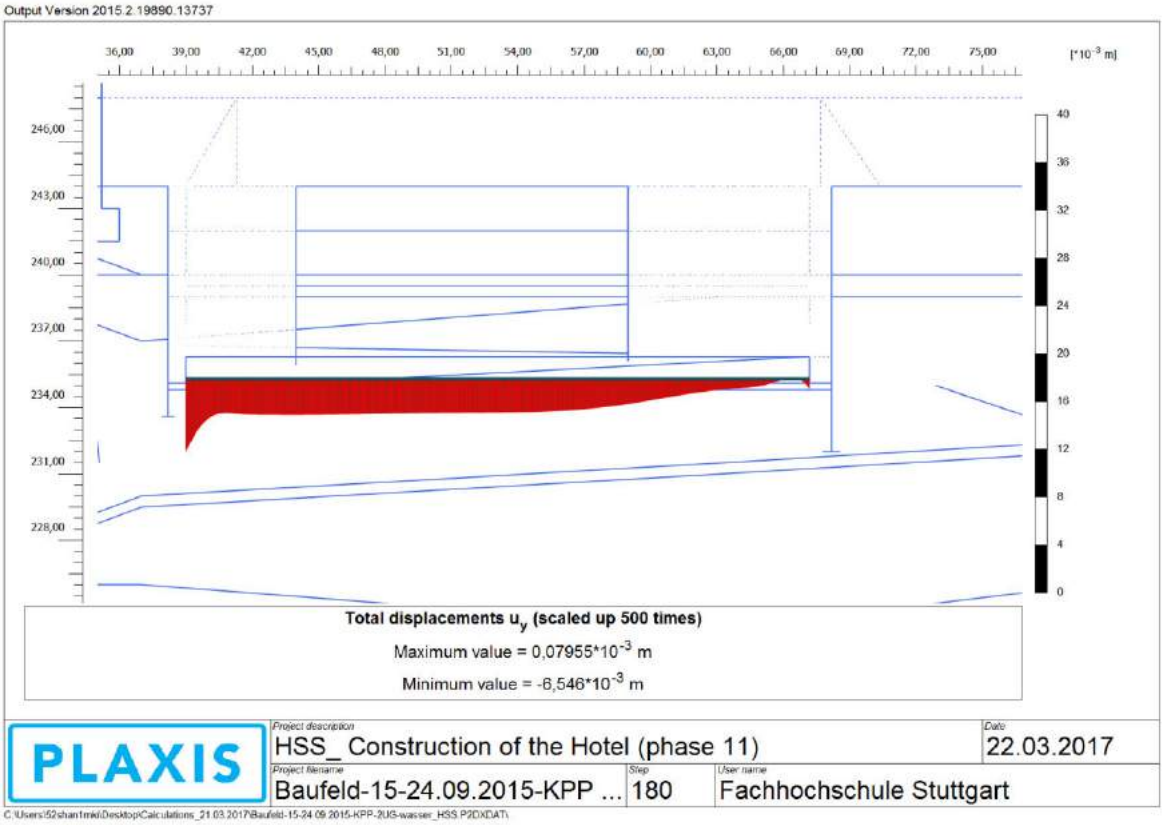

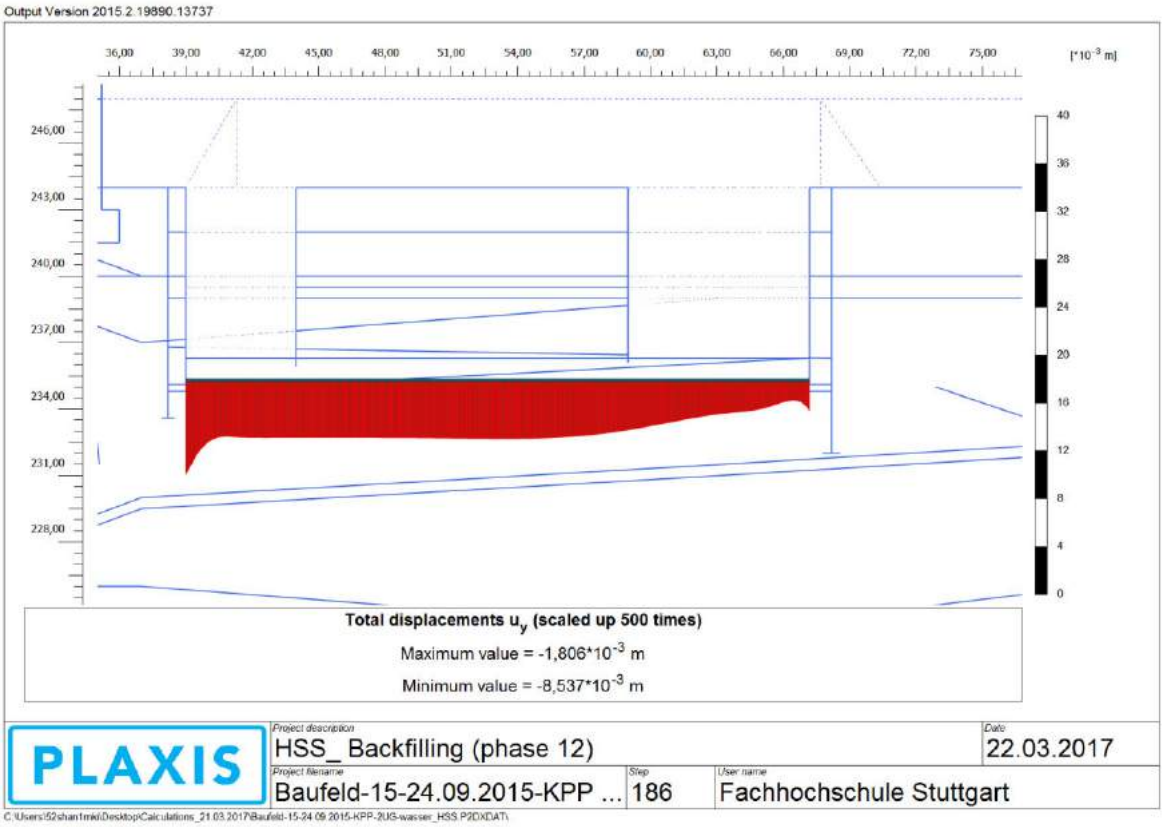

HSS_Hotel_Stresses

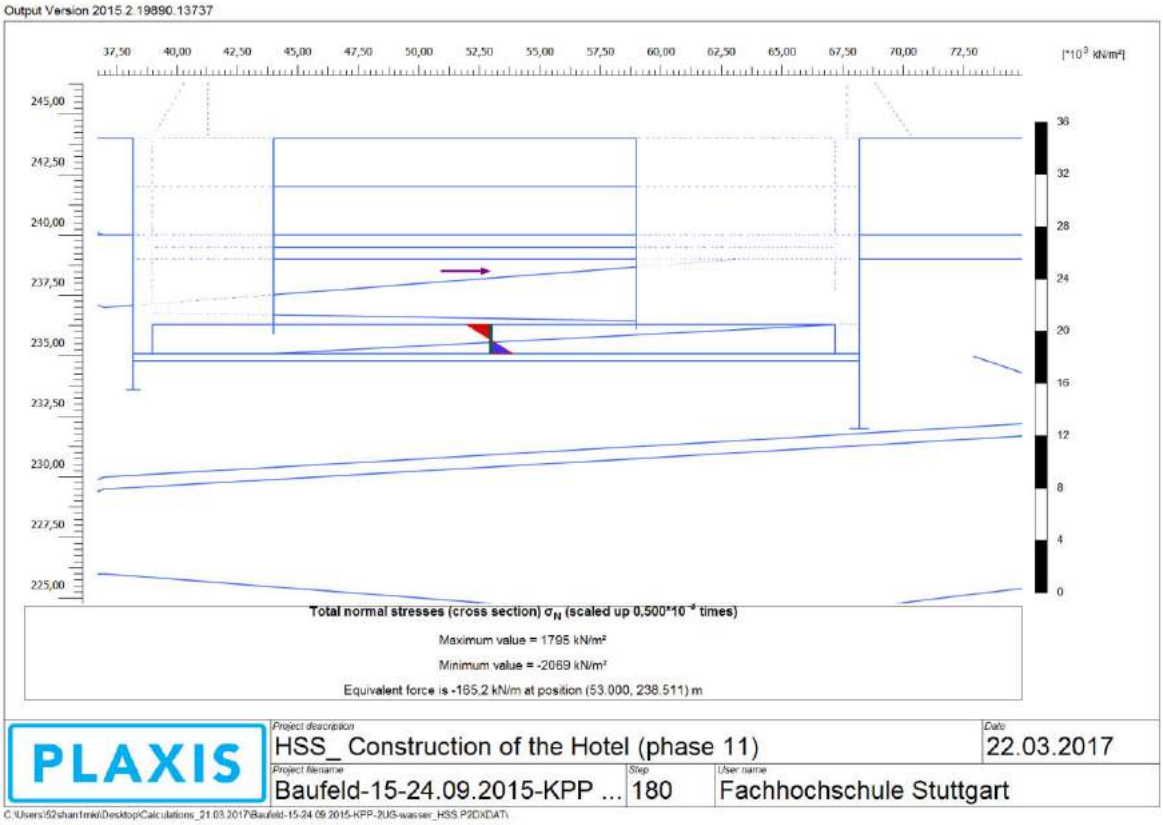

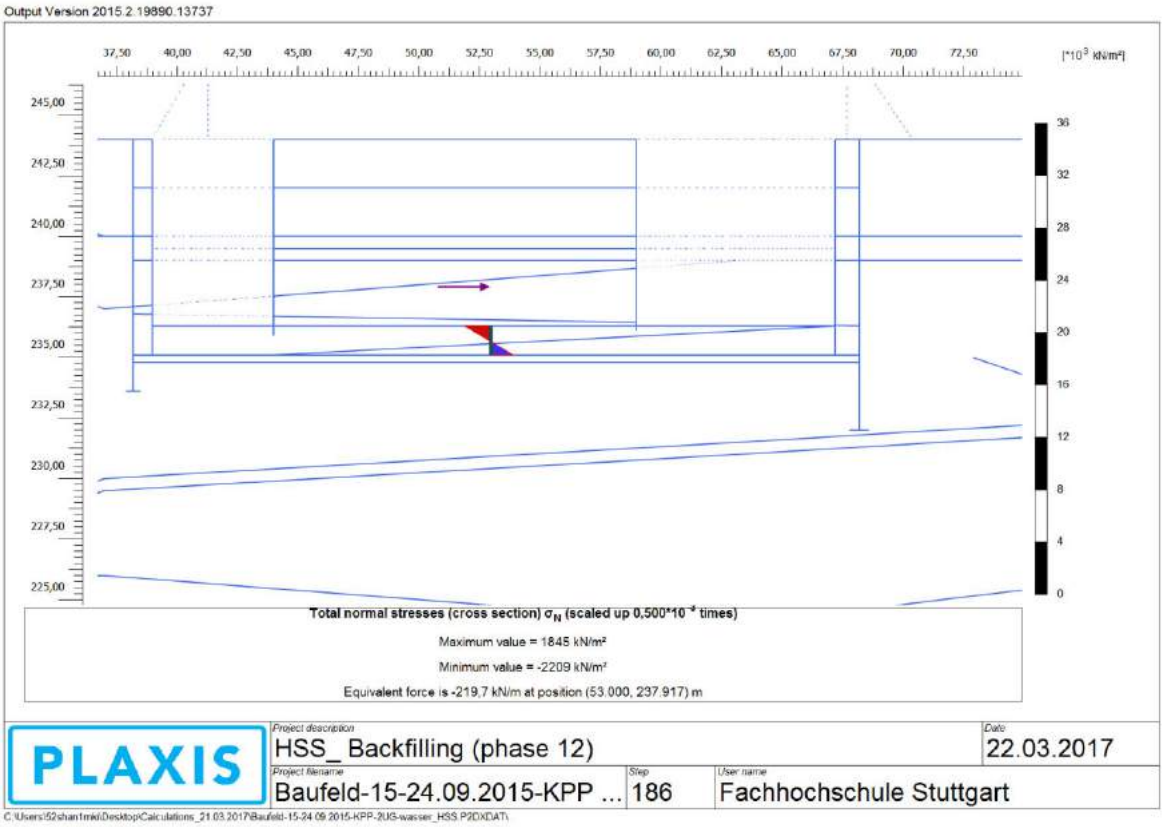

HSS_Hotel_Horizontal Displacement, u_x

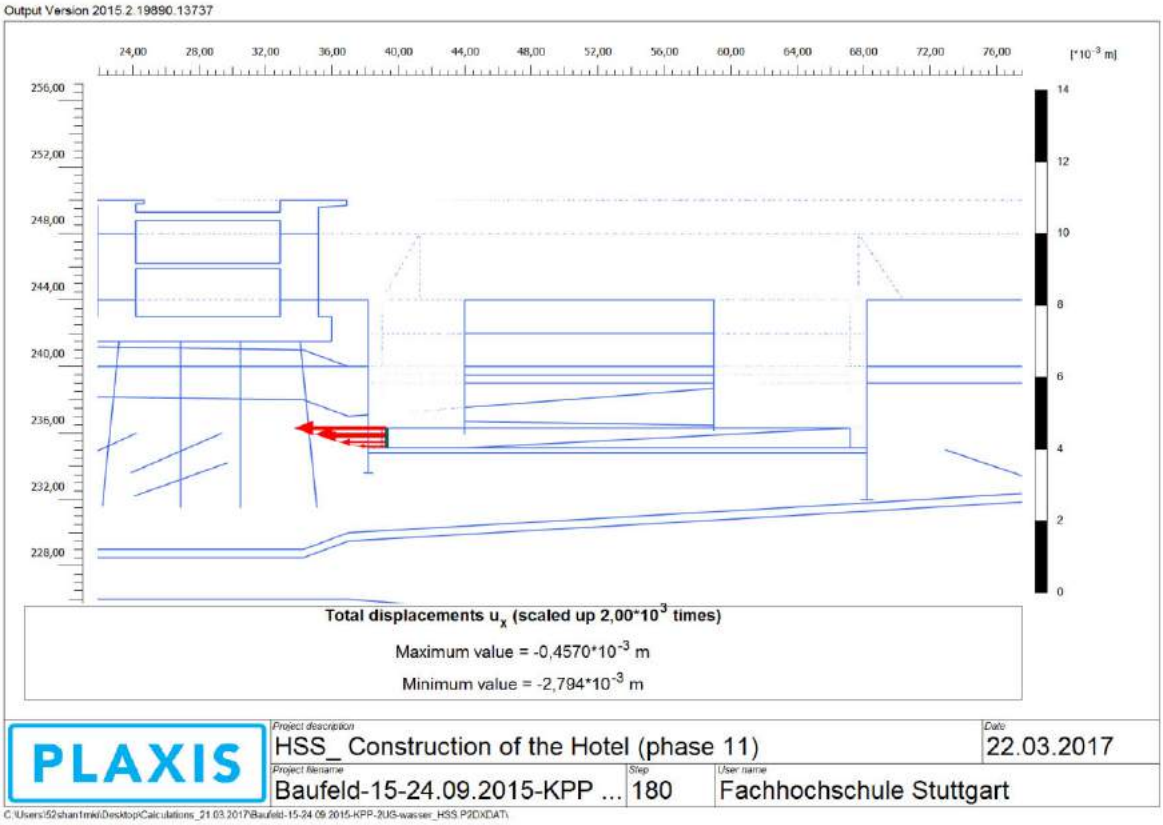

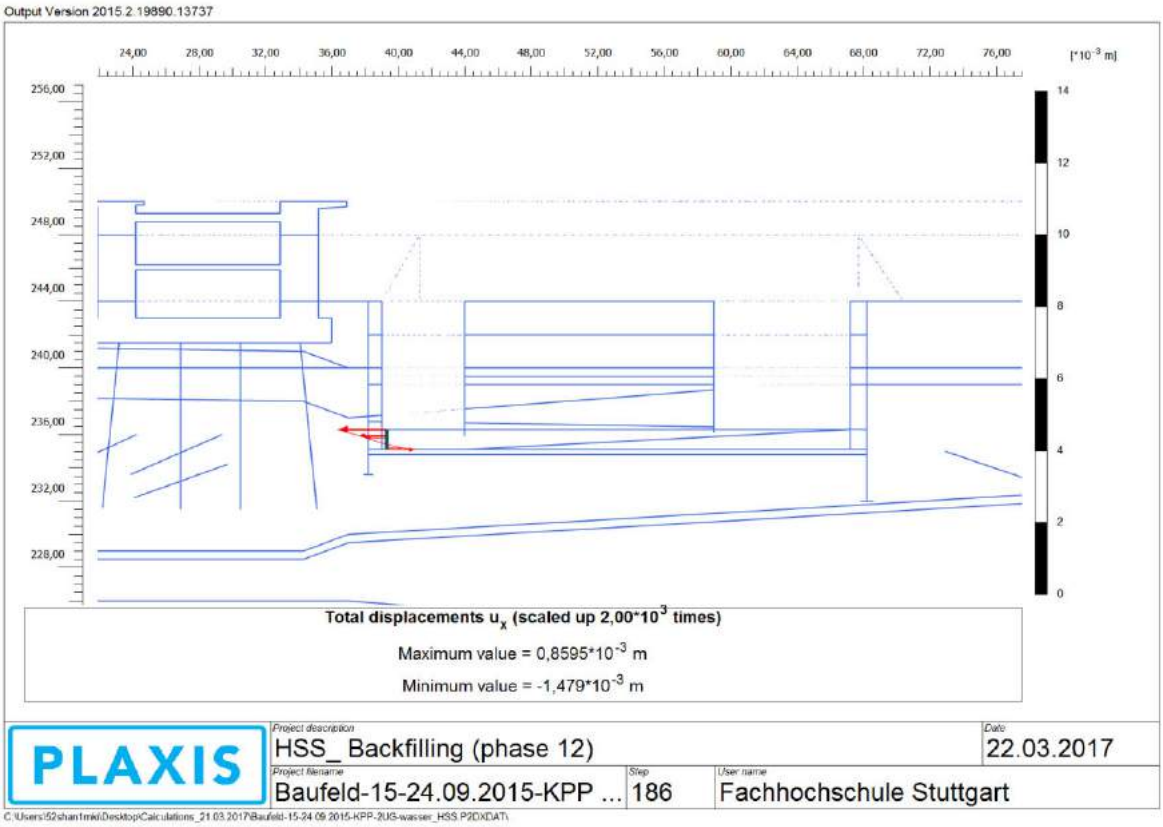

Output Version 2015.2.19890.13737

Total displacements u_x (scaled up $2{,}00*10^3$ times)

Maximum value = $-0{,}5711*10^{-3}$ m

Minimum value = $-2{,}501*10^{-3}$ m

PLAXIS	Project description: HSS_ Construction of the Hotel (phase 11)		Date: 22.03.2017
	Project filename: Baufeld-15-24.09.2015-KPP ...	Step: 180	User name: Fachhochschule Stuttgart

C:\Users\52shan1mki\Desktop\Calculations_21.03.2017\Baufeld-15-24.09.2015-KPP-2UG-wasser_HSS.P2DXDAT\

Output Version 2015.2.19890.13737

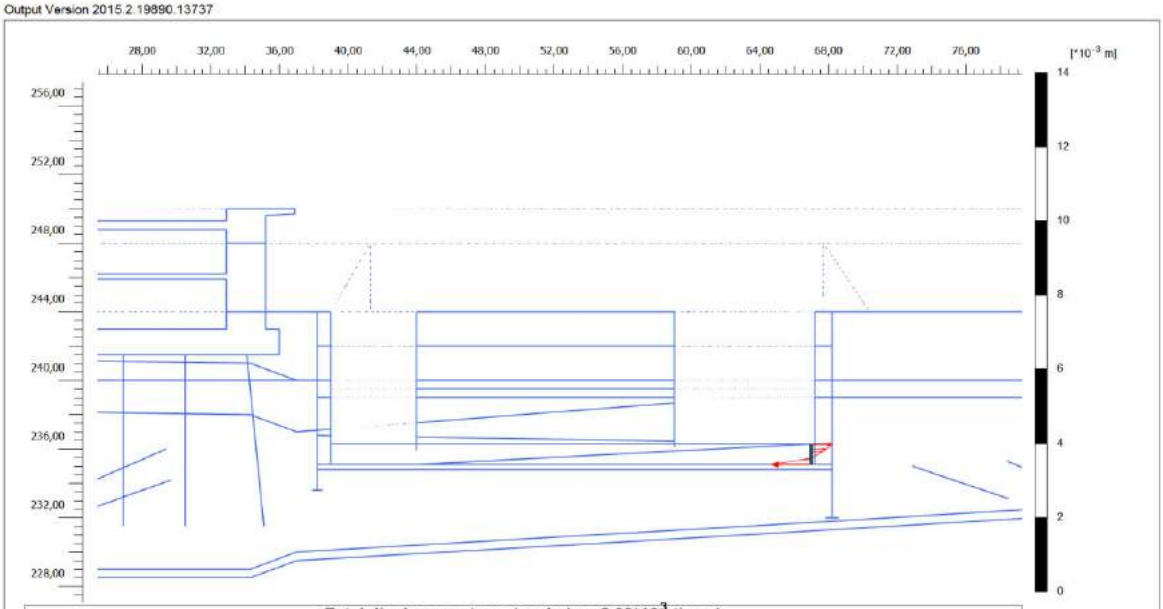

Total displacements u_x (scaled up $2{,}00*10^3$ times)

Maximum value = $0{,}6292*10^{-3}$ m

Minimum value = $-1{,}202*10^{-3}$ m

PLAXIS	Project description: HSS_ Backfilling (phase 12)		Date: 22.03.2017
	Project filename: Baufeld-15-24.09.2015-KPP ...	Step: 186	User name: Fachhochschule Stuttgart

C:\Users\52shan1mki\Desktop\Calculations_21.03.2017\Baufeld-15-24.09.2015-KPP-2UG-wasser_HSS.P2DXDAT\

HSS_Bearing Capacity of Soil